Refining the relationship between the mechanical demands on the spine and injury mechanisms through improved estimates of load exposure and tissue tolerance

by

Robert Jon Parkinson

A thesis
presented to the University of Waterloo
in fulfillment of the
thesis requirement for the degree of
Doctor of Philosophy
in
Kinesiology

Waterloo, Ontario, Canada, 2008

AUTHOR'S DECLARATION

I hereby declare that I am the sole author of this thesis. This is a true copy of the thesis, including any required final revisions, as accepted by my examiners.

I understand that my thesis may be made electronically available to the public.

Robert Jon Parkinson

Abstract

The low back loading to which an individual is exposed has been linked to injury and the reporting of low back pain. Despite extensive research on the spine and workplace loading exposures, statistics indicate that efforts to date have not led to large reductions in the reporting of these injuries. One possible cause for the apparent ineffectiveness of interventions may be a poorly defined understanding of the mechanical exposures of the spine during work related activities. There are sophisticated models that can predict spine loads and are responsive to how an individual moves and uses their muscles, however the models are complex and require extensive data collection to be implemented. This fact has prevented these models from being employed in industrial settings and the simplified surrogate methods that are being employed may not be predicting load exposures well. Therefore, this work focused on examining surrogate methods that can produce estimates of spine loading equal to our most complex laboratory based models. In addition, our understanding of spine tolerance to combined motion and load has been based upon in-vitro work that has not accurately represented coupled physiologic compression and flexion or has not investigated potentially beneficial loading scenarios. The result has been a lack of clear data indicating when motion should be treated as the primary influence in injury development or when load is the likely injury causing exposure. As a result, research was conducted to determine the interplay between load and motion in cumulative injury development, as well as investigating the potential of static rest periods in mitigating the effects of cumulative compression.

Study one examined the potential utility of artificial neural networks as a data reduction approach in obtaining estimates of time-varying loads and moments equal in magnitude to those of EMG-assisted and rigid link models. It was found that the neural network approach under predicted peak force and moment exposures, but produced strong predictions of average and cumulative

exposures. Therefore this method may be a viable approach to document cumulative loads in industrial settings.

Study two compared the load and moment estimates from a currently employed, posture match based ergonomic assessment tool (3DMatch) to those obtained with an EMG-assisted model and those predicted with a rigid link modeling approach. The results indicated that 3DMatch over predicted peak moments and cumulative compression. However, simple correction approaches were developed which can adjust the predictions to obtain more physiologic estimates.

Study three employed flexion/extension motion with repetitive compression loading profiles in an in-vitro study, with both load and motion profiles being obtained from measures in study 1. It was found that at loads above 30% of a spine's compressive tolerance, repetitive flexion/extension would not lead to intervertebral disc injury prior to an endplate or vertebral fracture occurring. However, as loads fall below 30% the likelihood of experiencing a herniation increases, while the overall likelihood of an injury occurring decreases. Comparison to relevant studies indicated that while repetitive flexion did not alter the site of injury it appeared to degrade the ability of the spine to tolerate compression.

Finally, study four employed dynamic compression while the spine was maintained in a neutral posture to investigate the effects of 'rest', or periods of static low level loading, on altering the amount of load tolerated prior to injury. It was found that there was a non-linear relationship between load magnitude and compressive tolerance, with increasing load magnitude exposures leading to decreasing cumulative load tolerances. Periods of low level static loading did not alter the resistance of the spinal unit to cumulative compression or impact the number of cycles tolerated to failure.

In summary, this work has examined methods that may allow for better predictions of spine loading in the workplace without the large data demands of sophisticated laboratory approaches.

Where possible, suggestions for optimal implementation of these surrogates have been developed. Additionally, in-vitro work has indicated a load threshold of 30%, above which herniation is not likely to occur during dynamic repetitive loading. Furthermore, the insertion of static rest periods into dynamic loading scenarios did not improve the spine's failure tolerance to loading, indicating that care should be exercised when determining optimal loading paradigms. In combination, the applied methods that have been developed and the information regarding injury development that has been obtained will help to refine our understanding of the exposures and tolerances that define mechanical injury in the spine.

Acknowledgements

Where to start, it has been a long haul and I have benefited from the influence of so many. First, I would like to thank my advisor, mentor, teacher, and perhaps most importantly friend Dr. Jack Callaghan. Academically and professionally you have provided countless hours of invaluable help and advice, for which I can never thank you. However, personally you have been an invaluable friend over the last 8 years and have helped me through some incredibly difficult times. Again, I cannot thank you enough. It is with great reservation that I will end my tenure in your lab, never to have defeated you in squash…although there was the one time you had to withdraw…

I must also acknowledge my best man and friend, Tyson Beach. Thanks for everything, I only hope we get the opportunity to work together again in the future as I know you are headed from some where very successful.

To my committee members Dr. Stu McGill, Dr. Steve Prentice, Dr. Clark Dickerson, Dr. Duane Cronin, Dr. Jennifer Durkin and Dr. Jim Potvin. I feel lucky to have had a committee of such strong scientists to help guide my development. Thank you all for taking the time to help me view my own work critically and to help me develop. I wish you all the best in the future.

Finally, I thank all the former lab members, visiting scientists and students I have had the pleasure of working with. Dr. Janessa Drake, Nadine Dunk, Diane Gregory, Erika Nelson-Wong, Adrian Holmes, Tyson Beach, Dr. Pete Stothart, Dr. Kermit Davis, Susan Kotowski, Stephanie Coke, Marty Bezaire, Lynne Pronovost, Katie Selman, Jeremy Noble, Steve Fischer, Sam Howarth, Dr. Steve Brown, Jon Singer, Jeff Rice, Wendell Prime, Ruth Gooding, Dr. Peter Kier, Jeremy Mogk, Dr. Sylvain Grenier and many others. Thank you all, for everything.

Dedication

To my beautiful bride, Christina. You are everything to me and I seldom say it but appreciate you more everyday. Thank you for being with me through all these years…We have come a long way from me cheating off your high school grammar!

To my mom, you are a shining example of what it takes to raise a family, through a range of experiences I could have never expected. I hope I can be for my kids what you are to me.

Finally, this thesis and everything that I do I dedicate to my father. There are no words to describe what you meant to me and our family. My deepest hope in life is that we will get to see each other again.

Table of Contents

List of Figures

List of Tables

Chapter 1
Introduction

The large volume of research that has been conducted on the relationships between the workplace, spinal loading and injury indicates that spine injury and low back pain have become a societal problem. Simply searching the key words 'low back pain' on the search engine Pubmed (www.pubmed.com) resulted in 12032 results dating back to 1949. In fact, low back pain has been deemed one of the top three occupational health problems to be watched by the World Health Organization for the Americas region (Choi *et al.*, 2001) and has been stated to be the most frequently filed compensation claim in the United States, with an estimated prevalence rate of 17.6% in 1988 (22.4 million cases)(Guo *et al.*, 1995). Of all the reported back pain cases in the United States for 1988, greater than 70% were attributed to the low back (Guo *et al.*, 1995). Despite all the research efforts, statistics do not support any substantial reduction in work related low back pain reporting (figure 1-1).

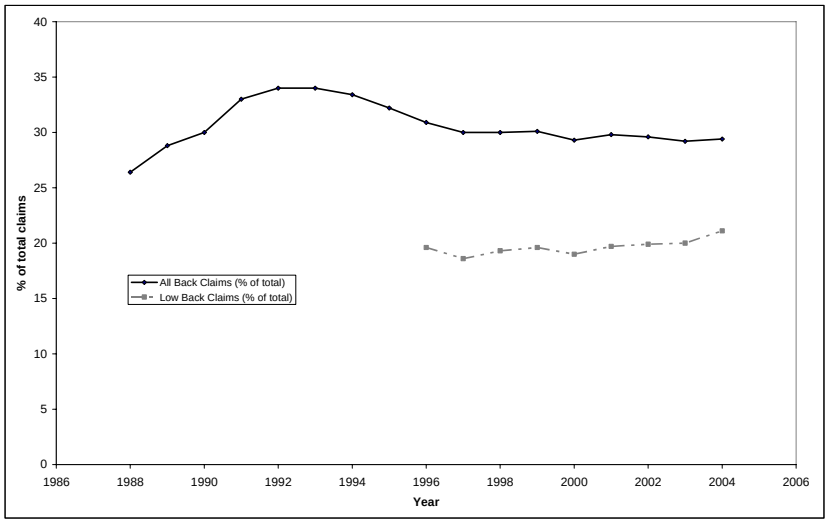

Figure 1-1: Solid line - The percentage of workers compensation claims attributed to the back in Ontario through the years of 1988 to 2004. Dashed line – The percentage of workers compensation claims attributed to the low back in Ontario through the years of 1996 to 2004. Data are taken from the 1995 and 2004 statistical supplements published by the Workplace Safety and Insurance Board (www.wsib.on.ca).

If the arguable assumption is accepted that the statistics regarding the reporting of pain are linked to the occurrence of injury in the spine it follows that research efforts have not been entirely successful in reducing work related spinal injury. In 1997, Professor McGill indicated that injuries in the spine occurred due to mechanical load exposure in excess of tissue tolerance limits (McGill, 1997). Although the contribution of numerous other factors to spinal injury have been highlighted, this relationship between load exposure and tolerance lies at the core of all injury theories (Marras, 2005). It has been suggested that the one reason for the ineffectiveness of research to date in reducing pain or injury is that causality may not be sufficiently understood to yield the desired benefits (Marras, 2005). This lack of understanding implies that the relationship between load exposure and tissue tolerance has not been sufficiently characterized to allow appropriate injury reducing interventions to be implemented. As stated by Parnianpour et al. (1997), "The fundamental inability to determine "How much of a risk factor is too much?" has been one of the most critical hindrances to the development of an ergonomics guideline for design of safe manual material handling tasks". One rationale for the poor causality may be that load exposures and tissue thresholds have not been adequately quantified in the appropriate settings.

In order to assess the load exposure of the spine several techniques have been employed, varying in complexity. Early attempts to estimate loading employed simplified two-dimensional models of the body combined with hand loads to estimate reaction forces in the spine (Smith *et al.*, 1982; McGill and Norman, 1985; Leskinen *et al.*, 1983a; Leskinen *et al.*, 1983b; Ekholm *et al.*, 1982). These models were followed by gradual increases in sophistication, starting with the movement to simplified three-dimensional models which ignored angular velocities and accelerations (Buseck *et al.*, 1988; Bush-Joseph *et al.*, 1988; Herrin *et al.*, 1986). Eventually, three-dimensional fully dynamic models were developed (de Looze *et al.*, 1992a; Kingma *et al.*, 1996a). While these

models were able to quantify loading due to external loads and body segment mass, they did not reflect the contribution of muscle forces to spinal loading. In order to more accurately reflect the loading of the spine, joint models have been developed. Initially these models began by employing one muscle force to represent the combined contribution of all back musculature, where the product of this force and its moment arm must balance the external moment (Bejjani *et al.*, 1984; Leskinen, 1985; Wood and Hayes, 1974; Morris *et al.*, 1961; Chaffin, 1969). As research has continued, these models have evolved to more accurately replicate spinal anatomy, including multiple muscles which can contribute to moments about all movement axes (flexion/extension, lateral bend and axial twist) (McGill and Norman, 1986; McGill, 1992b; Granata and Marras, 1995a; Marras and Sommerich, 1991a; van Dieen and Kingma, 2005). Some of these models have employed optimization algorithms to yield estimates of spinal loading through predictions of muscular activation (van Dieen and Kingma, 2005), while others use measured muscle activations as inputs to the model (McGill and Norman, 1986; McGill, 1992b; Granata and Marras, 1995a; Marras and Sommerich, 1991a). Although these models provide the most realistic estimates of spinal loads due to their anatomical detail, their high demand for multiple quality inputs (joint positions, velocities, muscle activation levels, external load measures) has limited their use in analyzing the load exposures experienced by workers performing industrial tasks outside of the laboratory environment (McGill *et al.*, 1996b; Mirka and Marras, 1993; Granata and Marras, 1995b; Lee *et al.*, 2003). As these models cannot be widely applied in industry, surrogate measures have been employed which do not have the same demands for inputs but also do not contain the same amount of biological fidelity. These measures may not have accurately determined the load exposure of various jobs and therefore we may not truly understand loads as they are experienced in industry. In order to address the limitations surrounding simplified estimates of work related spine loading, this thesis examined the use of artificial neural networks and posture matching (through 3DMatch, a custom software program) as potential methods

to provide estimates of joint moments and forces that would be equivalent to estimates produced with more demanding laboratory based methods. If these methods were proven successful despite the reduced information demands, it may be possible to document industrial spine loading more accurately and on a larger scale than is currently possible. In the future, these estimated loads can be incorporated into theoretical tissue injury models to enhance predictions of injury risk.

In addition to the issues surrounding the establishment of true load exposures, the development of tissue based load thresholds has also been subject to some limitations. Much of the early work surrounding spinal tissue failure focused on the resistance of the spine to acute compression (Callaghan and McGill, 1995; Edmondston *et al.*, 1997; Hansson *et al.*, 1980; Hansson and Roos, 1983; Hutton *et al.*, 1979; Roaf, 1960; Rockoff *et al.*, 1969; Thomsen *et al.*, 2002). As testing methodologies improved, researchers began to address the issues surrounding the dynamic nature of physiologic loading. Initial attempts to understand the response of the spine to dynamic loading involved the application of saw-tooth or sine compressive waveforms (Brinckmann *et al.*, 1988; Gordon *et al.*, 1991; Gardner-Morse and Stokes, 2003; Adams and Hutton, 1983a; Adams and Hutton, 1985; Liu *et al.*, 1983; Hansson *et al.*, 1987; Smeathers and Joanes, 1988; Hasegawa *et al.*, 1995). While these waveforms reflect the idea that load exposure of the spine is time-varying, they are not necessarily biological and likely reflect the limitations of the testing apparatuses. More recent work has been able to employ customized waveforms which will allow the application of dynamic loads as they are experienced in industrial tasks (Parkinson and Callaghan, 2006). Apart from the time-varying changes in load, researchers have developed methods to assess the impact of alterations in joint posture. Again, the initial work focused on the effects of static changes in posture and has progressed to time-varying posture change (Adams *et al.*, 1994; Adams and Hutton, 1982; Adams and Hutton, 1983b; Adams and Hutton, 1980; Gallagher *et al.*, 2005; Gallagher *et al.*, 2006; Gunning *et al.*, 2001; Callaghan and McGill, 2001). The results have indicated that postural changes under low

level loading can alter the injury mechanism, resulting in injury to the intervertebral disc (Callaghan and McGill, 2001), as opposed to the endplate and trabecular injuries observed with excessive load (Parkinson and Callaghan, 2007b). While the above studies have acknowledged the need to assess the impact of dynamic load and posture alterations, no research has yet been able to apply physiological load and posture changes concurrently to further determine the tissue threshold to injury. This research is further complicated by the multi-factorial exposure, making it difficult to determine which factor is responsible for the injury. Therefore, work contained within this thesis has been performed to identify a transition loading magnitude where the risk of a posture driven injury (intervertebral disc herniation) occurring increases. In addition, the effect of dynamic postural changes on the ability of the spine to tolerate cyclic loading will be addressed. In the future, this knowledge can be combined with loading estimates in a theoretical injury model to further improve estimates of injury risk and subsequently lead to improved injury prevention standards.

One interesting commonality with much of the previous tissue research is the consistent failure of vertebrae in the endplate and underlying trabecular bone when exposed to cyclic compression (Brinckmann *et al.*, 1988; Hansson *et al.*, 1987; Parkinson and Callaghan, 2007b). This consistency indicates that the central region of the vertebrae may be more prone to injury than the periphery. However, research has shown that when the endplate is loaded statically, the large central stresses decreased while the peripheral stresses increased (van Dieen *et al.*, 2001). This redistribution of stresses may present a viable injury prevention paradigm to enhance the tolerance of the endplate and underlying trabecular bone to cyclic compression. If this redistribution were effective, it could increase the cumulative compressive tolerance of the spine; however this mechanism has not yet been studied. The final study included in this body of work addresses this issue of load redistribution with the intent of improving the understanding of work cycles and rest, which in turn will provide valuable

information regarding methods of altering tissue tolerance, which can be incorporated into tissue injury models and lead to improved injury risk assessments.

Therefore, before research moves away from the theoretical injury models based on load exposure and injury threshold, attempts should be made to improve our estimates of industrial load exposure by implementing tools to provide the best possible load exposure estimates and at the same time improve tissue threshold estimates through the implementation of coupled load/motion profiles for in-vitro testing to better reflect industrial exposures. Enhancing the understanding of the types of injuries associated with different exposures (load vs. posture) may lead to an improved ability to focus interventions on the correct mode of injury. Additionally, examining mechanisms which may increase the cumulative tolerance of the osteoligamentous spine may provide insight into the design of adequate time-varying loading paradigms to limit the risk of vertebral fracture.

1.1 Global Thesis Questions and Hypotheses:

1. Can the data needed to use our most sophisticated biomechanical tools be reduced to a level that can be obtained in industry in order to facilitate large scale documentation of spinal load exposure in the workplace?

Hypothesis 1:

Artificial neural networks will allow for a reduction in the amount of input information needed to obtain estimates of spinal load and moment exposures equivalent to those of rigid link and EMG assisted spine models.

Study 1 addressed this hypothesis by examining the potential for artificial neural networks to develop relationships from a limited number of industrially obtainable inputs and relate these inputs to biologically meaningful outputs (moments and joint forces in the spine).

Hypothesis 2:

The errors associated with a quasi-dynamic posture matching tool (3DMatch) relative to rigid link and EMG-assisted models can be quantified and accounted for to allow physiologically reasonable estimates of spine loading in industrial settings.

Study 2 addressed this hypothesis by comparing estimates of joint moments and forces (compression and shear) between 3DMatch, a three-dimensional bottom-up inverse dynamic model and an EMG-assisted model.

2. Can new information regarding spinal exposure to compression and sagittal flexion/extension be used to expand our current understanding of tissue injury mechanisms and thresholds?

Hypothesis 1:

By applying physiologic dynamic kinetic and kinematic profiles to isolated porcine spinal units it will be possible to elucidate injury mechanisms associated with excessive load or excessive motion and from the combined loading paradigm identify a transition in injury mechanisms.

Study 3 addressed this hypothesis by exposing isolated porcine spinal units to differing combinations of dynamic load and flexion profiles (obtained from study 1) and recording the changes in the vertebrae and intervertebral disc that occur as injury progresses.

3. Is it possible that loads can be redistributed across the vertebral endplate in such a way as to enhance the ability of the spine to withstand cumulative compression?

Hypothesis 1:

By inserting periods of low level static loading between dynamic load applications the spinal unit will be capable of tolerating greater amounts of cumulative compression.

Study 4 addressed this hypothesis by exposing isolated porcine spinal units to differing combinations of dynamic load and static rest duration and monitoring changes in mechanical behaviour until injury occurred.

Chapter 2
General Review of Literature

2.1 Overview

While chapter 1 has highlighted the rationale for conducting the research contained within this thesis, the following sections will provide a more in depth review of literature focusing on the issues underlying this work. Specifically, this chapter will detail the background underlying spine modeling as it applies to force and moment predictions, provide a summarized history of artificial neural networks as they have been used in biomechanics, and summarize the progression of in vitro spine testing.

2.2 Rigid Link Modeling and Top-down vs. Bottom-up Approaches

Industrial surveillance has shown that the maximum moment a worker was exposed to was the most discriminating variable between those workers who were and were not at risk of developing low back pain in the workplace, with an odds ratio of 5.17:1 (Marras *et al.*, 1995). This finding signifies the influence joint moment may have on injury development and pain reporting in the low back, as well as the need for biomechanics researchers to accurately quantify this variable. Additionally, joint moments within the spine are used as inputs for sophisticated spine models where they can be decomposed into compression and shear forces within the joint (McGill and Norman, 1986; Marras and Sommerich, 1991a). These joint forces have been shown to result in injury of the spine if of sufficient magnitude (Gunning *et al.*, 2001; Callaghan and McGill, 1995; Yingling *et al.*, 1997; Allan *et al.*, 1990; Burklein *et al.*, 2001; Hansson *et al.*, 1987; McBroom *et al.*, 1985; Yingling *et al.*, 1999).

To understand the exposure of the spine to reaction forces and moments an inverse dynamics approach has been employed to estimate spine kinetics (Kromodihardjo and Mital, 1986; Lariviere and Gagnon, 1998; Lavender *et al.*, 1999; Freivalds *et al.*, 1984; Mital and Kromodihardjo, 1986; Gagnon and Gagnon, 1992; Kingma *et al.*, 1998a; Kingma *et al.*, 1998b; Kingma *et al.*, 1996b). In order to employ these methods, several pieces of information are required. First, anthropometric measures (mass, mass distribution and center of gravity) are required. Second, the location of the body segments in space must be known. In addition it is necessary to know any external force(s) and moment(s) applied to the segments. From this information the forces and moments at each joint can be predicted, with estimates at more proximal joints being obtained by proceeding through the distal rigid bodies until the desired joint is reached. As the process can be moved in any direction, it is theoretically possible to obtain the same force and moment estimates moving either from the hands to the spine (top-down) or from the feet to the spine (bottom-up) (figure 2-1) or completely through the linkage from one extremity to the other (i.e. hands to feet).

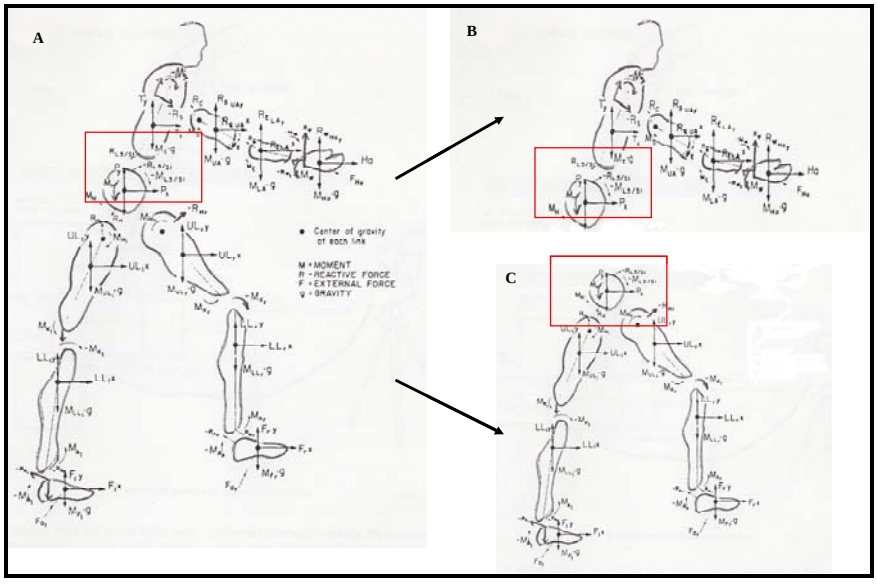

Figure 2-1: (A) Free body diagram of the whole body, the red squares indicate the forces and moments at the L5/S1 joint. **(B)** Isolation of the top-down portion of the model illustrating how information regarding the forces at the hands, body segment motion and body segment parameters could be employed to estimate the forces and moments at the L5/S1 joint. **(C)** Isolation of the bottom-up portion of the model illustrating how information regarding the forces at the feet, body segment motion and body segment parameters could be employed to estimate the forces and moments at the L5/S1 joint. The original figure was taken from Freivalds et al. (Freivalds et al., 1984).

This theoretical equality has allowed authors to test the agreement of their models and search for sources of error. Kingma et al. (1996b) compared the moments about L5/S1 as they were predicted from two-dimensional bottom-up and top-down models and found high correlations (0.990-0.997) for four types of lifting technique and two different anthropometric approaches. The model or anthropometric approach used did not significantly alter the absolute mean or peak differences, indicating that all approaches provided magnitude equivalent estimates (Kingma *et al.*, 1996b). Lariviere and Gagnon (1998) directly compared moments about L5/S1 predicted from three-dimensional bottom-up and top-down models and looked at the influence of changes in body segment parameters, lift asymmetry, load magnitude, lift rate and shoulder joint center location. For the bottom-up model each foot was placed on a force plate and calculations were performed segment by

segment. The bottom-up model was composed of 7 segments, including the feet, shanks, thighs and pelvis while the top-down model was composed of 9 segments, including the hands, arms, upper arms, head, T12/L1-shoulders and L5/S1-T12/L1. Hand forces were determined from the mass of the objects in the hand and the linear accelerations. Lariviere and Gagnon (1998) concluded that for static analysis no systematic differences existed between the models, finding the largest absolute difference between models for lateral bend moments (8.3 Nm). In contrast, the largest absolute difference in dynamic tasks was for extension moments (15 Nm). The study illustrated that the difference between the top-down and bottom-up models was much higher in dynamic tasks. The top-down approach appeared to underestimate the extension moment at the initiation of the lift (Lariviere and Gagnon, 1998). Both models were found to be sensitive to alterations in load magnitude and load distribution (between hands) while the downward model was shown to be more sensitive to alterations in anthropometric measures (segment mass, center of mass, radius of gyration). Movement of the L5/S1 joint center did not significantly alter extension moments in either model; however the models were sensitive to errors in marker location, with translation of the marker along the longitudinal axis of the pelvis leading to errors in moment estimation (Lariviere and Gagnon, 1998). However both models were similarly affected and the maximal differences between model estimates did not change. Use of differing shoulder joint center location methods had a greater effect on shoulder moments than those estimated at L5/S1, with errors of 14 and 2 Nm respectively (Lariviere and Gagnon, 1998).

In an earlier study it was shown that top-down and bottom-up models resulted in similar estimates of forces and moments at the L5/S1 joint, with correlations typically above 0.95 (Plamondon *et al.*, 1996). The lowest correlations were found for moments about the longitudinal axis for slow (0.76) and fast (0.78) lifting speeds. The root mean square difference between force estimates of the two models were larger for greater lifting speeds, but remained under 15 N.

Similarly, the root mean square difference in moment estimates was larger during the fast lifts and ranged from 4 to 9 Nm (Plamondon *et al.*, 1996). The maximum differences in force and moment estimates observed were 59 N and 38 Nm respectively (Plamondon *et al.*, 1996).

One argument against the use of a bottom-up model is that the use of a force plate may constrain foot placement (de Looze et al., 1994). Additionally, it has been shown that errors in the center of pressure location of 1 and 0.5 cm can lead to errors in moment estimation of 14 and 7% when averaged across the hip, knee and ankle joints (McCaw and DeVita, 1995). This finding supports the conclusions of Plamondon et al. (1996) who found that the bottom-up model was most sensitive to noise in the ground reaction force. Displacements in the joint center location of L5/S1 of 3-10mm can lead to differences in moment estimation up to 12 Nm in flexion/extension, 10 Nm in lateral bending and 3 Nm for axial torsion (Gagnon and Gagnon, 1992). Additionally, it has been shown that errors in the knee joint center location can lead to alterations in force and moment estimations at the joint (Nissan, 1980). In contrast top-down models are influenced by estimates of trunk mass (Pearsall et al., 1994), trunk mass locations and shoulder joint center identification. As inverse dynamic approaches assume that the links of the body are rigid and connected by simple articulations it stands to reason that the trunk may be more problematic as it is a flexible structure (Freivalds et al., 1984). Pearsall et al. (1994) provide information regarding inertial properties of the trunk, which are critical in a top-down model and contribute greatly to the estimated forces and moments about the L5/S1 joint (Lindbeck and Arborelius, 1991). The trunk represents the segment with the most divergent reported values of mass, ranging in the literature from 43.6% to 52.4% of total body mass (Pearsall *et al.*, 1994). The difficulty in accurately estimating trunk mass and mass distribution is reflected in the findings that top-down models are more sensitive to alterations in body segment parameters (Plamondon *et al.*, 1996). Kingma et al. (1996b) have shown that the trunk has the largest impact on moment estimation in the spine, with alterations in trunk mass or trunk center of

gravity estimates leading to the largest differences in moment estimation between top-down and bottom-up models. De Looze et al. (1992b) concluded that the largest variation in link length occurs in the trunk during motion (6.2% or 2.8 cm). Errors may also exist due to techniques of prediction. Typical analyses employ segment mass, length, center of gravity and radius of gyration. For the extremities these measures are more easily obtained as the pivot points are assumed at the joint centers and the center of mass falls near a line connecting two joint centers. The trunk is more complicated as the vertebral column permits many different types of motion and pivot points are not easily defined (Plagenhoef et al., 1983). These trunk associated errors may explain why work comparing estimates of the ground reaction force as determined through a top-down inverse dynamics assessment to measured ground reaction forces found a correlation of only 0.43, indicating substantial error (Freivalds et al., 1984). In contrast, when dealing with the lower extremities their contribution in terms of inertial effects is small (Lindbeck and Arborelius, 1991), and therefore errors in estimation of inertial properties may not exert as great an influence on joint load estimation.

As there is no method to determine systematic errors associated with the choice of top-down or bottom-up models, model selection becomes a choice dictated by the capabilities and goals of the researcher. Obtaining complete three-dimensional data during complex tasks is very demanding in terms of resources, regardless of model selection. Three-dimensional analysis demands a minimum of three non-collinear markers per segment. Based on a nine segment model top-down model, such as that employed by Lariviere and Gagnon (1998), this would require a minimum of 27 markers to be visible at all times throughout data collection (ignoring additional marker demands for calibration). This number could be reduced if a seven segment bottom-up model were used, although the demands for visibility are consistent. In terms of marker visibility range of motion must be considered. When performing lifting tasks, the hands and upper limb segments will cover a greater distance than the leg segments. Additionally, the rotation capability of the upper limb can result in hand and forearm

segment markers moving out of the visible field. Although the legs will also move, the motions are expected to be smaller and out of range rotations are not as likely to occur. Therefore a bottom-up model may provide a practical advantage in terms of positional data collection. In addition, measurement of external forces in a top-down model can be difficult. Top-down modeling requires either mounted force transducers, accelerometers, or the manipulation of Newton's second law, which can be represented by the equation F = ma. While the use of transducers can be complicated in a load return system due to cabling and interfacing the transducer between the hands and the objects handled, the estimation of force based on hand accelerations can lead to difficulty in determining when the load in is the hands (set down and lifted) and may induce errors at the initiation of the lift with large hand accelerations (Plamondon *et al.*, 1996). When these practical limitations in data collection are combined with the impact of trunk anthropometrics in joint kinetic estimates it appears that the bottom-up model may be a more practical approach in the laboratory.

However, the same conclusions may not be drawn for the estimation of joint loading in industry due to the practical issues in acquiring force and movement data. Bottom-up modeling requires the measurement of ground reaction forces, typically obtained with a force plate. The implementation of a force plate for data collection in industry is not practical due to the nature of the industrial environment and the need for workers to move through a larger area than that allowed by the instrument. Recent research has begun to investigate novel methods of obtaining forces and moments at the feet with wearable six degree of freedom load cells, with promising results (Carmichael et al., 2006). However further work needs to be conducted investigating industrial usability. A similar problem exists for top-down modeling in that instrumentation of industrial loads for direct force recording is also often impractical. Additionally, both approaches are limited in terms of motion analysis. The motion capture systems employed in the laboratory are expensive, require calibration of a limited capture space, and have extensive marker demands. These properties render

the systems impractical and therefore surrogate measures of three-dimensional motion and force exposure are necessary to obtain estimates of spinal loading. These surrogates may consist of positional data comprised of two or three-dimensional co-ordinates, joint angles (estimated from pictures, video data, or direct observation), static hand loads or self reported loading.

As no techniques or instrumentation can directly measure the moment or force exposure of the spine *in vivo* it is not known which of these methods or surrogate measures contain the necessary information to allow accurate prediction of spinal loading. In contrast, it is possible to measure external loads and movement in the laboratory with a much higher degree of accuracy, although this does not provide a direct estimate of industrial exposure. If research hopes to accurately predict industrial load and moment exposures it is necessary to be able to apply the laboratory techniques in the industrial setting. While this may not be physically practical, it may be possible through numerical techniques.

2.3 The EMG-assisted model

The joint model employed in this thesis was based on the joint model developed in the Ohio State Biodynamics Laboratory by Dr. Marras. This model has been chosen due to its ability to reflect anatomical differences due to gender and its previous implementation in the examination of industrial lifting scenarios. The following model timeline will describe the model from its initially reported state through the most recently published changes, highlighting those aspects which are relevant to the implementation of the model for this work.

1991

The model was initially described in 1991 as an approach to predict dynamic spinal loading under laboratory conditions (Marras and Sommerich, 1991a) and required the input of trunk EMG from 10 channels (bilaterally from the latissimus dorsi, erector spinae, rectus abdominus, and both internal and external obliques), subject characteristics (height, weight, trunk breadth and depth at L5), trunk kinematics (flexion angle and angular velocity) and kinetics (trunk moment). EMG data was normalized to maximal activation, and used to predict force output (Marras and Sommerich, 1991a). The EMG signal was then further adjusted for velocity, length, cross-sectional area and gain, where gain is the maximum force producing capability of the muscle per unit area. The force-velocity relationship was obtained by multiplying the EMG signal at each point by a ratio composed of the average normalized EMG signal obtained for a muscle at a certain trunk angle, external torque production, and 0 velocity (numerator) and the average EMG response at the same trunk angle, torque production at the velocity of the trial (denominator). This ratio was based on EMG signals within a database of the laboratory (Marras and Sommerich, 1991a). Not all muscles were adjusted for velocity, only the latissimus dorsi, erector spinae and internal obliques. The force-length relationship employed was stated to be obtained from equations derived from graphs in textbooks, in conjunction with trial and error. Force-length adjustments were only made to the

latissimus dorsi, erector spinae and rectus abdominus muscles. Muscle area was determined from trunk measures and coefficients from Schultz et al. (1982). The gain factor was an adjustable value used to ensure that predicted muscle forces resulted in an internal moment that balanced the external moment, compensating for deficiencies in other modulators (Marras and Sommerich, 1991a). The model was initially run with a gain value of 10 and the lateral torque due to muscle forces was determined. If this value was within 5% of the recorded average torque, the gain was determined to be sufficient and muscle forces and spinal loading were considered correct. If not the gain was increased and the process repeated. The initial model did not predict loads at all points within a trial, but at characteristic event times with linear interpolation used to fill in the remainder (Marras and Sommerich, 1991a). While this was the first full description of the model and its implementation in predicting absolute loads, an earlier version was published, but was limited to relative comparisons and did not make EMG-force adjustments (Reilly and Marras, 1989). Initial model architecture is depicted in figure 2-2.

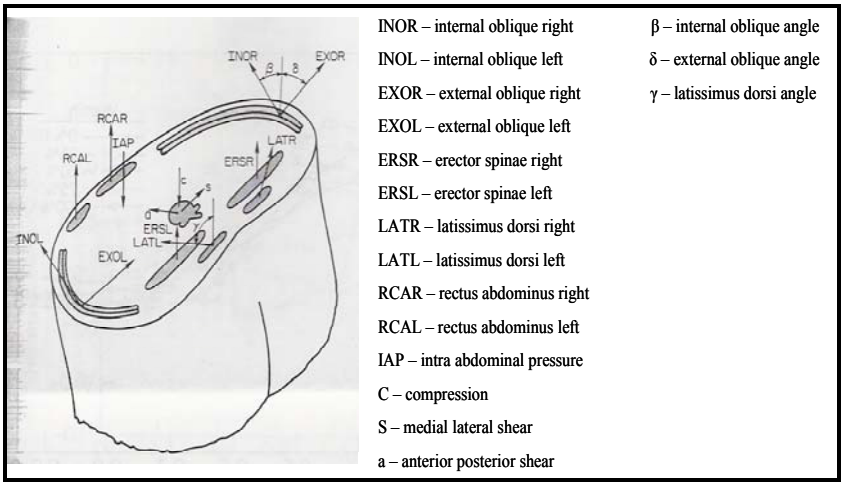

Figure 2-2: The original model architecture employed in the Ohio State Biodynamics laboratory, based on the work of Schultz and Andersson (1981). The figure has been taken from Reilly and Marras (Reilly and Marras, 1989).

1991

Marras and Sommerich conducted a validation of their model (1991b). As internal compression and shear cannot be measured to allow a direct validation of the model, predicted and measured joint torques about L5/S1 were compared (Marras and Sommerich, 1991b). Comparison of the torque estimates and measurements found that over 85% of the comparison pairs displayed correlation coefficients greater than 0.7. The authors concluded that this was a good correlation, given that the exertions were dynamic and included asymmetry (Marras and Sommerich, 1991b).

1993

In 1993, Granata and Marras reported on some adjustments to the model, including moving to a point by point analysis from the linear interpolation method initially used. Additionally, the

mechanics employed in modeling were extensively described. First, two co-ordinate systems were established. A sacral based axis system (coincident with the laboratory system) and a lumbar spine axis system are used. While both system origins are located in the sacrum, the lumbar spine system is free to move with the trunk. The systems are aligned with the subject in upright standing posture. Vector components of external moment are resolved in the lumbar reference frame and then transferred to the sacral frame to allow comparison and gain matching (Granata and Marras, 1993). Moments about L5/S1 attributed to muscles are predicted from the summation of vector products between moment arms and muscle forces. When the summed muscle moments equal the external moments it is assumed that the muscle forces are correct. Vector summation was then employed to determine spinal compression and shear (Granata and Marras, 1993). The model was further assumed valid if the gain values employed fall within the range of 30-100 N/cm^2. This model review highlighted the fact that over 80% of 2160 trials were predicted with a correlation coefficient of 0.8 or more (Granata and Marras, 1993).

1995

In 1995, the model was improved to allow prediction of joint loads in less constrained dynamic lifting scenarios (Granata and Marras, 1995a). The 10 muscle sites were the same as before, and the normalized EMG signal was again multiplied by several

modulating factors to allow estimation of muscle force. The normalized signal was subsequently multiplied by force-length and force-velocity factors (Granata and Marras, 1995a). This model description differed from the previous as it included the equations to determine the force-length and force-velocity coefficients:

Force-length (equations 2-1 and 2-2):

$$f(length) = -3.2 + 10.2(length) - 10.4(length)^2 + 4.6(length)^3 \quad \textbf{(2-1)}$$

For concentric velocities:

$$f(velocity) = 1.2 - 0.99(velocity) + 0.72(velocity)^2 \quad \textbf{(2-2)}$$

For eccentric velocities:

$$f(velocity) = 1.2$$

These equations employ length and velocity factors which are based on the muscle resting lengths. For this study, it was found that the average gain values in the sagittal plane were 64.9 ± 27.6 N/cm^2; while they were lower (50.2 ± 31.9 N/cm^2) in the lateral plane (Granata and Marras, 1995a). Gain values were found to differ significantly between subjects, but not within a subject. Velocity and exertion level did not significantly alter the gain value, although trunk asymmetry altered the gain value. Sagittal plane correlation coefficients averaged 0.81, while for the lateral plane the correlation coefficients averaged 0.76. The model predicted sagittal trunk moments with an average error of 17.5 Nm, less than 15% of the peak moment. The error in the lateral plane

was lower in terms of absolute magnitude (14.6 Nm); however this represented a higher relative error (24%) (Granata and Marras, 1995a).

Also in 1995, the model was applied to axial twist exertions (Marras and Granata, 1995). The authors conducted the study as previous attempts to model twisting motions resulted in non-physiologic estimates of muscle force capability, and therefore they could not replicate muscle forces. The unique contribution of this paper in terms of the model was a description of how the anatomy was employed. The 10 representative muscle vectors originated from a plane parallel to the iliac crest while insertions were given in a plane parallel to the 12^{th} rib (figure 2-3).

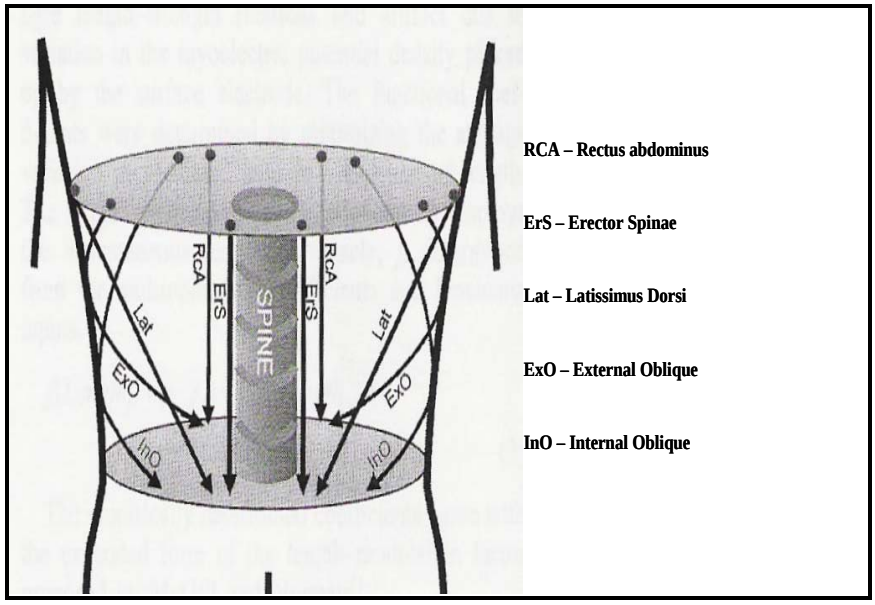

Figure 2-3: Schematic diagram depicting the more recent model architecture. The use of the planes allows the description of muscle origins and insertions as well as changes in these locations with alterations in the relationship between the planes. This figure was taken from Marras and Granata (1995).

These co-ordinates change with motion of the spine allowing muscle length and velocity changes to be accounted for (Marras and Granata, 1995). Scaleable three-dimensional co-ordinates were provided allowing determination of muscle properties in three-dimensions. Along with origin and insertions, muscle areas were also provided. In terms of model performance, the average gain value was 35.4±23.4 N/cm^2, well within the physiologic range. The average correlation coefficient for all trials was 0.8, with coefficients greater than 0.8 occurring in 65% of the trials. Correlation coefficients of 0.9 or greater occurred in 36% of the trials. Spinal loads were found to change depending on the

exertion level, direction of torque, and velocity of twisting (Marras and Granata, 1995). It was found that loading increased concurrently with increased velocity.

1997

The model has also been employed to examine the loading consequences of lateral bending exertions (Marras and Granata, 1997a). The authors hypothesized that increasing lateral bending velocity would require higher levels of co-contraction and result in higher levels of spinal loading. Modifications were made to the previously described model to more accurately reflect the force-velocity relationship at higher velocity rates (Marras and Granata, 1997a).

For concentric velocities:

$$f(velocity) = 0.65 + 0.35 \times \exp(-velocity/.025) \qquad \textbf{(2-3)}$$

For eccentric velocities:

$$f(velocity) = 1.5$$

In addition, the force-length equation was expanded to read:

$$f(length) = -3.25 + 10.20(length) - 10.40(length)^2 + 4.59(length)^3 \qquad \textbf{(2-4)}$$

It was found that the lateral bending moments were mainly induced by agonistic muscles with horizontal orientation vectors, including the ipsilateral latissimus dorsi, and the internal and external oblique muscles (Marras and Granata, 1997a). The model resulted in an average gain of 64.9 N/cm^2 with an average absolute error ranging

from 6-10%. The gain values were not altered by trunk angle, velocity or load magnitude. The average absolute error was found to be higher for dynamic contractions than for static. The average correlation coefficient for all trials was 0.91.

1998

The model has also been examined for its performance in lowering exertions (Davis *et al.*, 1998). Until this time, the spine model performance had only been examined in situations of concentric lifting, and it remained unknown if the empirical relationships within the model were robust to the direction of motion. In order to develop empirical relationships for force-length and force-velocity the average variation in the ratio between internal and external moments was minimized as a function of length and velocity (Davis *et al.*, 1998). The results for force-length were given in the form of a moment ratio vs. muscle length curve. It was found that the moment ratio – muscle length curve for lowering was very similar to that for lifting, with differences

appearing at the more extreme muscle lengths (figure 2-4).

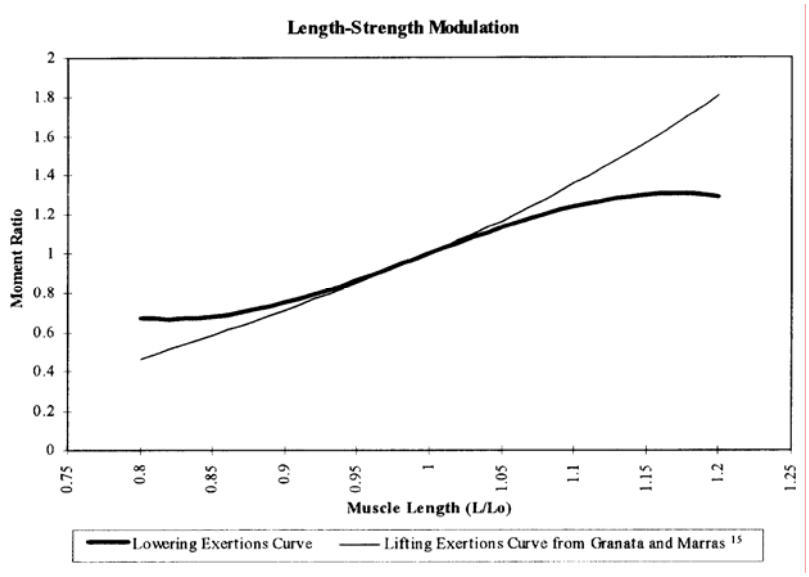

Figure 2-4: The length-strength (force-length) relationship obtained by Davis et al. while investigating lowering exertions. Figure taken from Davis et al. (1998).

The resulting moment ratio – muscle velocity curve (figure 2-5) resulted in an exponentially decreasing force generation at increasing concentric velocities while it was found that a constant modulation factor existed for lowering (1.56), indicating that subjects were 56% stronger while lowering (Davis *et al.*, 1998).

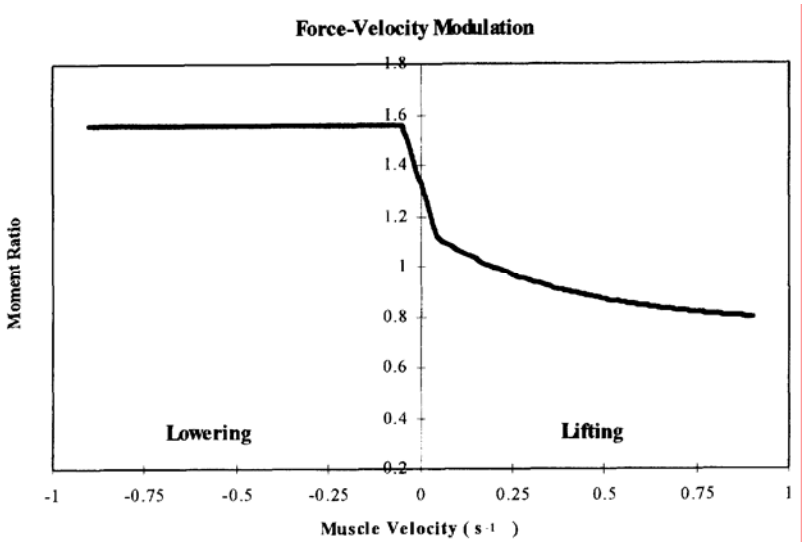

Figure 2-5: The force-velocity relationship obtained by Davis et al. while investigating lowering exertions. Figure taken from Davis et al. (1998).

Model performance was again assessed based on gain values, correlation coefficients and average absolute error. The results indicated that gain values were unchanged by the direction of loading and fell within the physiological range. It was found that coefficients of correlation between measured and predicted moment were higher for lowering exertions (0.95) than for lifting exertions (0.88). The same pattern was observed for joint moments, with higher agreement in moment magnitude for lowering than lifting, although sagittal moments for both directions were predicted within 10%. To further test the model, data were obtained from another study in which participants performed sagittally symmetric lifts of different

weights and speeds (Davis *et al.*, 1998). Implementation of the model with the above described relationships resulted in good agreement between measured and predicted moments ($r^2 = 0.91$ and average error of 7.23% of maximum sagittal moment).

1999

The model has also been tested for variability in estimation between trials occurring within the same day and trials performed on different days (Marras *et al.*, 1999). The model was shown to be quite stable. For within day analysis, the model performance parameters (gain, r^2, and average absolute error) were shown to be robust. Analysis of the sources of variability revealed that for the gain factor, subject specific properties exert the most influence (54-65% of variability), followed by the trial (17-25%). Investigation of the between day behaviour revealed that 20.6% of the gain variability was due to subject experience. Correlation variance was most influenced by the trial (42-49% of variation). However, experience was also a large contributor (31-34%). In terms of error, experience explained 22-37.38% while trial accounted for 34-51%. Weight was found to exert minimal influence (0.68-2%) (Marras *et al.*, 1999).

Gender Differences:

Although several anatomical differences have been noted in the male and female spines, such as the ratio of pelvic width to height (Brinckmann et al., 1981), moment arms of the trunk musculature at the T7, T12, L3 and L5 levels (Kumar, 1988b), cross-sectional area of the torso muscles (Reid and Costigan, 1985; Cooper *et al.*, 1992) and the amount of lumbar lordosis (Fernand and Fox, 1985), these studies did not present this information in such a way as to allow direct implementation into biomechanical models. However, more recent work has directly addressed gender differences in spinal anatomy.

Jorgensen et al. (2001) performed an examination of the gender differences in the moment arms of males and females in order to provide valuable data to those modeling the spine to account for gender differences. By improving the accuracy of the anatomy of the model, the content validity of the model rises and theoretically, the accuracy of the model predictions can be increased. Earlier studies which documented the moment arm length of female torso muscles were conducted on older women (Chaffin et al., 1990; Kumar, 1988a; Moga et al., 1993), which may not reflect the anatomy of young healthy females. The implementation of magnetic resonance imaging allowed the study of younger participants. As well as improving upon the current knowledge of male and female torso anatomy, the authors sought to develop equations that could be employed to predict gender specific moment arms based on external measures (Jorgensen *et al.*, 2001). Ten male and 10 female subjects were recruited for study. Eleven scans were obtained per subject, intersecting the vertebral bodies from T8 through to S1. The area centroid was obtained for each muscle within each scan through digital inscription of the scans. Muscle moment arms were determined as the absolute difference between the coordinates of the vertebral body centroid and the muscle area centroid in the sagittal and coronal planes (figure 2-6).

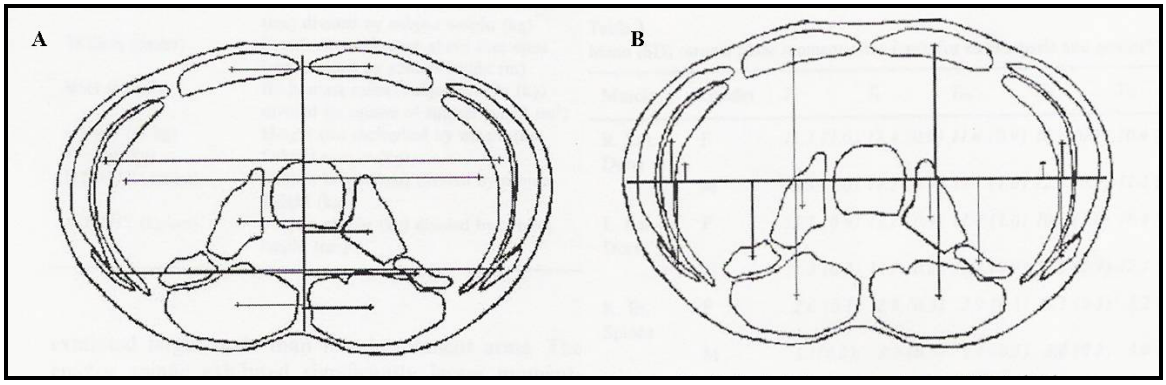

Figure 2-6: (A) Coronal plane moment arms at L3. **(B)** Sagittal plane moment arms at L3. Figure taken from Jorgensen et al. (Jorgensen *et al.*, 2001).

In the coronal plane it was found that the moment arms of the torso musculature differed between males and females, but these differences were not consistent among the spinal levels measured (Jorgensen *et al.*, 2001). The rectus abdominus was unusual in that for the left side, the moment arms were not found to differ. Moment arms were found to be larger for males than females at all levels for the latissimus dorsi, erector spinae (excluding right side, L4-S1), right rectus abdominus (not at L5) and the right external oblique, psoas major and quadratus lumborum. Overall, males exhibited 14.2% larger moment arms in the coronal plane. In the sagittal plane, the erector spinae moment arms for males were larger than for females with the exceptions of L1-L3 and L5 on the right (Jorgensen *et al.*, 2001). As well, the moment arms of the rectus abdominus were smaller in females except for the S1 level. Differences were not consistently observed for the internal obliques, external obliques or psoas major. When combined, the results indicate 17.5% longer moment arms for males in the sagittal plane. Several regression equations were developed, and it was found that the most significant predictor of female sagittal muscle moment arms was the product of height (m) and mass (kg). For males, it appeared that the best sagittal moment arm predictor was trunk depth measured at the xyphoid process. In the coronal plane, variations of height and mass (products, ratios) were all found to be significant predictors of female moment arms (Jorgensen *et al.*, 2001).

The same result was found for males. By providing the muscle moment arms for males and females, the authors provided a means through which future modeling of the spine can be made gender specific.

Employing the same methodology and participant pool as above, it was found that males exhibited larger anatomical cross sectional area (ACSA) of the torso muscles, as well as larger sizes of the vertebrae and trunk (Marras *et al.*, 2001). Additionally, symmetry was not maintained. Both males and females exhibited 10% larger right side latissimus dorsi when compared to the left (physiological cross sectional area – PCSA), and females displayed larger left side psoas major and quadratus lumborum. Regression equations were developed to allow prediction of muscle PCSAs from externally obtainable anthropometric measures. For male latissimus dorsi, height and mass combinations resulted in the best predictions, whereas for females measurements around the torso at the level of the xyphoid process were most predictive (Marras *et al.*, 2001). The erector spinae could be best predicted with combinations of height and mass for both genders. In terms of the abdominal musculature, the rectus abdominus PCSA of females was best predicted by measures of BMI and measures taken about the xyphoid process. For males, combinations of height and mass were significant predictors of rectus abdominus PCSAs. Measurements about the xyphoid process were the best predictors of female external obliques and male left external obliques (Marras *et al.*, 2001). Again, measures about the xyphoid process (as well as BMI) were significant predictors of the female internal obliques. For males, subject mass was the best predictor of internal oblique PCSA. While the correlation coefficients in this study ranged from 0.20 to 0.72, this was the first study to provide predictive regression equations for the determination of anatomically corrected muscle areas for such a variety of muscles across genders (Marras *et al.*, 2001).

The issue of gender specific moment arms was revisited by Jorgensen et al. in 2005 to try and address the issues associated with the supine posture used to study gender differences in moment

arms in their previous 2001 study (Jorgensen et al.). The use of a supine posture may result in under estimates of rectus abdominus muscle moment arms (McGill *et al.*, 1996a), and any such differences must be known and adjusted or corrected. Five female volunteers underwent upright sagittal and axial MRI scanning. The resulting scans were digitized and the borders of the intervertebral disc and rectus abdomini were outlined (Jorgensen *et al.*, 2005). Subsequently, the x and y co-ordinates of the muscle and disc centroid were recorded. Sagittal plane moment arms were determined as the distance between the intervertebral disc and muscle centroids. A correction was employed to adjust for the fact that the moment arms determined in the upright scans were obtained along a plane aligned with the orientation of the intervertebral disc, whereas previous studies (supine position) obtained the moment arms from transverse scans. It was found that the moment arms were largest at the upper and lower regions of the lumbar spine and shortest in the middle (Jorgensen *et al.*, 2005). Measurements indicated that the moment arms were symmetrical and not different from one another. When compared to the literature, it was found that the upright scanning procedure resulted in moment arms 27.5% longer than those obtained from supine analysis (7.3-43.7%), in strong agreement with the conclusions of McGill et al. (1996a). The resulting percentage differences may be employed in biomechanical models to account for the differences in muscle moment arms due to the supine postures of the participants during measurement (Jorgensen *et al.*, 2005).

Further MRI studies have found that males and females do not differ in lumbar lordosis, regardless of torso flexion angle, when lying on their side (Jorgensen *et al.*, 2003). Although this study was conducted to determine the effects of changing trunk angle on erector spinae moment arms, it also investigated these effects across genders. While females were again shown to display shorter moment arms, the moment arms of both males and females decreased with flexion from 0 to 45^0, with decreases of 8.9% and 9.7% for males and females at the L5/S1 level respectively (Jorgensen *et al.*, 2003). At the L4/L5 level, the difference in moment arm for the male erector spinae was 2.8 mm

(5.2%) and for females was 2.1 mm (3.6%). This study was also able to provide some of the strongest predictive equations for estimating sagittal plane moment arms of both males and females based on anthropometric measures (R^2 at L5/S1 of 0.76) (Jorgensen *et al.*, 2003).

Model Summary as Implemented in this thesis:

The model contains 10 muscle vectors that each originate at the L5/S1 level and insert at a higher level (T12 for this work). The origin of all muscle co-ordinates is taken at the center of the L5/S1 disc. The insertion points at the T12 level are rotated based upon the spine angles obtained from the LMM. As the LMM is mounted to the sacrum the assumption is made that it is measuring relative rotation of the T12 level relative to L5, so global rotations of both the origin and insertion co-ordinates prior to relative rotation is not necessary. Once rotated, the muscle force for each of the 10 muscles was predicted based upon the equation:

$$Force = Gain \times area \times \frac{EMG}{EMG_{\max}} \times f(length) \times f(velocity) \qquad \textbf{(2-5)}$$

EMG_{max} – muscle activation recorded during maximum voluntary contraction

Area – cross-sectional area of the muscle

$f(length)$ – Force-length modulation factor, calculated as (Granata and Marras, 1995a):

$$f(length) = -3.2 + 10.2(length) - 10.4(length)^2 + 4.6(length)^3 \qquad \textbf{(2-1)}$$

$f(velocity)$ - Force-velocity modulation factor, calculated as (Granata and Marras, 1995a):

$$f(velocity) = 1.2 - 0.99(velocity) + 0.72(velocity)^2 \qquad \textbf{(2-2)}$$

2.4 Artificial Neural Networks in Biomechanics

Artificial Neural Networks (ANN) are mathematical models designed to reflect the biological nervous system, being composed of 'neurons/units' and interconnected pathways. The unique property of ANNs that makes their application to biological systems promising is that they can 'learn' to map a set of inputs onto a set of outputs through adaptation of their structure. ANNs are composed of an input layer, an output layer, and one or more hidden layers, where the hidden units are contained (figure 2-7).

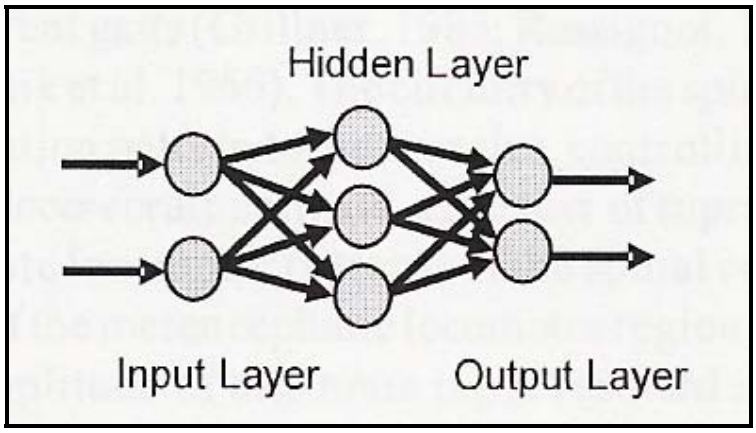

Figure 2-7: Schematic representation of an artificial neural network, taken from Prentice and Patla (2006).

These hidden units can be thought to act like a principal component analysis, where waveform features are characterized and subsequently used to recreate individual signals (Prentice *et al.*, 1998). To train the network, a series of inputs (with known outputs) are presented and based on initial network weights, an output prediction is obtained. This output is compared to the known output of the presented input, and if the error is sufficiently low training is terminated (figure 2-8). If not, the process is repeated, whereby the network weights are adjusted (or the number of hidden units is changed) and a new network prediction is obtained.

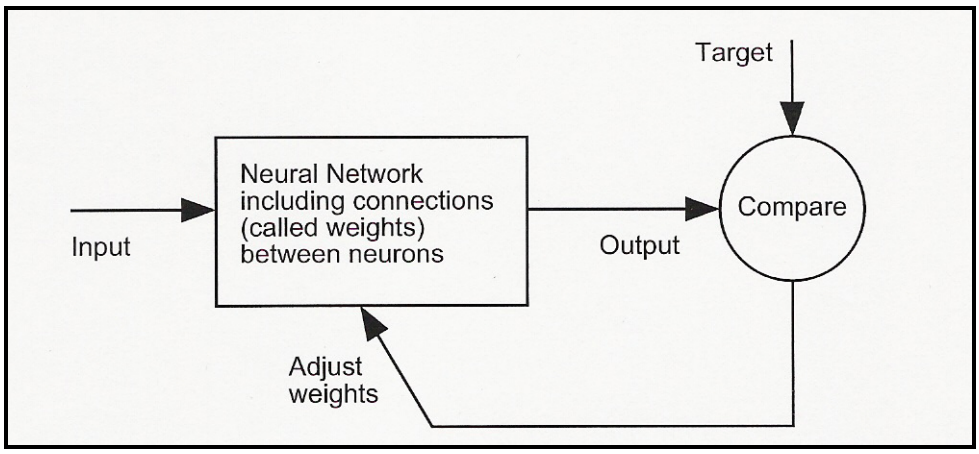

Figure 2-8: Schematic representation of the training process, indicating the feedback of error resulting in changes to the network. Figure taken from the Matlab Neural Network Toolbox User's Guide (Demuth *et al.*, 2006).

The training generated weights are then applied to new input signals as they move into the hidden layer and through the network to result in a novel output. The benefit of this modeling approach is that complex relationships can be represented with relatively simple model architecture (Prentice and Patla, 2006). These properties have been exploited by in several biomechanical studies for a large variety of reasons, ranging from classification of signals to modeling muscle activation dynamics. A summary of these studies is presented in table 2-1. Given the history of ANN use in biomechanics as well as the success of the models in accurately reproducing biomechanical relationships, it appears that the numerical technique may provide a means to obtain laboratory quality estimates of joint moments and forces with data that can be obtained in industry. Additionally, the variety of network architectures that can be developed may provide a means to allow neural networks to produce these predictions with a lower number of inputs than more complex models without the need for the explicit definition and development of a complex numerical model of the relationships between the reduced inputs and the target outputs.

Table 2-1: Summary of neural network applications in biomechanics.

MAPPING EMG SIGNALS TO JOINT MOMENTS						
Authors	*Inputs*	*Hidden Layer*	*Outputs*	*Training*	*Performance*	*Specifics*
Song and Tong (2005)	EMG: Biceps brachii, medial triceps brachii and brachioradialis Elbow angle and angular velocity	One layer Varied the number of nodes until a minimum error was found in terms of both training and test data	Elbow torque	Levenberg-Marquardt algorithm for back propagation training Terminated when sum of squared errors changes <0.5% over 50 iterations	RMS differences of 5.96% for full model, 12.42% for EMG input only	Output torque was used as a recurrent input Signals normalized between 0.1 and 0.9 Tested full model and model with only EMG inputs
Luh et al. (1999)	EMG: Biceps brachii and lateral triceps brachii Elbow joint angle and velocity	One layer No reduction in error of estimation with an increase in the number of nodes from 5 to 20	Elbow torque	Maximum 60,000 iterations Used a dynamic learning rate algorithm	Average r of 0.9, with average RMS difference of 0.1413	Signals normalized between 0.1 and 0.9
Uchiyama et al. (1998)	7 channels collected from shoulder and arm Elbow and joint angles	One layer 5 to 15 hidden units, no improvement in learning speed with greater than 10	Elbow torque	Based on ensemble average data Errors summed from all training data Training terminated when error of estimation < 0.01%	Not provided	Used to allow understanding of EMG and joint torque throughout a range of joint angles while allowing the input of constant muscular activation
Sepulveda et al. (1993)	EMG of 16 muscles	1 hidden layer, 32 hidden units	Angle and moment at the hip, knee and ankle through the gait cycle	Used data from another source for training A tolerance of 0.025 was used for EMG to joint angle	Perturbations to the training data of ± 20% resulted in differences in predicted outputs (joint angle and moment) of <	Looked at both EMG to joint moment and EMG to joint angle relationships All signals normalized

				mapping	7%	Looked at perturbations to the input signals used for training to generate the test data

MAPPING JOINT MOMENTS TO MUSCULAR ACTIVATION						
Authors	*Inputs*	*Hidden Layer*	*Outputs*	*Training*	*Performance*	*Specifics*
Nussbaum and Chaffin (1996)	Flexion, extension and right and left lateral bend moments measured about L3/L4	Tested 3 and 8 hidden unit models	Activation of the erector spinae, latissimus dorsi, rectus abdominus and external obliques bilaterally	15 of 60 load-position combinations were used for training	Assessed correctly 75% of the active muscle states Predicted activation levels with an error less than 0.63% for the 45 remaining load-position combinations Latissimus dorsi showed poor correlation values Correlations for the remaining muscles ranged from 0.87 to 0.98 Model predicted ↓ EMG levels at extrapolated larger moment applications	Assessed the model performance with external data sets as well as that collected for development and testing of the ANN ANN showed good agreement with optimization

Nussbaum et al. (1995)	Same as above	Tested a range of hidden unit numbers There was no improvement in the number of training cycles with >5 hidden units	Same as above	Training was found to be able to reduce the errors of estimation below 1%, however the threshold used for termination was not stated	Majority of errors were <6% ANNs with >3 hidden units showed higher correlations with measured levels than optimization Errors of estimation with ANN were <2.1%, compared to 5.3 and 3.4% for the optimization methods ANN predicted co-contraction	Compared results to that of optimization models
Lee et al. (2003)	Linguistic descriptors of trunk lateral moment	None – 2 layer network	Fuzzy rules regarding the activation level of 10 trunk muscles (same as above + internal obliques)	Not provided	Hybrid approach resulted in lower errors of estimation (6.4%) than reported for ANN alone Lower correlations (r^2 of 0.59) were found for hybrid approach than ANN alone (r^2 of 0.95)	Hybrid ANN and fuzzy modeling approach ANN was used to generate fuzzy rules
Nussbaum et al. (1997)	External moments about each of the anatomical axes	Two layers The second layer had 10 nodes, to mimic the 10 muscles of the torso (see above)	Internal moments about each of the anatomical axes	Training was conducted until the error in moment estimation was reduced below 3 Nm about each axis Used a back	ANN predicted joint moments with a standard error less than 1.66 Nm and correlation coefficient of 0.99 Model over predicted	The idea behind this ANN was to actually use the output of the second hidden layer to represent the contribution of each muscle to the moment about each axis

				propagation algorithm This technique can get stalled in local minima, but these occurrences were not analyzed	activation levels when activation was low Predicted activation levels well at higher levels Latissimus dorsi predictions were poorly correlated with measured levels	Used an inhibitory signal within the ANN

ANNs AS ALTERNATIVES TO OTHER MODELS						
Authors	*Inputs*	*Hidden Layer*	*Outputs*	*Training*	*Performance*	*Specifics*
Rosen et al. (1999)	EMG: Biceps brachii, triceps brachii (medial and lateral head), brachioradialis Elbow angle, angular velocity and shoulder angle	1 hidden layer Tested 100, 50 and 25 hidden unit configurations	Elbow moment	200,000 iterations	Hill-based muscle model resulted in an average error of 4.2 Nm, compared to 0.012 Nm with the ANN	Compared performance of the ANN to a Hill-type muscle model
Kingma et al. (2001)	EMG from erector spinae at T10 and L3 levels bilaterally Trunk tilt angle, angular velocity and linear accelerations of the trunk	Not provided	L5/S1 moment	Split data collected during repeated trunk motion into training and validation sets, but details of success not provided	EMG peak moment predictions exceeded those from the rigid link model by 25.5% ANN peak estimates were 17.3% lower than those of the rigid link model r^2 of 0.656 between the EMG and rigid link models, 0.744 between the ANN and	Compared a rigid link model, EMG estimation technique and ANN Lifting exertions

					rigid link model ANN predictions were the most repeatable	

MAPPING EMG TO KINEMATICS						
Authors	*Inputs*	*Hidden Layer*	*Outputs*	*Training*	*Performance*	*Specifics*
Dipietro et al. (2003)	EMG: pectoralis major, anterior and posterior deltoid, biceps and triceps brachii	1 hidden layer with 2 units	X and y co-ordinate trajectories of the wrist	Completed after 1,000,000 iterations Trained separately for each subject Used a validation set of data presented every 500 iteration to determine training effects	Average RMS difference of 0.092 units, or 9.2%	Recurrent back propagation approach to deal with time varying inputs and outputs Trials were not normalized in time
Koike and Kawato (1995)	Raw EMG input, signals from different muscles dependent upon joint were input to first layer (10 upper limb muscles collected) The second layer accepted the outputs of the first layer as well as joint angle and angular velocity	One hidden layer	Joint torque	Model was first trained to obtain the desired impulse response to describe the quasi-tension of the muscle using 10,000 data points Subsequent training was performed using both static and dynamic trials Training was continued until the error in the test data increased	Dynamic torque predicted with an r^2 of 0.887 Trajectory predicted with an r^2 of 0.948	Used a modular network, with different sections responsible for posture and movement Method also employed a gating network

MAPPING KINEMATICS TO EMG						
Authors	*Inputs*	*Hidden Layer*	*Outputs*	*Training*	*Performance*	*Specifics*
Prentice et al. (2001)	Horizontal and vertical displacement of hip and toe Sagittal hip and knee angles, frontal hip angle Velocity of all displacement inputs	1 hidden layer with 14 hidden units	Activation of medial gastrocnemius, soleus, tibialis anterior, peroneus longus, biceps femoris, rectus femoris, gluteus medius, erector spinae	Data was intentionally separated so that the trials remaining for model testing would assess both ANN interpolation and extrapolation Training was conducted until no further ↓ in error was observed	94 of 96 trials had RMS differences <0.10 units. 61% of trials showed r^2 >0.90, 94% > 0.80	Based on 1 subject, with variations in gait parameters (cadence, stride length, stance width, foot clearance) All signals normalized in amplitude and time
Prentice et al. (1998)	Temporal stride information (stride rate) represented with sinusoidal waves	1 hidden layer Tested the use of 16, 4, 2, or 1 hidden units	Muscle activation	Data was intentionally separated so that the trials remaining for model testing would assess both ANN interpolation and extrapolation Training was conducted until no further ↓ in error was observed	RMS difference < 20% for 83% of cases r^2 ranged from 0.1 to 0.9 The use of a higher number of hidden units resulted in better representation of the more subtle variations	Broke stride information into sine and cosine waves to use with ANN
Hou et al. (2004b)	Trunk kinematics (angle, velocity and acceleration) Trunk moments (about the anatomical axes) Participant anthropometrics Timing variable	2 hidden layers Subject variables were directly input into the 2nd hidden layer to give them higher importance 200 global hidden units,	Activation of 10 trunk muscles	Training was initially slow when data was input on a point by point basis, moved to a vector approach	Mean average error of prediction ranged from 0.9 to 11.1%	Authors employed a timing variable to avoid what they termed a "static model"

		35 regional				
Karwowski et al. (2006)	Fuzzy inputs Trunk moments about all three anatomical axes Pelvic tilt and rotation Sagittal, lateral and axial trunk angles	Not provided, although the hybrid model does not function in a purely ANN sense	Activation of 10 trunk muscles	Data from 10 subjects was used for training while data from an additional 10 subjects was used for testing	Errors of estimation were shown to range from 2.5-27.5%, with an average of 9.9%	Used a multiple input single output model (MISO), so created 10 ANNs Used a hybrid approach employing Fuzzification and an ANN

MAPPING EMG TO MUSCLE AND JOINT FORCES						
Authors	*Inputs*	*Hidden Layer*	*Outputs*	*Training*	*Performance*	*Specifics*
Liu et al. (1999)	Varied from 20 to 30 20 EMG inputs (20 points prior to point of interest) 10 kinematic data points (the 5 joint angles and velocities prior to the point of interest)	2 hidden layers, the first contained 20 hidden units, the second 10	Muscle force (soleus)	Looked at the inclusion of non-specific trials within the training and found no benefit Used a threshold error level, but did not report Reported to train network in 600 – 1000 iterations	Inter-animal testing revealed the model predicted muscle force with an $r > 0.9$ and RMS error < 15%. Inclusion of kinematic data did not improve estimates of force for inter-subject predictions Intra-animal predictions were found to result in r values ranging from 0.66 to 0.94, dependent upon speed Intra-session predictions showed r values ranging from 0.96 to 0.98 with an RMS error < 8%	Feline model Attempting to predict relationship between EMG and dynamic muscle force Muscles forces recorded with an implantable transducer

Hou et al. (2005)	Kinematics (trunk moment, angle, velocity and acceleration about all three axes) Subject anthropometrics Task variables (weight of object, lifting height, handedness and lifting style) EMG signals are an intermediate output and are fed back into the model as an input (10 trunk muscles)	1 hidden layer with 35 hidden units	Lateral shear, anterior-posterior shear and compression 10 trunk muscle activation levels	Not reported	Assessed through comparison to a biomechanical model Qualitatively comparisons showed some increase in error for nonsymmetrical motions Mean absolute errors ranged from 22.2 to 201.1 N	Recurrent hybrid neuro-fuzzy approach Incorporated kinematic-EMG and EMG-joint force relationships Normalized signals
Wang and Buchanan (2002)	Normalized EMG from 10 upper limb muscles	2 hidden layers, each with 15 hidden units	Muscle activation of the 10 muscles	Joint moment was used as the training comparator as muscle activation cannot be measured Data from one exertion level (75% of maximal exertion) was used for training Training error decreased below 3% after 1000 cycles and < 1.5% after 3000 cycles. Error was reduced to < 0.8% if training was continued to	Model predicted joint moments within 8.3% When examined at a lower exertion level than used in training, moments were predicted within 4.9% When used to predict joint moments for maximal contractions, the average relative error reached 34.2% ANN was shown to exhibit a 0.3-0.4 unit bias when EMG was zero	Believed previous efforts linking EMG directly to force ignored the explicit statement of some known relationships (such as force-velocity) Looked at using ANN to model activation dynamics and combining these activations with a Hill-type muscle model

				10,000 cycles		

USING ANNs AS CLASSIFICATION TOOLS						
Authors	*Inputs*	*Hidden Layer*	*Outputs*	*Training*	*Performance*	*Specifics*
Zurada et al. (1997)	Lift rate Peak twist velocity Peak moment Peak sagittal angle Peak lateral bend velocity	1 hidden layer with 10 hidden units	0 or 1, depending on low or high risk classification	148 jobs were used as the training data set (74 low risk and 74 high risk)	Classified 65 of 87 cases correctly 14 of 50 low risk jobs were classified incorrectly 8 of 37 high risk jobs were incorrectly classified This performance was better than that of either NIOSH equation	Looked at ANN as a tool to classify jobs in terms of potential to develop low back pain Signals normalized
Bishop et al. (1997)	Questionnaire data Spine motion trial information (velocity, shape and symmetry)	Not provided	Group (pain or no pain) Pain type	Not provided	Accurately distinguished between pain and no pain in 86% of cases Successfully classified 72% of the pain cases	Used 2 networks cascaded together Sort people first according to pain reporting and then classify those who report pain Used a radial basis function network
Kelly et al. (1991)	Power spectra density data of each muscle were used as inputs	Tested one and two hidden layer networks 2 hidden layer network had 8 hidden units Single layer network	Effort direction (flexion, extension, pronation and supination)	Training was terminated when a stable minimum error occurred	ANN was able to correctly identify contraction types 67 - 93% of the time Improved these results by having network	Classifying EMG signals to allow for control of a prosthesis

		functioned better in terms of accuracy and speed of training			function on pairs of data (correct classification in 71-95% of cases)	

USING ANNs TO AVOID OPTIMIZATION RELATED PROBLEMS						
Authors	*Inputs*	*Hidden Layer*	*Outputs*	*Training*	*Performance*	*Specifics*
Zatsiorsky et al. (2002)	Central neural drive	Some of the inputs passed straight through to the outputs to represent those muscles with connections to only one digit Muscles which connect to several fingers passed through the hidden layer 1 hidden layer	Finger forces	Back propagation algorithm, satisfactory results were obtained after 500 iterations Trained in several ways: 1. No validation data, all 15 sets used for training 2. 1 of 15 sets used as a validation set 3. Selective training using select data sets	Finger force production was estimated with a RMS error of 2.3 N Error in force estimation ↓ from 3.18 to 0.57 N when the number of fingers involved ↑ from 1 to 4	Looked at model as a way to predict neural input to the muscles of the hand Investigated the ceiling effect, where force production is less with multi-finger recruitment Also looked at enslaving effects Optimization approaches did not predict co-contraction

2.5 In-vitro Spine Testing

The following brief overview of in-vitro spine testing will highlight some of the relevant studies as they have progressed from acute load applications through to more complex, physiologic loading paradigms. This information is provided for the reader who may be interested in how some of the methods used in chapters 6 and 7 have been developed through past research.

2.5.1 Acute Loading

In order to understand the compressive properties of the spine and its constituent tissues, researchers have used axial compression of isolated vertebrae, vertebrae with adjacent intervertebral disc material, or spinal units (intervertebral disc and passive structures with the adjacent vertebrae). Acute compressive tests have been performed to investigate vertebral body compressive failure as caused by a singular load application (Roaf, 1960; Rockoff *et al.*, 1969; Hutton *et al.*, 1979; Hansson *et al.*, 1980; Hansson and Roos, 1983; Callaghan and McGill, 1995; Edmondston *et al.*, 1997; Thomsen *et al.*, 2002). In these experiments, including those where the intervertebral disc was present (in whole or in part), failure occurred in the vertebrae. Vertebral failures in experiments that have included intervertebral discs or disc material have revealed that the vertebrae are the weakest component of a spinal unit exposed to compression. Rockoff *et al*. (1969) performed preliminary experiments testing the compressive strength of the vertebral body and the intervertebral disc, concluding that the peak compressive strength of the intervertebral disc was in excess of the vertebral body strength.

The vertebral body is capped inferiorly and superiorly by cartilaginous endplates, which provide separation from the intervertebral disc (Genaidy *et al.*, 1993). The vertebral body is composed of a thin shell of cortical bone, which surrounds a cylindrical core of cancellous bone (Genaidy *et al.*, 1993). The cancellous (trabecular) bone is formed by relatively long trabeculae

connected by shorter transversely oriented bony elements (Fyhrie and Schaffler, 1994). Microstructure examination has shown that it is the transversely oriented components that fracture first, whereas the primary weight bearing trabeculae appear to accumulate microscopic matrix damage prior to buckling (Fyhrie and Schaffler, 1994). Upon buckling, vertebrae can exhibit multiple fracture patterns, including: stellate, step-like, endplate, transverse, edge, and Y-fractures, as well as disc intrusion (figure 2.1). More recent work has added another classification, denoted 'crack and defined by a single crack that ran across the endplate, without the height change that defines a step fracture (Parkinson and Callaghan, 2007b).

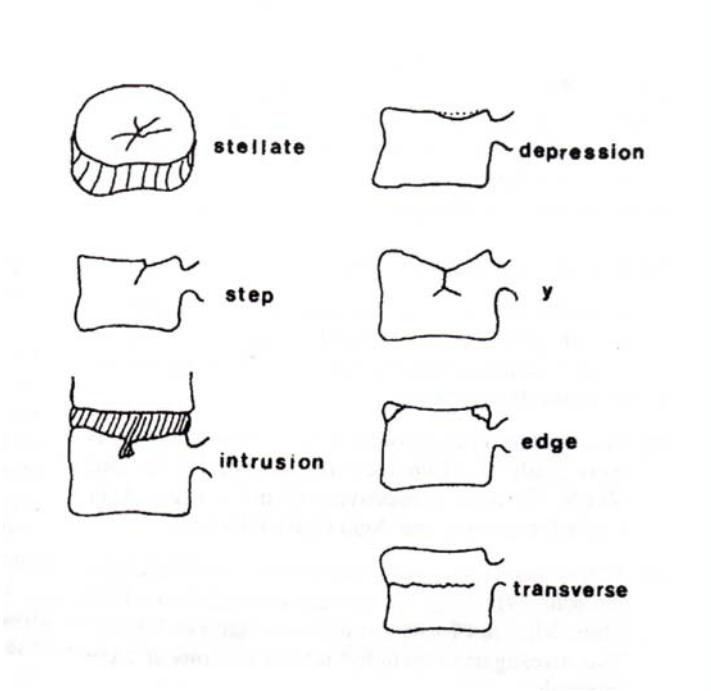

Figure 2-9: Fracture classifications as defined by Brinckmann *et al*. (1988), pg S11).

2.6 Cyclic Loading

2.6.1 Bone

The behavior of bone when exposed to cyclic loading has been the subject of much study. Carter and Caler (1983) obtained a non-linear relationship between strain range and cycles to failure in machined sections of cadaveric femoral bone during tensile and fully reversed testing protocols. The same research group (Caler and Carter, 1989) later tested machined femoral samples in compressive cyclic loading and found the relationship between normalized stress range (stress range/elastic modulus) and cycles to failure to be non-linear. From this data, Caler and Carter (1989) were able to conclude that the time to failure in compressive testing can be predicted by the accumulation of cycle dependent damage. The non-linear relationship between stress and cycles to failure was also exhibited in the work of Choi and Goldstein (1992), Michel *et al*. (1993), Bowman *et al*. (1998), and Ziopous and Casinos (1998). The behavior of trabecular bone in fatigue testing has been further quantified by Michel *et al*. (1993), who investigated changes in secant modulus (stiffness) in bovine trabecular bone exposed to fatigue testing. Interestingly, two distinctly different behavior patterns arose. In high cycle fatigue (lower strain – 1%) the bone samples showed an initial increase in modulus, whereas samples exposed to low cycle fatigue (higher strain – 2.1%) showed an immediate decrease (Michel *et al.*, 1993). The decrease in secant modulus has been confirmed in more recent studies of machined bone samples (Pattin *et al.*, 1996; Bowman *et al.*, 1998; Moore and Gibson, 2003b). However, more recently the increase in secant modulus (although attributed to end effects by the authors) has been reflected by an increase in stiffness of whole vertebrae exposed to repetitive cyclic compression (Lu *et al.*, 2004).

Bone samples have been characterized by an abrupt drop in modulus prior to failure (Michel *et al.*, 1993), also demonstrated in the work of Moore and Gibson (2003b). In addition, microscopic examination has revealed two distinct methods of fracture. Brittle-like fractures resulted in a fracture

with no identifiable buckling or buckling-like failure, which involved splitting and buckling of the trabeculae (Michel *et al.*, 1993). The fracture types were found to be related to the direction of loading, with brittle fractures occurring in trabeculae transverse to the direction of the load, and buckling-like failures occurring predominantly parallel or oblique to the loading axis (Michel *et al.*, 1993). Quantification of fracture behavior in bovine cortical bone exposed to cyclic loading has revealed that microcracks accumulate rapidly during the first 10,000 cycles, with a reduction in accumulation rate occurring until 50,000 cycles were reached (O'Brien *et al.*, 2003). After 50,000 cycles, crack accumulation occurred rapidly until failure. In addition, the propagation of microcracks was measured and found to occur in 8% of all cracks (O'Brien *et al.*, 2003). Stating that 92% of cracks do not propagate may be an over estimation, as the machining technique used to section the sample can lead to classification of a propagating crack in two staining stages, resulting in the incorrect assumption that they are individual cracks (O'Brien *et al.*, 2003). The use of multiple staining agents indicates that crack propagation only occurred from one end of the microcrack (O'Brien *et al.*, 2003). The propagation of the microcracks appears to be limited by the location of osteons and cement lines, as there are a low number of cracks within the osteons until 50,000 cycles are surpassed, at which time there is a large increase (O'Brien *et al.*, 2003). The accumulation of microfractures has also been shown in trabecular bone, when whole vertebrae were exposed to cyclic compression (Lu *et al.*, 2004). Microfractures were shown to increase in number when the applied cyclic load magnitude was increased (Lu *et al.*, 2004). The appearance of microcracks has been shown to correlate with a decrease in stiffness, with a stiffness loss of greater than 15% often indicating extensive damage (Burr *et al.*, 1998). As with many mechanical relationships of bone, the relationship between crack density and stiffness is non-linear (Burr *et al.*, 1998). While microfractures and microcracks have been treated as a tissue failure, there is also evidence that they may serve a role in protecting the bone from further damage. Sobelman *et al*. (2004) found that

cadaveric femoral bone samples with higher initial crack densities withstood a greater number of loading cycles prior to failure.

In addition to damage accumulating from the cyclically applied loads, it appears that creep may contribute to damage in fatigue testing. Cotton *et al*. (2003) demonstrated that permanent strain occurs during cyclic testing, and linked this accumulation to behavior observed in creep tests performed by several other researchers. Bowman *et al*. (1998) concluded that time to failure was also significantly related to stress range with a power law relationship, and that creep loading can lead to reductions in residual bone strength. Additionally, the authors indicated that early in fatigue testing, damage due to creep was a greater contributor to overall damage than damage/crack growth (Bowman *et al.*, 1998). As fatigue testing continues, the contribution of creep damage diminishes, but remains important throughout (Bowman *et al.*, 1998). These findings reinforce the statement of Carter and Caler (1985), who concluded that testing with a non-zero mean stress will include both creep and cycle dependent damage. The mathematical characterization of the creep-fatigue damage interaction performed by Carter and Caler (1985) is in agreement with the data of Bowman *et al*. (1998) which indicates a greater contribution of creep damage at low cycle numbers. However, recent work (Moore *et al.*, 2004) has argued against creep as a contributor to fatigue behavior as the predicted contributions of fatigue to the strain behavior of the bone samples was negligible in comparison to the actual strain behavior.

Although there is much evidence for damage due to fatigue loading, there exists a threshold level (endurance limit) below which there will be no observable change in the structural or mechanical properties of bone (Moore and Gibson, 2003b; Moore and Gibson, 2003a). Moore and Gibson (2003b), through extrapolation of their results, found a threshold level of 0.5% strain in compressive tests of bovine trabecular bone, below which they did not observe any changes in the mechanical properties of machined sections. Some microscopic damage was noted in control

specimens and those exposed to preload conditions only, however the damage was external and attributed to specimen preparation (Moore and Gibson, 2003a). Very little observable damage was found to occur until a yield strain of 0.8% was reached, and extrapolation of the results confirmed the threshold strain of 0.5% found in the mechanical testing (Moore and Gibson, 2003b). The results of Moore and Gibson (2003a; 2003b) support the earlier suggestion of Pattin *et al*. (1996) of a threshold (4000 microstrain) for mechanical property changes in cyclic compressive testing of bone.

The role of stress history or previous loading on the fatigue behavior of bone has been studied by Zioupos and Casinos (1998). The authors employed a two step loading protocol, with specimens being first cycled at a low or high stress level, followed by cycling at the opposite stress level until failure. It was demonstrated that the fatigue damage accumulation is affected by the initial stress level, the difference between applied stress levels, and the amount of damage caused in the first loading scenario (Zioupos and Casinos, 1998).

2.6.2 Spinal Units

The mechanical behavior of the intervertebral disc and vertebrae exposed to sub-failure cyclic loading has been investigated by several researchers. The intervertebral disc exposed to cyclic compression undergoes many changes. Geometric changes include a decrease in nucleus pulposus height and nucleus pulposus anterior-posterior length, an increase in anterior and posterior longitudinal ligament bulge, and an overall decrease in intervertebral disc thickness (Yu *et al.*, 2003). Cyclic loading has also been shown to result in dehydration, buckling of the annulus fibrosus, and bleeding (Yu *et al.*, 2003). *In vivo* porcine spinal units exposed to cyclic loading (50 N peak load at 5 Hz and 100N peak load at 5 Hz, separated by one hour of rest) responded with an initial rapid increase in displacement, followed by a stable, much less rapid constant increase (Ekstrom *et al.*, 1996). A similar study was able to show that the intervertebral disc will respond to loading at higher frequencies with increasing stiffness up to 20 Hz (a further increase in cyclic frequency to 25 Hz lead

to a decrease in stiffness, attributed to resonance) (Kaigle *et al.*, 1998). Additionally, the intervertebral discs exposed to several loading periods showed an increase in stiffness after the first load set, despite rest intervals between loading periods (Kaigle *et al.*, 1998). This observation is in agreement with the findings of Johannessen *et al*. (2004) who found that cyclic loading increased the stiffness of ovine spinal units *in vitro*. An increase in joint stiffness after cyclic loading has also been demonstrated in an *in vivo* murine model once tension develops, which occurs at greater angles due to an increase in joint laxity (Ching *et al.*, 2003).

Few authors (Liu *et al.*, 1983; Hansson *et al.*, 1987; Brinckmann *et al.*, 1988; Holmes and Hukins, 1994) have looked at the effects of cyclic axial compressive loads on the fatigue failure of spinal units. Holmes and Hukins (1994) tested the intervertebral disc with adjacent endplates under cyclic compressive loading to a peak of 1.9 kN. It was observed that displacement was small during the initial stages of testing, but increased rapidly until the cutoff value of 1.5 mm of endplate displacement was reached. Liu *et al*. (1983) tested specimens up to 10,000 cycles, but failed to report the cycle number where failure had occurred. The authors found two different responding groups, those that showed a stable increase in displacement, and those that responded abruptly. Radiographic examination after cyclic testing revealed that specimens showing an abrupt response had undergone subchondral bony failure within the vertebrae (Liu *et al.*, 1983). Failure in the cancellous bone was also responsible for the vertebral failure observed in the fatigue tests of Hansson *et al*. (1987). Loads ranging from 60 to 100 % of the estimated compressive strength of the spinal units were applied using a sine wave function until failure or 1000 cycles, resulting in the failure of 16 out of 17 specimens (Hansson *et al.*, 1987). In a more recent fatigue study, Brinckmann *et al*. (Brinckmann *et al.*, 1988) applied cyclic loads using a triangular function up to a maximum of 5005 cycles. Failure occurred prior to the cycle limit in 52 of the 70 spinal segments subjected to the fatigue tests. As with earlier fatigue studies, specimen failure occurred within the endplate or body of the vertebrae (Brinckmann

et al., 1988). More recently, Parkinson and Callaghan exposed porcine cervical spinal units to dynamic repetitive compression at normalized compressive loads of 40, 50, 70 and 90% and have shown there to be a highly non-linear relationship between the peak compressive load magnitude and the cumulative load tolerated to failure (Parkinson and Callaghan, 2007b). As the load magnitude increases, there is a disproportionate decrease in the ability to withstand cyclic loading, a relationship that should be considered when assessing injury risk.

2.6.3 The Role of Posture

The effects of postural change have progressed through time from the initial studies examining the effects static postures have on compressive tolerance to those which have examined dynamic loading profiles and their impact on injury development. In 1982, Adam and Hutton were able to demonstrate that flexion exceeding the normal range of motion in combination with compression was able to induce prolapsed intervertebral discs. Work examining the injury mechanisms with the spine in less extreme flexed postures found that the porcine cervical spine is able to tolerate 23-47% less compression than when in a neutral posture, dependent upon the prior loading history or hydration state (Gunning *et al.*, 2001).

While these studies are examples of how posture can affect injury behaviour in acute situations, loading is experienced dynamically so knowledge of how the spine responds during cyclic loading is critical. Gallagher et al. (2005) have shown that if the spine is statically flexed and then repetitively compressed, specimens in neutral postures are able to tolerate a far greater number of cycles to failure for equivalent loading exposures (8253±2895 cycles to failure for neutral posture, 3257±4443 cycles to failure for moderate flexion and 263±646 cycles to failure for the greatest amount of flexion). While this work illustrates that the neutral posture may allow for the greatest load tolerance, the postures applied were static and did not reflect those that someone would

experience in normal activities of daily living. Adams and Hutton (1985), through the application of dynamic compression and passive postural changes were able to show that disc herniation may result when the spine is exposed to combined compression and flexion. In order to isolate the effects of flexion, Callaghan and McGill (2001) exposed porcine cervical spinal units to repetitive flexion under low level static compressive loads and found that with high cycle numbers disc herniations were consistently observed, directly implicating dynamic, repetitive flexion motion as a major contributor to disc injury.

Chapter 3
Methodological Considerations

The following subsections provide some further insight into the methods adopted in the following chapters. It is the goal of this chapter to provide the reader with more detailed insight into the steps taken to arrive at some of the key assumptions and procedures underlying the work contained within this thesis.

3.1 Adjustments to the EMG-assisted Model

3.1.1 Force-velocity approach

While it is often cited that an eccentric cap be employed (a maximum force-velocity factor of 1.5 based upon Marras and Granata (1997a)) when muscles are producing force while lengthening, comparison of correlations indicated better agreement with no eccentric cap (table 3-1). As the purpose of the model was to best represent the loading the spine is exposed to (as compared to the predictions of net joint moments) it was felt that which ever method provided the highest agreement was the most reasonable. Application of this approach allowed force-length factors during eccentric contractions to reach values exceeding three.

Table 3-1: Correlations (r^2) between predicted muscle moments and reaction moments for sagittal lifting trials in which an eccentric maximum was not applied and those in which it was.

Subject	Without Eccentric Maximum	With Eccentric Maximum
Female 1, session 1	0.8328	0.6792
Female 1, session 2	0.8162	0.5571
Male 1, session 1	0.7977	0.8643
Male 1, session 2	0.8222	0.829
Male 2, session 1	0.7629	0.5889
Male 2, session 2	0.8052	0.5825
Female 2, session 1	0.8340	0.7182
Female 2, session 1	0.8139	0.665

3.1.2 Gain Factor Determination

In order to complete the force prediction, a gain factor must be obtained. In equation 2-5, it is assumed that the gain factor represents variation in maximum muscle stress. However, as it is a multiplier it can theoretically account for discrepancies across any of the modulators, as it is determined to ensure that a sum of all modeled muscle forces balance the external or net joint moment. For this work only the sagittal moment was used in determining the gain value. In all sessions, participants completed a floor to waist lift and lower, which was used to determine the gain value for all lifts and lowers completed during that session. No attempt was made to gain the model on a point by point basis, rather to provide the best amplitude fit for the entire gain trial.

In order to determine if this provided the best estimate of the gain value, several participants were chosen at random and multiple trials were analyzed to determine the gain value. It was found that in general the sagittal lift provided the highest correlations between the predicted muscle moments and reaction moments obtained through inverse dynamics, so it was decided to apply this approach as a rule

across all participants. Examples of the values obtained with this approach are found in table 3-2. Additionally, the stability of the gain value was examined by having several subjects perform 5 repeats of the calibration lift. The results indicated that the gain predictions were stable (Table 3-3).

Table 3-2: Correlations (r^2) and root mean square errors (RMSE) between the predicted muscle moments and the external reaction moments for one male and one female participant. The gain trial is in bold lettering.

Male				**Female**			
Lift Type	*Gain*	R^2	*RMSE*	*Lift Type*	*Gain*	r^2	*RMSE*
Center waist to shoulder, light	53.03	0.791	11.29	Center floor to shoulder, heavy	10.91	0.421	27.99
Left floor to right shoulder, heavy	37.19	0.778	12.83	Left waist to shoulder, light	39.12	0.586	11.68
Center waist to shoulder, heavy	56.26	0.799	12.18	Left waist to shoulder, light	46.44	0.6347	17.43
Left floor to shoulder, heavy	37.39	0.669	19.91	Center waist to shoulder, light	46.29	0.597	10.76
Sagittal calibration	**50.69**	**0.7595**	**11.17**	**Sagittal calibration**	**9.256**	**0.834**	**17.02**

Table 3-3: Gain value from sagittal calibration trial, for five repeats within a testing session.

Subject 1 Session 1	Subject 1 Session 2	Subject 2 Session 1	Subject 2 Session 2	Subject 3 Session 1	Subject 3 Session 2	Subject 4 Session 1	Subject 4 Session 2	Subject 5 Session 1	Subject 5 Session 2
6.63	5.14	5.21	10.35	24.87	9.83	10.6	14.71	109.50	44.80
6.02	3.51	4.26	7.35	24.86	7.15	10.4	14.34	135.20	37.25
6.20	4.01	4.20	8.09	19.24	7.27	10.9	10.99	107.50	32.54
7.00	4.03	5.06	6.71	14.45	7.23	5.13	12.80	112.70	34.92
7.78	4.10	4.01	6.65	13.05	7.95	9.66	15.40	100.50	31.85

3.1.3 Gender Specific Anatomy and Passive moments:

In order to enhance the biologic fidelity of the model, it was developed to contain two sets of anatomy, one for males and one for females. The moment arms and vector lines of action, while not scalable for each individual, provided the gender specific muscle orientation based upon the MRI work of Jorgensen et al. (2001). In addition, individually scalable muscle cross-sectional areas were obtained from the MRI work of Marras et al. (2001).

To further enhance the physiologic relevance of the model, gender specific passive moments were also included. The passive moments were determined based on the instantaneous position of the spine about all three axes, and were included as restorative moments. The equations for these passive moments were adapted from Dolan et al. (1994) for male and female trunk flexion, while extension, lateral bend and axial twist moments were predicted based upon equations provided in McGill et al. (1994). These equations were applied to the reaction moment as determined with the inverse dynamics approach, and therefore impacted the subsequent gain determination. Examination of the effect of passive moment inclusion on the gain values found that accounting for passive moment contributions resulted in lower gain values, small changes in correlations and decreases in the root mean square error (Table 3-4). One limitation of this approach was that the equations to predict the passive moments when the spine was flexed required that the flexion angle was normalized to a maximum range of motion (Dolan *et al.*, 1994). The experimental setup employed for studies one and two did not allow for maximum range of motion trials to be collected, therefore literature values for maximum ranges of motion (table 3-5) were applied as obtained from Van Herp et al. (2000)

Table 3-4: Gain value, coefficient of determination (r^2) and root mean square error (RMSE) for sagittal calibration trials with and without the inclusion of gender specific passive moments. Percentage differences relative to the predictions with inclusion of passive moments are also included.

	With Passive Moments			**Without Passive Moments**					
Subject	*Gain*	r^2	*RMSE*	*Gain*	*% Difference*	r^2	*% Difference*	*RMSE*	*% Difference*
1, session 1	33.74	0.7943	18.2	50.26	-48.96	0.7707	2.97	28.6	-57.14
1, session 2	53.34	0.7903	15.0	93.14	-74.62	0.7941	-0.48	25.3	-68.67
2, session 1	9.12	0.8320	17.3	12.11	-32.79	0.8320	0	22.6	-30.64
2, session 2	9.32	0.8113	15.7	12.82	-37.55	0.7848	3.27	22.8	-45.22
3, session 1	15.96	0.8081	18.0	22.63	-41.79	0.8598	-6.40	20.6	-14.44
3, session 2	10.30	0.7563	14.0	18.31	-77.77	0.8051	-6.45	20.2	-44.29

Table 3-5: Maximum range of motion values (degrees) taken from Van Herp et al. (2000) for males and females aged 20-29.

Direction	**Male**	**Female**
Flexion	58.9	56.4
Extension	37.0	22.5
Right Lateral Bend	26.3	25.8
Left Lateral Bend	25.1	26.2
Right Axial Twist	18.6	14.4
Left Axial Twist	18.6	12.8

3.1.4 Nodal Points:

Initial work with the model produced extremely large predictions of posterior muscle force when participants were lifting, due to the large amount of spine flexion. It was determined this was due to the straight-line muscle representation vectors developing a line of action much more parallel to the shear axis of the joint when the end range of motion was approached. As there were no physical constraints programmed into the model to ensure that the muscles wrapped around the spine and did not pass through structures in a non-realistic fashion, the muscle lines of action were

assuming non-physiologic directions. In order to correct for this, muscle co-ordinates were taken from Jorgensen et al. (2001) for the latissimus dorsi and erector spinae muscle vectors at the L4 level. Subsequent use of the model employed a proportional rotation of the L4 co-ordinates (21.8% of flexion, 20.7% of lateral bend, and 15.4% of axial twist) to determine the location of the nodal point through which these muscles were constrained to pass. Once employed, these nodal points resulted in more reasonable shear values through the range of postures observed in studies 1 and 2. This indicates that interpretations of shear magnitudes must be made with caution, as they are heavily reliant on the predicted model anatomy.

3.2 Artificial Neural Network Development

Overview:

While the final neural network approach is described in chapter 4, it was felt that the reader of this thesis might benefit from some additional information. Therefore, the following section will briefly highlight some of the steps taken in determining the eventual network configurations as well as present the necessary weighting factors and bias values in order to allow testing and use of the networks external to this work.

The linear transfer function:

As many researchers (Song and Tong, 2005; Luh *et al.*, 1999; Uchiyama *et al.*, 1998; Nussbaum *et al.*, 1995; Nussbaum *et al.*, 1997; Dipietro *et al.*, 2003; Koike and Kawato, 1995; Taha *et al.*, 1997; Liu *et al.*, 1999; Wang and Buchanan, 2002; Rosen *et al.*, 1999) have reported the use of non-linear transfer functions in previous biomechanical neural network applications, this was the first approach employed in network development. However, it was found that the mean square error in

training was higher when employing the non-linear transfer functions (tansig function, Neural Network Toolbox™ (Matlab 7.4.0, The Mathworks, MA, USA)). Further examination of the data indicated that the predicted outputs of the neural network were 'capped' at a maximum value when using this approach (figure 3-1) due to the inherent dictation of maximums when using such a non-linear function. In order to try and work around the limitation associated with a fixed maximum prediction, networks were also developed that had a linear transfer function in the output layer, which followed the non-linear transfer function approach employed in the hidden layer. However, this combination approach did not improve the results as the 'capped' maximum values were still observed.

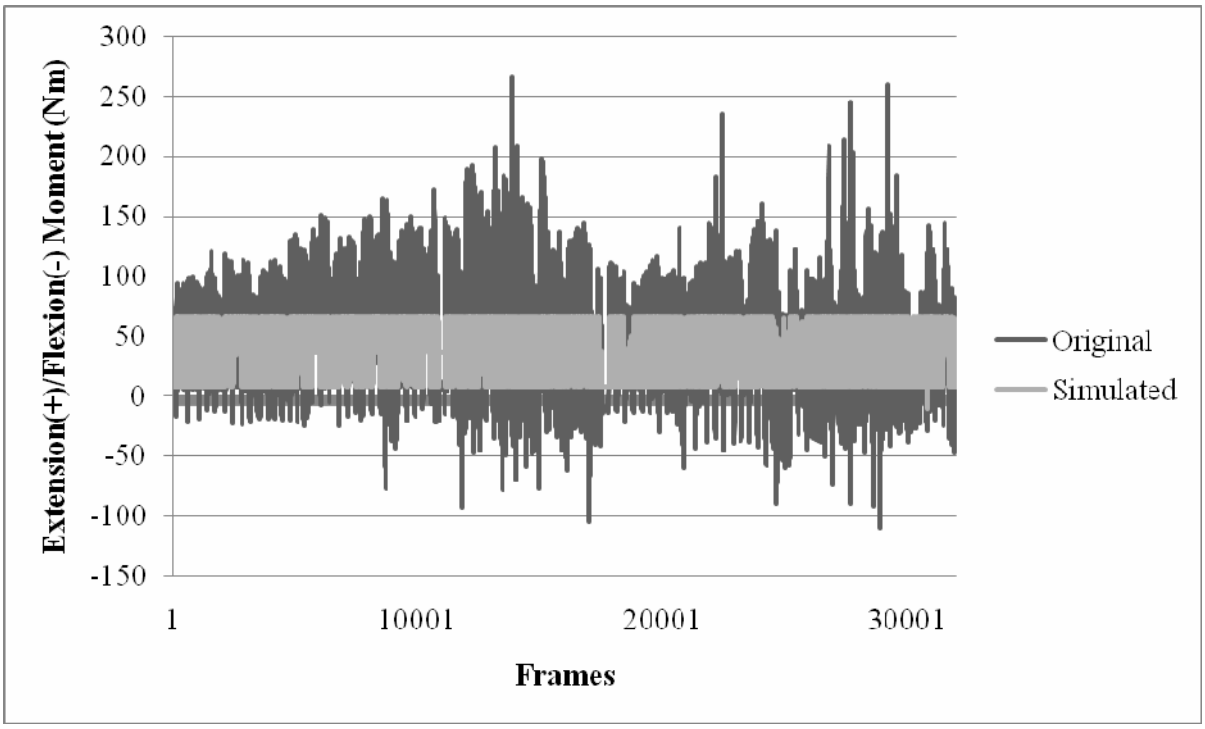

Figure 3-1: Time series of extension (+)/flexion(-) moments (Nm) for all participants downsampled to 8 Hz. Notice that the predictions obtained with the neural network employing a non-linear transfer function (simulated, grey line) have a maximum limit and do not replicate variations in peak moment exposure well relative to the moments determined with an inverse dynamics approach (Original, black line).

Do the networks perform better with all of the time varying inputs?

In order to answer this question, various tests were conducted based upon the neural networks designed to predict the spine loads. First, a network was designed to account for spine angle, spine angular velocity and spine angular acceleration. The training results indicated no improvement over the reduced approach. Second, a network was designed that would employ all channels of EMG along with spine angle and anthropometry (18 total inputs). While the results of including all of the data in training indicated an improvement in the mean squared error, the magnitude of the improvement was not large enough to warrant the necessary additional data collection. Additionally, as the muscle activations of the erector spinae and internal obliques were also correlated with each other (although not strongly) a network was designed to employ only one muscle activation pattern, which may represent all muscles. However, it was found that the training error increased indicating that important information can be obtained by employing the other muscle activations. The mean square error differences from all of the approaches were similar enough that one could argue for the strength of each approach. It was decided to employ the study 1 approach (four channels of EMG). There is inherent value in these EMG channels that can be obtained (fatigue measures, gaps analysis, etc) so if the data can be obtained reasonably it is of value apart from this neural network approach. As four channels of EMG can be obtained with a portable data logger, this method was selected. The training data is summarized in table 3-6. Note that these tests were conducted on data from one participant.

Table 3-6: Root mean square error (RMSE) and epoch number determined during training of the neural network to data from one female. The 5 reduced data approaches from study 1 (approach 1), an approach involving spine velocities and accelerations (approach 2), an approach using all time varying inputs (approach 3) and an approach using only one channel of EMG are included for comparison (right erector spinae is approach 4, left erector spinae is approach 5).

Approach 1		Approach 2		Approach 3		Approach 4		Approach 5	
RMSE	Epoch	RMSE	Epoch	RMSE	Epoch	RMSE	Epoch	RMSE	Epoch
521.2 N	351	469.5 N	851	519.6 N	251	540.5 N	100	550.4 N	226

Can the network be too simple?

While the network architecture presented in this thesis is quite simple, it could be further reduced, perhaps representing the desired relationships with as little as one hidden unit. In order to test the possibility, a network with only one hidden unit was developed and trained with the data from the same participant as the above tests reported in Table 3-6. Again, it was found that this architecture did not greatly alter the mean square error during training (525.9 vs. 521.2 N from table 3-6 above). However, as increasing the number of hidden units is known to improve the generalizing ability of neural networks, it was felt that the limited increase in network complexity associated with employing five hidden units versus one was justified if a better generalizing network was desired (see tables 3-7 and 3-8 for weighting coefficients and biases of the study 1 neural networks). The cost of increasing the number of hidden units in a neural network is in the potential for over fitting of the data, resulting in noisy predictions. In order to avoid over fitting, two approaches can be employed. The first is to ensure an adequate number of data points (Demuth *et al.*, 2006). Given the number of data points in this work and the need for down sampling this goal was achieved. Second, presenting the network with validation and test sets of data, along with the data used for training can allow the network to stop training when the error between the provided and predicted test data increases, even

when the error for training may still be decreasing (Demuth *et al.*, 2006). This procedure was used in all neural network tests described in the thesis in order to ensure over training was not a concern.

Table 3-7: Weighting coefficients and biases for the network used to relate spine posture and hand forces to joint moment.

Layer 1	**Flexion Angle**	**Lateral bend angle**	**Axial twist angle**	**Right vertical hand force**	**Left vertical hand force**	**Height**	**Weight**	**Gender**
Unit 1	-1.0663	-0.462	-1.0586	0.2125	1.5621	0.0135	-0.9361	-0.7364
Unit 2	-0.1094	0.9781	0.1656	-0.5647	0.0567	0.7116	-0.3075	0.5755
Unit 3	-0.1384	0.6363	0.1341	0.2655	-0.0425	-0.1778	-0.0241	-0.5943
Unit 4	-0.7678	1.1566	1.0741	0.5476	0.6446	-0.5015	0.0012	-1.3417
Unit 5	0.6561	-0.2945	0.0597	0.2502	-0.3868	0.2973	-0.7693	-0.2003

Layer 1 continued	**Trunk width**	**Trunk depth**	**Flexion acceleration**	**Bend acceleration**	**Twist acceleration**	**Bias**
Unit 1	0.1346	-0.1711	0.4478	-0.1142	-0.206	-0.3574
Unit 2	1.1606	-0.3672	-0.3798	-0.2785	0.8624	-0.749
Unit 3	-0.3664	0.7547	0.8101	-0.8409	0.41	-0.3378
Unit 4	-0.5019	0.3248	-0.1818	0.1054	-0.5061	0.1939
Unit 5	-0.1614	-0.3194	1.0025	0.0932	-0.4361	0.8174

Layer 2	**Unit 1**	**Unit 2**	**Unit 3**	**Unit 4**	**Unit 5**	**Bias**
Unit 1	-0.5256	-0.6092	0.2029	-0.3823	-0.3283	-0.0742
Unit 2	0.4029	-0.5952	-0.1212	-0.8972	-0.4842	0.8387
Unit 3	-0.0039	-0.0217	-0.0317	-0.0194	0.0138	-0.6409

Table 3-8: Weighting coefficients and biases for the network used to relate spine posture and muscle activation to joint forces.

Layer 1	**Right erector spinae**	**Left erector spinae**	**Right internal oblique**	**Left internal oblique**	**Spine flexion**	**Height**	**Weight**	**Gender**
Unit 1	-0.8468	0.2605	-0.0081	-0.5667	-0.953	-0.2975	1.3575	0.2012
Unit 2	-0.7925	-0.2633	-0.9445	-0.2774	-0.9913	-0.4486	-2.4661	-0.501
Unit 3	1.9937	0.0524	0.6787	-0.1291	1.6884	1.0564	1.5999	-0.2175
Unit 4	0.1005	0.6117	-0.5188	-0.4871	1.1128	1.3392	0.2286	0.6235
Unit 5	1.7853	2.0953	0.9022	-0.3668	2.7477	0.4197	1.6528	-0.3005

Layer 1 continued	**Trunk width**	**Trunk depth**	**Bias**
Unit 1	-5.0441	-2.1127	0.2821
Unit 2	5.2767	1.7417	-0.0114
Unit 3	-5.1384	-2.4719	-0.2778
Unit 4	-0.1217	0.7311	0.805
Unit 5	-2.9224	-0.9622	0.0273

Layer 2	**Unit 1**	**Unit 2**	**Unit 3**	**Unit 4**	**Unit 5**	**Bias**
Unit 1	0.9935	-0.4095	1.6053	0.0175	-0.7899	0.3638
Unit 2	-2.0111	1.3412	-0.7277	-0.4481	-0.3979	0.1572
Unit 3	4.8761	-4.5067	4.2983	-0.1485	2.1787	-0.405

Was the limitation in the number of hidden units a contributor to the observed differences?

Although multiple hidden unit numbers were examined with the data in study 1 (5, 15 and 25) the volume of data that was being used in training prohibited any effects of a larger numbers of hidden units from being studied. In order to ensure that any observed differences were not due to the number of hidden units employed, a set of only 200 data points (representing the sagittal calibration lifts from one male) was isolated and used to train neural networks to predict joint forces based on the reduced inputs employed in study 1. Two networks were created, one employing a hidden layer of five hidden units, and one with a hidden layer containing 100 hidden units. Examination of the maximum and average errors as well as the correlation coefficients between the EMG-assisted predictions of joint force and those obtained from the neural network indicated that being able to

increase the number of hidden units beyond the maximum of 25 examined in study 1 was not likely to alter the results (table 3-9).

Table 3-9: Maximum difference, average difference and correlation coefficient between the EMG-assisted predictions of spine compression and those obtained using two different neural networks, one with a 5 unit hidden layer, another with a 100 unit hidden layer.

Variable	5 Hidden Units	100 Hidden Units
Maximum Difference	1853.0	1853.0
Average Difference	-3.09×10^{-7}	4.23×10^{-4}
R	0.85	0.85

3.3 A Comparison of 3DMatch and Lumbar Motion Monitor Predicted Spine Angles

Overview:

While the neural network and 3DMatch studies (chapters 4 and 5) are clearly related in that they are attempts to better understand tools that may be used in place of more complex models, they share common inputs – three-dimensional spine angles. While the work examining neural networks and EMG-assisted modeling obtained spine angles from the Lumbar Motion Monitor (LMM, Biomec Inc., Cleveland, USA), spine angles for the rigid link model underlying 3DMatch are based upon video observer based posture matching. In order to quantify the differences in spine angles between the two methods 23 trials from the larger data set employed in chapter 5 were randomly selected and a comparison was performed between 3DMatch predicted spine angles and those obtained with the LMM.

The results of paired t-tests indicated that the two methods of angle determination differ in maximum extension angle ($p = 0.04$), average flexion angle ($p = 0.005$) and peak right (maximum) twist ($p < 0.0001$). There were no differences in predicted peak flexion, peak left twist or average

twist angles (figure 3-2). While differences were found, it is important to note that the magnitudes of angle differences are quite small. Additionally, statistics were not performed for any of the lateral bend measures as lateral bend was not predicted using 3DMatch in any of the analyzed trials. In terms of agreement in time series, flexion angle was shown to have an average correlation coefficient of 0.87±0.16 between the two approaches, while axial twist was found to show much lower agreement (0.27±0.17). Again, the agreement in lateral bend was not quantifiable as lateral bend as documented by the video observer using 3DMatch did not show any time variation.

Based on these results, there is now evidence that 3DMatch angles, particularly in flexion agree well with those obtained concurrently using the LMM. However, care should be taken if attempting to replace LMM based inputs for the neural network with those obtained from 3DMatch due to the issue of binning (see chapter 5) and the reduced sample rate (5 Hz) in calculating velocities and accelerations.

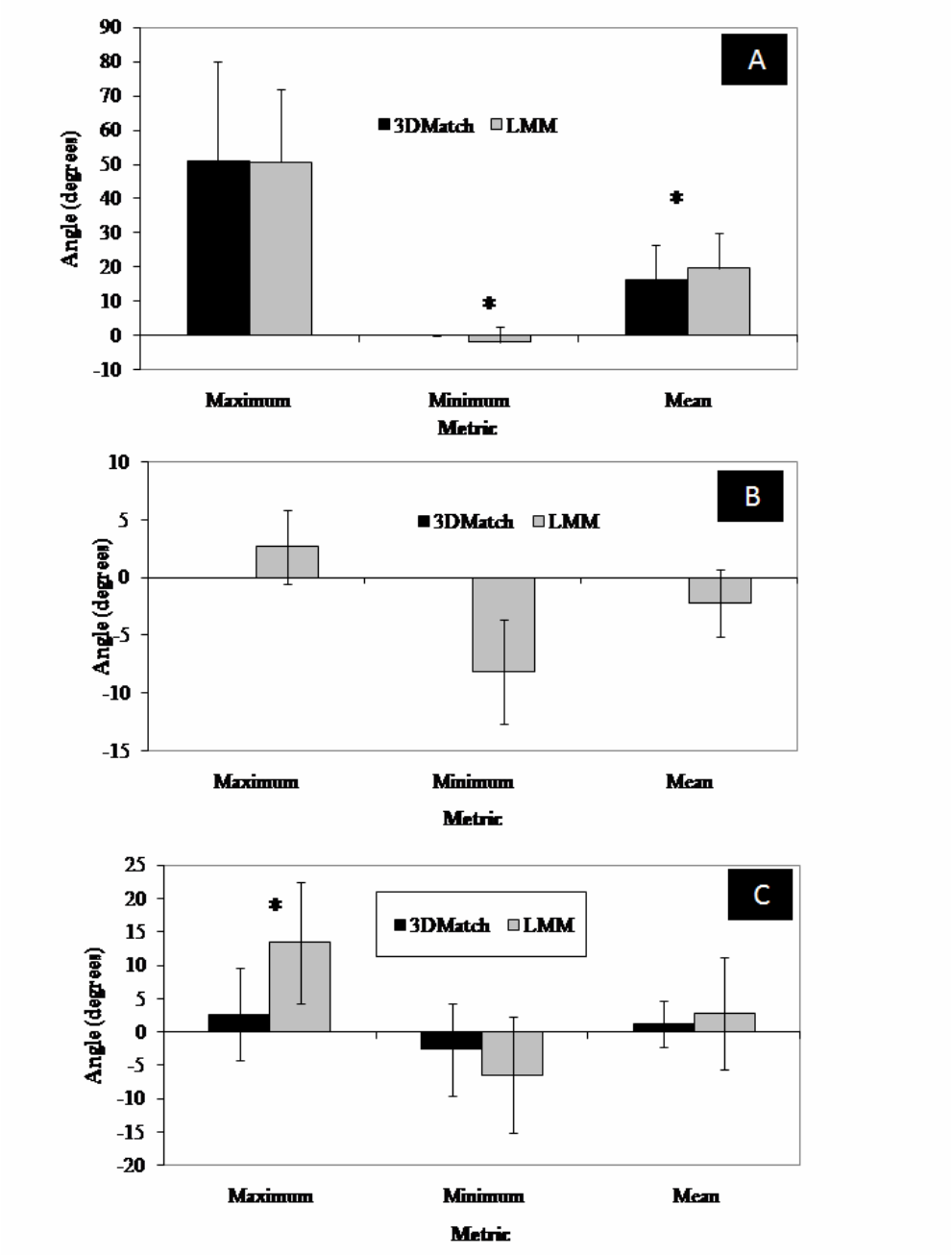

Figure 3-2: (A) Barplot of average maximum, minimum and mean (±1 standard deviation) spine flexion angle as predicted using 3DMatch and the LMM. **(B)** Barplot of average maximum (right), minimum (left) and mean (±1 standard deviation) lateral bend angle as predicted using 3DMatch and the LMM. **(C)** Barplot of average maximum (right), minimum (left) and mean (±1 standard deviation) axial twist angles as predicted using 3DMatch and the LMM. Statistically significant comparisons are denoted with a (*). There were no comparisons performed for lateral bend as the 3DMatch approach did not predict any deviation from neutral.

3.4 Issues in Tissue Testing

3.4.1 The Use of a Porcine Animal Model

In order to conduct the tissue research included in this thesis, porcine cervical spinal units were employed as an analog to the human lumbar spine. While this approach has the obvious scientific benefit of allowing large samples to be tested, it is subject to some limitations. The following section will outline the work that has led to the choice of the porcine cervical spine as a suitable model.

When performing *in vitro* tests for the purposes of determining safe limits for the human body, it would be ideal to use human tissues. However, cadaveric materials can be difficult to obtain and costly (Yoganandan *et al.*, 1996). Furthermore, cadaver use would act to increase the variability of testing results by providing a non-homogenous population (Allan *et al.*, 1990). The variability of results will be increased with the use of cadaveric material as it has been shown that age, activity, degeneration and ethnic background can affect the physical and mechanical properties of the intervertebral tissues (Gower and Pedrini, 1969; Andersson and Schultz, 1979; Horst and Brinckmann, 1981; Postacchini *et al.*, 1983; Koeller *et al.*, 1986; Porter *et al.*, 1989; Bush *et al.*, 1956). Due to differences between people in these factors as well as those of genetics, diet and illness, it would not be possible to obtain a homogenous experimental population. The use of an animal model allows control over these factors (Gunning *et al.*, 2001; Yingling *et al.*, 1999), decreasing the variability in experimental results by providing a more homogenous population.

Many animal models have been used in the study of spinal tissues and structures, including canine (Fitzgerald, 1975), ovine (Costi *et al.*, 2002; Kettler *et al.*, 2000; Wilke *et al.*, 1998; Mitton *et al.*, 1997), bovine (van Dieen *et al.*, 2001; Race *et al.*, 2000b; Oden *et al.*, 1998), (Race *et al.*, 2000b; Oden *et al.*, 1998) and porcine (Gunning *et al.*, 2001; Tsai *et al.*, 1998; Callaghan and McGill, 2001; Oxland *et al.*, 1991). One issue with the listed models is that the animals are quadrupeds, with

gravity acting along the spine perpendicular to the direction in a biped. This may indicate that quadruped spines are not loaded in axial compression like the spines of bipeds. However, researchers have shown that the muscular action in a quadruped leads to a loading pattern similar to that in humans (Smit, 2002). This conclusion is based on the direction of trabeculae growth (Lin *et al.*, 1997). Based on Wolff's law (that tissues, in this case trabeculae, are aligned in the direction of force application), it was concluded that the quadruped spine is loaded mainly in axial compression (Lin *et al.*, 1997; Smit, 2002).

In a recent article on comparative morphology, McLain *et al*. (2002) stated that the choice of a proper animal model can aid in avoiding incongruencies and assumptions, which can lead to improved research. For a study on injury mechanics, it is important that the chosen model has a similar structure and exhibits the same mechanism of failure. Anatomic comparisons of porcine and human vertebrae have concluded that porcine vertebrae are generally smaller (Yingling *et al.*, 1999; McLain *et al.*, 2002). However, it has been found that the facet and ligamentous structures of porcine and human spines are similar, despite the presence of anterior processes on the porcine cervical spine (Oxland *et al.*, 1991; McLain *et al.*, 2002; Yingling *et al.*, 1999). The anterior processes do not appear to serve any load-bearing purpose, and therefore would not affect mechanical testing (Oxland *et al.*, 1991). More recently, dissection work has shown that while the porcine cervical intervertebral disc is smaller than that of the human lumbar spine and contains fewer annular layers the fiber orientation and general structure make it a suitable model in studies examining repetitive flexion and extension (Tampier, 2006).

In 1999, Yingling *et al*. investigated the response of porcine vertebral motion segments to compression, and compared their results to human data available in the literature. The authors concluded that common compression fractures occurring in human vertebrae (stellate and edge

fractures) also occur in the porcine vertebrae (Yingling *et al.*, 1999). Porcine tissues also showed results in shear loading consistent with those in cadaveric material (Yingling *et al.*, 1999).

Based on the anatomical similarities and consistency of mechanical behaviour it was felt that the porcine cervical intervertebral joints (C3/C4 and C5/C6) would provide a reasonable representation of human lumbar joint behaviour while allowing for the testing of a large number of homogenous specimens. The homogeneity of the specimens has been previously confirmed between independent samples obtained from the supplier used in this work, illustrating that separate samples did not differ in average endplate size, bone mineral content or compressive tolerance (Parkinson *et al.*, 2005).

3.4.2 Frozen Storage

Given the current laboratory and specimen supply infrastructures, it was not realistic to test numerous specimens concurrently, nor was it possible to test each specimen as soon as materials became available. Therefore, it was necessary to store the tissues so that they could be obtained when available and tested when possible. In order to accomplish this, many authors have slowly frozen the tissues (Adams and Hutton, 1983a; Oxland *et al.*, 1991; Asano *et al.*, 1992; Holmes *et al.*, 1993; Lin *et al.*, 1997; Tsai *et al.*, 1998; Gunning *et al.*, 2001). The slow freezing process has the potential to injure or alter the tissues. Slow freezing causes the extracellular matrix to freeze first leading to solute exclusion, water then moves out of the cells to achieve equilibrium across the membrane, causing cellular dehydration (Knox *et al.*, 1980; Rubinsky *et al.*, 1990). Upon thawing, the water moves back into the cell, leading to large amounts of swelling (Knox *et al.*, 1980). Therefore, both the formation of ice crystals and the water movement have potential to injure the tissues of interest, individually or in combination.

The effects of freezing on ligament tensile behavior were examined by Woo *et al*. (1986). Rabbit was chosen as the animal model, and the medial collateral ligament was examined. The use of this model allowed paired specimens to be used in the comparison. The investigators subjected the ligaments to -20^0 C for 1.5 and 3 months. No difference was found between fresh and frozen specimens in terms of the load, deformation, and energy absorbing capability at failure (Woo *et al.*, 1986). Furthermore, no changes were found in the cyclic stress relaxation or the load-deformation characteristics (Woo *et al.*, 1986). The researchers did find that hysteresis in the stored samples was significantly lower than in the fresh samples, but this difference was diminished with repeated loading and reached non-significant levels (Woo *et al.*, 1986).

Frozen storage effects on the material of the intervertebral disc have also been studied. Hickey and Hukins (1979) used x-ray diffraction to look for the effects of freezing on the distribution of the collagen within the annulus fibrosus of rabbits. They found that preservation through freezing in liquid nitrogen, freezing, and fixation in saline were all acceptable, as none of the methods led to disruption of the collagen fibril arrangement (Hickey and Hukins, 1979). Furthermore, freezing had no effect on the collagen molecules within a fibril (Hickey and Hukins, 1979). The effects of freezing on the mechanics of the intervertebral disc have also been examined. A 1997 study examining the effects of freezing on the creep properties of porcine intervertebral discs found that the permeability of frozen discs (-20^0 C) was 82% higher than fresh and the swelling pressure was 25% lower (Bass *et al.*, 1997). However, permeability was determined with a mathematical model and did not isolate a biological change in the disc. The investigators also observed that repeated creep cycles did not decrease the magnitude of the differences between fresh and frozen specimens, indicating that the damage due to freezing may be permanent (Bass *et al.*, 1997). In contrast, Dhillon *et al*. (2001) used the same 3 parameter fluid transport model and showed that freezing of cadaveric intervertebral discs at -20^0 C did not affect the creep behavior in terms of endplate permeability, strain dependence, or

annular creep. Due to the non-destructive nature of the tests, the same segment was tested prior to and after freezing, removing the variability that may be present in studies examining intervertebral discs from different donors. The authors also tested adjacent levels, which eliminated the effects of the prolonged testing protocol required to test the same specimen twice and reached the same conclusions (Dhillon *et al.*, 2001). The effects of frozen storage on trabecular bone have also been examined. Machined sections of tibial bone were obtained and stored at -20^0 C for 1, 10, or 100 days (Linde and Sorensen, 1993). Thawed tibial specimens were then compressed to 0.45% strain, and stress-strain curves were plotted. Freezing did not significantly alter the stiffness, elastic energy, or hysteresis of the bone samples (Linde and Sorensen, 1993).

Although testing of isolated ligaments, intervertebral discs, and trabecular bone has been performed, it is necessary to test freezing effects upon these structures when they are combined into a functional unit as they would be in the body. Gleizes *et al*. (1998) looked at segments of sheep spine containing three vertebrae and found that freezing at -18^0 C did not significantly affect the range of motion or stiffness of the intervertebral disc in flexion-extension or right and left lateral flexion. The researchers did report that the C6/C7/T1 fresh and frozen segments did respond differently; however the conditions of validity were not met so statistical analysis was not performed (Gleizes *et al.*, 1998). Panjabi *et al*. (1985) also tested the effects of frozen storage (-18^0 C) on cadaveric thoracic motion segments. Segments were tested fresh, frozen for 21 days, or frozen for 232 days. No significant differences were noted between the three groups for measures of anterior shear, axial rotation, and lateral bending (Panjabi *et al.*, 1985). Smeathers and Joanes (1988) quantified the effects of -18^0 C frozen storage on the hysteresis and axial dynamic compressive stiffness of cadaveric lumbar intervertebral joints. It was found that freezing caused less than a 1% change in the hysteresis and compressive stiffness during cyclic testing, indicating that no damage had occurred (Smeathers and Joanes, 1988). The consistency of stiffness between fresh and frozen specimens was supported by

Callaghan and McGill (1995). It was also found that the displacement at failure and failure mechanism are not altered by frozen storage at -20^0 C for 1 month (Callaghan and McGill, 1995). However, their investigation of the compressive properties of porcine cervical spinal units revealed that frozen storage increases the energy absorbed to failure by 33% and the ultimate compressive load by 24% (Callaghan and McGill, 1995).

It is clear from the available literature that there is controversy regarding the effects of freezing on intact intervertebral joints as well as the tissues that comprise them. However, due to limitations in infrastructure and specimen availability it is necessary to continue to freeze spinal tissues to allow storage. Since all specimens were treated in the same fashion it was assumed that any changes observed would be due to the experimental treatments and not attributable to any artifact due to storage.

3.4.3 Hydration

As the tissues that make up the spine are viscoelastic, their hydration state may affect the measure of interest. The effects of hydration on the properties of vertebral cancellous bone were examined by Mitton *et al*. (1997). The authors found that the stiffness of the bone (quantified using Young's modulus) was significantly lowered in the hydrated sample ($p = 0.0015$) (Mitton *et al.*, 1997). However, the authors failed to maintain a constant temperature exposure (hydrated samples tested at body temperature, air samples tested at room temperature), which may have created or contributed to the observed differences. Similarly, Costi *et al*. (2002) concluded that spinal units tested in saline solution were less stiff than those tested in air. Similarly to Mitton *et al*. (1997), the temperatures used were not equivalent so changes may not be entirely attributable to hydration state. Although temperature may have influenced the results of the above-mentioned studies, their results have been supported by the findings of other studies. In an investigation of the effects of hydration

on bovine intervertebral discs, Race *et al*. (2000a) found that specimens exposed to long term creep, that induced dehydration, showed a rapid increase in compressive stiffness over the first 30 minutes followed by a slower continuous increase.

The effect of hydration on the material of the intervertebral disc (annulus fibrosus) was studied as early as 1967 by Hirsch and Galante . The authors immersed strips of annulus in various solutions and measured the tensile properties at multiple times. It was found that swelling resulted with immersion, and subsequently the material became more extensible, and that energy dissipation increased while recovery decreased (Hirsch and Galante, 1967).

Apart from affecting the stiffness of the vertebral bone and intervertebral discs, hydration state can also affect compressive strength as well as the failure mechanism. When the maximum compressive strength of vertebral cancellous bone was adjusted for apparent bone density, bone samples tested in saline were less resistant to compression (Mitton *et al.*, 1997). This decreased strength was also found in the intervertebral discs of porcine cervical spines (Gunning *et al.*, 2001). The investigators observed that super hydrated specimens (placed unloaded in physiological saline solution for 6 hours) displayed 71-78% of the strength of dehydrated specimens (Gunning *et al.*, 2001). Furthermore, dehydration was found to alter the compressive failure mechanisms, with dehydrated specimens displaying edge fractures significantly ($p < 0.001$) more often than the other three hydration states (Gunning *et al.*, 2001). However, there is conflicting literature available. Callaghan (1994) investigated the effects of testing in a chamber filled with air and testing in a physiological saline filled chamber on the compressive strength, slope, maximum deformation, energy absorbed to failure, and the nature of injury. Immersion in saline produced no significant effects on any of the mechanical properties measured (Callaghan, 1994). During testing, the specimens were loaded while immersed in the saline, which can act to control swelling (Pflaster *et al.*, 1997), and therefore may limit changes in the mechanical properties.

Given the evidence in the literature that indicates hydration state can alter the results of mechanical testing of viscoelastic tissues, there are varied techniques for controlling hydration. Some authors have developed chambers that expose the test segment to solution or 100% humidity (Adams and Hutton, 1983a; Adams and Hutton, 1985; Brinckmann *et al.*, 1988; Asano *et al.*, 1992; Hasegawa *et al.*, 1995). However, to avoid damaging the sensitive measuring equipment (Wilke *et al.*, 1998), corrosion effects (Wilke *et al.*, 1998), and greatly complicating the experimental setup and procedures, many authors wrap the specimen in saline soaked gauze and/or wrap the specimen in plastic (Gordon *et al.*, 1991; Holmes and Hukins, 1994; Adams *et al.*, 2000; Callaghan and McGill, 2001; Gardner-Morse and Stokes, 2003). Regardless of the chosen method, equal application across all load groups to ensure consistency of experimental conditions will prevent confounding factors of varying hydration state on study results. Given the amount of motion necessary with the apparatus used in studies three and four, it was felt that a saline soaked gauze wrap was the most appropriate approach.

3.4.4 Synchronization of the Angular and Vertical Motion Systems

In order to apply motion and load profiles together, two separate systems were employed. For vertical loading, an Instron materials testing system (8872, Instron Canada, Toronto, Canada) was employed while a Galil motion controller (Galil DMC-18x0) was used to control the application of rotations through a rotational motor (Kollmorgen AKM23D-BNCNC-00) in series with a torque transducer (SensorData T120-106). This approach was limited by the fact that although the Instron load and position channels were sampled by the Galil program, adjustments to the Instron system itself through this control system were not possible. Similarly, it was not possible to drive the rotational motor through the Instron system's software. The independence of the systems presented a difficulty in ensuring that the desired angular positions and load applications were occurring at the

correct time relative to one another. In order to deal with this, the Galil program was designed to ensure that the rotational motor did not induce motion until after a certain load magnitude was reached. As the duration of each load and motion cycle was maintained constant, this would ensure synchronization. In situations where the two systems became poorly timed, the Galil program would simply wait until the next cycle to resume motion. In only four of fifty tests was this approach unable to maintain proper timing.

Chapter 4

The use of Artificial Neural Networks to reduce data collection demands in determining spine loading: A laboratory based analysis.

Robert J. Parkinson, and Jack P. Callaghan

Submitted to Computer Methods in Biomechanics and Biomedical Engineering

4.1 Abstract

The data collection demands required to perform three-dimensional inverse dynamics or to employ a joint model to estimate spinal loading exposures creates a barrier to the development of advanced injury prevention standards in the workplace. Alternative methods of obtaining exposure estimates of equal quality to laboratory estimates without the equivalent data demands are desirable. This work examined the potential of feed forward artificial neural networks (ANNs) for this purpose and compared predictions to three-dimensional rigid link (RLM) and EMG-assisted (EMG) models. Data were collected on 10 males and 10 females who performed a variety of free dynamic lifts on each of two testing days. All modeling approaches were applied and comparisons of predicted joint moments (RLM vs. ANN) and joint forces (EMG vs. ANN) were evaluated. The results indicated that while the ANN significantly under predicted peak extension moments ($p = 0.0261$) and peak joint compression ($p < 0.0001$), predictions of average ($p = 0.5744$) and cumulative extension moments ($p = 0.8293$) as well as average ($p = 0.7710$) and cumulative joint compression ($p = 0.9557$) were not different between the model types. Testing the ANN with novel data not used in the training process did not alter these conclusions. These results indicate that ANNs may be used to obtain laboratory quality estimates of average and cumulative exposure variables with greatly reduced input demands, however they should not be applied to determine the peak loading demands of a worker's exposure.

Keywords: Spine, cumulative loading, artificial neural network

4.2 Introduction

The reporting of low back pain and the occurrence of injury have been associated with mechanical loading measures, such as compression and moment exposures (Norman *et al.*, 1998; Kumar, 1990; Marras *et al.*, 1995). In order to assess these exposures several techniques have been employed, varying in complexity. Early attempts to estimate loading employed simplified two-dimensional models of the body combined with hand loads to estimate reaction forces in the spine (Smith *et al.*, 1982; McGill and Norman, 1985; Leskinen *et al.*, 1983a; Leskinen *et al.*, 1983b; Ekholm *et al.*, 1982). These models were followed by gradual increases in sophistication, starting with the movement to simplified three-dimensional models which ignored angular velocities and accelerations (Buseck *et al.*, 1988; Bush-Joseph *et al.*, 1988; Herrin *et al.*, 1986). Eventually, three-dimensional fully dynamic models were developed (de Looze *et al.*, 1992a; Kingma *et al.*, 1996a). While these models were able to quantify loading due to external loads and body segment mass, they did not reflect the contribution of muscle forces to spinal loading. In order to more accurately reflect the loading of the spine, joint models need to be partnered with the reaction forces and moments calculated. Initially these models began by employing one muscle force to represent the combined contribution of all back musculature, where the product of this single force vector and its moment arm must balance the calculated external moment (Bejjani *et al.*, 1984; Leskinen, 1985; Wood and Hayes, 1974; Morris *et al.*, 1961; Chaffin, 1969). As research has continued, these models have evolved to more accurately replicate spinal anatomy, including multiple muscles which can contribute to moments about all movement axes (flexion/extension, lateral bend and axial twist) (McGill and Norman, 1986; McGill, 1992b; Granata and Marras, 1995a; Marras and Sommerich, 1991a; van Dieen and Kingma, 2005). While these models may provide the most realistic estimates of spinal loads due to their anatomical detail, their high demand for multiple quality inputs (segment positions, angular velocities, muscle activation levels, external load measures) has limited their use in analyzing

load exposures experienced by workers performing industrial tasks outside of the laboratory environment (McGill *et al.*, 1996b; Mirka and Marras, 1993; Granata and Marras, 1995b; Lee *et al.*, 2003).

This limitation has led to the implementation of simplified approaches in order to estimate risks, which can be categorized as examining peak loading or time-varying (cumulative) loading. Tools examining peak loading investigate postural and load demands at a single point in time, and involve measures of the task dimensions along with manipulative equations to determine risk (such as the NIOSH equation (Waters *et al.*, 1993)) or posture matching, whereby mannequins are manipulated into a position mimicking that of the worker and calculations of loading are performed based on an underlying rigid link model (such as Three-Dimensional Static Strength Prediction Program™ (3DSSPP)). Other work has examined the prediction of joint forces through implementation of regression equations based on industrially attainable measurements (location of load to be lifted, travel distances, anthropometrics, etc)(Potvin *et al.*, 1992; Potvin, 1997). While these methods can identify instances of excessive loading, they cannot account for individual variation in task performance through time, or differences in joint loading due to varied muscle recruitment patterns. Individual muscle recruitment patterns can contain valuable information and have shown potential in separating individual's who experience pain due to low level activation from those that do not (Veiersted *et al.*, 1993). If multiple frames are analyzed for a given task, it is possible to use these approaches to obtain time-series data of load exposures. However this process is time-consuming, which may limit its usefulness in large scale industrial studies. This has led researchers to look for ways to obtain time-series estimates of spine loading with less time-intensive methods than required of posture matching. Mientjes et al. (1999), based on the work of Potvin et al. (1990), employed compression normalized EMG as a method of tracking spine compression, reporting an average amplitude error of 14.9% as obtained from amplitude probability distribution

function analysis, with a range of 15.5-46.5%. In another attempt to track spine loading Fathallah et al. (1999) employed regression models capable of predicting continuous estimates of compression, in addition to anterior-posterior (AP) and medial lateral (ML) shear. The simplest regression model was able to predict spine compression with a standard error of 1001 N, AP shear with a standard error of 241 N and ML shear with a standard error of 136 N. More recently, researchers have employed artificial neural networks (ANN) as a method to obtain estimates of time-varying joint moment (Kingma *et al.*, 2001) and joint force (Hou *et al.*, 2004a; Hou *et al.*, 2005; Hou *et al.*, 2007). Kingma et al. (2001) were able to demonstrate that an ANN, trained with EMG and trunk motion variables, was able to predict L5/S1 moments with a root mean square difference of 31.4 Nm and a correlation of 0.744 when compared to predictions obtained from a dynamic three-dimensional rigid link model. On average, the ANN under predicted the average moment by 3.1% when compared with the rigid link model approach, while under estimating the peak moment by 17.3%. When the ANN moment predictions were compared with moments determined with an EMG based approach the ANN over predicted the average moment by 17.7%, again under predicting the peak moment (37.2%). Examination of the graphed time-series data (figure 1, page 341) indicates that the EMG based approach predicts faster rise and fall times in joint moments, along with larger peak estimates and shorter exposure durations. These predicted patterns of moment exposure, if integrated through time, may yield similar estimates of cumulative moment. Similarly, Hou et al. (2007) have shown that a recurrent fuzzy neural network can be employed to successfully predict the amplitude and timing of both EMG signals and spine loads (ML shear, AP shear and compression) with mean absolute errors of 12.5, 52,7 and 147.7 N respectively. As with the work of Kingma et al. (2001), visual examination of the graphical data provided (figures 6 and 7, page 107) indicates that the neural network predictions may provide good estimates of cumulative exposure when compared with those obtained from an EMG-assisted model, however this was not quantified.

The potential for ANNs to yield strong predictions of joint moments and joint loads in combination with their ability to obtain these predictions through time with reduced inputs (compared to a three-dimensional rigid link or EMG-assisted joint model) may make them an ideal approach to obtain laboratory quality estimates of spine loading in industry. While previous research has indicated that an ANN approach can provide reasonable estimates of load exposure, to the authors' knowledge these findings have not been extended to examine the estimation of cumulative exposures. Therefore, this study was conducted to examine the potential utility of ANNs as a data reduction approach to provide high quality estimates of cumulative spine loading.

4.3 Methods

4.3.1 Participant Selection

Twenty participants (10 male and 10 female, table 4-1) were recruited from the University of Waterloo population for involvement in this study. Participants attended two testing sessions, separated by a minimum of one week. The study received ethics clearance through the University of Waterloo Office of Research Ethics and individuals were required to provide written consent and to have had no non-muscular low back pain for the previous 12 months.

Table 4-1: Average subject age (years), mass (kg) and height (m). Standard deviations are expressed in parentheses.

	Age(years)	**Mass(kg)**	**Height(m)**
Male	25.2(3.3)	86.8(7.9)	1.82(0.08)
Female	22.2(2.2)	69.7(8.0)	1.66(0.07)

4.3.2 Task Description

In order to replicate industrial conditions, participants were asked to perform multiple lifting and lowering trials of an instrumented lifting rig, between the floor and shelving located at 0.67 (approximating waist height) and 1.2m (approximating shoulder height). Participants completed these lifts under two load conditions (level 1 – 7.6 kg and level 2 – 9.7 kg) and through various directions and combinations of lifting asymmetry (right, center, and left). In order to prevent fatigue, participants only completed four trials in which they altered direction, these were moving from the right floor to left shoulder under light and heavy conditions, and moving from the left floor to right shoulder heights under light and heavy conditions. These lifts were chosen to represent a 'worst case' ergonomic lifting situation. These combinations resulted in a total of 132 lifts and 132 lowers (22 lifting trials×6 lift/lower cycles) representing both symmetric and asymmetric tasks for each participant. During the lifts, participants were free to perform the lift in any manner as long as they remained on the force plate; technique and lifting speed were not controlled. Participants completed all of the required lifts during each testing session, with the order of presentation being randomized for all sessions. Due to the large size of the force plate participants were free to move in any way they felt comfortable and could complete the lifts at a self-selected pace (figure 4-1).

Figure 4-1: Male participant performing a left floor to right shoulder lift.

4.3.3 Data Collection and Analysis

In order to estimate the reaction forces and moments at the L5/S1 joint, a bottom-up, three-dimensional, dynamic rigid link model (RLM) was employed. Ground reaction forces and moments were measured at 2048 Hz with a force plate (900mm × 900mm, Model BP900900, Advanced Medical Technology Inc., Watertown, USA) while segment kinematics were determined from infrared light emitting diodes (IREDS) that were affixed on cuffs attached to the lower legs, thighs, and pelvis. Diodes were applied directly over the first and fifth metatarsal bones, heel and dorsum of the foot, as well as the acromion processes to allow for tracking of the trunk and feet. Segment based co-ordinate systems were determined from an upright standing calibration trial in which the medial and lateral malleoli, medial and later epicondyles of the knee (aligned to flexion/extension axis of the joint) and greater trochanter were also identified through placement of additional IREDS. Marker

position in three-dimensions was recorded at 32 Hz using an optoelectronic system (Optotrak Certus, Northern Digital Inc, Waterloo, Canada). Marker co-ordinates and voltages recorded from the force plate were input into Visual3D motion analysis software (C-Motion, Inc., Ontario, Canada) where inverse dynamic calculations were performed in order to determine reaction forces and moments at the L5/S1 joint using a bottom-up approach. Prior to model calculations, all raw marker data was low-pass filtered (dual pass) with a Butterworth filter (6 Hz cut-off frequency). The calculated moments and forces were dual pass filtered with a low-pass Butterworth filter (2.5 Hz cut-off) prior to being exported from the software. Additionally, upper body joint (elbow, wrist) angles were determined at 32 Hz for all lifts using the locations of markers placed over the 3rd metacarpal, wrist, elbow and shoulder joint centers. Bilateral hand loads were also collected with two force cubes mounted in the rig (Model MC3A – 500, Advanced Medical Technology Inc., Watertown, USA) during all lifts. This data, when combined with trunk angle represented the time-varying information needed to implement a top-down model capable of predicting joint loads at the L5/S1 joint. This data was obtained for use in ANN development as it was felt that a top-down model would better reflect industrial data collections. Research has shown correlations of 0.990-0.997 between bottom-up and top-down two-dimensional models (Kingma *et al.*, 1996b), while analysis of magnitude differences in a dynamic three-dimensional model found the largest absolute differences to be 15 Nm (Lariviere and Gagnon, 1998). Therefore, it was felt reasonable to assume that moments predicted from the bottom-up model would reasonably represent those that would be expected from a full three dimensional top-down approach.

An EMG-assisted model was employed to obtain estimates of bone on bone (joint) compression and (joint) shears. Muscle activation levels were recorded from five bilateral trunk muscle sites, including the erector spinae (at the L3 level), latissimus dorsi, internal oblique, external oblique and rectus abdominus (Mirka and Marras, 1993) using self-adhesive surface electrodes (Blue

Sensor, Medicotest Inc., Ølstykke, Denmark). EMG signals were band pass filtered (10-1000 Hz) and differentially amplified (common mode rejection ratio of 115 dB at 60 Hz, input impedance of 10 GΩ, Model AMT-8, Bortec Biomedical Ltd., Calgary, Canada). In order to allow normalization of EMG levels, maximum voluntary contractions were performed for the extensor musculature through exertions with the participant lying prone with their lower body supported on a table while they attempted to maximally extend their back. Maximum abdominal exertions were obtained through a series of contractions in which the participant attempted to maximally flex, bend and twist about their low back. For the extensor and abdominal exertions resistance was applied manually by the researcher to limit motion. Maximal latissimus dorsi activation was achieved through a pull-down type contraction, where the participant pulled down on a handle that was rigidly fixed to the ceiling. The handle was adjustable to ensure that participants could assume a posture in which their upper arm was abducted and externally rotated 90^0 and their elbow flexed 90^0. All EMG data was sampled at 2048 Hz and synchronized to the marker and force plate data through the collection software (NDI-Toolbench v3.00.39). Post-collection, raw EMG data was high-pass filtered at 33 Hz to remove contamination from heart rate (Drake and Callaghan, 2006) and the Optotrak system, and notch filtered to remove any 60 Hz contamination (Mello *et al.*, 2007a). This filtered data was then full-wave rectified and low pass-filtered using a low-pass 2.5 Hz cut-off Butterworth filter (Brereton and McGill, 1998). In addition, spine posture was measured using the Lumbar Motion Monitor (LMM, Biomec Inc., Cleveland, USA), sampled at 2048 Hz and dual pass filtered (1.5 Hz low pass Butterworth filter (Beach *et al.*, 2006)).

The EMG-assisted model employed was based upon the work of Granata and Marras (1995a) and includes gender specific anatomy (Jorgensen *et al.*, 2001; Marras *et al.*, 2001) and gender specific passive moments (McGill *et al.*, 1994; Parkinson *et al.*, 2004; Dolan *et al.*, 1994). Passive moments were determined based upon the instantaneous position of the spine, and their contribution to the

bending moment about each axis was accounted for. The EMG-assisted model also included nodal points that the erector spinae and latissimus dorsi muscles pass through at the L4 level in order to prevent excessive shear forces from developing when participants near full flexion. The model was scaled for gender, participant height and mass as well as trunk dimensions. A model gain trial was performed in which the participant lifted a mass (7.56 or 14.2 kg) from the floor to waist height, and returned it to the ground. This allowed for the determination of a participant and session specific gain value based on the rationale that the predicted muscle moment must be equal in magnitude to the reaction moment. Only the moment about the flexion/extension axis was used for determination of the gain value. The trial (7.56 vs. 14.2 kg) that was selected provided the best agreement between the measured and predicted traces (r value) for each participant. Once determined, this gain value was applied to all lifts conducted within the same testing session.

4.3.4 Artificial Neural Network Development

Building on the evidence that both moment and force exposures can be related to the likelihood of reporting low back pain or experiencing injury, two ANNs were developed, one to predict three-dimensional joint moments and one to predict three-dimensional joint forces. Each set of network inputs was based upon the type of model, which would be employed to obtain estimates of the values in the laboratory. Therefore, the network designed to predict low back moments incorporated motion variables of the trunk and arms, hand forces, and anthropometric measures as these inputs represent those that would be used in a top-down rigid link model to obtain the same estimates. In contrast, the network designed to predict bone on bone forces was based upon trunk motion, anthropometrics and EMG, as these inputs reflect those that would be needed to obtain bone on bone forces from an EMG-assisted joint model. In order to allow data reduction, correlations were calculated between all time-varying input variables and the desired out come measures. Those

variables that showed the strongest correlations, along with anthropometric measures, were subsequently used as inputs for the neural networks.

Once the inputs were identified, network architecture was determined. For this work a three-layer feed forward network architecture was employed where both the hidden layer and output layer employed linear transfer functions. The number of inputs was determined based upon the correlation analysis, while the number of outputs was fixed at three for both models. The number of hidden units was determined from the training error (mean square error between network predicted moments and forces and those predicted from the RLM or EMG-assisted approaches, respectively), where the minimum number of hidden units necessary to achieve stable error estimates dictated the final architecture. Trials from the first testing session were used to develop a network training set. In order to improve generalization and achieve early stopping in training, the session one (training) data was further divided by randomly selecting 60% of the data for training, 20% for validation and 20% for testing. In order to ensure stable determination of network parameters, networks were trained three times with newly initialized parameters (weights and biases). All training was conducted using back propagation, employing a momentum technique which can avoid local minima by providing information on the error surface (Demuth *et al.*, 2006). Data from the second experimental day was used to test the networks ability to generalize predictions to a 'partially novel' data set. The data is only partially novel as the network was trained on the same people with the same anthropometrics; however it had not seen any time-varying data from the second day in training. Additionally, data from two males and three females was withheld from the network in order to be able to test the ability of the network to predict joint load exposures when presented with completely novel data. The ANN approach employed in this study used the Neural Network Toolbox^{TM} (Matlab 7.4.0, The Mathworks, MA, USA) that has also been used in previous ANN studies (Song and Tong, 2005; Rosen *et al.*, 1999).

4.3.5 Statistical Analysis

Statistical comparison of the outcome measures (peak and average moments about the flexion/extension, lateral bend and axial twist axes and cumulative extension moment along with peak and average compression, AP shear, ML shear and cumulative compression) was performed using a two-way analysis of variance (data source (original or simulated) and gender), with subject nested in gender. Comparisons between data source and gender were conducted for the session 1 training data (source data) as well as the session 2 test data (partially novel). Only the comparisons between data source were carried out for the novel data, gender effects were not assessed due to the small number of participants (two male and three female). All tests with $p < 0.05$ were considered statistically significant.

4.4 Results

4.4.1 Joint Moments

4.4.1.1 Network Development

Removal of data for testing of network generalization, as well as the loss of one female data set due to technical issues resulted in complete training data from eight males and six females. Due to the very large data set, incorporating all trials sampled at 32 Hz resulted in memory errors when trying to train the networks, so only those trials in which the upper limb markers remained visible (192/244 session 1 trials, table 4-2) were employed and data was further down sampled to 8 Hz for network training. The correlation analysis indicated that trunk angles (flexion, twist and lateral bend) were most highly correlated with the time-varying joint moments (table 4-3). Additionally, the vertical hand forces were among the most strongly correlated variables with joint moment. However, none of the variables demonstrated what would be classified as strong correlations with any of the

three moments (table 4-3). Based on these results, spine angles and vertical hand forces were selected for use within the neural network. In addition, the spine accelerations about each of the three axes were included as it was felt that they may exhibit a strong relationship with the moments ($\sum$moments = inertia×angular acceleration or $\sum M = I\alpha$) and they would require no additional data collection above that required to obtain the spine angles. This resulted in eight time-varying inputs, four anthropometric measures (participant height, mass, trunk depth and trunk width at the level of the umbilicus) and one gender factor (1 for males, 0 for females). A hidden layer was designed to contain 5 hidden units, as this architecture was capable of producing moment estimates in training similar to those when hidden layers containing 15 and 25 hidden units were employed, with no meaningful change in the number of training epochs (table 4-4). The training data set was too large to employ hidden layers with greater than 25 hidden units. ANN predicted were further down sampled to 4 Hz for all subsequent analysis. A summary of network performance can be found in table 4-5.

Table 4-2: Table indicating the number of trials from each lifting condition chosen from session 1 for development of the artificial neural network used to predict joint moments.

	Starting position for load level 1 lifts								
	right floor	**right waist**	**right shoulder**	**center floor**	**center waist**	**center shoulder**	**left floor**	**left waist**	**left shoulder**
Right floor	xxxxxx	xxxxxx	xxxxxx	xxxxxx	xxxxxx	xxxxxx	xxxxxx	xxxxxx	xxxxxx
Right waist	**2**	xxxxxx	xxxxxx	xxxxxx	xxxxxx	xxxxxxx	xxxxxx	xxxxxx	xxxxxx
Right shoulder	**5**	**8**	xxxxxx	xxxxxx	xxxxxx	xxxxxx	**11**	xxxxxx	xxxxxx
Center floor	xxxxxx	xxxxxx	xxxxxx	xxxxxx	xxxxxx	xxxxxx	xxxxxx	xxxxxx	Xxxxxx
Center waist	xxxxxx	xxxxxx	xxxxxx	**9**	xxxxxx	xxxxxx	xxxxxx	xxxxxx	xxxxxx
Center shoulder	xxxxxx	xxxxxx	xxxxxx	**7**	**5**	xxxxxx	xxxxxx	xxxxxx	xxxxxx
left floor	xxxxxx	xxxxxx	xxxxxx	xxxxxx	xxxxxx	xxxxxx	xxxxxx	xxxxxx	xxxxxx
Left waist	xxxxxx	xxxxxx	xxxxxx	xxxxxx	xxxxxx	xxxxxx	**4**	xxxxxx	xxxxxx
Left shoulder	**7**	xxxxxx	xxxxxx	xxxxxx	xxxxxx	xxxxxx	**3**	**8**	xxxxxx
	Starting position for load level 2 lifts								
	right floor	**right waist**	**right shoulder**	**center floor**	**center waist**	**center shoulder**	**left floor**	**left waist**	**Left shoulder**
Right floor	xxxxxx	xxxxxx	xxxxxx	xxxxxx	xxxxxx	xxxxxx	xxxxxx	xxxxxx	xxxxxx
Right waist	**2**	xxxxxx	xxxxxx	xxxxxx	xxxxxx	xxxxxx	xxxxxx	xxxxxx	xxxxxx
Right shoulder	**6**	**7**	xxxxxx	xxxxxx	xxxxxx	xxxxxx	**8**	xxxxxx	xxxxxx
Center floor	xxxxxx	xxxxxx	xxxxxx	xxxxxx	xxxxxx	xxxxxx	xxxxxx	xxxxxx	xxxxxx
Center waist	xxxxxx	xxxxxx	xxxxxx	**7**	xxxxxx	xxxxxx	xxxxxx	xxxxxx	xxxxxx
Center shoulder	xxxxxx	xxxxxx	xxxxxx	**3**	**2**	xxxxxx	xxxxxx	xxxxxx	xxxxxx
left floor	xxxxxx	xxxxxx	xxxxxx	xxxxxx	xxxxxx	xxxxxx	xxxxxx	xxxxxx	xxxxxx
Left waist	xxxxxx	xxxxxx	xxxxxx	xxxxxx	xxxxxx	xxxxxx	**6**	xxxxxx	xxxxxx
Left shoulder	**8**	xxxxxx	xxxxxx	xxxxxx	xxxxxx	xxxxxx	**6**	**8**	xxxxxx
	Single lifts								
	Light calibration		Heavy calibration		Right lateral bend		Left lateral bend		Standing
	33		11		7		9		4

Table 4-3: Coefficients of determination (r^2) between the time-varying measured variables and the predicted joint moments and bone on bone forces. Underlined variables were chosen for use as inputs to the artificial neural network.

Joint Moments				**Bone on Bone Forces**			
Variable	*Flexion/ Extension*	*Lateral Bend*	*Axial Twist*	*Variable*	*ML Shear*	*AP Shear*	*Compression*
Flexion Angle	0.39	0.06	0.07	**RL3**	0.05	0.12	0.27
Left Vertical Hand Force	0.36	0.01	0.01	**LL3**	0.04	0.12	0.24
Right Vertical Hand Force	0.35	0.03	0.02	**RIO**	0.06	0.11	0.26
Lateral Bend Angle	0.09	0.07	0.19	**LIO**	0.04	0.11	0.25
Axial Twist Angle	0.02	0.27	0.17	**Flexion Angle**	0.06	0.21	0.24
Right Wrist Angle	0.04	0.01	0.02	**Lateral Bend Angle**	0.03	0.05	0.06
Left Wrist Angle	0.03	0.01	0.01	**Axial Twist Angle**	0.06	0.03	0.01
Right Elbow Angle	0.03	0.01	0.01	**Right Lat**	0.10	0.07	0.09
Left Elbow Angle	0.02	0.01	0.01	**Left Lat**	0.03	0.05	0.10
Right AP Hand Force	0.07	0.04	0.02	**REO**	0.02	0.02	0.05
Left AP Hand Force	0.09	0.02	0.02	**LEO**	0.01	0.03	0.04
Right ML Hand Force	0.02	0.03	0.01	**RRA**	0.02	0.03	0.06
Left ML Hand Force	0.02	0.02	0.01	**LRA**	0.02	0.03	0.06

ML – medial/lateral, AP – anterior posterior, Right and Left Lat – Right and left Latissimus dorsi activation, RL3 and LL3 – right and left erector spinae (L3 level) activation, RRA and LRA – right and left rectus abdominus activation, REO and LEO – right and left external oblique activation, RIO and LIO – right and left internal oblique activation.

Table 4-4: The average training error (MSE – mean square error) and average number of epochs resulting from training attempted with 5, 15 and 25 hidden units in the hidden layer. Standard deviations are in parentheses.

	Joint Moments		**Bone on Bone Forces**	
Hidden Unit #	*MSE*	*Epochs*	*MSE*	*Epochs*
5	373.9(2.6)	180.7(20.6)	141828.3(804.4)	105.3(12.7)
15	367.4(1.1)	274.3(19.7)	144773.7(785.7)	114.7(43.0)
25	372.4(3.6)	148.7(55.7)	144648.7(1056.0)	144(72.1)

Table 4-5: Average network performance parameters (mean absolute error (MAE) and correlation coefficients(r)) for the source data, partially novel data and novel data for the joint moment neural network (Moment, based upon the flexion extension moments) and joint force (Force, based upon compression force) neural network. Standard deviations are in parentheses.

	Source		**Partially Novel**		**Novel**	
	Moment	*Force*	*Moment*	*Force*	*Moment*	*Force*
MAE	19.2(4.8) Nm	392.4(79.3) N	19.1(5.2) Nm	419.8(140.2) N	21.7(7.3) Nm	645.8(374.5) N
r	0.8(0.06)	0.6(0.06)	0.8(0.06)	0.6(0.06)	0.8(0.1)	0.6(0.06)

4.4.1.2 Peak Moments

Analysis indicated that the ANN significantly under predicted the following moments: peak extension ($p = 0.0261$), peak right bend (significant gender×data source interaction ($p = 0.0151$), $p = 0.0028$ for males, $p = 0.0107$ for females), peak left bend ($p = 0.0084$), peak right twist in males ($p = 0.003$, significant gender×data source interaction ($p = 0.0115$)), and peak left twist ($p = 0.0074$) for the source data, while peak flexion was not significantly different between the original and simulated data sets ($p = 0.1773$, figure 4-2a, the ranges of peak differences are provided in table 4-6). In terms of the partially novel data, significant differences existed between the original and simulated data for peak flexion moment ($p = 0.0463$), peak extension moment ($p = 0.0479$), peak right bend moment ($p = 0.0041$), peak left bend moment ($p = 0.0041$), peak right twist moment for males (significant gender×data source interaction ($p = 0.0181$), $p = 0.0019$) and peak left twist moment ($p = 0.0023$, figure 4-2b). Additionally, males demonstrated significantly greater peak extension moments than females (151.9±46.5 vs. 123.9±15.1 Nm, $p = 0.0479$). In contrast, when the novel data was presented to the network, peak flexion ($p = 0.0702$), peak extension ($p = 0.1431$), and peak left bend ($p = 0.1104$) predictions were not different between original and simulated data. However, significant differences were found between peak right bend ($p = 0.0349$), peak right twist ($p= 0.0012$) and peak left twist moments ($p = 0.0099$, figure 4-2c).

Table 4-6: The range of maximum (expressed in both absolute magnitudes and normalized to original data average peak values (%)) and average differences in predicted extension moments (Nm) and predicted joint compressive forces (N), along with the range of correlation coefficients within each data group.

	Extension Moment			**Joint Compression**		
Data Group	*Source*	*Partially Novel*	*Novel*	*Source*	*Partially Novel*	*Novel*
Average Peak Value	171.1 Nm	155.9 Nm	167.8 Nm	5770.1 N	7015.7 N	8071.1 N
Maximum Peak Difference	287.7-37.9 Nm	213.1-38.6 Nm	220.2-46.5 Nm	6537.5-1712.2 N	17158.0-1714.8 N	8052.4-4939.8 N
% Range	168.1-22.2%	136.7-24.8%	131.2-27.7%	113.3-29.7%	244.6-24.4%	100.2-61.2%
Average Peak Difference	9.4-(-10.3) Nm	5.5-(-17.5) Nm	20.7-(-3.5) Nm	407.2-(-361.5) N	716.2-(-490.3) N	1267.8-104.1 N
r	0.88-0.63	0.90-0.65	0.86-0.58	0.72-0.54	0.72-0.52	0.68-0.55

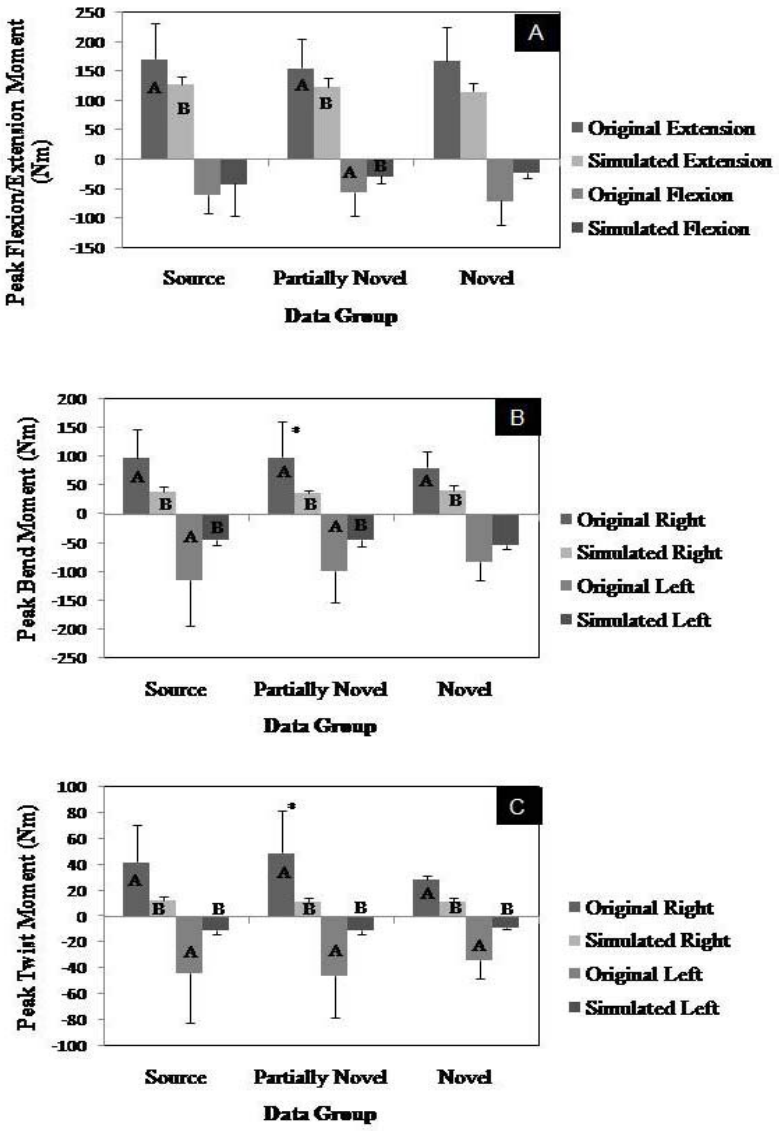

Figure 4-2: (A) Bar plot of average peak extension moment (+ 1 standard deviation) and average peak flexion moment (- 1 standard deviation) averaged within a data source group. **(B)** Bar plot of average peak right lateral bend moment (+ 1 standard deviation) and average peak left lateral bend moment (- 1 standard deviation) averaged within a data source group. **(C)** Bar plot of average peak right axial twist moment (+ 1 standard deviation) and average peak left axial twist moment (- 1 standard deviation) averaged within a data source group. In all plots significant differences are denoted with capital letters. Comparisons marked with (*) showed a significant gender×data source interaction, although both genders shared the same relative relationship as the grouped data. Rigid link model based predictions are labeled as 'original', artificial neural network predictions as 'simulated'.

4.4.1.3 Average and Cumulative Moments

There were no significant differences in average extension moment ($p = 0.5744$, ranges of differences in average extension moment are provided in table 4-6), average lateral bend ($p = 0.5262$) or average axial twist moment ($p = 0.1707$) for the source data. Gender had a significant effect on the average extensions moment ($p = 0.0270$), with males experiencing greater average extension moments (table 4-6). Similarly, cumulative extension/flexion moment predictions were not different between the original and simulated data ($p = 0.0602$, figure 4-3c). When the partially novel data was presented to the network, there were no significant differences for any of the average moments ($p = 0.2471$, 0.7599 and 0.6737 for extension, lateral bend and axial twist, respectively, table 4-7). Additionally, there was no significant differences between the original and simulated data for cumulative extension/flexion moment ($p = 0.7016$), although males were shown to have significantly higher average cumulative loading than females (18462.1±8492.5 vs. 6958.0±2818.0 Nms, $p = 0.0089$). As with the other data sets, there were no significant differences in average predicted extension ($p = 0.1338$), lateral bend ($p = 0.2111$) or axial twist moments ($p = 0.1666$) when the novel data was presented to the network (table 4-7). Cumulative extension/flexion moment predictions were not significantly different between the original and simulated data sets ($p = 0.0955$, figure 4-3c).

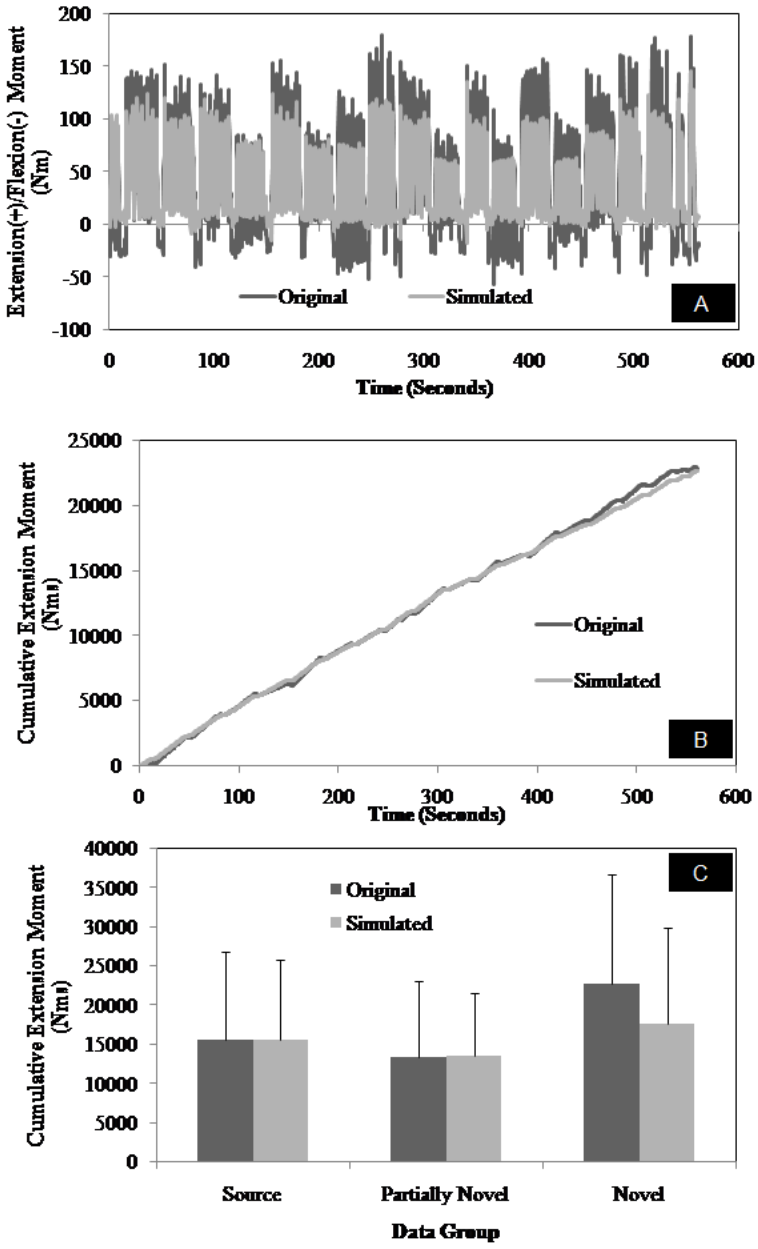

Figure 4-3: (A) Time series of extension (+) and flexion (-) moment as predicted using a rigid link model (denoted as 'original') and an artificial neural network (denoted as 'simulated') obtained from one participant. Note that the data was concatenated for viewing and therefore should not be viewed as continuous lifts. **(B)** The cumulative extension moment (Nms) as determined through trapezoidal integration of the extension/flexion time series in (A). **(C)** Bar plot of average cumulative extension moment (+ 1 standard deviation) for the source, partially novel and novel data sets. There were no significant differences between the rigid link model (original) and artificial neural network (simulated) based estimates.

Table 4-7: The average moments about each movement axes for the original (O) and neural network simulated (S) data, separated by gender. Source data was used for training the neural network, while partially novel and novel data was used to test generalization. Standard deviations are in parentheses. The only significant difference occurred for gender, for average extension moment in the source data, denoted by the letters a and b.

	Source				**Partially Novel**				**Novel**	
Gender	**Male(a)**		**Female(b)**		**Male**		**Female**		**All**	
	O	*S*	*O*	*S*	*O*	*S*	*O*	*S*	*O*	*S*
Extension	38.3	37.0	32.4	33.1	33.1	35.7	24.3	26.3	41.5	32.6
(a,b)	(11.2)	(8.1)	(12.0)	(8.8)	(11.6)	(7.2)	(10.9)	(12.4)	(12.4)	(7.6)
Lateral	-1.0	-2.3	-3.2	-3.3	-2.3	-2.7	-1.2	-1.8	-0.3	-2.3
Bend	(5.9)	(4.2)	(5.0)	(5.2)	(9.0)	(5.2)	(3.1)	(5.2)	(5.6)	(5.2)
Axial	1.2	0.7	-0.2	0.9	1.4	0.7	-0.6	0.8	-0.8	0.7
Twist	(1.6)	(0.2)	(1.8)	(0.2)	(3.5)	(0.3)	(1.9)	(0.3)	(19.8)	(15.8)

4.4.2 Joint Forces

4.4.2.1 Network Development

After removing two males and three females to create a novel data set, the data from eight males and seven females was used. As with the joint moment approach, it was necessary to reduce the total number of trials used due to data volume. In order to do this, only trials in which the correlation coefficient between the EMG-assisted extension moments and RLM extension moments was equal or greater than 0.5 were used (246/560 session 1 trials, table 4-8) and this data was further down sampled to 8 Hz for network development. While this approach may represent the use of the best case data by excluding trials in which correlations were poor, it was felt to be justified in this work examining the potential utility of artificial neural networks. The correlation analysis indicated that only four channels of EMG explained more than 10% of the variance in bone on bone compression, and were subsequently included as inputs for the neural network (table 4-3).

Additionally, spine flexion angle appeared among the most strongly correlated variables and was included as an input to the network. As with the joint moment correlations, none of the input variables exhibited very strong correlations to the output measures (table 4-3). The correlation analysis resulted in five time-varying inputs, four anthropometric measures (participant height, mass, trunk depth and trunk width at the level of the umbilicus) and one gender factor (1 for males, 0 for females) for a total of 10 inputs. Subsequent network training again indicated that implementation of 5 hidden units resulted in errors lower than those predicted with an increased number of hidden units, with a lower number of training cycles required (table 4-4). After network development and simulations, all data was down sampled to 4 Hz for further analysis. A summary of network performance can be found in table 4-5.

Table 4-8: Table indicating the number of trials from each lifting condition chosen from session 1 for development of the artificial neural network used to predict joint forces.

	Starting position for load level 1 lifts								
	right floor	**right waist**	**right shoulder**	**center floor**	**center waist**	**center shoulder**	**left floor**	**left waist**	**left shoulder**
right floor	xxxxxx	xxxxxx	xxxxxx	xxxxxx	xxxxxx	xxxxxx	xxxxxx	xxxxxx	xxxxxx
right waist	**2**	xxxxxx	xxxxxx	xxxxxx	xxxxxx	xxxxxxx	xxxxxx	xxxxxx	xxxxxx
right shoulder	**6**	**7**	xxxxxx	xxxxxx	xxxxxx	xxxxxx	**10**	xxxxxx	xxxxxx
center floor	xxxxxx	xxxxxx	xxxxxx	xxxxxx	xxxxxx	xxxxxx	xxxxxx	xxxxxx	Xxxxxx
center waist	xxxxxx	xxxxxx	xxxxxx	**12**	xxxxxx	xxxxxx	xxxxxx	xxxxxx	xxxxxx
center shoulder	xxxxxx	xxxxxx	xxxxxx	**10**	**11**	xxxxxx	xxxxxx	xxxxxx	xxxxxx
left floor	xxxxxx	xxxxxx	xxxxxx	xxxxxx	xxxxxx	xxxxxx	xxxxxx	xxxxxx	xxxxxx
left waist	xxxxxx	xxxxxx	xxxxxx	xxxxxx	xxxxxx	xxxxxx	**4**	xxxxxx	xxxxxx
left shoulder	**7**	xxxxxx	xxxxxx	xxxxxx	xxxxxx	xxxxxx	**6**	**8**	xxxxxx
	Starting position for load level 2 lifts								
	right floor	**right waist**	**right shoulder**	**center floor**	**center waist**	**center shoulder**	**left floor**	**left waist**	**Left shoulder**
right floor	xxxxxx	xxxxxx	xxxxxx	xxxxxx	xxxxxx	xxxxxx	xxxxxx	xxxxxx	xxxxxx
right waist	**3**	xxxxxx	xxxxxx	xxxxxx	xxxxxx	xxxxxx	xxxxxx	xxxxxx	xxxxxx
right shoulder	**7**	**8**	xxxxxx	xxxxxx	xxxxxx	xxxxxx	**10**	xxxxxx	xxxxxx
center floor	xxxxxx	xxxxxx	xxxxxx	xxxxxx	xxxxxx	xxxxxx	xxxxxx	xxxxxx	xxxxxx
center waist	xxxxxx	xxxxxx	xxxxxx	**9**	xxxxxx	xxxxxx	xxxxxx	xxxxxx	xxxxxx
center shoulder	xxxxxx	xxxxxx	xxxxxx	**10**	**10**	xxxxxx	xxxxxx	xxxxxx	xxxxxx
left floor	xxxxxx	xxxxxx	xxxxxx	xxxxxx	xxxxxx	xxxxxx	xxxxxx	xxxxxx	xxxxxx
left waist	xxxxxx	xxxxxx	xxxxxx	xxxxxx	xxxxxx	xxxxxx	**7**	xxxxxx	xxxxxx
left shoulder	**7**	xxxxxx	xxxxxx	xxxxxx	xxxxxx	xxxxxx	**6**	**9**	xxxxxx
	Single lifts								
	Light calibration		Heavy calibration		Right lateral bend		Left lateral bend		Standing
	35		13		8		9		4

4.4.2.2 Peak Forces

Statistical analysis of the original and simulated source data indicated that the neural network approach significantly underestimated the peak bone on bone forces in all directions ($p < 0.01$), with $p < 0.0001$ for compression (the ranges of differences in peak and average compression are provided in table 4-5), $p = 0.0003$ for anterior shear, $p < 0.0001$ for posterior shear, $p < 0.0001$ for right shear and $p = 0.0106$ for left shear (figure 4-4). The same significant underestimations occurred for the partially novel data, with $p = 0.0002$ for compression, $p = 0.0002$ for anterior shear, $p < 0.0001$ for posterior shear, $p = 0.0001$ for right shear and $p = < 0.001$ for left shear (figure 4-4). Peak left shear force was also significantly ($p = 0.0424$) smaller in males than in females (-286.9±370.9 vs. -496.0±508.9 N). Again, the significant underestimation was also observed when the novel data was presented to the network, with $p = 0.0017$ for compression, $p = 0.0121$ for anterior shear, $p = 0.0142$ for posterior shear, $p = 0.0086$ for right shear and $p = 0.0013$ for left shear (figure 4-4).

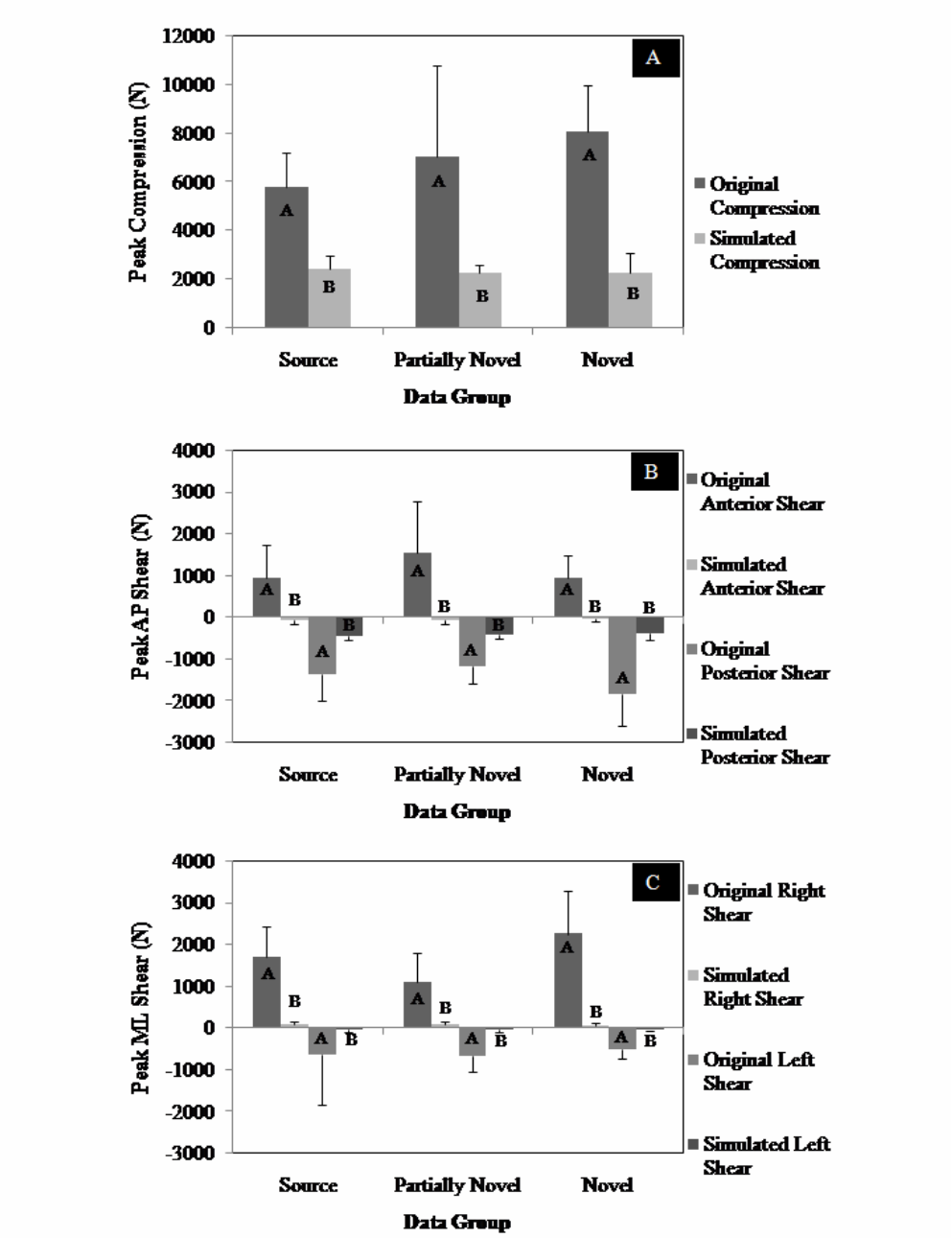

Figure 4-4: (A) Bar plot of average peak compression (+ 1 standard deviation) averaged within a data source group. **(B)** Bar plot of average peak anterior shear (+ 1 standard deviation) and average peak posterior shear (- 1 standard deviation) averaged within a data source group. **(C)** Bar plot of average peak right lateral shear (+ 1 standard deviation) and average peak left lateral shear (- 1 standard deviation) averaged within a data source group. In all plots marked with different letters analysis indicated a significant difference between the rigid link model and artificial neural network predictions.

4.4.2.3 Average and Cumulative Forces

There were no significant differences in the average ML shear ($p = 0.4432$), AP shear ($p = 0.8532$) or compression ($p = 0.7710$) predicted with the EMG-assisted or neural network based approaches for the source data. However, both average AP shear ($p = 0.0031$) and average compression ($p = 0.0363$) were significantly affected by gender, with males showing higher force magnitudes in both cases (-208.8±76.2 vs. -120.1±76.4 N for AP shear and 1097.2±255.0 vs. 834.2±206.5 N for compression). As with the source data, the partially novel data did not display any significant differences between the original and simulated ML shear ($p = 0.9452$), AP shear ($p = 0.4762$) or compression ($p = 0.3918$). AP shear again exhibited significant gender effects, with males exhibiting higher magnitudes of loading than females (-238.2±80.0 vs. -127.7±81.8 N, $p = 0.0160$). When the novel data was examined, it was found that AP shear and compression were not significantly different ($p = 0.2057$ and 0.0676, respectively) while average ML shear was found to be significantly greater in the model based data than in the simulated data, and was of the opposite direction ($p = 0.0158$, table 4-9). Cumulative compression was not found to be significantly affected by gender ($p = 0.0609$, $p = 0.1009$, and $p = 0.0788$ for source, partially novel, and novel data respectively) or method ($p = 0.9557$, $p = 0.7290$ and $p = 0.0788$ for source, partially novel and novel data respectively, figure 4-5).

Table 4-9: The average bone on bone force along each axis for the original (O) and neural network simulated (S) data, separated by gender. Source data was used for training the neural network, while partially novel and novel data was used to test generalization. Standard deviations are in parentheses. Values that displayed gender differences are italicized within a data group. Values that displayed differences between the original and simulated data are bold.

	Source				**Partially Novel**				**Novel**	
Gender	**Male**		**Female**		**Male**		**Female**		**All**	
	O	*S*	*O*	*S*	*O*	*S*	*O*	*S*	*O*	*S*
ML Shear	38.1 (71.7)	34.7 (49.0)	10.5 (64.2)	-16.6 (39.8)	12.5 (44.7)	34.2 (46.7)	10.5 (42.2)	-11.0 (42.8)	**80.6 (57.7)**	**-6.3 (24.4)**
AP Shear	*-244.9 (62.3)*	*-226.7 (63.9)*	*-107.6 (92.4)*	*-132.7 (61.2)*	*-248.8 (89.2)*	*-227.6 (74.1)*	*-128.9 (102.9)*	*-134.4 (79.0)*	-208.7 (76.2)	-149.2 (68.0)
Comp	*1096.8 (294.8)*	*1097.6 (229.1)*	*851.0 (197.6)*	*817.3 (219.7)*	1025.2 (263.4)	1098.8 (280.1)	983.0 (318.0)	794.1 (285.5)	1374.4 (447.3)	850.5 (300.8)

ML – medial/lateral, AP – anterior/posterior, Comp - compression.

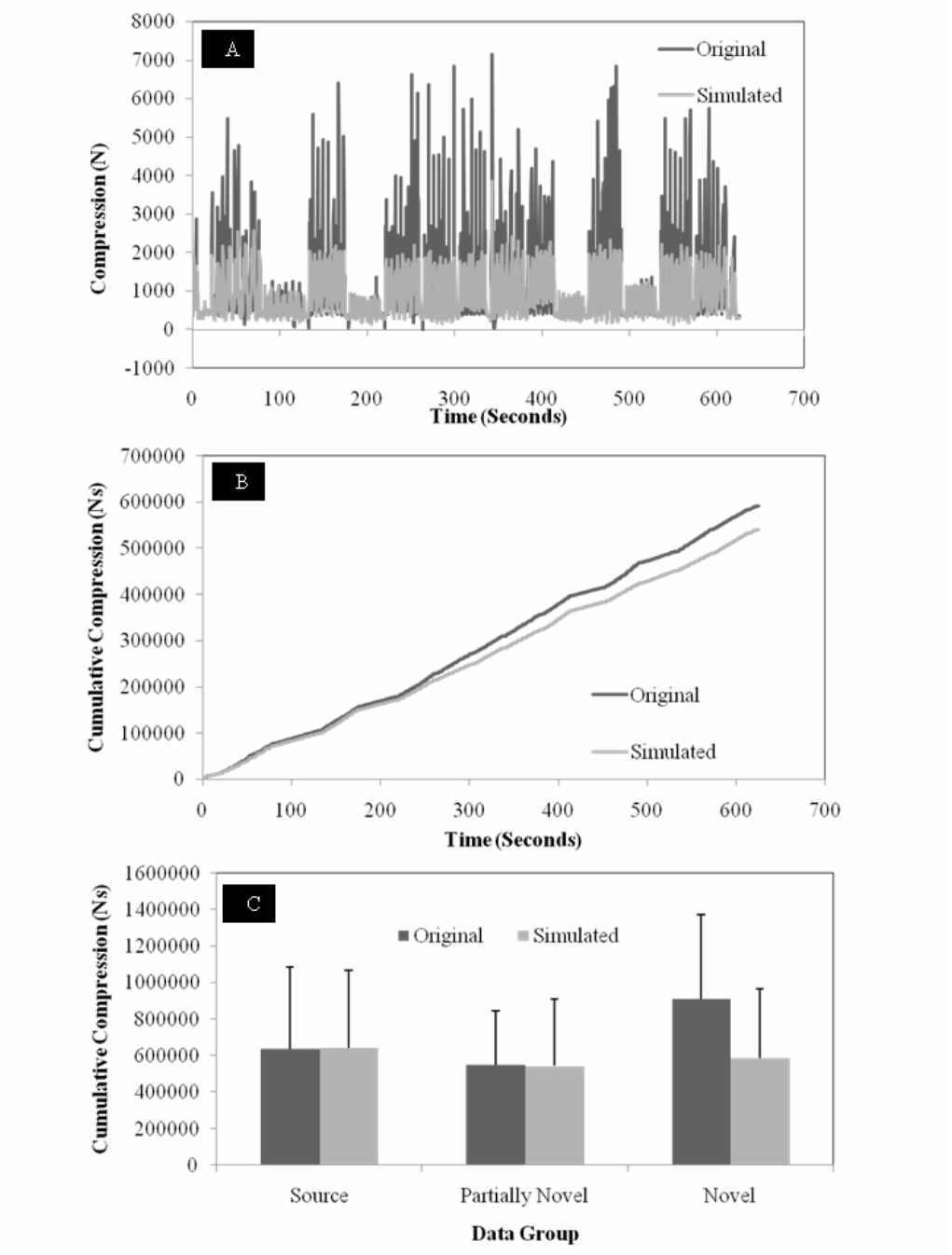

Figure 4-5: (A) Time series of compression (N) as predicted using a rigid link model (denoted as 'original') and an artificial neural network (denoted as 'simulated') obtained from one participant. Note that the data was concatenated for viewing and therefore should not be viewed as continuous lifts. **(B)** The cumulative compression (Ns) as determined through trapezoidal integration of the compression time series in (A). **(C)** Bar plot of average cumulative compression (+ 1 standard deviation) for the source, partially novel and novel data sets. There were no significant differences between the rigid link model (original) and artificial neural network (simulated) based estimates.

4.5 Discussion

The results of this study indicate that simple ANNs can be used in combination with a reduced number of inputs to yield estimates of average and cumulative joint moments and joint forces equivalent to methods that are used in the laboratory (three-dimensional dynamic rigid link modeling and EMG-assisted joint models), that have much greater input demands. These relationships were consistent with increasingly novel inputs to the network, indicating that the network architecture was successful at generalization. This statement must reflect the fact that novel, in the sense employed in this work, related to data that had not been included within the network training sets. It did not reflect novel tasks, such as pulling instead of lifting. Future work should test the robustness of the ANN to respond to such novel tasks. The necessary inputs to drive both of the developed artificial neural networks can be obtained in industry with the LMM, four channels of EMG and dynamic hand loads. The strength of these results lies in the fact that these measures can be obtained with a portable data logger (the LMM is wireless) removing the need to tether a worker to a collection station. Additionally, no kinematics beyond spine angles are required, removing the expense and time intensive labour of video based analysis. These findings highlight the potential of this approach to be implemented in field investigations of cumulative loading of the low back. However, it is clear that the ANNs employed significantly under predicted the peak moments and forces acting on the spine. In situations where the risk of an acute injury is high, application of the ANN approach could lead to a severe under prediction of the risk of injury. Additionally, it should be noted that although the averaged data indicated that the ANN predicted equivalent magnitudes of average and cumulative loads its implementation at the participant level resulted in both over and under estimates of exposure relative to the more complex models. Therefore, although this method appears promising for large scale studies where average exposures are of interest, it does not appear a reasonable approach to

obtain individualized estimates of exposure based upon the range of predicted errors observed for both peak moments and forces.

Comparison of the moment and force estimations of this work with those from similar studies indicates that the under prediction of peak moments and strong prediction of average moments may be an inherent property of the networks employed. Kingma et al. (2001) found that an ANN trained to predict L5/S1 moments under predicted peak moments by 17.3% when compared to a RLM and under predicted an EMG based moment prediction by 37.2%. When the average moments were compared, the ANN under predicted the RLM model by 3.1% and over predicted the EMG based approach by 17.7%. Additionally, examination of the graphical data (pg. 107, figures 6 and 7) provided by Hou et al. (2007) indicates the dynamic recurrent fuzzy neural network also under predicted peak spine loads although peak differences were not quantified. As the neural networks employed here were trained to minimize the error between the target signal (RLM moments or EMG-assisted forces in this work) they did not react to short duration peaks and valleys causing errors in peak estimates, while they strongly reflected the general trends in the training data leading to strong agreement in average and cumulative predictions (figure 4-6). However, other research examining constrained movements, such as repetitive flexion/extension of the elbow at a controlled velocity has found much lower errors between measured and predicted moments (Song and Tong, 2005), while also employing the Matlab Neural Network™ toolbox to train the network based on minimization of the squared error, similar to the approach employed here. While the inputs to obtain joint moments were different (EMG and joint angle in the work of Song and Tong (2005) vs. spine kinematics in this study) it may be that the ability of participants in this study to complete the lifting tasks at any rate and using any technique that they chose induced a larger amount of variability into the relationship between the input variables and moment predictions that cannot be as strongly accounted for in the

network approach employed. Evidence for this variation is found in the low correlation values between all time-varying inputs and the RLM based estimates of joint moment.

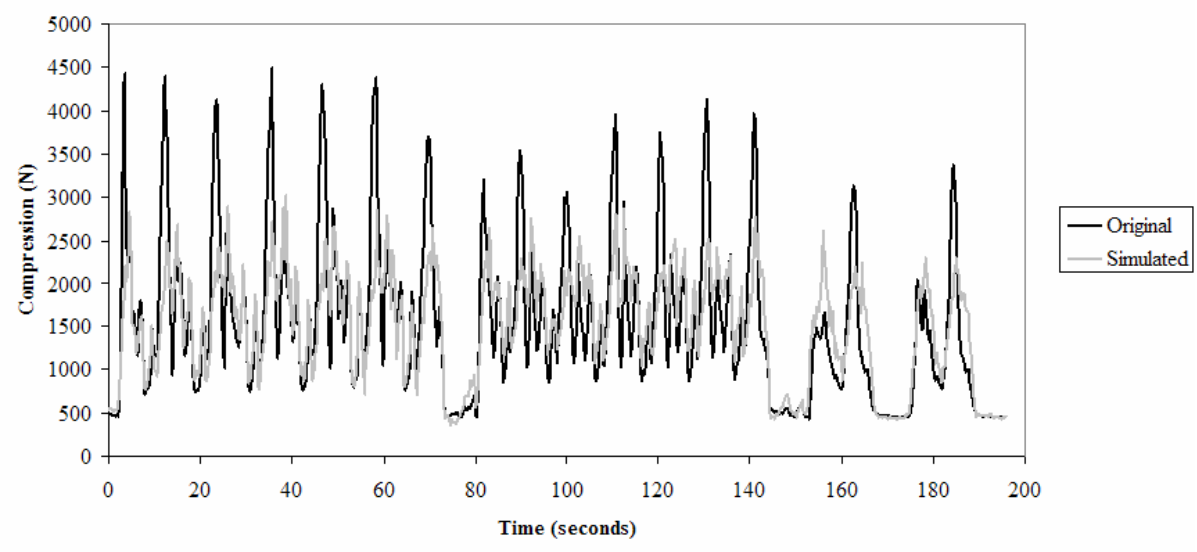

Figure 4-6: Small window of time series compression from one participant, illustrating how the artificial neural network (ANN) predicted compression (grey line) follows the trend of the EMG-assisted predicted compression (black line). Note that although the ANN prediction follows the general shape of the EMG-assisted compression, it does not replicate the peaks.

Interestingly, the insensitivity of network performance while increasing the number of hidden units above 5 is in direct agreement with the work of Nussbaum et al. (Nussbaum *et al.*, 1995) who found that in using a feed forward neural network to predict muscle activations from input joint moments there were no differences in the number of required training cycles while the criterion error was reached in all configurations. Luh et al. (Luh *et al.*, 1999), in estimating elbow joint torque from surface EMG and joint kinematics, also found no improvement in network performance with an

increase in the number of hidden units above 5. The use of simple network architecture is further supported by the conclusions of Sietsma et al. (Sietsma and Dow, 1991) who found in simulated classification problems that smaller networks (with repetitive and useless hidden units removed through pruning) are better able to generalize to new data .

As with all research, this study was subject to several limitations. First, although participants were free to move while completing the lifts, they were limited to lifting only two relatively light loads. While restriction of the loads was intentional to prevent fatigue related changes in the EMG amplitude (Dolan *et al.*, 1995; Potvin and Norman, 1993), it is possible that the inclusion of larger loads may have improved the predictions of the network. However the effects of increasing the load lifted on other predictive models have been dichotomous, where increases in load during symmetric lifting have improved estimates of spinal compression, while decreasing accuracy of compression estimates in asymmetrical lifting (Fathallah *et al.*, 1999).

Additionally, there are a great number of network architectures that exist. While it was a goal of this work to develop simple networks that can be implemented with out high level programming experience, this may not have lead to an optimal network configuration. One characteristic of networks that was not used in this work was that of recurrence, or having data from an earlier time step fed back into the network to provide information on a previous state (as in (Hou *et al.*, 2004a; Hou *et al.*, 2005)). As RLMs employ determinations of angular accelerations and the EMG-force equation underlying the EMG-assisted model employs velocity correction factors, there is clearly a time-dependence within the models. However, the ability to assimilate data from many participants along with the randomization of that data into training, validation and test sets precluded the use of recurrent inputs as it would have been necessary to isolate participant data and maintain the order of the time-series. While this study focused on developing models based upon group data, recurrence in individual models may improve the prediction of peak loads and moments. Another limitation was in

the size of the novel data set, comprised of only two males and three females, one testing session each. Although each testing session was comprised of a large number of lifts and lowers the low participant number prevents comparisons of network simulations between males and females. Future research should expand upon this novel data set by increasing the number of males and females, and also look to include experienced workers. As research indicates that increased lifting experience leads to lower spinal compression loads at lower moment exposure levels (Marras *et al.*, 2006) and that experienced lifters have been shown to take less time to complete a lifting task (Smith *et al.*, 1982) it would be an important assessment of the network to see if altered lifting strategies based upon experience would be reflected in average and cumulative loading predictions.

Despite the limitations, this study represents the first attempt at extending the use of artificial neural networks into determinations of cumulative exposures. The examination of industrially relevant lifting tasks indicates promise for this tool as a means to obtain high quality estimates of time-varying spine loads without the need for extensive data collections. For example, implementation of the artificial neural network described to estimate joint forces requires only the collection of 4 channels of EMG and spine flexion obtained with the lumbar motion monitor in contrast to the full laboratory method which required the collection of ten channels of EMG, all three spine angles as obtained with the lumbar motion monitor along with the force plate data and full marker set-up as required to perform inverse dynamics to obtain joint moments and allow gain setting for implementation of the EMG-assisted model. Additionally, data processing time is drastically reduced from several minutes for a 60 second trial to seconds, which is an additional benefit if large scale implementation is desired. These results are based on the strongest obtained data (highest correlations between the rigid link model and EMG-assisted predictions of extension moment) and therefore represent a best case scenario, and may have been altered with the inclusion of the lower quality trials.

While the neural networks do not appear to predict peak loads well, future work should be conducted to determine the usability of this approach in documenting cumulative exposures, exploiting its potential to predict loading through extended periods of time. Additionally, future work may be targeted at developing alternative networks that are better able to predict peak spine loads which may in turn further improve the ability of the neural networks to predict cumulative load on an individual level as the results of this study are based upon average network performance.

Chapter 5

A comparison of low back kinetic estimates obtained through posture matching, rigid link modeling and an EMG-assisted model.

Robert J. Parkinson, Marty Bezaire and Jack P. Callaghan

Submitted to Applied Ergonomics

5.1 Abstract

The purpose of this study was to examine any errors introduced by a video based posture matching approach (3DMatch) relative to a dynamic, three-dimensional rigid link model (Visual3D) as well as an EMG-assisted model on low back kinetics. Eighty-eight lifting trials composed of various combinations of starting and finishing heights (floor, 0.67, 1.2 m), asymmetry (left, right and center) and mass (7.6 and 9.7 kg) were videotaped while spine postures, ground reaction forces, segment orientations and muscle activity levels were simultaneously documented. Calculations were performed to obtain three-dimensional joint moments (L5/S1) as well as reaction and joint forces. The results indicated that posture matching over predicted the peak, average and cumulative extension moment ($p < 0.0001$ for all variables); however correction factors were developed that reduced these differences. There was no difference between the peak compression estimates obtained with posture matching or the EMG-assisted approaches ($p = 0.7987$), although the posture matching approach over predicted the cumulative ($p < 0.0001$) compressive loading due to a large compressive bias in upright standing. Use of an individualized bias correction eliminated these differences. These results demonstrate that posture matching approaches provide a method to analyze three-dimensional industrial lifting exposures that will predict kinetic values similar to those of a rigid link model and EMG-assisted approach, provided necessary corrections are applied.

Keywords: Spine loading, posture matching, 3DMatch

5.2 Introduction

The collection of motion and electromyographic (EMG) data related to spine loading in industry is difficult as it is restricted by the cost of the collection equipment, environmental constraints, access to employees, tethering of equipment to personnel and the cost of manufacturing interruptions to the company. This has lead researchers to look for less invasive methods to obtain estimates of spinal loading. One approach is to combine video based estimates of posture with rigid link modeling. This is advantageous as workers and tasks can be captured on video in the workplace, providing valuable information regarding task demands and worker performance that would not be obtained in a laboratory mock up. Additionally, video can be preserved indefinitely and analyzed at the researcher's or ergonomists's convenience. These advantages have been reflected in the use of video in both industrial and laboratory settings (Callaghan *et al.*, 2001; Neumann *et al.*, 2001; Daynard *et al.*, 2001; Jager *et al.*, 2000; Norman *et al.*, 1998). A recent survey of the existing literature has found video based posture analysis to be the most commonly employed tool in assessments of cumulative loading (Waters *et al.*, 2006). While video analysis provides a non-invasive and cost effective approach to assess workplace loading, it is not sensitive to individual levels of muscle activation which have been shown to vary based on gender (Marras *et al.*, 2002) and simultaneous mental processing (Davis *et al.*, 2002), despite constant external task demands.

One tool developed to analyze video to estimate low back loading is 3DMatch (University of Waterloo, Waterloo, Canada). The software allows for captured video to be opened into an interactive user interface, which guides the user through the selection of postures that correspond to those of the worker captured on the video. These postures, along with subject anthropometrics and hand forces are combined with a 'hands-down' quasi-dynamic three-dimensional rigid link model (RLM) to predict the external loads and moments acting on the spine (Hogan, 2005; Callaghan *et al.*, 2003). Predicted moments are used in conjunction with a polynomial equation (McGill *et al.*, 1996b)

to adjust for the role of the torso musculature in spinal compression (Callaghan *et al.*, 2003). Muscle based anterior/posterior (AP) shear is based on the implementation of a single muscle equivalent, employing a 6 cm moment arm (McGill and Norman, 1987) and 5.3^0 extensor line of pull. Previous assessments of 3DMatch performance found that when the calculated moments were compared to those from a two-dimensional RLM, 3DMatch underestimated the extension moment in a sagittal symmetric lifting task in both frame-by-frame and cumulative instances, although errors were below 15% (Callaghan *et al.*, 2003). However, 3DMatch predictions of low back kinetics have not been compared to a dynamic three-dimensional RLM, nor have the model based estimates of compression and shear been compared to those obtained from an EMG-assisted spine model. Recently, Sutherland *et al.* (2008) compared the spine kinetics derived from 3DMatch based postures to spine kinetics derived from postures obtained with an eight sensor electromagnetic tracking system. The study employed the same underlying quasi-dynamic three-dimensional model and found strong agreement in cumulative extension moment and compression, although a dynamic comparison was not performed (Sutherland *et al.*, 2008). As early 3DMatch research has indicated potential for this software to become a valuable tool in ergonomic assessments of low back kinetic exposures, this study was conducted to compare 3DMatch based moment predictions to those obtained from a dynamic, three-dimensional RLM. Additionally, it is critical to quantify any differences that may exist between the bone on bone forces obtained with the polynomial and single muscle equivalent approaches employed in 3DMatch and force estimates obtained with an EMG-assisted model that is sensitive to an individual's task performance.

5.3 Methods

5.3.1 Participant Selection

Data for this study was obtained from a larger data set that included full analysis of 10 male and 10 female participants, recruited from the University population. Although 20 participants were involved in data collection, given the large number of trials performed in each session data analysis was limited to 6 males and 6 females (Table 5-1). These participants were chosen in order to ensure one representative trial for each gender, lifting condition and session. No attempt was made to balance the design between the 12 participants. The trials to be analyzed were chosen based on ease of identification of the start and end frames (determined by light trigger in the video) as well as the clarity of the video data. As a result, 88 trials were analyzed as in four lifting conditions only three trials were available due to video quality. Each trial consisted of six continuous lifts and lowers. The study received ethics clearance through the University Office of Research Ethics and participants were required to provide written consent to participate and have had no low back pain for the previous 12 months.

Table 5-1: Average subject height (m), mass (kg) and age (years). Standard deviations are expressed in parentheses.

Gender	Height	Mass	Age
Male	181.8(6.7)	88.3(8.5)	26.2(2.9)
Female	168.0(7.1)	72.5(7.6)	22.3(2.6)

5.3.2 Task Description

In order to replicate industrial conditions participants were asked to perform multiple lifting and lowering trials using an instrumented rig between the floor and shelving located at approximately waist (0.67m) and shoulder heights (1.2m). Participants completed these lifts under two load

conditions (level 1 – 7.6 kg and level 2 – 9.7 kg) and through each combination of directions (right, center, and left). In order to prevent fatigue, participants only completed four trials in which they altered direction, these were moving from the right floor to left shoulder heights under light and heavy conditions, and moving from the left floor to right shoulder heights under light and heavy conditions. It was felt that these lifts would represent a worst case scenario in terms of postural demands. During the lifts, participants were free to perform the lift in any manner as long as they remained on the force plate; technique and lifting speed were not controlled.

5.3.3 Data Collection and Analysis

5.3.3.1 Rigid Link and EMG-assisted models

In order to estimate the forces and moments acting on the spine, a bottom-up, three-dimensional, dynamic RLM was employed. Ground reaction forces and moments were measured at 2048 Hz with a force plate (900mm × 900mm, Model BP900900, Advanced Medical Technology Inc., Watertown, MA, USA) while segment kinematics were determined from infrared light emitting diodes that were affixed on cuffs attached to the lower legs, thighs, and pelvis. Diodes were applied directly over the first and fifth metatarsal bones, heel and dorsum of the foot, as well as the acromion processes to allow for tracking of the trunk and feet. Segment based co-ordinate systems were determined from an upright standing calibration trial in which the medial and lateral malleoli, medial and later epicondyles of the knee (aligned to flexion/extension axis of the joint) and greater trochanter were also identified through placement of diodes. Marker position in three-dimensions was recorded at 32 Hz using an optoelectronic system (Optotrak Certus, Northern Digital Inc, Waterloo, Canada). Marker co-ordinates and voltages recorded from the force plate were input into Visual3D motion analysis software (C-Motion, Inc., Kingston, Canada) where a geometric model of each participant was constructed and inverse dynamic calculations were performed in order to determine forces and

moments at the L5/S1 joint. Visual3D predicted moments and forces were dual pass filtered with a low-pass Butterworth filter (2.5 Hz cut-off).

In addition to the Visual3D approach, an EMG-assisted model was also employed to obtain estimates of bone on bone (joint) compression and bone on bone (joint) shear. Muscle activation levels were recorded from five bilateral trunk muscle sites, including the erector spinae, latissimus dorsi, internal oblique, external oblique and rectus abdominus (Mirka and Marras, 1993) using self-adhesive surface electrodes (Blue Sensor, Medicotest Inc., Ølstykke, Denmark). EMG signals were band pass filtered (10-1000 Hz) and differentially amplified (common mode rejection ratio of 115 dB at 60 Hz, input impedance of 10 GΩ, Model AMT-8, Bortec Biomedical Ltd., Calgary, Canada). In order to allow normalization of EMG levels, maximum voluntary contractions (MVCs) were performed for the extensor musculature through exertions with the participant lying prone with their lower body supported on a table and the upper body hanging. MVCs for the abdominal musculature were obtained through a series of contractions in which the participant attempted to maximally flex, bend and twist about their low back. For the extensor and abdominal exertions resistance was applied manually by the researcher to limit motion. Latissimus dorsi MVCs were performed using a pull-down type contraction where the participant pulled down on a handle that was rigidly fixed to the ceiling. The handle was adjustable to ensure that participants could assume a posture in which their upper arm was abducted and externally rotated 90^0 and their elbow flexed 90^0. All EMG signals were sampled at 2048 Hz and synchronized to the marker and force plate data. Post-collection, raw EMG data was high-pass filtered at 33 Hz to remove contamination from heart rate (Drake and Callaghan, 2006) and the Optotrak system, and notch filtered to remove any 60 Hz contamination (Mello *et al.*, 2007b). This filtered data was then full-wave rectified and low pass-filtered using a low-pass 2.5 Hz cut-off Butterworth filter (Brereton and McGill, 1998). In addition, spine posture was measured

using the Lumbar Motion Monitor (LMM, Biomec Inc., Cleveland, USA), sampled at 32 Hz and dual pass filtered using a 1.5 Hz low pass Butterworth filter (Beach *et al.*, 2006).

The model employed was based upon the work of Granata and Marras (1995a) and includes gender specific anatomy (Jorgensen *et al.*, 2001; Marras *et al.*, 2001) and gender specific passive moments (McGill *et al.*, 1994; Parkinson *et al.*, 2004; Dolan *et al.*, 1994). The EMG-assisted model included nodal points that the erector spinae and latissimus dorsi muscles pass through at the L4 level in order to prevent excessive shear forces from developing when participants near full flexion. The model was scaled based upon gender, participant height and mass as well as trunk dimensions. A model gain trial was performed in which the participant lifted a mass (7.56 or 14.2 kg) from the floor to waist height, and returned it to the ground. This allowed for the determination of a participant and session specific gain value based on the rationale that the predicted muscle moment must be equal in magnitude to the reaction moment. Only the moment about the flexion/extension axis was used for determination of the gain value. The trial (7.56 vs. 14.2 kg) was selected based upon the magnitude of agreement between the measured and predicted traces (r value) for the participant.

5.3.3.2 Video Data and 3DMatch

Video data was collected using a digital video camera (Panasonic Digital Palmcorder, Model PVDV202-K, Matsushita Industrial Electric Company Ltd., Saijo Ehim, Japan) oriented at 90^0 from the sagittal plane with the participant facing forward. Video data was synchronized to the Optotrak collection system using a light source visible in the camera view, which was triggered by a voltage signal generated on initiation of the Optotrak system. All video data was converted to AVI format and reduced to a 5 Hz sample rate from the original 30 Hz (Callaghan *et al.*, 2001). All video files were imported into 3DMatch and posture matched by a single user. Posture match bins included six for trunk flexion/extension, three options for lateral bend, three options for trunk rotation, four bins

for neck flexion/extension and two for neck lateral bend. There were six bins for shoulder flexion, four for shoulder abduction and three bins for elbow flexion (Sutherland *et al.*, 2008). Resulting posture files were combined with dynamic hand loads obtained from force cubes mounted in series with the handles of the load rig (Model MC3A – 500, Advanced Medical Technology Inc., Watertown, MA, USA). The dynamic hand forces were collected at 32 Hz, low pass-filtered using a dual pass Butterworth filter with a cut-off frequency of 1.5 Hz, interpolated and resampled to 5 Hz to match the frequency of the 3DMatch posture data.

The combined posture and force data were used to drive a three-dimensional quasi-static RLM within the 3DMatch software. The RLM produces joint moments which are translated into bone on bone compression using a polynomial equation (McGill *et al.*, 1996b) that employs the moments about all three axes, while AP bone on bone shear is predicted using a single equivalent muscle approach employing a 6 cm moment arm (McGill and Norman, 1987) and 5.3^0 angle of pull.

5.4 Statistical Analysis

A two-way analysis of variance (ANOVA) was used to test for significant method (Visual3D, 3DMatch, EMG-assisted) or gender based differences in peak and cumulative moments as well as the peak and cumulative forces (compression and AP shear). In cases where a significant gender×method interaction was observed the data was assessed using a one-way ANOVA within gender. Where indicated by significant main effects a Tukey's post hoc test was employed to isolate between group differences. All tests with $p<0.05$ were considered significantly different.

5.5 Corrective Factors

In situations where differences between extension moments existed, corrective factors were determined based upon the average error between the variable of interest as determined by 3DMatch

and that predicted with Visual3D (Visual3D was assumed to be the 'gold standard' rigid link modeling approach, equation 5-1). The differences in predicted values were calculated for each trial and then averaged prior to determination of the corrective factors. Once the corrective factor was determined it was multiplied by the 3DMatch predicted value for each trial, and the corrected values were subsequently used in further analysis. The Visual3D approach was chosen to act as the main comparator as the methodology is well established, whereas various EMG-assisted models are in use (McGill and Norman, 1986; van Dieen, 1997; Marras and Granata, 1997b) and subsequently a greater variance in predicted moments and loads would be expected. In cases where there were differences in predicted bone on bone compression, a correction was applied to account for the large bias present in the polynomial approach (McGill *et al.*, 1996b). This correction involved adjusting the polynomial based prediction of compression in upright standing (1068 N in the presence of 0 moments used in 3DMatch) to equal the compression in upright standing predicted by the EMG-assisted method. Focus was given to flexion/extension moment and bone on bone compression as they have been associated with the risk of low back pain and injury (Marras *et al.*, 1995; Norman *et al.*, 1998; Seidler *et al.*, 2001; Seidler *et al.*, 2003), although this principle of corrective factors could have been applied to all variables.

$$Corrective\ Factor = \frac{1}{\left(1 + \frac{1}{88}\sum_{i=1}^{88}\left[\frac{3DMatch_i - Visual3D_i}{3DMatch_i}\right]\right)} \quad \textbf{(5-1)}$$

5.6 Results

5.6.1 Peak Moments

Statistical analysis indicated that there was a significant effect of the method employed in determining peak extension moment ($p<0.0001$). It was found that 3DMatch predicted significantly greater peak extension moments than either the EMG-assisted or Visual3D approaches, which were also significantly different (figure 5-1a). Application of the correction factor (0.62 based upon equation 5-1) eliminated the significant difference between the Visual3D and 3DMatch methods and resulted in a change from a 53.2% average overestimate to a 4.8% average underestimate. There were no significant interactions ($p = 0.4072$) or gender effects ($p = 0.1984$). 3DMatch predicted significantly lower positive (right) lateral bend moments than either the EMG-assisted or Visual3D methods (figure 5-1b, $p < 0.0001$). Neither the gender effects ($p = 0.2374$) nor the interaction were statistically significant ($p = 0.6160$). However, a significant interaction was found for negative (left) lateral bend ($p < 0.0001$). Examination of within gender effects indicated that for males there was a significant method effect ($P < 0.0001$), with 3DMatch predicting lower bending moments than either Visual3D or EMG-assisted approaches, which were significantly different from each other. For the females, 3DMatch predicted lower moments than the EMG assisted approach, but did not differ from the Visual3D method (figure 5-1c). Peak right and left twisting moments were found to be significantly different depending upon the method of determination ($p < 0.0001$), with no interaction ($p = 0.1741$ (right) and $p = 0.6613$ (left)) or gender effects ($p = 0.3755$ (right) and $p = 0.2730$ (left)). For left and right twist, the EMG-assisted and Visual3D approaches predicted moments significantly larger than 3DMatch, but were not significantly different from each other.

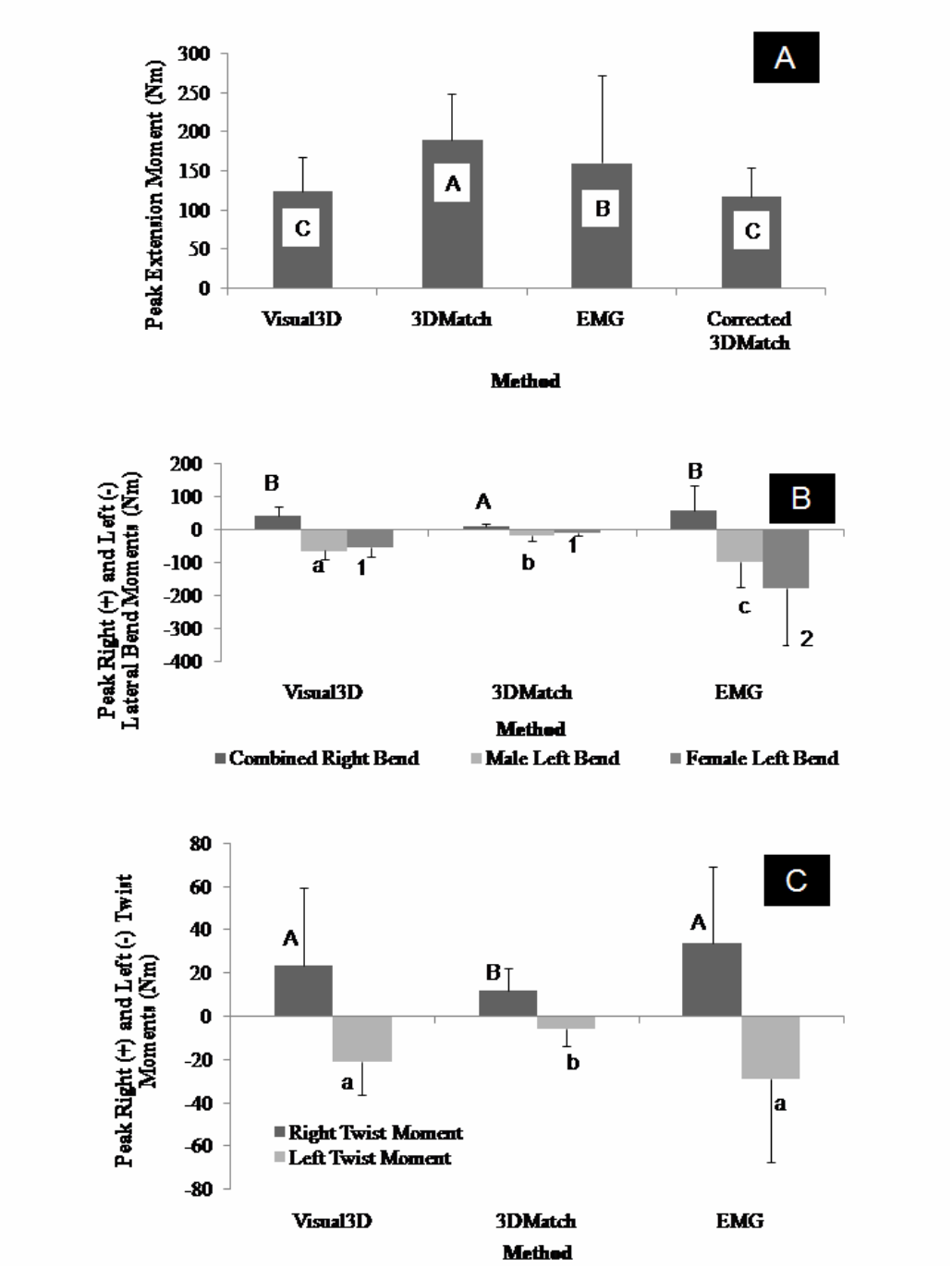

Figure 5-1: (A) Bar plot of average (+ 1 standard deviation) peak extension moment (Nm). **(B)** Bar plot of average (+ 1 standard deviation) peak lateral bend moment (Nm). **(C)** Bar plot of average (+ 1 standard deviation) peak axial twist moment (Nm). Bars denoted by the same capital or lowercase letter are not significantly different when compared within a direction.

5.6.2 Cumulative Moments

A significant gender×method interaction was found for cumulative extension moment ($p = 0.0054$). For males, a significant method effect was observed ($p<0.0001$), with the 3DMatch and RLM approaches (which did not differ) predicting significantly greater cumulative moments than the EMG-assisted approach (figure 5-2). For females, a significant method effect was also observed ($p < 0.0001$) where 3DMatch predicted significantly greater moments than either the Visual3D or EMG-assisted approach while the Visual3D method predicted significantly greater cumulative moment exposure than the EMG-assisted method. Although males did not exhibit statistically significant differences between the Visual3D and 3DMatch approach in predicting cumulative moment, a corrective factor of 0.836 was found. Application of this corrective factor resulted in a reduction in average error from 19.65 to 0.03%. For females, a corrective factor of 0.518 was found and applied, successfully eliminating the significant difference between the 3DMatch and Visual3D approaches (figure 5-2), with the percentage difference decreased from 92.92 to 0.07%.

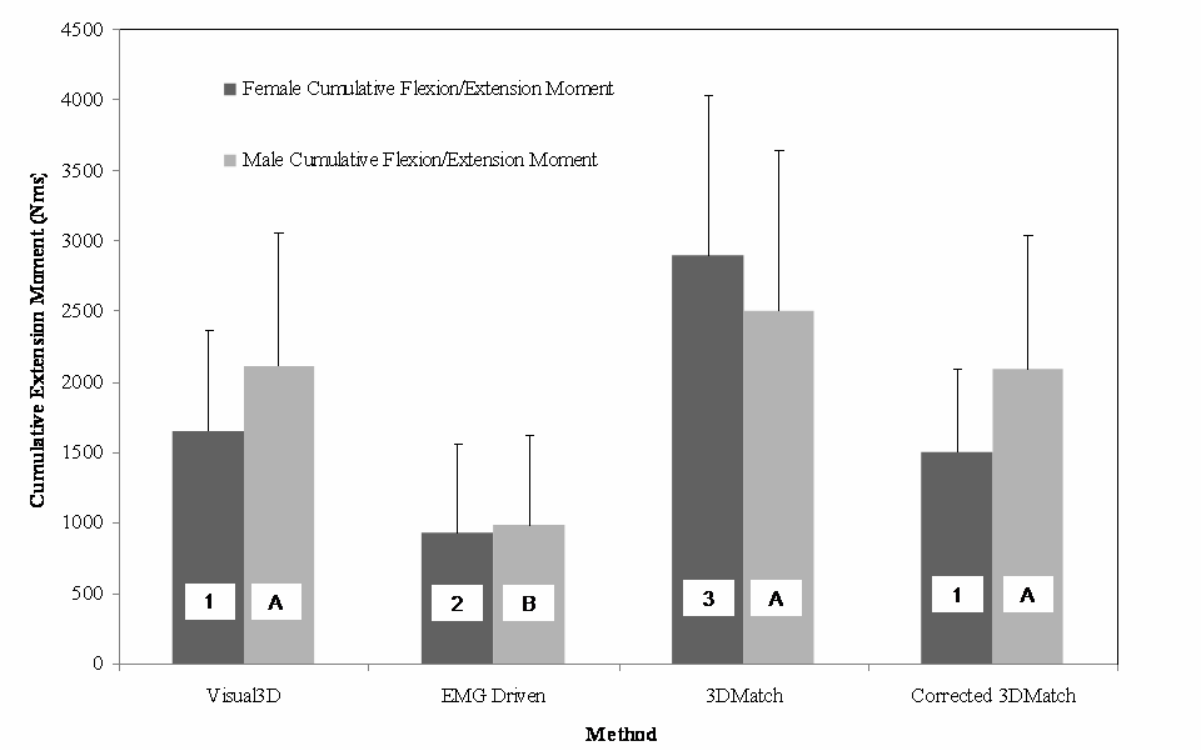

Figure 5-2: Bar plot of average (+ 1 standard deviation) cumulative extension moment (Nms). Bars denoted by the same letter are not significantly different for males, while bars denoted by the same number are not significantly different for females.

A significant gender×method interaction was also found for cumulative ($p = 0.0071$) and average ($p = 0.0125$) lateral bend moment. Subsequent analysis of method effects within gender revealed no significant differences in cumulative ($p = 0.6257$) lateral bend moment for males, regardless of the method of determination. However, cumulative lateral bend moment predictions were significantly different dependent upon the method used for females ($p < 0.0001$). Post hoc analysis revealed that 3DMatch predicted significantly different cumulative lateral bend moments (73.5±95.9 Nms, right) than the Visual3D (-146.4±333.5 Nms, left) or EMG-assisted (-443.3±615.5 Nms, left) approaches.

No gender×method interaction was found for cumulative axial twist ($p = 0.9627$), however significant method and gender effects were observed ($p = 0.0067$ and $p = 0.0003$, respectively). Post hoc analysis indicated that the 3DMatch and EMG-assisted approaches predicted cumulative axial twist moments were not significantly different and shared the same directionality (figure 5-3a). In contrast, the Visual3D approach predicted significantly lower cumulative moments with the opposite polarity. Analysis of gender effects indicated that significantly higher cumulative axial twist moments were found for males than females ($p = 0.0067$, figure 5-3b).

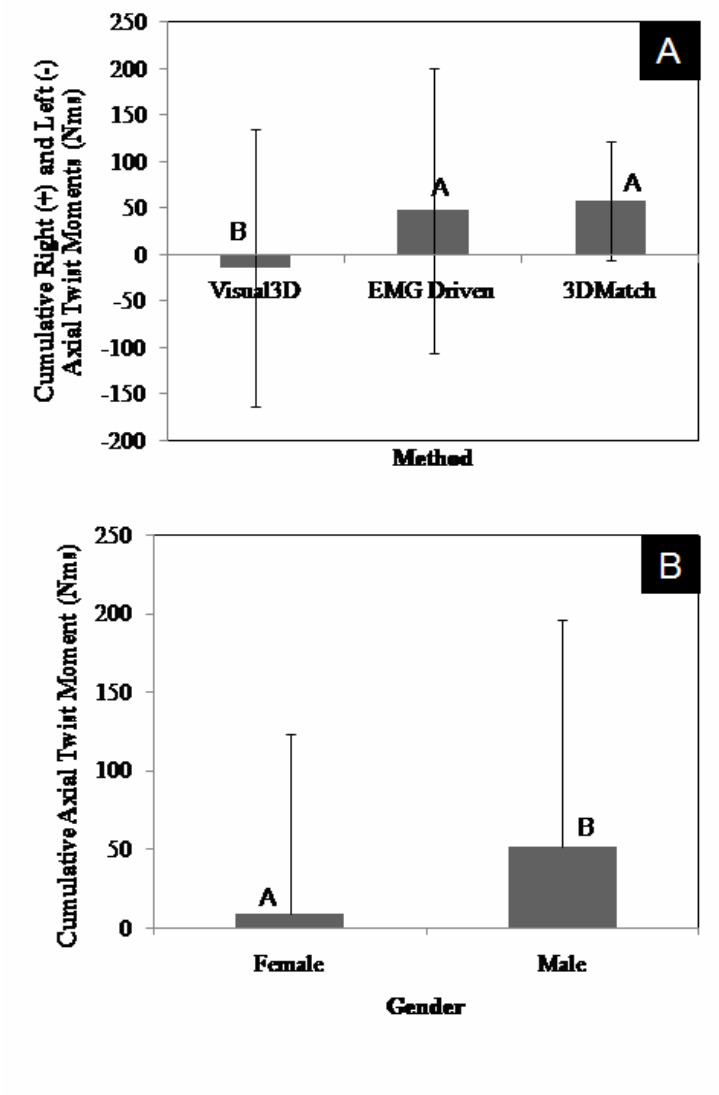

Figure 5-3: (A) Bar plot of average (± 1 standard deviation) cumulative axial twist moment (Nms) isolated by method. **(B)** Bar plot of average (+ 1 standard deviation) cumulative axial twist moment (Nms) isolated by gender. Bars denoted by the same letter are not significantly different.

5.6.3 Reaction Compression and AP Shear

As the EMG-assisted model does not predict reaction forces, only the Visual3D and 3DMatch approaches are included in these results. A significant gender×method interaction was found for reaction compression ($p = 0.0480$), although males ($p < 0.0001$) and females ($p < 0.0001$) both

exhibited significant method effects with Visual3D predicting higher reaction compression than 3DMatch for both genders (figure 5-4). In contrast there were no significant interaction ($p = 0.4313$), gender ($p = 0.8653$) or method ($p = 0.4284$) effects for AP shear.

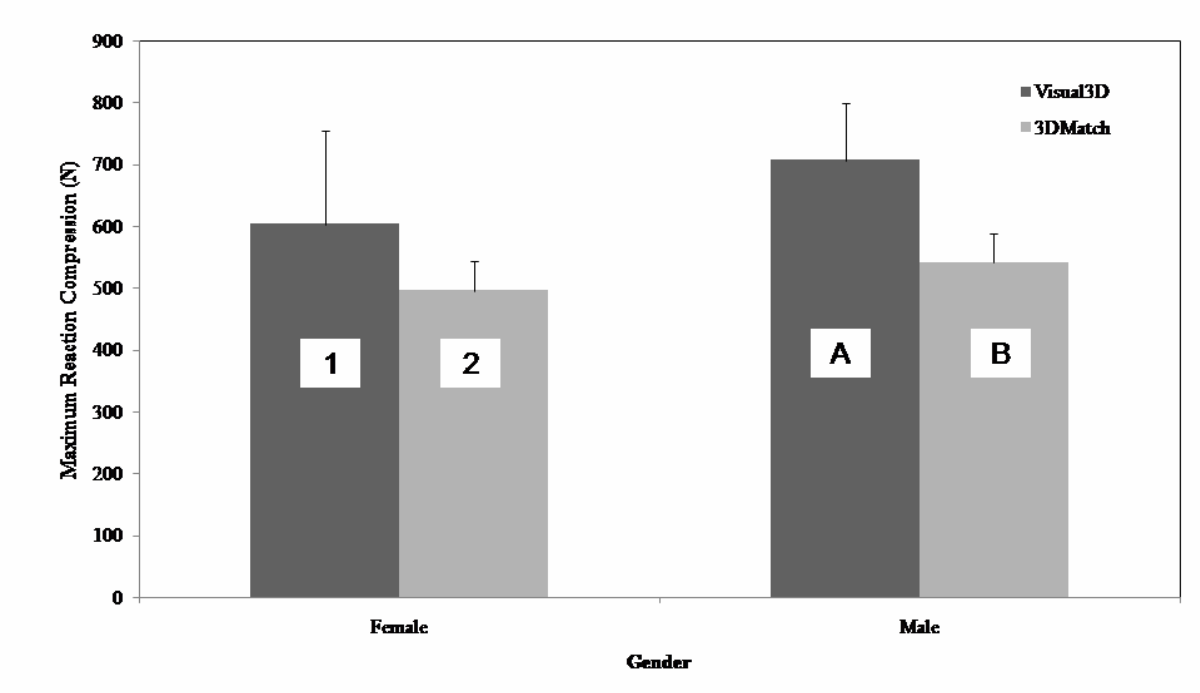

Figure 5-4: Bar plot of average (+ 1 standard deviation) reaction compression (N). Bars denoted by the same letter are not significantly different for males, while bars denoted by the same number are not significantly different for females.

5.6.4 Bone on Bone Forces

The peak bone on bone compression predicted using 3DMatch (3769.2±1216.6 N) and the EMG-assisted (3703.0±2118.8 N) approaches were not found to be significantly affected by gender ($p = 0.1308$) or method ($p = 0.7987$) or gender×method interaction ($p = 0.2376$). Cumulative compression also exhibited no significant interaction ($p = 0.1268$) or gender ($p = 0.3099$) effects, with method significantly altering the determination of cumulative compression ($p < 0.0001$). The 3DMatch method predicted significantly greater cumulative compression than the EMG-assisted

approach, however when the individualized compressive bias correction was applied, this difference was decreased to non-significant levels (figure 5-5), over-estimation reduced from an average percentage error of 73.05 to 12.96%). Peak posterior shear forces were found to be significantly different dependent on the method of determination (table 5-2, $p < 0.0001$), while unaffected by gender ($p = 0.6633$) or gender×method interaction ($p = 0.8534$). Peak anterior shear force exhibited a significant gender×method ($p = 0.0065$), where male predictions were not affected by method ($p = 0.0944$) while female predictions were (table 5-2, $p = 0.0016$).

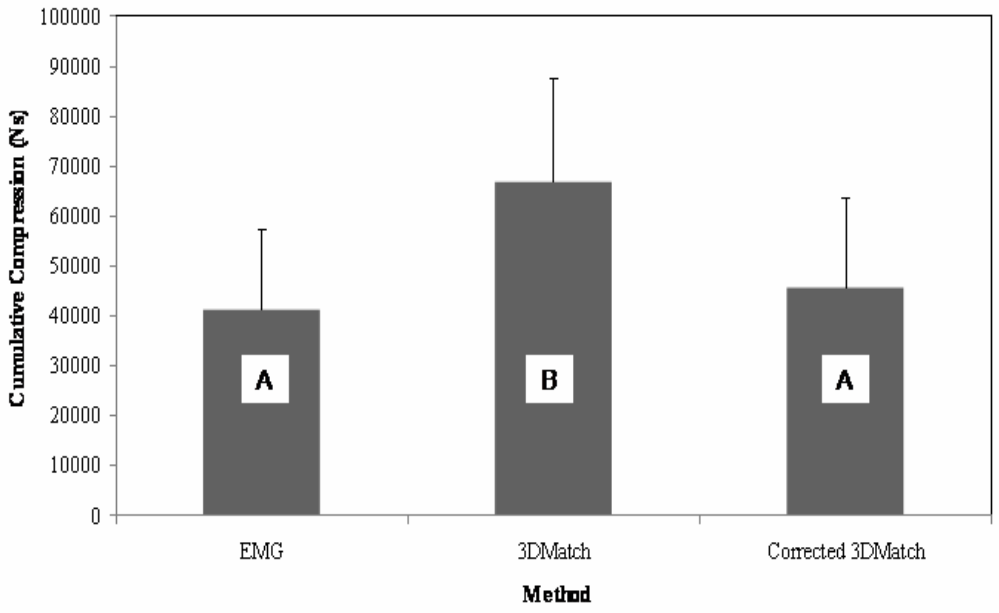

Figure 5-5: Bar plot of average (+ 1 standard deviation) cumulative compression (Ns). Bars denoted by the same letter are not significantly different.

Table 5-2: Average peak shear forces (±1 standard deviation) as predicted using EMG-assisted and 3DMatch approaches. Significant differences existed between posterior shear force and female anterior shear force. Values of male anterior shear force were not significantly different.

Method	Posterior Shear Force (N)	Anterior Shear Force (N)	
		Female	Male
EMG-assisted	735.0±435.1	669.4±1078.0	186.1±274.8
3DMatch	165.43±90.0	124.1±29.5	115.7±24.7

5.6.5 Correlation Values

As each trial consisted of 6 lifts and 6 lowers (figure 5-6), it was possible to determine the correlation coefficient (r) between the various methods of variable estimation. In terms of flexion/extension joint moment prediction, the greatest agreement was found between the Visual3D and 3DMatch methods, although correlations between all methods exceeded 0.6 (figure 5-7). Much lower correlations were observed for lateral bend and axial twist moments, regardless of the methods used. In terms of force, the lowest correlations were observed for reaction compression and bone on bone AP shear (table 5-3). Reaction AP shear and bone on bone compression both exhibited correlation coefficients greater than 0.5.

Table 5-3: Minimum, maximum, average and standard deviation of correlation coefficients for reaction and bone on bone forces. Reaction force comparisons were between 3DMatch and Visual3D methods, while bones on bone comparisons were between 3DMatch and EMG-assisted methods.

	Reaction Forces		Bone on Bone Forces	
	Compression (N)	AP Shear (N)	Compression (N)	AP Shear (N)
Minimum	-0.435	-0.518	-0.038	-0.739
Maximum	0.939	0.962	0.875	0.833
Average	0.243	0.577	0.541	0.193
Standard Deviation	0.421	0.343	0.208	0.442

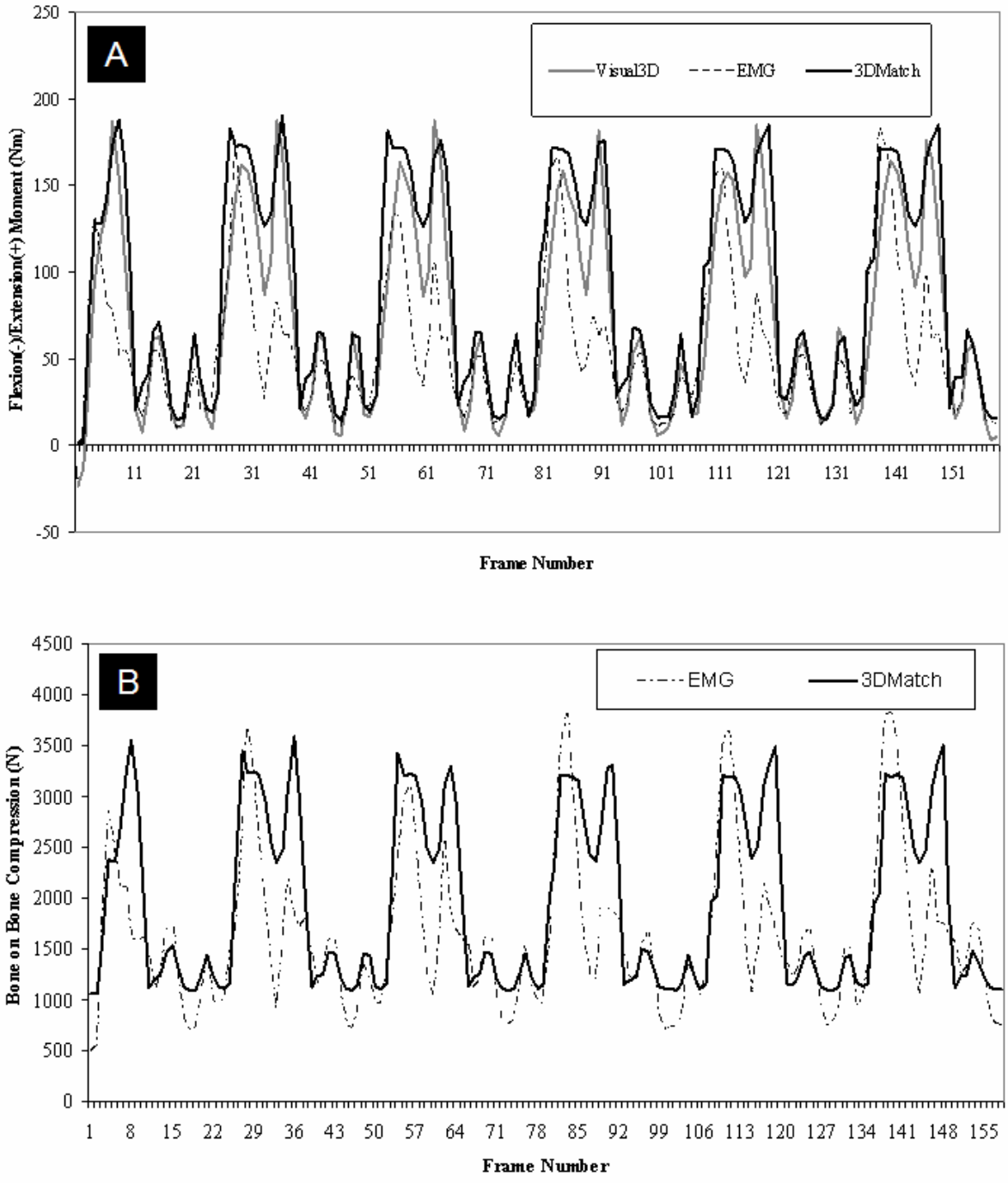

Figure 5-6: (A) Time series of flexion/extension moment (Nm) as determined using a rigid link model (Visual3D, grey line), EMG-assisted model (dashed black line) and 3DMatch (solid black line). **(B)** Time series of compression (N) as determined using an EMG-assisted model (dashed black line) and 3DMatch (solid black line). Note that both (A) and (B) are from the same trial.

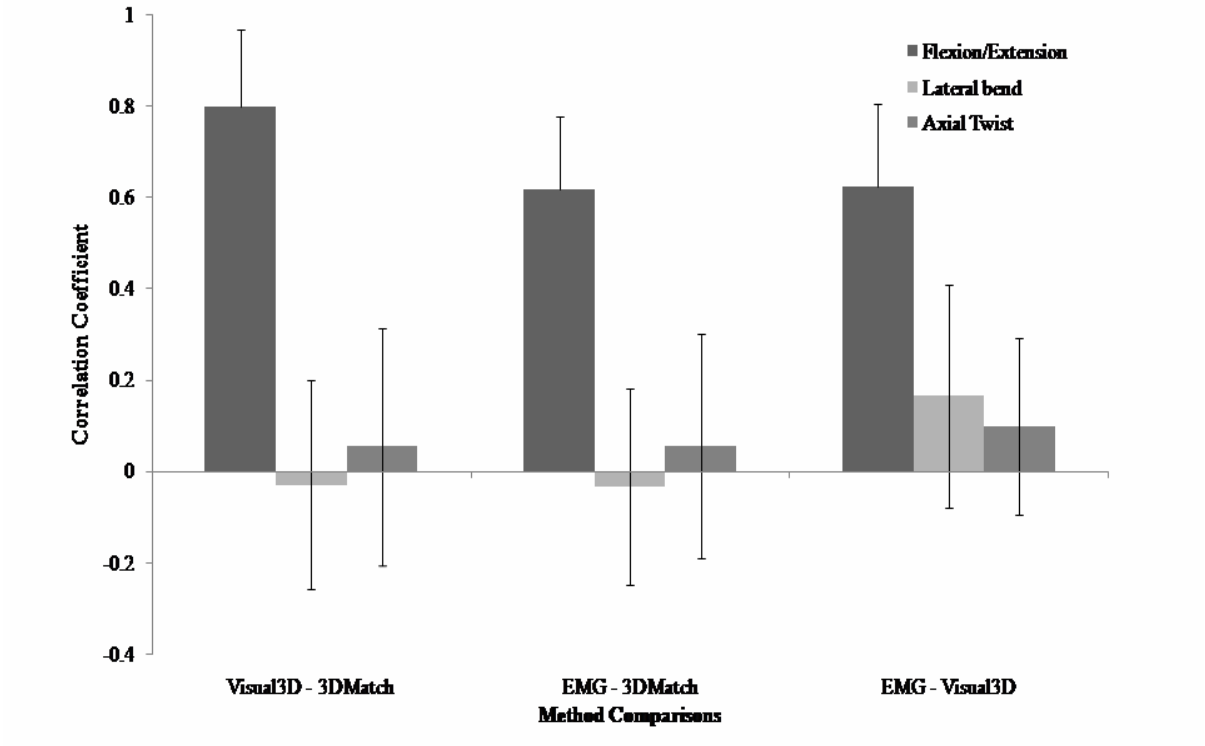

Figure 5-7: Bar plot of average (+/- 1 standard deviation) correlation coefficient across comparison and moment axis.

5.7 Discussion

The results of this study indicate that 3DMatch is a viable tool for determining kinetic exposures of the low back, although corrective factors need to be implemented. In the case of peak, average and cumulative flexion/extension moment, it is clear that the uncorrected 3DMatch approach will over estimate the exposure level, subsequently leading to a conservative determination of risk level. Several factors may have contributed to the observed differences in peak extension moment. 3DMatch employs a quasi-dynamic model that includes dynamic hand loads while ignoring the inertial components of the segments. The error associated with this approach varies widely in the literature, ranging from overestimating fully dynamic peak extension moments by as much as 25% (McGill and Norman, 1985) to underestimates of 3% (Lindbeck and Arborelius, 1991). Additionally,

3DMatch implements a hands down modeling approach, which has been shown to lead to over estimates in average extension moment of 3.6%, with overestimates in peak moment of 10.9% when compared to a bottom-up approach (de Looze *et al.*, 1992a), as employed in the RLM method used here. While the impact of these potential sources of error has not been quantified in this study, the application of a simple correction factor can reduce the differences in moment predictions to non-significant levels, leading to much improved estimates of joint moment exposure. Female differences required lower correction values, reflecting a greater over estimation in moment magnitude by 3DMatch than determined with the RLM approach. Some portion of this difference may be due to the anthropometric model underlying 3DMatch, which incorporates gender specific segment mass calculations while the determination of segment length and center of mass locations are based upon height and are not corrected for gender differences. In average and cumulative flexion/extension moments, the EMG-assisted approach yielded the lowest predictions. Examination of the moment traces indicates large drops in EMG-assisted predictions when participants are fully flexed. This occurrence is likely due to a drop in muscular activity near full flexion (Callaghan and Dunk, 2002; Dickey *et al.*, 2003). Additionally, in lifting conditions where participants chose to perform the task using more of a twisting motion to maneuver the load around the shelving as opposed to pulling the load closer to themselves (when lifting from the waist height to shoulder height) the EMG-assisted approach predicted much lower extension moments than the other methods. While differences in moment predictions about the other axes (lateral bend and twist) were also observed, the moment magnitudes were small and therefore corrective factors are not likely to reflect meaningful biological differences. The observed correlation coefficients were much higher for flexion/extension than for other axes, although they indicated that time-variations in the various predictions were not consistent between methods. This result is not surprising when the number of differences in data collection and

signal processing are considered (such as variations in filter cut-offs, down sampling to match sample rates, etc.).

In terms of predicted loads, it appears that where peak compression is of interest 3DMatch predicts values equal to those predicted with a more detailed anatomical EMG-assisted approach. As 3DMatch employs a polynomial derived from predictions made using an EMG-assisted approach (McGill *et al.*, 1996b) this would be the expected outcome, however the EMG-assisted model used to determine the polynomial was not the same as the EMG-assisted model employed in this study. The consistency of results supports not only the use of 3DMatch in determining peak compressive forces, but also provides an indirect means of validating the equivalence of two different EMG-assisted approaches. For this work, the specific EMG assisted approach was selected due to its ability to account for gender, however a large variety of models exist so caution should be extended to not treat this particular model as a 'gold standard' in predicting joint loads.

When 3DMatch is used to predict loads over time (either as an average or cumulative approach) it greatly overestimates the loading. This is a result of the large bias in upright standing, which overestimated the predicted upright standing compression in this study by an average of 569 N. Removal of this bias (which could be determined for an individual as the difference between 3DMatch predicted compression in upright stand and an estimate of upper body mass obtained through anthropometrics) resulted in large decreases in this overestimation, eliminating any significant differences. Peak AP shear loads were shown to be much higher when employing the EMG-assisted approach than 3DMatch, likely due to instances of greater muscle activation translating into greater force exposure. As 3DMatch does not account for individual task performance through muscle activation it does not predict these instances of greater loading. The higher instances of loading with the EMG-assisted approach are also reflected in greater average shear loads. Additionally, 3DMatch employs a constant muscular angle of pull (5.3^0) regardless of gender or

posture. Anatomical differences and flexion of the spine during lifting will alter this angle of pull and may lead to altered predictions of shear. One final contributor to the differences in shear may be the binning method employed in 3DMatch, which assigns a segment angle value equal to the mid-point of the posture bin. For example, if the 15-45^0 trunk flexion bin is selected, the trunk angle would be assigned a value of 30^0, regardless if the actual angle was 16 or 44^0. In comparison, the EMG-assisted approach would incorporate the measured angle and would not be subject to the effects of binning. This limitation has been discussed previously (Sutherland *et al.*, 2008).

While this study presents a first attempt at examining the quality of 3DMatch predictions of joint moments (relative to a fully dynamic, three-dimensional bottom-up rigid link model) and joint loads (relative to a gender specific scalable EMG-assisted model) it is subject to several limitations. First, it is not a true repeated measures design. As trials were chosen from a larger research study based upon the quality of video data, the participants were not represented in equal numbers. Due to the comparative nature of the study, with each method within each trial being obtained from one participant, it was not felt that this would alter the observed relationships. Additionally, only two loads were employed, both of relatively low magnitude. These loads were chosen to allow examination of multiple load levels without leading to muscular fatigue, due to the large number of lifts involved for each participant. While larger load levels may improve the generalization of the results, it is reasonable to expect improved agreement in the cumulative and average compression measures as load levels would greatly exceed those in upright standing, reducing the relative contribution of the bias of the polynomial approach. One additional limitation is the comparison of force predictions to only one EMG-assisted approach. While the EMG-assisted approach used here has been well developed (Granata and Marras, 1995a; Marras and Sommerich, 1991a), several others exist (McGill and Norman, 1986; McGill, 1992a; van Dieen, 1997) which incorporate different anatomy, as well as length and velocity modulators. Therefore the EMG-assisted approach employed

for this work should not be treated as a 'gold standard' of comparison, and caution should be employed when relating these findings to other joint models. Finally, the joint model and RLM calculations were performed about the L5/S1 joint, not L4/L5 like 3DMatch. Based upon the anatomy, there is an expectation of slightly higher loads at L5/S1 due to additional mass above the joint location, however this difference would likely be compensated for by the increased forward tilt of L5/S1 relative to L4/L5, which would result in a lower amount of the vertical load being projected onto the compressive axis. However, this would increase the amount of shear loading and therefore the absolute magnitude of shear values presented should be interpreted with caution.

Based on this research 3DMatch has the potential to be a valuable ergonomic tool in industry, where video is often the most realistically useable tool. In its current form, 3DMatch overestimates extension moments and cumulative compression. However, the errors in variable determination are easily corrected with the developed correction factors. The correction factors are designed to correct for the average amount of error between the posture matching and inverse dynamics based estimates of error should be implemented in studies examining multiple workers. However, caution should be extended that they represent the average error and when applied to an individual prediction of loading may alter the loading predictions unpredictably if another measure (such as RLM based estimations of moments) is not present to ensure correction is necessary. It is worth noting that these correction factors are based upon the industrial situation for which 3DMatch was created, that being lifting. While it is unknown how these corrections may be altered in situations of altered loading exposures, for example one handed pushing, it is felt that implementation of these factors would still result in better predictions of loading when applied to grouped data than currently available. In contrast, the correction approach developed for predictions of cumulative compression should always be applied, as the bias is always present. Additionally, the similarity of the 3DMatch based predictions of peak compression those using the more sophisticated EMG-assisted model supports the use of the

polynomial approach in estimating compression from joint moments and provides evidence of strong agreement between different EMG-assisted approaches in their ability to predict peak loads. Future work should be conducted to determine if these relationships will be consistent when the tool is used in industry, in particular examining the consistency of the corrective factors to ensure that the best possible estimates of exposure are being used in any determination of injury risk.

Chapter 6

The role of dynamic flexion in spine injury is altered by increasing dynamic load magnitude.

Robert J. Parkinson and Jack P. Callaghan

Submitted to Clinical Biomechanics

6.1 Abstract

Evidence indicates that the loads and postures to which an individual is exposed are related to their risk of reporting low back pain or incurring a spine injury. *In-vitro* research has shown that cyclic flexion under static compressive loads can lead to disc herniation, while repetitive compression in neutral or flexed postures leads to vertebral failure. However, no research has examined the likelihood of altering injury site (disc vs. bone) when dynamic load exposures are varied concurrently with cyclic flexion. In order to address this issue, 50 porcine cervical spinal units were assigned to one of five groups based on peak normalized loads of 10, 30, 50, 70 and 90% of the unit's predicted tolerance. Specimens underwent passive range of motion tests to determine individual range of motion. Once individualized loads and angles were determined, specimens were cyclically compressed and flexed based on profiles obtained from a floor to waist height lift, until failure occurred or 12 hours elapsed. Upon failure specimens were dissected to identify injury site, and cumulative exposures sustained to failure were calculated. Disc injury was not observed when peak loads exceeded 30% of the tolerance, while they occurred with increasing frequency when decreasing from the 30 and 10% groups. Those specimens exhibiting disc injury tolerated significantly greater number of cycles to failure ($p < 0.0001$), greater cumulative compression ($p < 0.001$), shear ($p < 0.001$) and angular excursion ($p < 0.001$). These results indicate that people exposed to greater levels of load, in the presence of repetitive flexion, are more likely to exhibit vertebral fracture. In contrast,

the likelihood of disc injury in the presence of repetitive flexion increases as peak load levels decrease.

Keywords: Spine, posture, load, fracture, herniation

6.2 Introduction

Evidence has shown that spinal injury and reporting of low back pain may be due to accumulated load (Kumar, 1990; Norman *et al.*, 1998; Seidler *et al.*, 2001; Seidler *et al.*, 2003), and therefore research has been conducted to understand injuries due to cyclic loading. In 1983, Liu et al. exposed spinal units to cyclic compressive loads shaped with a sine waveform for up to 10,000 cycles, concluding that specimens showing an abrupt increase in displacement had developed a fracture within the vertebrae (Liu *et al.*, 1983). Fracture of the vertebral bone was also the injury mechanism observed in 16 of 17 cyclically compressed spinal units in the work of Hansson et al. (1987) and 52 of the 70 spinal units loaded by Brinckmann et al. (1988). These conclusions are supported by more recent research which has implemented physiologic loading profiles, also showing that cyclic repetitive compression leads to vertebral fracture (Parkinson and Callaghan, 2007b).

While this evidence implicates repetitive compression in vertebral fracture, it has focused on neutral postures. Additional research has shown that flexion significantly reduced the compressive strength of the spinal unit when compared to the neutral posture, 32-47% depending on the prior loading history (Gunning *et al.*, 2001). More recently, cadaveric units were tested for their resistance to loading while in one of three postures based on trunk flexion of 0, 22.5 and 45^0 (Gallagher *et al.*, 2005). Spinal units were cyclically compressed at load rates and magnitudes based on predictions of loading at each of the three fixed torso angles while holding a 9 kg load. It was found that loading in

a flexed posture resulted in a significantly lower tolerance to compression, with specimens most flexed lasting only 263 cycles compared to 3257 cycles for those moderately flexed and 8253 cycles for those loaded while in a neutral posture (Gallagher *et al.*, 2005). Injury assessment of the vertebrae after loading found failure typically occurred in the endplate, regardless of posture. The morphology of the injury appeared posture dependent, with neutral postures resulting in endplate depression with no macroscopic disruption, while clear fractures occurred with joint flexion (Gallagher *et al.*, 2005). While these studies indicate a role of posture in modifying vertebral tolerance to compression, injury occurred in the vertebral bone and endplates. Therefore, static postural changes may modify the likelihood of injury, but they do not appear to change the site of occurrence.

In 2001, Callaghan and McGill extended the study of postural effects on the injury mechanisms of the spine through the application of a controlled dynamic kinematic profile. Each specimen was assigned one of three low-level compressive magnitudes (260, 867 or 1472 N) and subjected to cyclic flexion. It was found that intervertebral disc herniation could be induced with low levels of compression through high cycle numbers (Callaghan and McGill, 2001). Specimens exposed to the lowest magnitude of compression did not display any herniations, regardless of the number of applied cycles.

While this study demonstrated that dynamic application of postural changes can lead to injury in the intervertebral disc, damage occurred under the application of static compression. As other work has shown that exposure to higher levels of acute or repetitive compression in neutral postures leads to failure in the endplate and underlying vertebral bone, it remains unknown how the spine may become injured with concurrent dynamic applied loads and postures. Based on the evidence from static postural tests, it would appear that vertebral fracture occurs when the spine is exposed to excessive load, regardless of posture. However, if the load is not of sufficient magnitude to lead to bone or endplate failure (as in Callaghan and McGill (2001)) injury may be induced in the

intervertebral disc in the presence of concurrent flexion. As this relationship has not yet been quantified, the purpose of this work was to examine the role of concurrent dynamic motion and loading in determining injury risk and location.

6.3 Methods

6.3.1 Specimen Preparation

Fifty cervical Functional Spinal Units (FSU, C3/4 and C5/6) were isolated from porcine spines. These adjacent spinal levels have been previously shown to be equivalent in endplate area, bone mineral content and compressive strength (Parkinson *et al.*, 2005). Spines were obtained frozen and allowed to thaw prior to dissection. Surrounding musculature was removed in order to isolate the osteoligamentous segment, consisting of two vertebrae, the intervertebral disc and all associated ligaments. The exposed endplates of the superior and inferior vertebrae were measured along the midline in the anterior-posterior (A) and medial-lateral (B) directions allowing calculation of endplate area ($\pi/4 \times A \times B$), and averaging of the resultant areas. This average represented the area of the FSU and was used to predict the compressive tolerance of the spinal unit without destructive testing (Parkinson *et al.*, 2005), allowing for normalization of the peak loads.

Prior to mounting, the anterior processes and exposed facets were trimmed to ensure that the endplates were responsible for load carriage across the segment. Screws were inserted into the anterior processes and 19 gauge wires were looped around the lamina and tightened against custom aluminum cups. Once specimens were rigidly fixed to each aluminum cup, non-exothermic dental plaster (Denstone, Miles, South Bend, USA) was placed around the segment to enhance fixation between the specimen, wires, screws and the aluminum cup. Specimens were then injected with approximately 0.7 cm^3 of barium sulphate (radio-opaque), blue dye (Coomassie Brilliant Blue G-mix:

0.25% dye, 2.5% MeOH, 97.25% distilled water), and distilled water in a relative mixture of 2:1:2 (Callaghan and McGill, 2001) and an initial sagittal plane X-ray was obtained from the specimen's right side. X-rays were developed using a digital X-ray system (Kodak DirectView CR500, Carestream, Toronto, Canada) and were repeated throughout testing, although the frequency of examination was altered depending on the load level (10% - every 3000 cycles, 30% - every 3000 cycles, 50% - every 200 cycles, 70 and 90% - after failure).

6.3.2 Loading

The superior cup was mounted to a custom flexion/extension rig which was rigidly fixed to the load cell of a servo-hydraulic materials testing machine (8872, Instron Canada, Toronto, ON, Canada). Flexion/extension moments were applied to the rig through a rotational brushless servomotor (Kollmorgen, Model AKM23D-BNCNC-00, Danaher Motion, Il., USA) and subsequently to the upper vertebrae. Moments were measured with a moment transducer (SensorData Technologies Inc., Model T120-106-1K, Sterling Heights, MI., USA) mounted in series with the servomotor. Control of the servomotor was accomplished through an ISA bus motion controller (model DMC18x0, Galil Motion Control, Rocklin, USA). The lower cup rested on a bearing table allowing anterior-posterior and medial-lateral translations and axial rotation (figure 6-1).

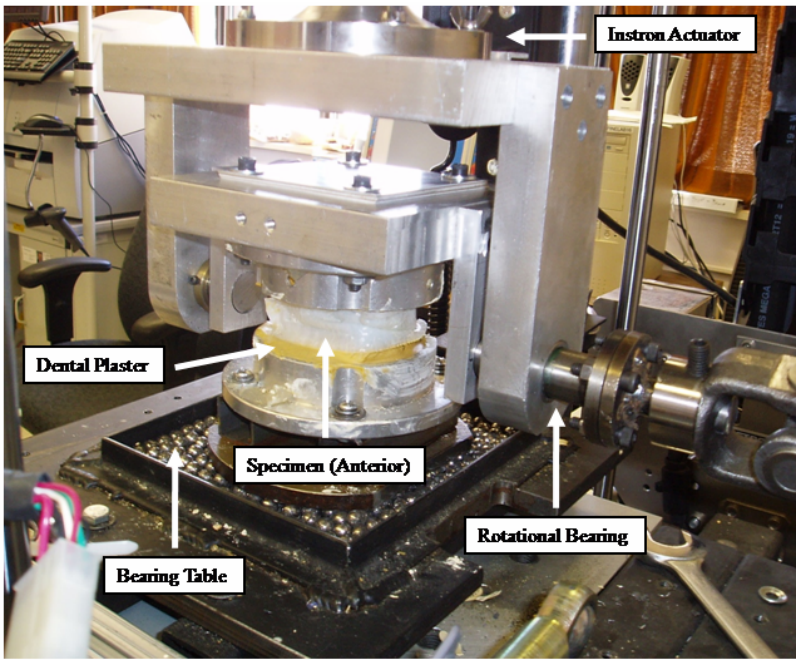

Figure 6-1: A mounted specimen prior to loading.

After mounting, each FSU was preloaded at 300 N for 15 minutes (Callaghan and McGill, 1995; Gunning *et al.*, 2001; Yingling *et al.*, 1999) prior to cyclic testing. During this period, the servomotor sought a position for which no external moment was present (elastic equilibrium), this position was taken as neutral. In order to determine a specimen specific range of motion (ROM), passive flexion extension was performed while under 300 N of compression in order to obtain moment-angle curves. Three repeats of the ROM test were performed; maximum flexion and extension angles were obtained from the third cycle. Maximum flexion and extension angles were determined by identifying the angle where the moment-angle curve began to deviate from linearity (figure 6-2).

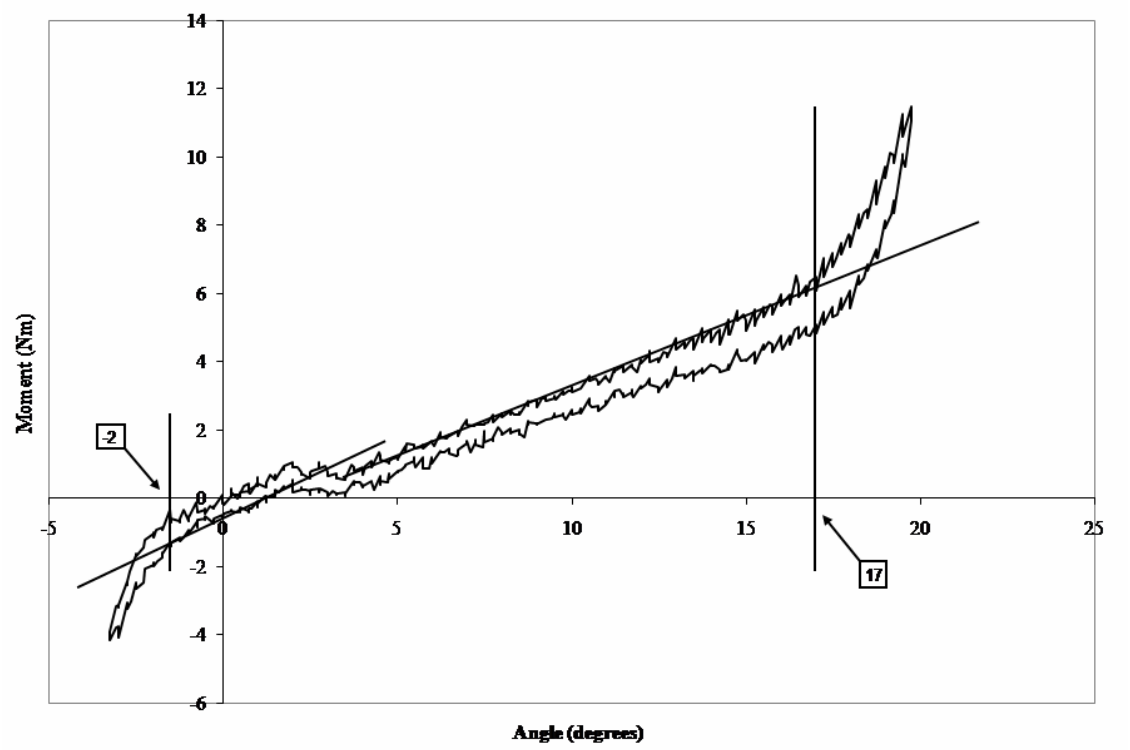

Figure 6-2: Moment-angle curve obtained from the third cycle of a passive range of motion test. Straight lines have been added to the linear portion of the curve to improve visualization of how test flexion and extension angles were chosen.

Upon completion of the preload and ROM tests, specimens were randomly assigned to one of five normalized loading groups, corresponding to peak loads of 10, 30, 50, 70 and 90% of the compressive tolerance of the specimen. Both load and motion profiles were obtained from a floor to waist height lift performed by a male. Joint compression was determined through the use of an EMG-assisted spine model based upon the work of Granata and Marras (1995a), while spine angle was measured using the Lumbar Motion Monitor (Biomec Inc., Cleveland, OH, USA). Spine angle and compression were normalized in time to match the desired cycle frequency of 0.5Hz as well as normalized in amplitude to allow scaling to appropriate normalized compression and ROM values (figure 6-3).

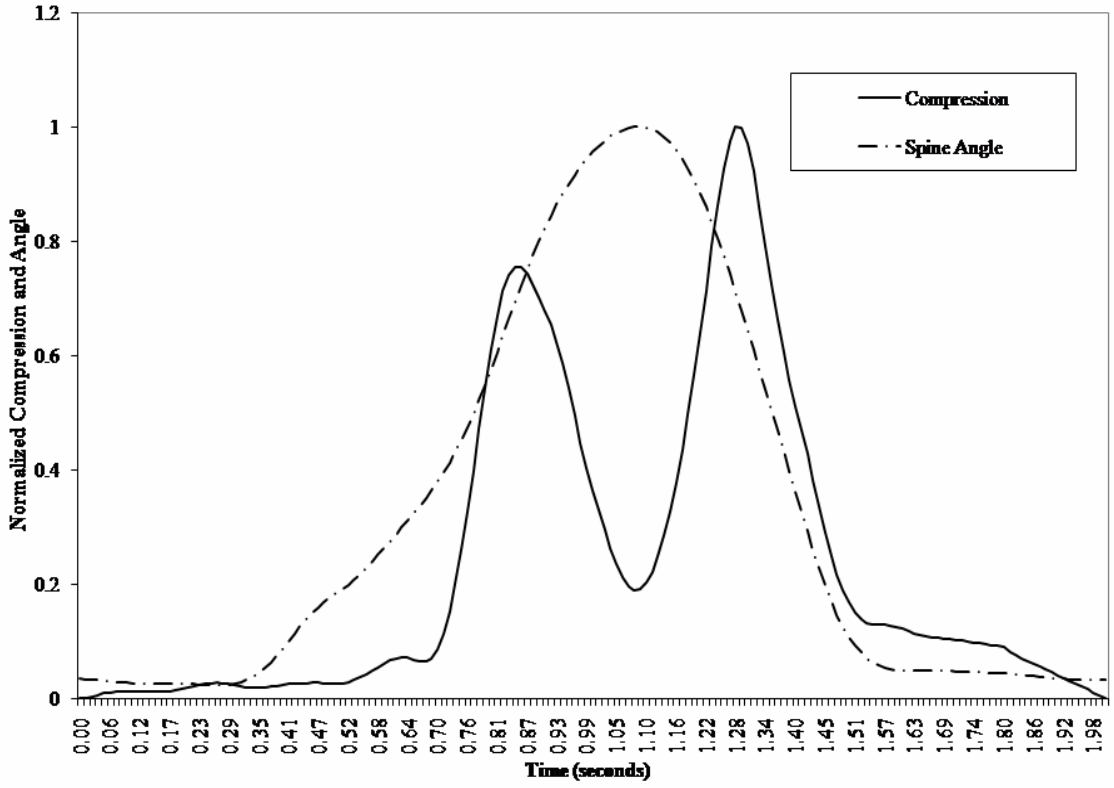

Figure 6-3: Sample compression and angle curves normalized in amplitude (0 to 1) and time (0.5 Hz loading frequency). The compression curve was obtained using an EMG-assisted spine model while a male subject performed a single floor to waist height lift. The spine angle was obtained during the same lift using the Lumbar Motion Monitor.

The compression waveform was scaled to run from a minimum of 300 N up to the desired peak load, with 300 N being chosen to represent the weight of the upper body during upright standing. Additionally, this load has been identified in our laboratory as resulting in an equalization of height with no excessive creep over a 15 minute period for in-vitro testing. Note that the applied compressive load is not the compression experienced across the joint (except at 0^0) as it is translated into compressive and shear components through the loading rig. Therefore the global angle of the rig was also calculated to allow determination of the anatomical compression and shear values.

6.3.3 Failure Analysis

All specimens were cyclically compressed and flexed until failure occurred or a maximum of 12 hours (21600 cycles) had elapsed. If failure was indicated through height loss (more than 9 mm) or X-ray documentation, testing was stopped. Failure was identified in X-rays by the loss of nuclear visualization, nuclear presence within the vertebral body or the appearance of nuclear material in the posterior annular layers. Throughout testing, compressive load, vertical position, joint angle and rotational moment were sampled at 25 Hz. Determination of the injury cycle in bone failure was based upon stiffness and displacement. When fracture occurs, it is indicated by a drop in compressive stiffness (equation 3) and an increase in vertical displacement (Brinckmann *et al.*, 1988; Hansson *et al.*, 1987; Parkinson and Callaghan, 2007b). Failure based upon X-ray analysis was taken to occur at the last cycle prior to obtaining the X-ray in which the injury was observed. Cycles to failure, height loss at failure, cumulative excursion (time integrated angular displacement), cumulative moment, and cumulative compression to failure were also determined. All cumulative variables were calculated using trapezoidal integration.

$$Cycle\ Stiffness\ (\frac{kN}{mm}) = \frac{(Peak\ Cycle\ Load\ (kN) - Minimum\ Cycle\ Load\ (kN))}{(Peak\ Cycle\ Displacement\ (mm) - Minimum\ Cycle\ Displacement\ (mm))} \quad \textbf{(6-1)}$$

Upon termination of cyclic loading, specimens were dissected to determine the site of injury. First, the posterior elements were removed to determine if there were any visible signs of injury to the posterior disc. Second, the external vertebral surfaces were examined for signs of fracture and finally the intervertebral disc was cut to allow visualization of any endplate fractures or internal disc damage. Endplate fractures were classified as crack (Parkinson and Callaghan, 2007b), step (Brinckmann *et al.*, 1988), stellate (Brinckmann *et al.*, 1988) or crush (Hansson *et al.*, 1987). The direction and location of any disc damage was identified by the presence of blue dye in the posterior annular layers.

6.3.4 Statistical Analysis

Specimen randomization was assessed using a one-way analysis of variance (ANOVA) to test for load group differences in endplate area, ultimate load, maximum flexion angle, and maximum extension angle. A one-way ANOVA was also performed to identify any between group differences in injury cycle, maximum and minimum moment exposure, cumulative compression, cumulative excursion, cumulative shear, and cumulative moments due to load exposure. One-way ANOVAs were performed to identify significant differences in these measures between those specimens that exhibited failure and those that did not, as well as between those that underwent bony failure and those that experienced disc damage. Significant pair-wise differences (where necessary) were identified through a Tukey's post hoc test. All tests with $p<0.05$ were considered statistically significant.

6.4 Results

6.4.1 Specimen Randomization

Due to difficulties in synchronization of the compression and flexion/extension axes, two specimens in each of the 10 and 30% loading groups were excluded, resulting in a total of 46 samples. Based on these samples, there were no significant differences found between the loading groups for endplate area ($p = 0.447$), maximum flexion angle ($p = 0.8718$) or maximum extension angle ($p = 0.6317$). No significant differences were found in these measures when specimens that underwent failure were compared with those that did not (endplate area ($p = 0.0948$), maximum flexion angle ($p = 0.5929$), maximum extension angle ($p = 0.0855$)). When comparisons were performed based on injury site (disc vs. bone), there were no significant differences in these values (endplate area ($p = 0.9442$), maximum flexion angle ($p = 0.6664$), maximum extension angle ($p = 0.3481$)) (Table 6-1).

Table 6-1: Specimen number, average endplate area, maximum flexion angle and maximum extension angle of specimens tested under each loading condition, those specimens which failed and those which survived, as well as for specimens which developed disc injury and those that exhibited bone injury. Standard deviations are presented in parentheses. There were no significant differences in endplate area, flexion or extension angles between any load groups.

Group	Specimen Number	Endplate Area (mm^2)	Maximum Flexion Angle (degrees)	Maximum Extension Angle (degrees)
10%	8	692.7(35.4)	14.9(2.9)	4.1(2.8)
30%	8	660.9(49.9)	14.3(3.0)	2.9(3.0)
50%	10	653.1(39.2)	15.0(2.8)	4.0(1.7)
70%	10	669.8(65.4)	14.5(6.1)	3.7(2.1)
90%	10	654.1(47.0)	16.0(2.1)	4.4(2.4)
Failed	41	664.7(48.3)	14.8(4.1)	4.2(2.1)
Non-Failed	5	703.3(35.5)	15.8(2.3)	2.4(1.7)
Bone Injury	34	660.8(48.7)	15.0(3.8)	3.9(2.0)
Disc Injury	7	659.3(51.5)	14.3(3.5)	4.7(2.8)

6.4.2 Load Magnitude

Analysis revealed a significant effect of load magnitude exposure on the number of cycles tolerated to failure (Table 6-2, $p<0.0001$). Post hoc analysis indicated that the 50 and 70%, and 70 and 90% comparisons were not significantly different, with those specimens exposed to higher compressive loads sustaining fewer cycles to injury. Significant between group differences were also identified for cumulative compression (figure 6-4a, $p < 0.001$). Specimens loaded to 10% of their estimated tolerance tolerated a greater amount of cumulative compression than those loaded to 50, 70 or 90%. Specimens loaded to 30% of their maximum tolerance sustained more cumulative compression than those loaded to 50, 70 or 90%, which were not different from one another. The same relationships were found for cumulative shear (figure 6-4b, $p < 0.0001$). Cumulative excursion was also found to differ between the loading groups (figure 6-4c, $p < 0.0001$), with the 50-70%, 70-90% and 50-90% between group comparisons being non-significant. Specimens exposed to the lowest levels of compression (10 and 30%) tolerated significantly higher cumulative moment exposures than those exposed to greater loads (figure 6-4d, $p < 0.0001$), although they did not differ

from each other. Specimens loaded to 50, 70 or 90% did not differ statistically in terms of cumulative moment exposure. Load magnitude significantly altered height loss at failure ($p = 0.0012$), with those specimens loaded to a maximum of 30% of their estimated tolerance exhibiting significantly greater height loss than specimens exposed to greater loads. No statistical difference in height loss was observed between the 10 and 30% groups (Table 6-3).

Table 6-2: Average injury cycle. Values marked with the same letter are not significantly different within a comparison group. Standard deviations are presented in parentheses. *As all non-failed specimens tolerated 21600 cycles, no variance exists and statistical comparisons were not performed.

Average Injury Cycle with Load Magnitude (%) Grouping				
10%	*30%*	*50%*	*70%*	*90%*
14400(6858.6)	5030.7(3943.9)	154.7(167.0)	21.8(26.2)	3.7(2.8)
A	D	B	BC	C

Average Injury Cycle Number for Failed	**vs.**	**Average Injury Cycle Number for Non-Failed**
2782.2(5445.0)		21600(NA)
*		*

Average Injury Cycle Number for Disc Injuries	**vs.**	**Average Injury Cycle Number for Bone Injuries**
9000(5477.2)		929.9(3754.4)
A		B

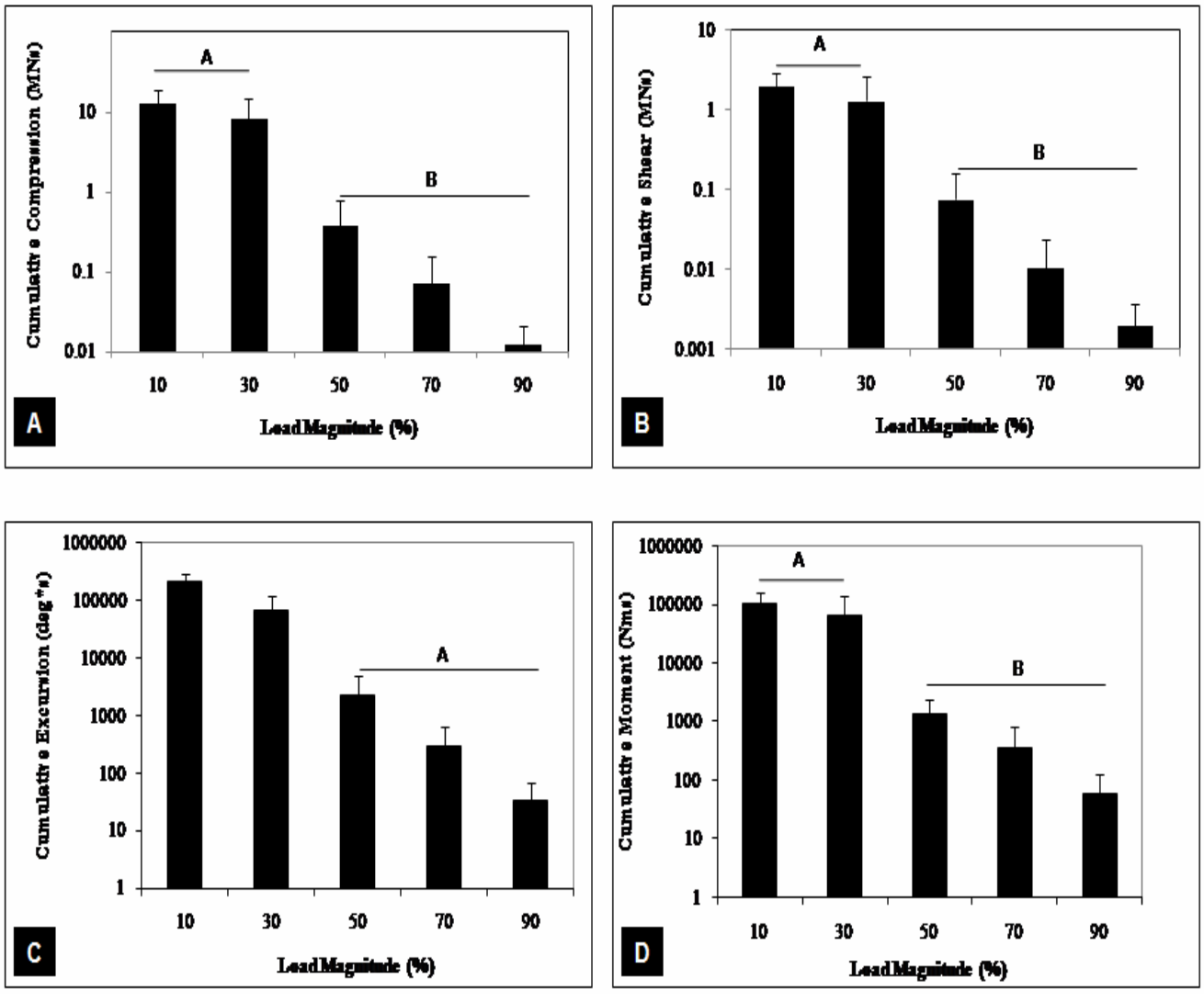

Figure 6-4: (A) Bar chart of average cumulative compression (MNs + 1 standard deviation) tolerated to failure at each level of peak load magnitude. **(B)** Bar chart of average cumulative shear (MNs + 1 standard deviation) tolerated to failure at each level of peak load magnitude. **(C)** Bar chart of average cumulative excursion (degrees + 1 standard deviation) tolerated to failure at each level of peak load magnitude. **(D)** Bar chart of average cumulative moment (Nms + 1 standard deviation) tolerated to failure at each level of peak load magnitude. For all figures, groups marked by the same letter are not significantly different.

Table 6-3: Average height loss at failure (mm). Values marked with the same letter are not significantly different within a comparison group. Standard deviations are presented in parentheses.

Average Height Loss Within Load Magnitude (%) Group				
10%	*30%*	*50%*	*70%*	*90%*
3.3(0.4)	4.7(1.3)	2.6(1.6)	2.3(1.8)	1.5(1.2)
AB	B	A	A	A
Average Height Loss for Failed Specimens vs. Average Height Loss for Non-Failed Specimens				
2.9(1.7)			4.3(2.6)	
A			A	
Average Height Loss for Disc Injuries vs. Average Height Loss for Bone Injuries				
4.1(1.0)			2.4(1.7)	
A			B	

6.4.3 Failed vs. Non-failed

Of the 46 specimens tested, five survived 2 hours (four from the 10% group, 1 from the 30% group). Surviving specimens were exposed to significantly lower peak loads (1618.9±916.0N vs. 4886.8±2255.2 N, $p = 0.003$ for compression, 298.4±246.5 N vs. 1070.8±698.9 N, $p = 0.0203$ for shear) and tolerated a greater number of cycles (Table 6-2). All cumulative variables reflected this relationship, with surviving specimens tolerating greater cumulative compression (22.9±8.0 MNs vs. 3.3±5.8 MNs, $p < 0.001$), cumulative excursion (305961.2±34092.5 degs vs. 39642.9±77156.6 degs, $p < 0.0001$), cumulative shear (3.4±1.5 MNs vs. 0.5±1.0 MNs, $p < 0.0001$) and cumulative moment (244058.6±98243.3 Nms vs. 26545.7±53214.7 Nms, $p < 0.001$). The surviving specimens exhibited greater height loss, but the difference was not statistically significant (Table 6-3, $p = 0.1209$).

6.4.4 Disc Injury vs. Bone Injury

Observable disc injuries constituted 17.1% of all injuries (41). Three of these injuries occurred in specimens loaded to a maximum of 10%, while the remainder occurred in the 30% load group. Specimens exhibiting vertebral fracture received significantly higher load applications (6155.3±2032.1 vs. 2132.1±969.9, $p < 0.001$ for compression, 1299.6±687.3 vs. 570.4±332.1, $p =$

0.0097 for shear) and tolerated significantly fewer cycles to failure (Table 6-2, $p < 0.0001$). Cumulative exposure measures reflected this relationship, with specimens exhibiting vertebral fracture tolerating lower cumulative compression (10.9±6.4 MNs vs. 1.1±3.4 MNs, $p < 0.001$), cumulative excursion (130809.7±72519.2 degs vs. 12714.7±53102.3 degs, $p < 0.001$), cumulative shear (1.8±1.3 MNs vs. 0.2±0.5MNs, $p < 0.001$), and cumulative moment (88328.3±63536.0 Nms vs. 8367.4±33117.7 Nms, $p < 0.001$). Specimens exhibiting bony failure lost significantly less height prior to failure (Table 6-3, $p = 0.0172$).

6.4.5 Injury Analysis

Examination of the injury site determined that in all specimens exposed to peak loads equal to or exceeding 50% failure occurred within the endplate or vertebral bone. In 27 of 34 cases the resulting fracture exhibited the crack morphology (Table 6-4). The next most frequently observed injury was endplate depression, which occurred in 4 cases. Bone failure was also observed at lower load magnitudes, but at decreasing frequencies. When exposed to peak normalized loads of 30%, bone and disc injuries occurred in 43 and 57% of failed specimens, respectively. Bone/endplate failure comprised only 25% of the observed injuries when peak loads of 10% were employed. In two instances the fracture occurred in one of the external endplates in contact with the aluminum cup. While this occurs infrequently, it indicates that the applied compressive loads are being carried through the endplates as intended. Intervertebral disc damage only occurred in the two groups receiving the lowest amounts of compression. In all cases the herniation traveled in a posterior direction and was indicated by a loss of visible nuclear material in X-ray and an accumulation of blue dye in the annular layers (figure 6-5). Complete prolapse was observed in only 1 case, although in another specimen the blue dye was clearly visible in the outer annular layers prior to dissection of the disc. The observation of rare complete prolapse is likely due to the study goal of attempting to

identify the injury as close to the initiating cycle as possible. If the tests were allowed to progress beyond the termination point it is possible that more of the disc herniations would have progressed to complete prolapse.

Table 6-4: Number of occurrences of fracture type grouped according to normalized peak load magnitude.

	Fracture Type				
Load Magnitude (%)	*Crack*	*Endplate Depression*	*Step*	*Stellate*	*Crush*
10%	1	0	0	0	0
30%	2	1	0	0	0
50%	7	2	1	0	0
70%	7	1	0	1	1
90%	10	0	0	0	0

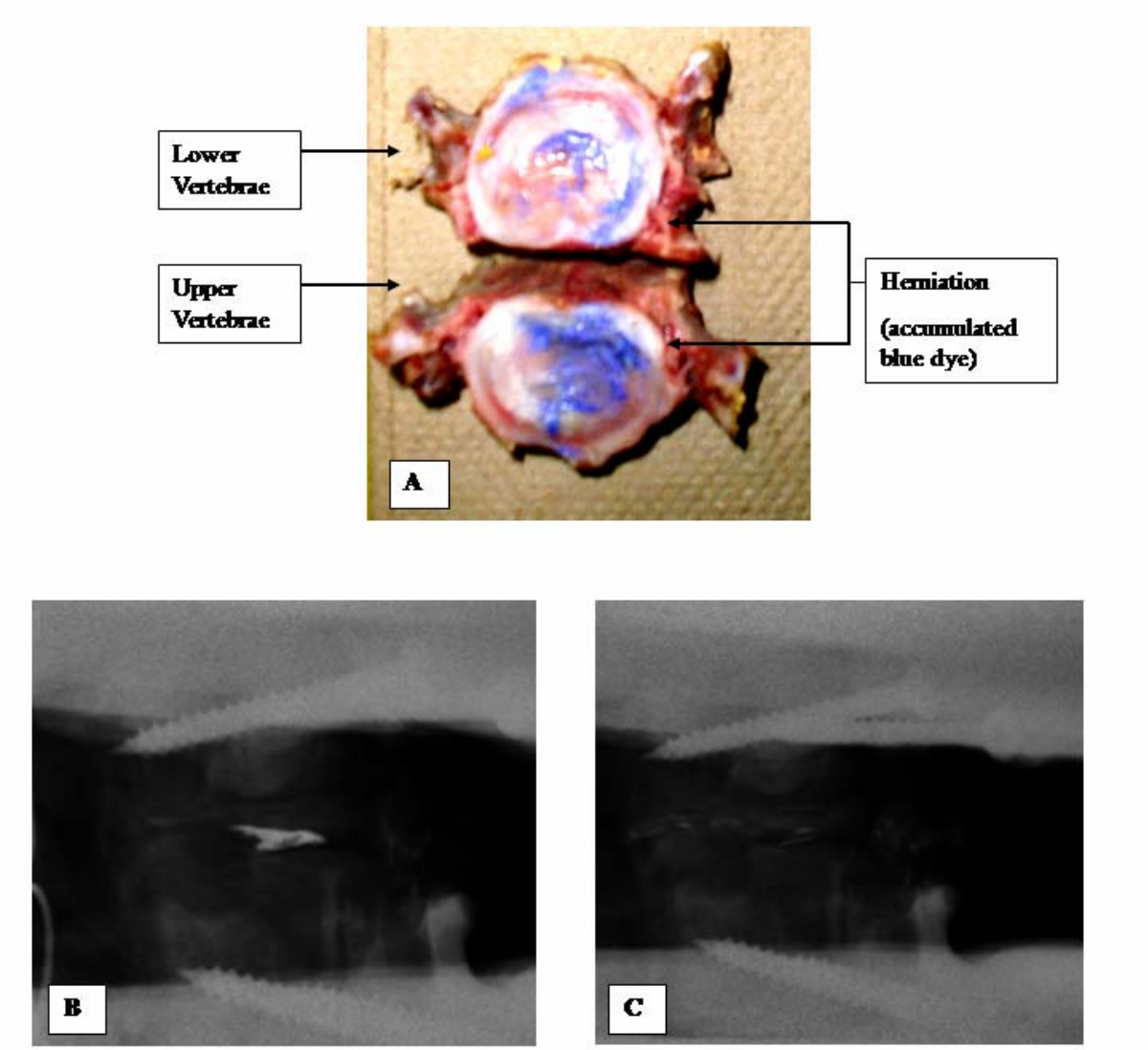

Figure 6-5: (A) Photograph of a herniated specimen. Note the presence of blue dye in the posterior annulus. X-rays of the same specimen taken prior to **(B)** and after **(C)** disc damage. Notice the absence of any visible radio-opaque solution in the post injury X-ray. Due to the sagittal nature of the X-ray, the screws inserted through the anterior processes are visible; however they have not entered the vertebral body.

6.5 Discussion

The results of this study indicate that in scenarios where peak load magnitudes exceed 50% of a spinal level's estimated compressive tolerance, the presence of concurrent dynamic flexion will not

change the site of injury from the vertebrae to the intervertebral disc. This conclusion supports epidemiologic evidence that the lifting of loads is not associated with the appearance of intervertebral disc injury (Kelsey, 1975). More recent epidemiologic evidence indicates that there may be instances where disc injury can be observed under larger exposures, however the loads must be quite large (>11.3 kg) and the relative lifting frequency high (>25 times/day) (Kelsey *et al.*, 1984). However, as peak loads decrease below this level the likelihood of sustaining a disc injury becomes greater than that of sustaining a bone or endplate injury. However, this decrease in load exposure also reduces the over-all likelihood of any injury occurring. The presence of repetitive flexion did not alter the existence of a non-linear relationship between peak load magnitude exposure and injury cycle, as described in earlier work (Parkinson and Callaghan, 2007a). The decrease in tolerated cycles to failure in those groups exposed to higher loading is reflected in decreases in tolerance to cumulative compression, cumulative shear, cumulative excursion and cumulative moment. The same conclusions can be drawn when comparing those specimens, which exhibited injury to those that did not, or when comparing those specimens that experienced disc injury to those that experienced vertebral fracture. Those joints in which a disc injury was observed were exposed to lower loads and exhibited significantly greater height loss. This enhanced height loss may indicate the presence of a greater creep component prior to failure, also explaining the significantly greater height loss exhibited in the lowest loading groups.

Although posture does not appear to be the primary injury mechanism at larger loads, it appears to play a substantial role in reducing compressive tolerance when compared to the data from earlier work. Earlier work found compressive tolerances (average number of cycles at injury) of 2.8 MNs(434), 1.1 MNs(129.4), and 0.1 MNs(8.6) for porcine cervical spine specimens exposed to cyclic compression in a neutral posture with peak load exposures of 50%, 70% and 90% respectively (Parkinson and Callaghan, 2007a). The same peak magnitude load exposures employed in this study

resulted in cumulative compressive tolerances (average injury cycles) of 0.4 MNs(154), 0.07 MNs(21.8), and 0.01 MNs(3.7). The specimens tested in the current study exhibited much lower tolerance to cumulative compression, with the major experimental difference being the application of concurrent dynamic flexion. Although other experimental differences exist in that slightly different compressive profiles were employed in the studies and that the specimens in the current study were injected with solution for X-ray purposes, the large differences in observed tolerances are most likely due to the inclusion of postural changes as flexion has been shown to reduce compressive tolerances when applied statically (Gunning *et al.*, 2001). Examination of the number of cycles to injury in those specimens undergoing disc injury reveals that dynamic compression may alter tolerance to cyclic flexion. Previous work examining the role of dynamic repetitive flexion in intervertebral disc herniation reported the lowest injury cycle number of 34974 to occur under the largest static compressive load of 1472 N (Callaghan and McGill, 2001). While this cycle number is higher than that of the current study (9000±5477.2) for specimens displaying disc injury, the maximum applied compression in this study was larger (2132.1 N). However, this represents only the peak load of a dynamic profile. The average compressive load, taken across all specimens that exhibited disc injury is 667 N. As the same animal model was used under similar test conditions (the earlier study testing was conducted at body temperature; however this would be expected to accelerate injury due to accelerating tissue deterioration) it is reasonable to attribute the large differences in tolerated cycle numbers to the difference in static and dynamic loading profiles. This relationship provides underling mechanical evidence for the fact that workers in sedentary jobs, particularly those who operate motor vehicles (which would induce low level dynamic load profiles and flexed postures) are at higher risk of developing intervertebral disc herniation (Kelsey, 1975). The lower average compressive load may also explain the large differences in reported height loss between the two studies.

A major limitation of this study lies in the need to identify injury through crude measures. In order to identify disc injury, an X-ray approach was taken. While this approach has been used previously (Callaghan and McGill, 2001), it is limited as it requires removal of the specimen from the loading apparatus in order to allow an X-ray to be obtained. This limits the frequency of imaging, leading to coarse measures in the number of cycles to failure. In order to allow for improved identification of the injury cycle, different X-ray intervals were applied based upon the peak load exposure with specimens exposed to higher peak load magnitudes being imaged more frequently. When an injury was identified, it was assumed to have occurred at the last loading cycle prior to imaging. It was felt that this would provide a conservative estimate of the injury cycle number and was applied as a rule to all specimens. Identification of fractures, although based upon distinct changes in displacement and stiffness behaviour, was done after testing was stopped based on height loss (>9mm). Therefore, in some cases the initial injury may have occurred many cycles prior to termination of loading and for this reason the morphology of the fracture may have been altered from the injury at initiation.

Additionally, an animal model was employed which may limit the direct transferability of the results to human samples. This was done to ensure an adequate sample number, as well as to control for diet, activity, genetics, illness and age. The anatomical and functional similarities between the human and porcine spine have been previously demonstrated (Yingling *et al.*, 1999; Oxland *et al.*, 1991) and additional work has determined that the trabeculae display similar architecture (Lin *et al.*, 1997). A very recent dissection study has shown that although differences between species do exist, the porcine cervical disc is a reasonable analog to the human lumbar disc for studies involving repetitive flexion/extension (Tampier, 2006). Additionally Haddock et al. (2004) have indicated that trabecular bone may show similar fatigue response in different species. Previous work on porcine cervical samples from the same supplier developed an equation that allows estimation of the

compressive strength of a spinal unit without the need for destructive testing (Parkinson *et al.*, 2005). This allows normalized loads to be applied, leading to enhanced comparison between studies as well as improved interpretation when compared to human *in vivo* loading scenarios. In this regard, the applied angles were also normalized to each specimen's maximum flexion and extension range to ensure consistent motion demands within the experiment as well as improve transferability to examinations of human motion.

Based on this work, it appears that the spine is at greater risk of intervertebral disc herniation when loads are lower (below 30% of the estimated compressive tolerance) and at greater risk of vertebral fracture if the loads are larger. When the loads exceed 50%, intervertebral disc herniation will not occur prior to fracture, if the dynamic flexion does not exceed the normal range of the joint. Although disc herniation will not occur, it appears that the inclusion of repetitive flexion at higher loads may lead to a decrease in the ability of the joint to tolerate loading. Conversely, the application of a dynamic loading profile in concert with repetitive flexion appears to lead to disc herniation at much lower cycle numbers than would be observed if the motion was coupled with low level static loading. The coupling of dynamic flexion with cyclic compression resulted in non-linear relationships between peak load magnitude levels and cumulative exposure variables. The results of this study can be applied to improve understanding of injury, focusing attention on the disc as the tissue likely to be injured in low level loading and the vertebrae in instances of larger compressive loads. Future work should be conducted to further understand the interactions between load and posture, specifically focused on identifying the exact location where intervertebral disc herniations will begin to occur.

Chapter 7

Can Periods of Static Loading be used to enhance the Resistance of the Spine to Cumulative Compression?

Robert J. Parkinson and Jack P. Callaghan

Journal of Biomechanics, 40(13), 2944-2952

7.1 Abstract

Results of in-vitro studies conducted on isolated bone specimens have indicated a higher tolerance to static load than exists when exposed to cyclic loading, when controlled for creep rate. If this difference in load tolerance exists it may be exploited to extend the life of vertebral bone exposed to repetitive compression, and potentially alter the development of spinal injury. However, little work has been conducted on functional spinal units to determine if bone displays this characteristic within an intact joint. Additionally, static loading may result in load redistribution within the intervertebral disc forcing more of the compressive load towards the periphery of the endplate away from the nucleus. In order to examine these potential mechanisms, 218 osteoligamentous porcine functional spinal units were assigned to one of fifteen loading scenarios. This involved one of three normalized peak load magnitudes (50, 70 and 90% of estimated compressive tolerance) and one of five normalized static load applications (0%, 50%, 100%, 200% and 1000% of the total dynamic work duration). Load magnitude significantly altered the resistance to cumulative compression, with decreased peak magnitudes corresponding to both increased cumulative load tolerance and increased height loss. Static load periods did not alter the resistance of the spinal unit to cumulative compression or impact the number of cycles tolerated to failure. The insertion of static load periods impacted the total survival time to failure, but only for the 1000% static load group, an exposure unlikely to occur for most in-vivo exposures. The insertion of static load periods decreased the

amount of height loss during testing which may play a protective role by allowing load redistribution within the vertebral bone and intervertebral disc.

Keywords: Spine, cumulative load, compression, fracture, creep

7.2 Introduction

Previous in-vitro work has shown that repetitive compression of the spine leads to failure in vertebrae at load magnitudes below those tolerated under acute loading (Brinckmann *et al.*, 1988; Hansson *et al.*, 1987; Parkinson and Callaghan, 2007b). Although these studies differed in testing conditions a commonality exists in that failure occurred within the trabeculae underlying the vertebral endplate and the endplate itself. Therefore efforts should be directed toward investigating mechanisms to improve resistance of the bone to cumulative fatigue. Such a mechanism may provide a means to reduce the risk of spinal injury through alterations in load exposure.

The fatigue behaviour of isolated bone has been studied under both tensile and compressive cyclic loading (Moore and Gibson, 2003b; Moore *et al.*, 2004; Lu *et al.*, 2004; Carter and Caler, 1983; Carter and Hayes, 1976; Pattin *et al.*, 1996; Michel *et al.*, 1993; Bowman *et al.*, 1998; Zioupos *et al.*, 2001; Ganguly *et al.*, 2004; Carter and Caler, 1985; Haddock *et al.*, 2004; Rapillard *et al.*, 2006; Caler and Carter, 1989). One finding of interest is that specimens exposed to static loading will survive longer than those exposed to cyclic loading (Bowman *et al.*, 1998). This conclusion was extended by Moore et al. (2004) who performed creep calculations based on the work of Bowman et al. (1998), and determined that statically loaded specimens survive one to four times longer than if loaded cyclically.

These studies indicate that bone exposed to time varying loading regimes would fail before bone loaded statically. As these studies were conducted on isolated bone the survival time would be due to properties of the bone, not to interactions with surrounding tissues. Van Dieën et al. (2001),

while using a bovine model, provided a potential mechanism for changes within the joint induced by compressive creep loading that may alter the fatigue resistance. Under sustained compression, larger stresses initially observed in the inner area of the endplate decreased while stress in the outer area of the endplate increased, leading to an increased uniformity of stress and a larger distribution area (van Dieen *et al.*, 2001). This redistribution may be beneficial in protecting the central endplate area, known to be a compression failure site, through transference of the loads to stronger trabecular and endplate regions. However, isolated bone testing indicates that trabeculae in the periphery may be less capable of bearing load, with central regions being 1.16 to 1.26 times stronger than the periphery (Keller *et al.*, 1989; Keller *et al.*, 1989; Lin *et al.*, 1997). In contrast, more recent work has demonstrated that the central endplate region is weaker than the peripheral endplate areas in isolated cadaveric endplates (Grant et al., 2001; Grant et al., 2002). These studies indicate a potential mechanism where periods of static loading may increase the fatigue resistance of the intervertebral joint.

As no previous work has tested these mechanisms we were driven to examine the effects of static load duration on the resistance of the spinal unit to repetitive compression. Numerous studies (Moore and Gibson, 2003b; Moore *et al.*, 2004; Haddock *et al.*, 2004; Michel *et al.*, 1993; Rapillard *et al.*, 2006; Caler and Carter, 1989) have indicated an effect of load magnitude on the fatigue resistance of bone and spinal units (Hansson *et al.*, 1987; Brinckmann *et al.*, 1988; Parkinson and Callaghan, 2007b), necessitating an examination of load magnitude effects and any interaction with static load duration.

7.3 Methods

7.3.1 Specimen Dissection

218 porcine cervical functional spinal units (FSU) were obtained frozen from a local abattoir (111 C3C4 and 107 C5C6). Spines were stored frozen and thawed overnight prior to dissection, during which the osteoligamentous FSU was isolated by removal of surrounding musculature. Once isolated the exposed endplates were measured along the midline in the anterior-posterior (A) and medial-lateral (B) directions allowing calculation of endplate area based on the surface area of an ellipse ($\pi/4 \times A \times B$). The surface area of the two exposed endplates was calculated and the average represented the FSU.

FSUs were mounted in aluminum cups, aligning the midplane of the intervertebral disc parallel to the surface of the cups. In order to maintain natural lordosis of the segments, dental plaster (Denstone, Miles, South Bend, IN, U.S.A.) was placed in the cups and allowed to harden around the endplates to support the segment without reinforcing the exterior surface of the vertebrae. The superior cup was mounted to the load cell of a servo-hydraulic materials testing machine (8872, Instron Canada, Toronto, ON, Canada). The lower cup rested on a bearing table allowing anterior-posterior and medial-lateral translations and axial rotation (figure 7-1).

After mounting, the FSU was preloaded at 300 N for 15 minutes (Callaghan and McGill, 1995; Gunning *et al.*, 2001; Yingling *et al.*, 1999) prior to cyclic testing. Throughout testing specimens were wrapped in saline soaked gauze and plastic to prevent moisture loss.

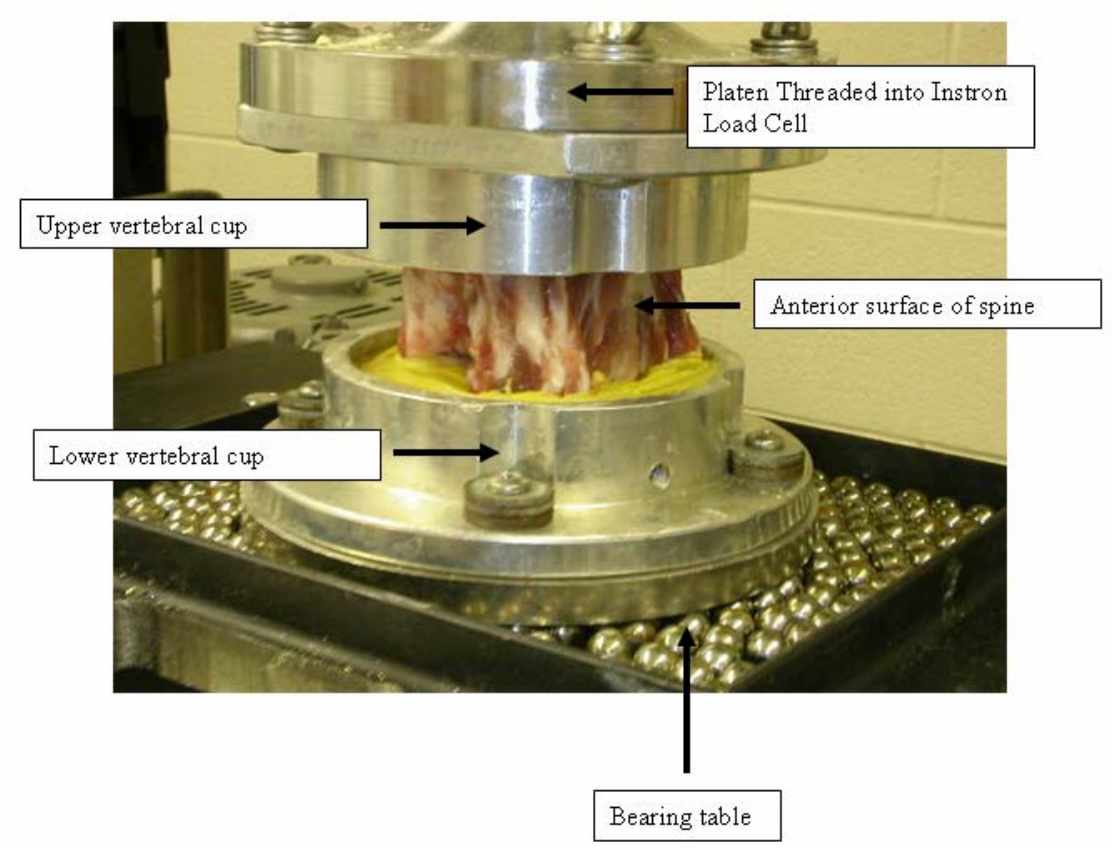

Figure 7-1: A mounted specimen prior to loading. The saline soaked gauze and plastic have been removed to allow visualization of the spinal unit.

7.3.2 Loading Scenario

In order to interpret the results of this animal model study in terms of human load exposures, lifting was chosen as a representative activity. To mimic this physiologic exposure an L4/L5 joint compression profile was obtained using a biomechanical rigid link model during a floor to waist height lift. Loads were estimated for the L4/L5 joint as it has been examined in in-vivo studies examining the links between cumulative loading and the reporting of low back pain (Norman *et al.*, 1998). This waveform was normalized to run from 0 to 1 (figure 7-2).

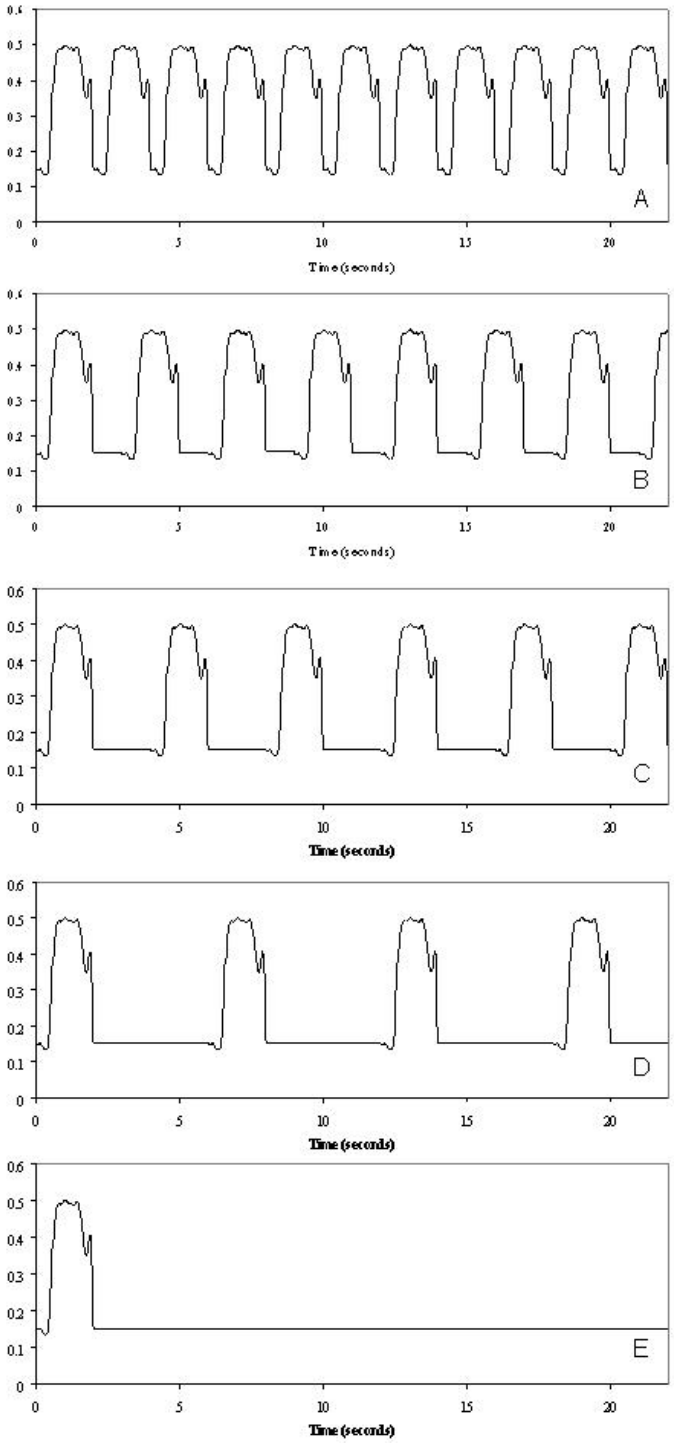

Figure 7-2: Sample compressive loading curves, normalized to peak loads of 0.5 (50% of the estimated compressive tolerance). (A) 0% rest, (B) 50% rest, (C) 100% rest, (D) 200% rest, (E) 1000% rest.

The desired peak compressive load was then used to scale the waveform to run from a minimum of 300 N up to the desired peak load. 300 N was chosen to represent the weight of the upper body during upright standing. This load has been identified in our laboratory as the load that resulted in an equalization of height with no excessive creep over a 15 minute period for in-vitro testing. Maximum compressive tolerance was estimated using the average endplate area and a previously developed regression equation (Parkinson *et al.*, 2005). Three peak loading magnitudes of 50, 70 and 90% of the maximum compressive tolerance were investigated. In addition, each specimen was assigned to one of five static load durations, expressed as a percentage of the 0.5 Hz loading cycle (Holmes and Hukins, 1994; Brinckmann *et al.*, 1988; Hansson *et al.*, 1987; Parkinson and Callaghan, 2007b). Normalized durations of 0, 50, 100, 200 and 1000% of the loading cycle (2 seconds) were examined. During these periods the load was returned to 300 N. Cyclic loading was continued until failure or the maximum test duration of 12 hours was reached. Load and displacement data were sampled at 10 Hz. Average cycle stiffness was calculated for each cycle (equation 6-1, chapter 6), which was comprised of the dynamic load application and static load period. Failure was identified by an increase in displacement and decrease in cycle stiffness (Brinckmann *et al.*, 1988; Hansson *et al.*, 1987; Parkinson and Callaghan, 2007b). Height loss at failure was calculated as the difference in displacement (the minimum cycle displacement) between the first cycle and the failure cycle. Survival duration and cycles to failure were documented for each specimen. Cumulative load, in units of MNs, was calculated through trapezoidal integration of the loading profile up to the failure cycle. After failure, specimens were dissected and fracture morphology was recorded.

7.4 Statistical Analysis

To assess the success of specimen randomization a two-way (rest duration by load magnitude) analysis of variance (ANOVA) was used to test for differences in endplate area. A two-way ANOVA was performed to analyze between group differences for cumulative load tolerated to failure, number of cycles tolerated to failure, survival time and height loss. A one way ANOVA was employed to test for differences in the height loss between specimens which survived the testing and those that failed. A protected least significant difference post hoc test was used to identify significant between group differences. All tests with $p<0.05$ were considered statistically significant.

7.5 Results

7.5.1 Specimen Randomization

Specimens were successfully randomized as no differences were found in the endplate areas between groups (table 7-1, $p = 0.535$). One specimen exhibited an extremely high cumulative load tolerance in the 50% load magnitude and 50% static load duration group. This specimen had an endplate area below the group mean (627 mm^2 vs. 668 mm^2) with a peak load exposure of 4.6 kN and tolerated 12400 cycles to failure and 74.5 MNs of cumulative compression. All group analyses excluded this specimen.

Table 7-1: Average endplate area (mm^2) and total number of specimens tested for each combination of normalized load magnitude and normalized static load period. Standard deviation of the endplate area is expressed in parentheses. There were no significant differences in area between any of the load magnitude or static load period groups.

		Load Magnitude (% of Compressive Tolerance)		
		50%	**70%**	**90%**
Static Load Duration (% of load cycle)	**0%**	699(91) N = 14	671(52) N = 16	646(59) N = 14
	50%	668(45) N = 14	652(47) N = 14	694(56) N = 14
	100%	676(62) N = 15	665(58) N = 15	685(53) N = 14
	200%	670(65) N = 15	662(62) N = 14	687(58) N = 16
	1000%	663(68) N = 14	655(58) N = 15	679(38) N = 14

7.5.2 Specimen Survival

Examination of the survival numbers indicated the highest survival rate among load magnitudes occurred for cyclic loading to a peak load of 50% (table 7-2). The lowest survival rate occurred in specimens exposed to static load durations of 100% (table 7-2).

Table 7-2: Percentage of spinal units tested at each combination of normalized load magnitude and normalized static load period that tolerated 12 hours of loading without failure.

		Load Magnitude (% of Compressive Tolerance)			
		50%	**70%**	**90%**	**Total**
Static Load Duration (% of load cycle)	**0%**	28.57	0	0	9.09
	50%	14.29	0	0	4.76
	100%	6.67	0	0	2.27
	200%	20.00	0	0	6.67
	1000%	14.29	6.67	0	6.98
	Total	16.67	1.35	0	5.96

7.5.3 Fracture Morphology

All fractures occurred adjacent to the intervertebral disc and displayed one of four fracture patterns including: crack (Parkinson and Callaghan, 2007b), step (Brinckmann et al., 1988), stellate (Brinckmann et al., 1988) and crush (Hansson et al., 1987). Fractures exhibiting the crack morphology occurred most often, while step fractures were observed in the fewest number of cases (figure 7-3). It appeared that increasing periods of static loading did not greatly alter the fracture type, however increasing the load magnitude above 50% led to a large increase in the number of stellate and crush type fractures (figure 7-3).

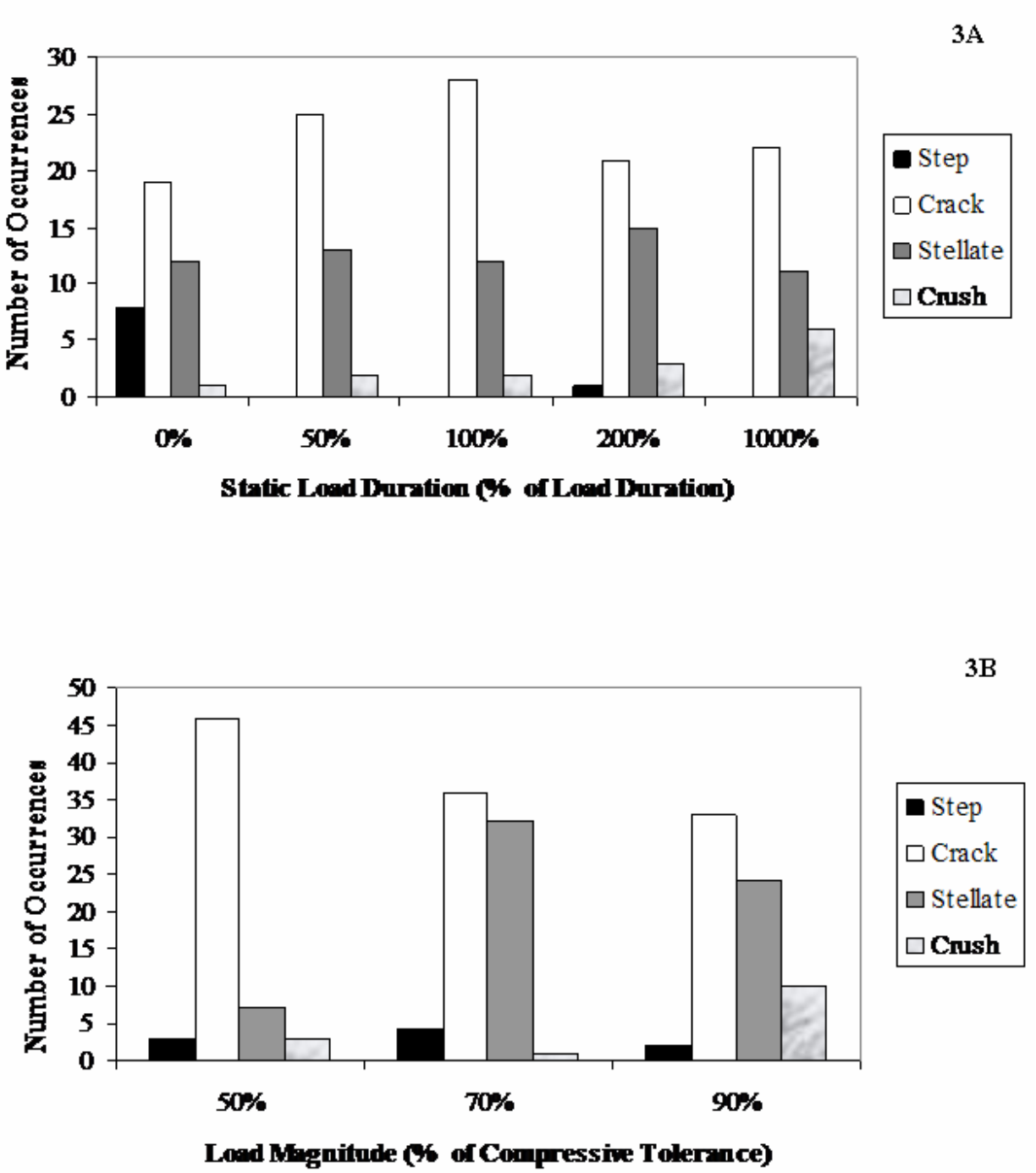

Figure 7-3: (A) A histogram depicting the number of specimens displaying each of the fracture types separated according to static load duration. **(B)** A histogram depicting the number of specimens displaying each of the fracture types separated according to load magnitude exposure.

7.5.4 Cumulative Load Tolerance

Cumulative load tolerated to failure was not significantly affected by insertion of static load periods ($p = 0.1646$). Although not statistically significant, moderate static load periods (50 and 100%) result in lower cumulative tolerances than 0 or 1000% durations at moderate load magnitudes, resulting in a "u" shaped relationship (Figure 7-4a). Load magnitude significantly altered cumulative load tolerance ($p<0.0001$), with specimens in the 50% loading group exhibiting higher cumulative load tolerance than those in the 70 and 90% groups (Figure 7-4b).

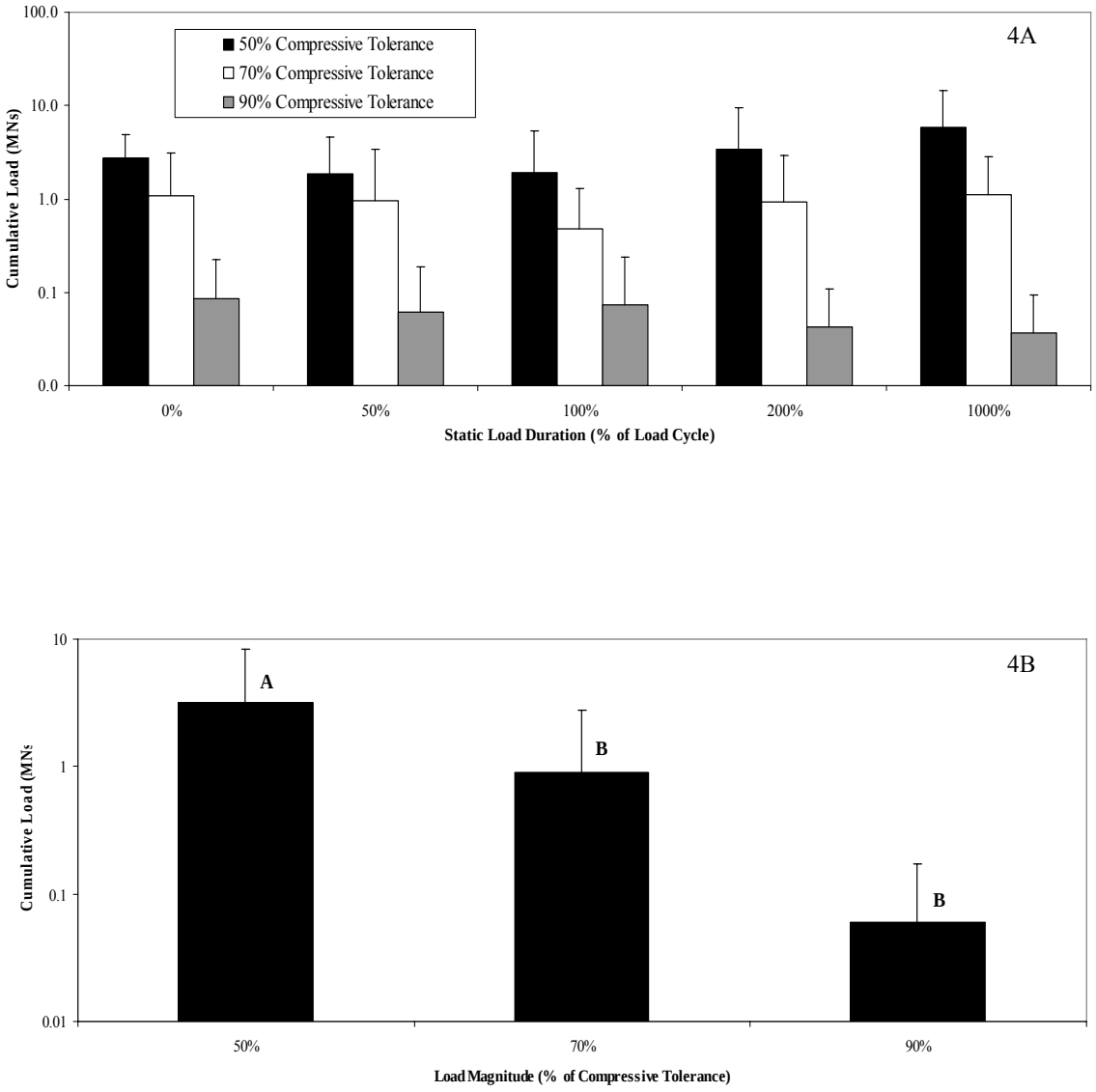

Figure 7-4: (A) Bar chart of average cumulative load (MNs + 1 standard deviation) tolerated to failure at each level of static load duration. No significant differences were found for between group comparisons. **(B)** Bar chart of average cumulative load (MNs + 1 standard deviation) tolerated to failure at each level of load magnitude. Significantly different groups are marked with different letters; groups marked by the same letter are not significantly different. Note that in (A) and (B) the Y axes are logarithmic.

7.5.5 Height Loss

Height loss was significantly altered by load magnitude ($p < 0.0001$) and static load duration ($p = 0.0301$), with no interaction between these variables ($p = 0.4262$). Post hoc analyses indicated that increased peak loading levels resulted in decreased height loss prior to failure, with all between group comparisons significant (figure 7-5a). At moderate load levels, 50 and 100% static load durations resulted in the lowest height loss (figure 7-5b). Surviving specimens demonstrated greater height loss than those that failed (4.76mm vs. 2.11mm, $p < 0.0001$).

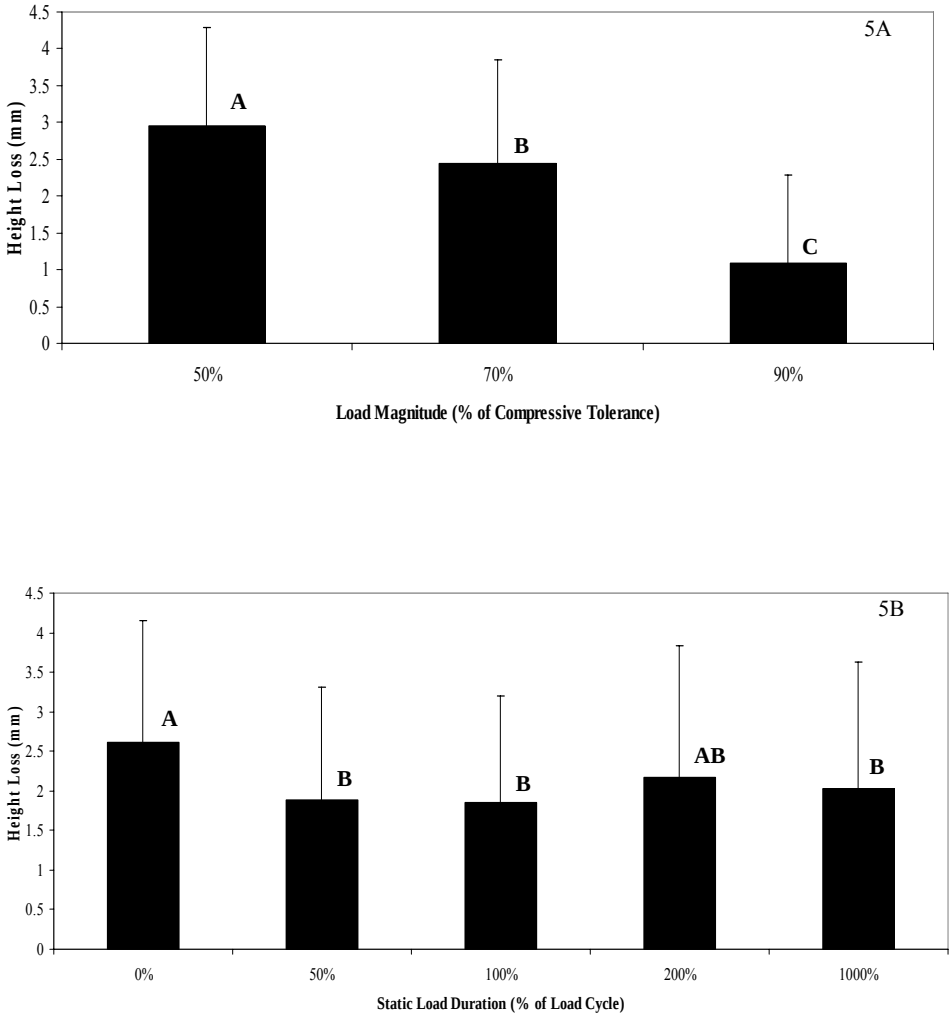

Figure 7-5: (A) Bar chart of average height loss (mm + 1 standard deviation) tolerated to failure at each level of load magnitude. Significantly different groups are marked with different letters. **(B)** Bar chart of average height loss (mm + 1 standard deviation) tolerated to failure at each level of static load duration. Those specimens that had no static load exposure demonstrated significantly greater height loss than those receiving 50%, 100% or 1000% static load durations. Significantly different groups are marked with different letters; groups marked by the same letter are not significantly different.

7.5.6 Survival Time

A significant interaction was found between load magnitude and static load duration effects on survival time ($p = 0.0002$). Examination of the effects of static load duration at each load level

revealed that static loading only significantly effected survival time at 50% ($p = 0.0076$) and 70% ($p = 0.0190$) load magnitudes. Post hoc analysis of the results for the 50% and 70% loading groups revealed that insertion of 1000% static load durations resulted in a greater increase in survival time than all other load periods (table 7-3). Analysis of load magnitude effects at each rest duration revealed that specimens exposed to static load periods of 0% ($p = 0.0003$), 200% ($p = 0.0303$) and 1000% ($p = 0.0062$) were significantly influenced by the peak load magnitude. Post hoc analysis indicated those specimens loaded to a peak magnitude of 50% lasted significantly longer than those exposed to 70% or 90% (table 7-3).

Table 7-3: Average survival time (seconds) for each combination of normalized load magnitude and normalized static load period. Standard deviations are expressed in parentheses. Groups marked with an asterisk (*) do not significantly differ in survival time when compared within a load magnitude and across static load duration. Groups with different letters display a significantly different survival time when compared within a static load period and across load magnitude.

	Static Load Duration (% of work cycle)					
Load Magnitude (% of Compressive Tolerance)		**0%**	**50%**	**100%**	**200%**	**1000%**
	50%	867.8 (673.6) A *	906.8 (1434.8) A *	1227.4 (2342.4) A *	2972.5 (5311.9) A *	10796.5 (15288.5) A
	70%	258.9 (500.3) B *	370.5 (978.0) A *	209.6 (351.8) A *	562.7 (1187.0) B *	1769.4 (2669.7) B
	90%	17.1 (28.9) B *	15.6 (29.9) A *	27.4 (62.0) A *	22.5 (35.1) B *	53.4 (75.1) B *

7.5.7 Cycles to Failure

Analysis of cycles to failure found that load magnitude significantly altered the number of cycles to failure ($p < 0.0001$) with those loaded to a peak of 50% tolerating a higher number of cycles prior to failure than either the 70% or 90% groups, which were not significantly different (Figure 7-6). Static load duration did not alter the number of cycles tolerated to failure ($p = 0.8344$).

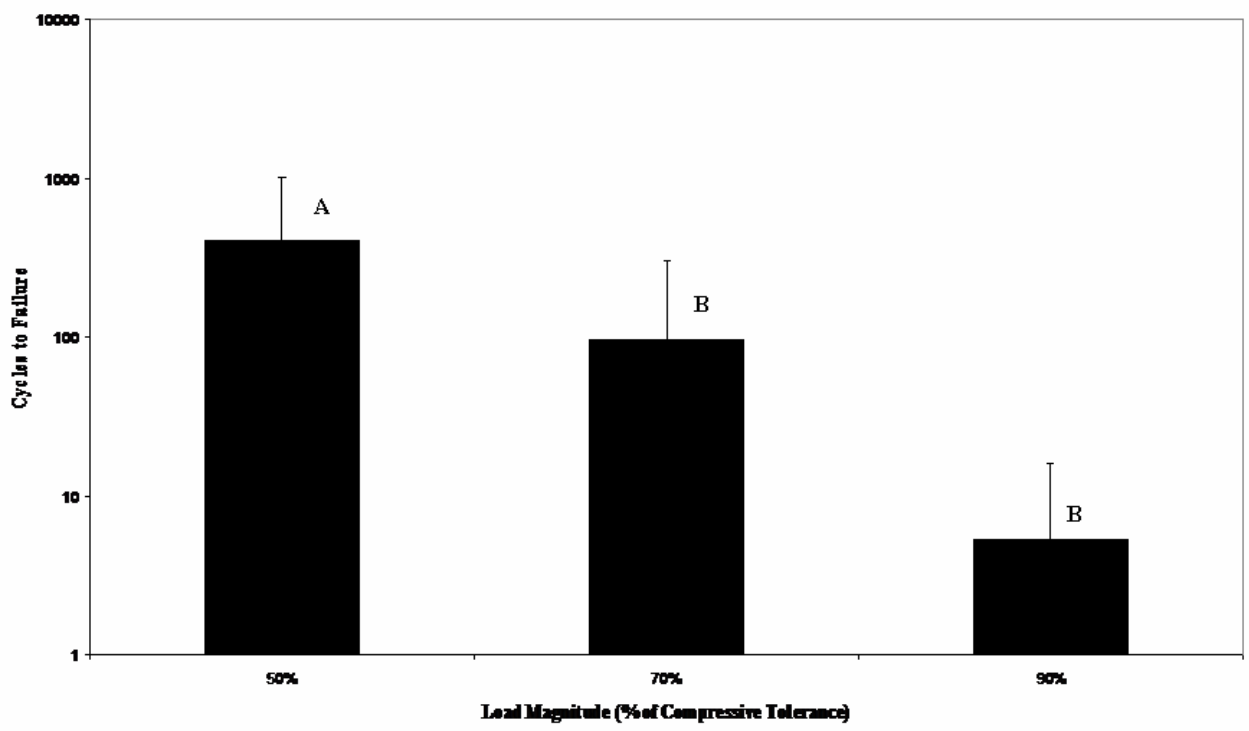

Figure 7-6: Bar chart of average number of cycles (+ 1 standard deviation) tolerated to failure at each level of load magnitude. Significantly different groups are marked with different letters; groups marked by the same letter are not significantly different. Note the Y axis is logarithmic.

7.6 Discussion

This study has shown that long static load periods (1000%) increased the time to failure in the porcine cervical spine. It appears that static load periods impact the cumulative load tolerated to failure but differences were not statistically significant due to high variability in response. Similarly, differences in cycles to failure were not significantly altered by static load exposure. Load magnitude was found to affect the survival rate, cumulative load, cycles to failure, height loss and the survival time of the spinal units.

The effects of load magnitude on cumulative load tolerance were expected based on previous research (Parkinson and Callaghan, 2007b). Additionally, studies examining fatigue failure in bone have shown that increasing load magnitudes decreased tolerance to loading (Michel *et al.*, 1993; Bowman *et al.*, 1998; Caler and Carter, 1989; Haddock *et al.*, 2004; Moore *et al.*, 2004; Moore and Gibson, 2003b; Zioupos *et al.*, 2001; Rapillard *et al.*, 2006). Higher loads also resulted in significantly lower amounts of height loss prior to failure, a result not found in the work of Parkinson and Callaghan (2007b). This may indicate a different mechanism of failure, with intervertebral disc changes (creep) not being as influential at higher loading magnitudes due to a decreased exposure time prior to failure. The amount of height lost across load groups may also be influenced by load rate. To maintain the curve shape and loading frequency the loading rate differed between load groups, with the largest difference occurring between specimens loaded to peaks of 90% and 50%, with the larger load application resulting in a load rate 1.7 times greater. Research has found that spinal units subjected to higher loading rates lose less height than those loaded at lower rates (Yingling *et al.*, 1997; Race *et al.*, 2000b).

Based on previous in-vivo work which found static loading generated larger intervertebral disc height loss than dynamic loading (Ching *et al.*, 2003) it was expected that exposure to the longest static loading duration would create the greatest height loss. However, specimens which did not

receive static loading lost the most height. This may be due to an inability to maintain fluid content within the intervertebral disc without static load periods. To prevent fluid loss to the atmosphere, specimens were surrounded in saline soaked gauze and plastic, however no measures were taken to prevent fluid loss or transfer between tissues of the FSU. The absence of static low level load periods may have prevented fluid recovery and led to increased height loss.

Specimens displaying the greatest height loss may have received beneficial effects from associated changes. Creep loading, which induces height loss (Adams *et al.*, 1996; Keller *et al.*, 1987; Race *et al.*, 2000b; McNally and Adams, 1992), has been shown to alter load distribution within the disc. With creep an increasing amount of load is carried in the periphery of the disc and less load is carried centrally (Adams *et al.*, 1996; McNally and Adams, 1992). This redistribution of load may improve the fatigue resistance of the centrally located trabeculae which appear to be the site of failure under fatiguing compressive loads (Brinckmann *et al.*, 1988; Hansson *et al.*, 1987; Parkinson and Callaghan, 2007b) by increasing the load distribution area (van Dieen *et al.*, 2001). This transfer of load from the central area of the disc to the periphery has been demonstrated in injured segments (Adams *et al.*, 2000) providing a mechanism for continued load carriage despite injury. If this redistribution mechanism does alter the load tolerance of the spine it appears to play a role in the duration of loading tolerated and did not influence the cumulative load or cycle tolerance of the FSU. It was found that the surviving specimens exhibited more than twice the average height loss of the failed specimens, perhaps indicating an ability of survivors to redistribute load throughout the disc and thereby extend the life of the FSU and underlying bone.

This study is subject to several limitations that should be acknowledged, the first of which is the use of a porcine model. The porcine spine model has been heavily employed (Callaghan and McGill, 2001; Callaghan and McGill, 1995; Yingling *et al.*, 1997; Gardner-Morse and Stokes, 2003; Goertzen *et al.*, 2004; Tsai *et al.*, 1998) and allows control over age, size, genetics, illness and diet of

the animals. Previous research has shown that separate spine samples obtained from the current supplier did not differ in size, bone mineral composition, or compressive tolerance indicating a homogenous sample (Parkinson *et al.*, 2005). The anatomical and functional similarities between the human and porcine spine have been demonstrated (Yingling *et al.*, 1999; Oxland *et al.*, 1991) and additional work has determined that the trabeculae display similar architecture (Lin *et al.*, 1997). Additionally Haddock et al. (2004) have shown a similarity in behaviour between young bovine and aged human trabecular bone indicating that trabecular bone may show similar fatigue response in different species.

The potential effects of repair and recovery should be acknowledged. This study employed cycle numbers exceeding those previously reported, which were less than 7000 (Brinckmann et al., 1988; Hansson et al., 1987; Holmes and Hukins, 1994). One thousand cycles has been previously chosen to simulate an hours worth of vigorous activity (Hansson et al., 1987). Here, the maximum cycle number allowed was dictated by a 12 hour time limit and varied based on the static load duration, ranging from 21600 to 1964 cycles for 0% and 1000% static load duration respectively. The greater cycle number allowed fractures to develop at lower loads, which may not have occurred with lower cycle numbers. Although it is important to acknowledge that no physiological repair processes were occurring, their impact would have been minimal over the durations observed. Lotz et al. (1998) concluded that murine intervertebral discs exposed to one week of compression failed to fully recover one month after removal of compression while researchers investigating fracture repair of bone obtained measures of bone repair initiation one week after injury (Garavello-Freitas et al., 2003; Tami et al., 2003), although clotting can occur at a fracture site within 6 to 8 hours of injury (Tortora and Grabowski, 1996). As 93% of the specimens that failed in this study failed within 1 hour, tissue repair would not have affected the fatigue responses. In addition to the lack of cellular

repair, physiologic fluid flow (blood, extracellular) does not exist in this testing approach and its effects are unknown.

An additional limitation exists in the prediction of the maximum compressive tolerance of the spinal units. The equation used had an error of estimation of 11% (Parkinson *et al.*, 2005), which could have resulted in under and over estimation of the peak loads applied in this work. It was expected that errors in estimation would be equally distributed between over and under estimations and would therefore not alter the relationships observed. While these errors are acknowledged and may contribute to the variability reported, earlier research indicates that the implementation of more sophisticated tools in estimation of ultimate compressive strength do not lead to any improvements (Parkinson *et al.*, 2005).

The results of this study indicated that the cumulative load tolerance of vertebral trabecular bone in intact spinal units is significantly altered by the loading magnitude but not significantly altered by the insertion of static load periods. Static load periods extend the survival time of spinal units if the load periods are sufficiently long although they did not alter the cumulative load tolerance at moderate load magnitudes. At high load magnitudes (90% of the estimated compressive load tolerance) static load periods of any duration did not alter cumulative load tolerance or survival duration. Therefore the cumulative compressive tolerance of the spinal unit cannot be significantly increased by the insertion of periods of static load. The inclusion of moderate length static loading periods may even lower the resistance to cumulative compression by limiting height loss and load redistribution which may function to enhance resistance to loading. Based on these results, it does not appear that periods of static rest can be employed to reduce the risk of compression induced injuries of the spine. These results have been used to generate a weighting approach that can be used to account for the effects of load magnitude and rest exposure on the risk of injury due to cumulative

loading (Appendix A). Future research should be conducted to examine the impact of dynamic rest to determine if it may be more effective in reducing the risk of injury.

Chapter 8
Conclusions

8.1 Addressing the Global Hypothesis

1. Can the data needed to use our most sophisticated biomechanical tools be reduced to a level that can be obtained in industry in order to facilitate large scale documentation of spinal load exposure in the workplace?

Hypothesis 1:

Artificial neural networks will allow for a reduction in the amount of input information needed to obtain estimates of spinal load and moment exposures equivalent to those of rigid link and EMG assisted spine models.

The results of study one have indicated that artificial neural networks may provide a method to allow documentation of cumulative and average moments and load exposures through time. However, they do not appear capable of providing accurate peak exposure predictions and should not be implemented in scenarios where it is believed that the risk of acute excessive loading is the primary injury mechanism.

Hypothesis 2:

The errors associated with a quasi-dynamic posture matching tool (3DMatch) relative to rigid link and EMG-assisted models can be quantified and accounted for to allow physiologically reasonable estimates of spine loading.

Study two has shown that 3DMatch based estimates of peak loads should be corrected for over estimation errors, and these corrections should be gender specific (0.62 for male and female peak extension moment, 0.836 for males and 0.518 for females when predicting cumulative extension moments). In terms of load exposures, 3DMatch proved to provide peak bone on bone compression estimates equal in magnitude to those obtained with an EMG-assisted model. If 3DMatch is to be used for determination of cumulative exposure, it should be corrected for the compression bias that exists under zero-moment or low external moment conditions.

2. Can new information regarding spinal exposure to compression and sagittal flexion/extension be used to expand our current understanding of tissue injury mechanisms and thresholds?

Hypothesis 1:

By applying physiologic dynamic kinetic and kinematic profiles to isolated spinal units it will be possible to elucidate injury mechanisms associated with excessive load or excessive motion and from the combined loading paradigm identify a transition in injury mechanisms.

The loading paradigm employed in study three was able to produce a clear delineation of where intervertebral disc herniation becomes the dominant injury mechanism (at loads less than 30% of the

estimated compressive tolerance of the spine). Disc herniation is not likely to be the primary injury mechanism when loads exceeding 30% are applied, in these scenarios the endplate or vertebral bone will fracture first. However, it does appear that the application of repetitive flexion and extension motion decreases the ability of the spinal unit to tolerate compression. This information can be used in ergonomic assessments to help in focusing on load and motion as separate injury mechanisms based upon the particular exposure.

3. Is it possible that loads can be redistributed across the vertebral endplate in such a way as to enhance the ability of the spine to withstand cumulative compression?

Hypothesis 1:

By inserting periods of low level static loading between dynamic load applications the spinal unit will be capable of tolerating greater amounts of cumulative compression.

By examining various lengths of low level static 'rest' periods study four was able to show that the inclusion of these periods between dynamic loading cycles did not result in an enhancement of the spine's resistance to cumulative loading. In fact, it appeared that periods of moderate static rest might actually decrease tolerance to this dynamic load profile. Therefore care should be taken when attempting to manipulate work rest scenarios to ensure that the targeted changes are actually beneficial, not neutral or even detrimental.

8.1.1 Summary

This work has highlighted several approaches that may be used to document peak and cumulative load and moment exposures while industrial tasks are performed. These tools were compared to the most sophisticated biomechanical models that are currently employed in laboratory settings. While relative errors between the methods have been quantified and corrective approaches identified, the work has not yet been extended into industry. While the conclusions of studies one and two support the viability of the posture matching and artificial neural network approaches, research must still be performed to determine how well the obtained exposure estimates will relate to the reporting of injury.

In addition, tissue based evidence has been provided to clarify the effects of rest and posture on injury development in the osteoligamentous spine. Based upon the observations, it would appear that disc herniation is not a likely injury mechanism when load exposures are sufficiently large and are more likely to occur in jobs that require repetitive flexion under very light loads. Additionally, the results of study four indicate that static periods of rest do not enhance the ability of the osteoligamentous spine to tolerate cumulative load and therefore the use and benefit of rest periods in work cycles must be interpreted with caution.

The four studies included in this thesis are all related in that they provide new information regarding methods that may be used to predict load exposures and tissue tolerances. The studies regarding artificial neural network and 3DMatch provided kinematics, joint moments and joint load exposures that were used to determine the loading profile used in examining the role of motion in cumulative injury development (figure 8-1). The predicted joint kinetics can also be used in future work to determine reasonable load exposures given similar task demands. The tissue based studies provided valuable new information on spine tolerances to load, motion and rest that can be incorporated into current tissue injury models.

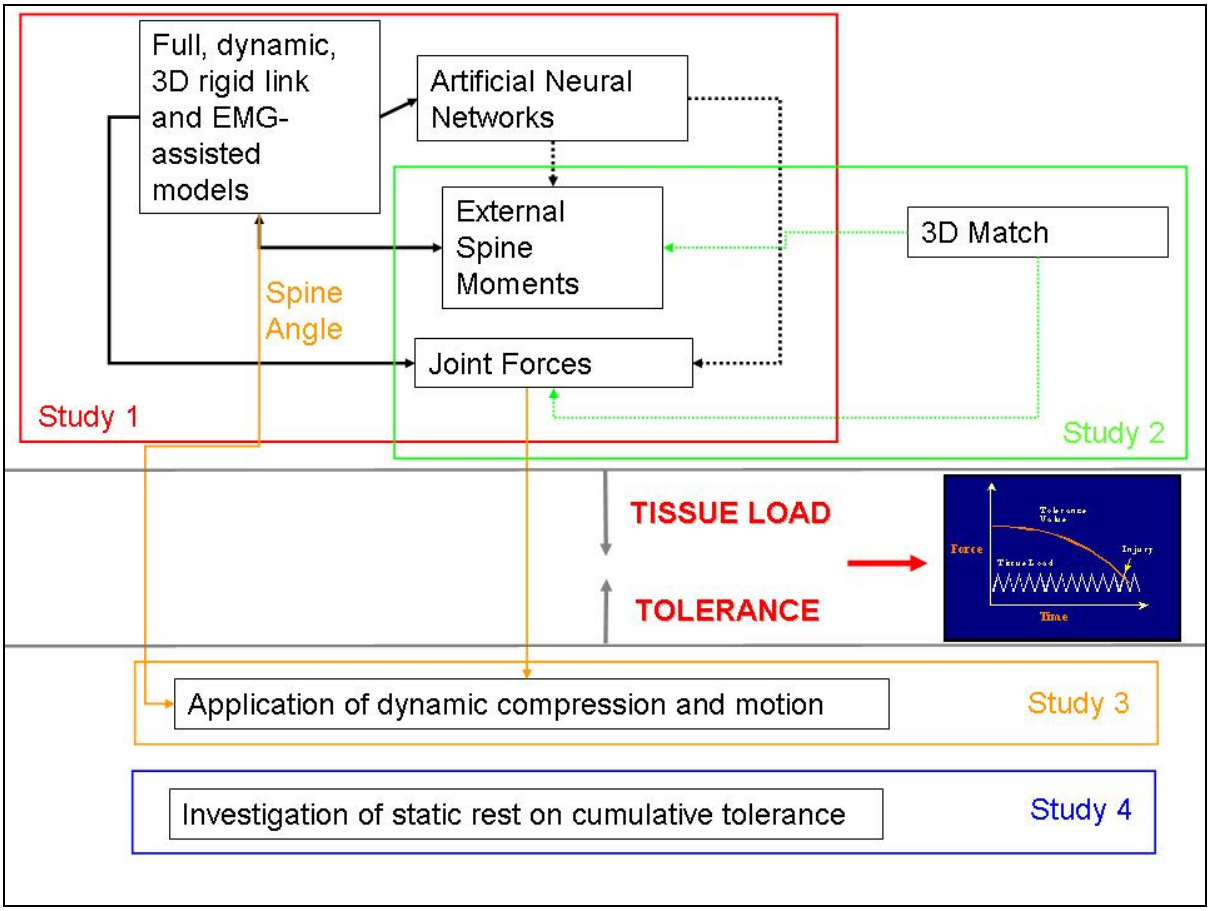

Figure 8-1: Flow chart highlighting the interconnections between the studies comprising this thesis. Note that the dashed lines indicate results obtained from simplified models. The orange lines indicate variables which were carried directly from the in-vivo studies to the in-vitro studies.

8.1.2 Future Directions

Although this work stands as a new contribution to the fields of biomechanics, injury determination and ergonomics, perhaps its greatest strength is in the development of future lines of inquiry. The obvious extension of any laboratory based study is to take the new methods and conclusions and test them in an applied setting, in this case industrial based manual materials handling tasks. To truly determine the effectiveness of the artificial neural networks and 3DMatch

approaches they need to be assessed under true industrial conditions to assess their ability to isolate jobs that pose a greater risk of injury from those that do not. In doing such experimentation it is hoped that these tools will also allow for the documentation of industrial exposures as they are altered by personal factors that may influence loading exposures despite constant task demands. Additionally, it is hoped that this work will raise the profile of artificial neural networks as a potential tool in predicting joint loads. While a thorough approach was applied to try and develop the best neural network configurations for the desired predictions there may have been inherent limitations present in using the preset network forms contained within the Matlab software. It may be possible to develop neural networks that are more accurate in their prediction of peak and cumulative loads, and it would be a disservice to the potential of this approach to not explore alternative configurations. In addition, it would be beneficial to examine a wider variety of industrially related tasks to determine the ability of the neural network and 3DMatch approaches to adapt to more novel exposures.

The tissue based values determined in this thesis are intended to improve our understanding of how tissue tolerance can be altered by modifying factors, an understanding which is critical in assessments of injury risk. However, this work was based upon an animal model and as such should not be taken to reflect the absolute magnitude of exposures expected to lead to injury in the human spine, but should be understood to reflect the general shape of the exposure-injury curves due to morphological and mechanical similarities between the human and animal spines. Future work should be undertaken to determine proper scaling or transfer functions that may allow for a direct comparison of the animal model resultant magnitudes to those of humans. This line of research will need to marry the results from animal, cadaver, and epidemiological studies.

Appendix A

The following paper, entitled 'Quantification of the relationship between load magnitude, rest duration and cumulative compressive tolerance of the spine: development of a weighting system for adjustment to a common injury exposure level' presents the results of chapter 7 as they were employed to develop weighting factors to account for the role of load and rest in the development of cumulative injuries. The data is presented in a more theoretical manner and equations are provided to allow determination of appropriate weighting factors based upon peak load exposures and rest durations. It is intended to illustrate how knowledge about tissue tolerance can be transferred out of the laboratory and employed in situations of injury risk determination.

Theoretical Issues in Ergonomics Science
Vol. 9, No. 3, May June 2008, 255 268

Taylor & Francis
Taylor & Francis Group

Quantification of the relationship between load magnitude, rest duration and cumulative compressive tolerance of the spine: development of a weighting system for adjustment to a common injury exposure level

ROBERT J. PARKINSON and JACK P. CALLAGHAN*

Department of Kinesiology, Faculty of Applied Health Sciences,
University of Waterloo, 200 University Avenue West, Waterloo,
Ontario N2L 3G1, Canada

(*Received 4 September 2006; revised 8 January 2007; in final form 13 January 2007*)

The objective of this study was to quantify the relationship between load magnitude, rest duration and cumulative compression tolerance in the spine. A total of 218 porcine cervical spinal units were dynamically compressed in one of 15 loading paradigms. Each paradigm was a combination of one of three normalized peak load magnitude exposures (50, 70 and 90% of the units estimated compressive tolerance) and one of five normalized rest durations (0, 50, 100, 200 and 1000% of the 2 second work duration). At the lowest load exposure level (50%) the spinal units sustained significantly greater amounts of cumulative compression prior to failure than units exposed to 70 or 90% peak loads, which did not differ. Rest did not significantly increase the resistance of the spine to cumulative compression; however, it appears that moderate durations of rest (50 and 100%) may decrease the tolerance of the spine to cumulative compression at moderate load levels. Attempts to adjust the measured cumulative loads to a common injury exposure level based on previously developed weighting methods were unsuccessful, prompting the development of a weighting method using the three-dimensional relationship between load magnitude, rest duration and cumulative compression. Load magnitude and rest duration impact the cumulative load tolerance of the spine, with load magnitude exerting greater influence. These results indicate that rest may not reduce the risk of osteoligamentous spine injury.

Keywords: Cumulative load; Spine; Weighting; Compression; Rest

1. Introduction

Increased cumulative compression in the low back has been associated with an increase in the reporting of low back pain among institutional aides (Kumar 1990) and automotive assembly workers (Norman *et al.* 1998) as well as an increased appearance of symptomatic osteochondrosis, spondylosis and concomitant disc herniation (Seidler *et al.* 2001, 2003). Cumulative compression is calculated as the time-integrated compression exposure and is therefore subject to modification based on several factors, such as posture, load magnitude and pattern of exposure duration. While recent evidence has demonstrated an effect of joint posture on the

ability of the osteoligamentous spine to resist cumulative compression (Gallagher *et al.* 2005), little is known about the interaction of load magnitude and rest exposure on injury development within the intervertebral joint.

Until recently, the relationship between load magnitude and cumulative load tolerated prior to failure had not been quantified. Earlier work described a non-linear relationship between load magnitude and the number of cycles to failure (Hansson *et al.* 1987, Brinckmann *et al.* 1988); however, attempts to convert the reported load exposure data into cumulative compression revealed high variability in the data, with subsequent poor quantification of the relationship between load magnitude and cumulative load tolerance (Callaghan 2006). Based on the poor relationship characterization brought on by the high variability in the earlier studies, Parkinson and Callaghan (2007) investigated the relationship between load magnitude and cumulative load tolerance using a controlled porcine animal model. Their results revealed a highly non-linear relationship between load magnitude and cumulative load tolerance and provided adjustment factors to be used in future summations of cumulative load to reflect the greater impact of larger load magnitudes on the development of cumulative compression injuries. While previous work had implemented a non-linear weighting of load magnitudes (Jager *et al.* 2000, Seidler *et al.* 2001), this animal model study was the first to present quantitative tissue-based evidence supporting the need to adjust calculations based on load exposure.

As cumulative load reflects the load exposure over a period of time, the insertion of rest may influence the potential for injury development and may interact with load magnitude in the modulation of tissue tolerances. The inclusion of rest during repeated trunk flexion has been shown to increase the endurance time in both pain free and chronic recurring low back pain reporters as well as decrease the rate of discomfort development (Keyserling *et al.* 2005). Additionally, increased rest breaks have been shown to reduce the presence of musculoskeletal symptoms in agricultural workers exposed to labour requiring large amounts of spinal flexion and static loading (Faucett *et al.* 2007). The above studies examining the impact of varying work rest schedules on pain and discomfort development in the back were based on self-reports and were not intended to isolate or identify the affected tissue(s). Animal model evidence indicates that the insertion of rest periods can act to alleviate neuromuscular dysfunction (Sbriccoli *et al.* 2007). It was shown in a feline model that a work : rest ratio of 1 is optimal in preventing neuromuscular disorders elicited by static lumbar flexion (Sbriccoli *et al.* 2007). However, this conclusion was only supported for loading durations of 30 min. For loading durations exceeding 30 min, long-term rest was not able to restore proper function even when the rest duration exceeded that of the loading period (Sbriccoli *et al.* 2007). Rest periods may become more important to the recovery of neuromuscular function as the number of load repetitions increases, as an increase in the number of load repetitions has been shown to lead to an increase in the severity of dysfunction (Sbriccoli *et al.* 2004). Although the impact of loading on neuromuscular function should not be ignored, it has been shown that recovery of the viscoelastic tissues of the spine takes a much longer period of time than that of the neuromuscular system (Solomonow *et al.* 2000). This tissue-dependent recovery may indicate that differences exist in the ability of various tissues to tolerate load and, as such, investigations into cumulative loading and potential rest effects should isolate the behaviour of isolated spinal tissues to allow identification of injury sites and tolerance limiting structures.

As repetitive compression of the spine has been shown to lead to fractures of the vertebral endplate and the underlying trabecular bone (Hansson *et al.* 1987, Brinckmann *et al.* 1988, Parkinson and Callaghan 2007), this region should be examined.

Due to a lack of quantitative investigation into the impact of rest periods on the development of cumulative compression injuries within the intervertebral joints of the spine, this study was conducted to determine the effects of varying rest durations on the cumulative load tolerance of porcine spinal units. The study was designed to also identify any potential interactions between load magnitude and rest exposure. Additionally, analyses were performed to assess the impact of previously developed weighting factors (Parkinson and Callaghan 2007) on the adjustment of measured cumulative loads for the non-linear influence of load magnitude on injury development.

2. Methods

2.1. *Specimen dissection and mounting*

A total of 218 frozen porcine cervical functional spinal units (FSU two adjacent vertebrae, intervening disc and passive tissues) were obtained from a local abattoir. Spines were allowed to thaw overnight prior to dissection, during which the osteoligamentous spine was isolated through removal of the surrounding musculature. Both the C3C4 and C5C6 FSUs were used for testing as previous work has shown them to be similar in compressive strength, endplate area and bone mineral content (Parkinson *et al.* 2005). Only non-degenerated specimens (grade 1) on the scale proposed by Galante (1967) were included in this study. As in previous work (Parkinson and Callaghan 2007), the endplates were measured along the midline in both the anterior posterior (A) and medial lateral (B) directions to allow calculation of endplate area based on the surface area of an ellipse ($\pi/4*A*B$). Once the surface area of the two exposed endplates was calculated, an average was determined and used to represent the FSU.

After dissection, isolated FSUs were mounted in aluminium cups such that the midplane of the intervertebral disc was aligned parallel to the surface of the aluminium cups. In order to maintain the natural lordosis of the segments, non-exothermic dental plaster (Denstone, Miles, South Bend, IN, USA) was placed in the cups and allowed to harden around the exposed endplates to support the segment and preserve neutral joint posture. Plaster was not allowed to provide reinforcement around the exterior surface of the vertebrae. The lower aluminium cup was fastened to a steel plate, which sits on a bearing table, allowing anterior posterior and medial lateral translations as well as axial rotations. The superior vertebral cup was mounted to a custom platen threaded directly into the actuator of a servohydraulic materials testing machine in series with a 25 kN load cell (8872; Instron Canada, Toronto, ON, Canada). After the specimen was mounted within the system, the FSU was preloaded at 300 N for 15 min (Callaghan and McGill 1995, Yingling *et al.* 1999, Gunning *et al.* 2001) prior to the initiation of cyclic testing. Throughout testing, specimens were wrapped in saline-soaked gauze and plastic to prevent moisture loss.

2.2. *Loading scenario*

Prior to data collection, a rigid link model (GOBER; University of Waterloo, Waterloo, On, Canada) was employed to obtain an estimate of the L4L5 joint compression during a single floor to waist height lift. The resulting profile amplitude was subsequently scaled to run from 0 to 1. The scaled waveform was then adjusted to run from a minimum load of 300 N up to the desired percentage of maximum compressive tolerance. Maximum compressive tolerance was estimated using the average endplate area of the FSU and an equation developed previously on a porcine cervical FSU sample (Parkinson *et al.* 2005). In this study, three peak load magnitudes were investigated, corresponding to 50, 70 and 90% of the estimated maximum compressive tolerance. Once a specimen was assigned to a load magnitude group it was then allotted to one of five rest durations, expressed as a percentage of the loading cycle (2 seconds load duration based on 0.5 Hz loading frequency (Hansson *et al.* 1987, Brinckmann *et al.* 1988, Holmes and Hukins 1994, Parkinson and Callaghan 2007)). Five rest periods were examined resulting in normalized durations of 0, 50, 100, 200 and 1000% of the work duration. In essence, the absolute length of the duty cycle was maintained at 2 seconds for all conditions and the total cycle time was altered by varying the rest component in multiples of the duty cycle.

Cyclic loading was performed on the servohydraulic materials testing machine using the associated software (Single Axis Max; Instron Canada) until failure occurred or a maximum test duration of 12 hours was reached. During testing the load and displacement data were sampled at 10 Hz. Average cycle stiffness was calculated for each cycle (equation 1), where one cycle comprised the load application and entire rest period.

$$Cycle\ Stiffness\left(\frac{kN}{mm}\right) = \frac{(Maximum\ Cycle\ Load\ (kN) - Minimum\ Cycle\ Load\ (kN))}{(Maximum\ Cycle\ Displacement\ (mm) - Minimum\ Cycle\ Displacement\ (mm))} \quad (1)$$

As in previous research, failure was identified by an abrupt increase in the sampled displacement and an accompanying decrease in the cycle stiffness (Hansson *et al.* 1987, Brinckmann *et al.* 1988, Parkinson and Callaghan 2007). These structural property changes correspond to macroscopic failure within the vertebrae. Cumulative load tolerance was calculated through trapezoidal integration of the loading profile up to the failure cycle and was reported in MNs.

2.3. *Implementation of previously developed weighting factor*

Earlier work attempted to produce a weighting factor to adjust for the influence of load magnitude on cumulative compression-induced injury (Parkinson and Callaghan 2007). In order to assess the impact of these weighting factors, they were implemented using two methods. The first weighting method (WM1) involved normalizing the applied load on a point by point basis (10 Hz), determining the appropriate weighting factor and using the product of the load magnitude (kN) and weighting factor at each point in the determination of cumulative load exposure.

The second weighting method (WM2) applied the weighting factor only once, determining the weighting factor corresponding to the peak normalized load application and multiplying it with the total cumulative load exposure prior to failure.

2.4. *Surface characterization and weighting factor development*

In order to mathematically describe the three-dimensional relationship between normalized load magnitude (load), normalized rest duration (rest) and cumulative load tolerance, a sigmoid surface with an offset was fit to the raw data based on equation 2, where A, B, C, D, E and F are the coefficients for fitting the surface, 'rest' is the normalized rest duration and 'load' is the normalized compression magnitude.

$$cumulative\ load\ (MNs) = \frac{A}{((1 + e^{(B-C\times rest)}) \times (1 + e^{(D-E\times load)}))} + F \qquad (2)$$

The following steps were taken to develop the weighting factors based on the sigmoid surface fit to the original data:

2.4.1. Step 1 – Predicted load generation. Predicted cumulative load tolerances were generated for all combinations of load magnitude (1 100% in 0.5% increments) and rest duration (0 1000% in 10% increments) using equation 2, resulting in a 199 by 101 array of predicted cumulative load tolerances.

2.4.2. Step 2 – Minimum value adjustment. The minimum value of the 199 by 101 array was found. As this value was negative, the absolute value of the minimum was added to all values in the array to set the minimum to zero. This resulted in a positive shift of the surface with no alteration to the shape.

2.4.3. Step 3 – Inverse value calculation. The inverse of all 199 by 101 values was calculated.

2.4.4. Step 4 – Determination of final adjustment value. The average inverse value for all load magnitude-rest duration combinations below 37.5% load magnitude was calculated and this average value was subtracted from 1. The ratio between the previously calculated average inverse value and this difference (1 average inverse value) was determined.

2.4.5. Step 5 – Threshold establishment. Based on previous work (Parkinson and Callaghan 2007), all weighting factors for load magnitudes less than 37.5% (regardless of rest duration) will be set equal to 1.

2.4.6. Step 6 – Proportional increase. The ratio determined in step 4 was then used to proportionally increase all of the inverse values obtained for all load

magnitude-rest duration combinations at or above load magnitudes of 37.5%, using the following equation:

$$weighing\ factor = inverse + (ratio \times inverse) \quad (3)$$

The result of these manipulations was a 199 by 101 look-up table containing the weighting factor for each combination of load magnitude and rest duration.

2.5. *Statistical analysis*

In order to test for differences in specimen size, a two-way ANOVA was used to compare the endplate area between each of the 15 testing groups (five normalized load levels by three normalized rest durations). Subsequently, a two-way ANOVA was performed to analyse differences between the testing groups for the cumulative load tolerated to failure for each calculation method (unweighted, WM1 and WM2). A least significant difference post hoc test was used to identify significant between-group differences. In order to assess the impact of the weighting factors for each load level, least square means tests were performed within each rest level. All tests with $p < 0.05$ were considered statistically significant.

3. Results

Statistical analysis indicated that specimen randomization was successful, as no differences were found in the average endplate areas of the FSU between groups (table 1; $p = 0.535$). Due to random assignment of the FSUs, there is slight variation in the number of specimens tested within each group (table 2). One specimen exhibited an unusually high tolerance to cumulative load in the 50% load 50% rest group, showing a tolerance greater than 40 times the group mean. Determination of the failure cycle and cumulative load tolerated to failure resulted in values of 12 400 cycles and 74.5 MN, respectively. This specimen exhibited an endplate area below the mean of the group (627 mm^2 vs. 668 mm^2) and was loaded to an absolute peak load of 4.6 kN. All group analysis excluded this specimen.

Table 1. Average endplate area (mm^2) of specimens tested for each combination of normalized load magnitude and normalized rest period (standard deviation of the endplate area is expressed in parentheses)

		Load magnitude (% of compressive tolerance)		
		50%	70%	90%
Rest duration (% of load cycle)	0%	699 (91)	671 (52)	646 (59)
	50%	668 (45)	652 (47)	694 (56)
	100%	676 (62)	665 (58)	685 (53)
	200%	670 (65)	662 (62)	687 (58)
	1000%	663 (68)	655 (58)	679 (38)

Note: There were no significant differences in area between any of the load magnitude or rest duration groups.

Examination of the number of surviving specimens per group indicated that at high loading exposures (90%), there was no occurrence of survival. When FSUs were exposed to dynamic loading up to a peak of 70%, survival was only documented in the 1000% rest group. Overall, the highest rate of specimen survival occurred when FSUs were exposed to a maximal peak load of 50% and given no rest (table 2). In terms of rest duration, the lowest survival rate occurred in those specimens exposed to rest durations of 100%, while specimens that received no rest periods exhibited the highest occurrence of survival.

Analysis of the cumulative load tolerated to failure showed no statistically significant impact of rest ($p = 0.1646$). Despite the lack of significant differences, it appears that moderate rest levels (50 and 100%) result in lower cumulative tolerances than either the 0 or 1000% rest durations at moderate load magnitudes, resulting in a 'u' shaped relationship (figure 1). However, if exposed to high (90%) peak loading magnitudes, the cumulative load tolerance appears to be unaffected by rest periods. Load magnitude was shown to significantly alter cumulative load tolerance

Table 2. Total number of functional spinal units tested for each combination of normalized load magnitude and normalized rest period (the number of surviving specimens is indicated in parentheses)

		Load magnitude (% of compressive tolerance)			
		50%	70%	90%	Total
Rest duration (%)	0%	14 (4)	16	14	44
	50%	14 (2)	14	14	42
	100%	15 (1)	15	14	44
	200%	15 (3)	14	16	45
	1000%	14 (2)	15 (1)	14	43
	Total	72	74	72	218

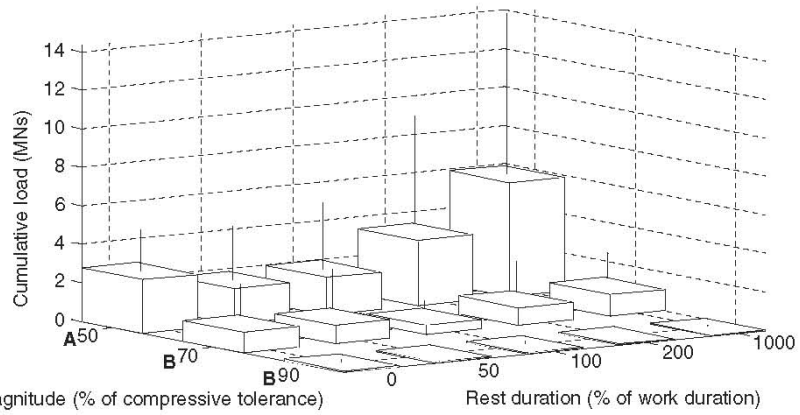

Figure 1. Three-dimensional bar chart of average cumulative load (MN + 1 SD) tolerated to failure at each level of load magnitude and rest duration. Significantly different load groups are marked with different letters; groups marked by the same letter are not significantly different. No significant differences were found between the rest groups and therefore no designations were applied.

Table 3. The between-group differences in cumulative compression tolerance based on load magnitude exposure (the differences were calculated based on unweighted cumulative compression as well as those calculated using method 1 (point by point) and method 2 (one time adjustment))

Load magnitude comparison	Unweighted cumulative load (MN)	Weighted method 1 (MN)	Weighted method 2 (MN)
50–90	3.1*	2.9*	2.7*
50–70	2.3*	1.6*	1.1
70–90	0.8	1.2*	1.6*

*Differences were significantly different.

Table 4. Resulting p-values as determined through least square means analysis comparing the unweighted cumulative load tolerance value with the weighted cumulative load tolerance value as determined using the point by point method (weighting factor method 1 (WM1)) and the weighted cumulative load tolerance value as determined using the one time adjustment method (weighting factor method 2 (WM2))*

Load comparison	Method	0% Rest	50% Rest	100% Rest	200% Rest	1000% Rest
50(u) – 50(w)	WM1	0.8589	0.9211	0.8863	0.9009	0.9175
	WM2	0.8110	0.8858	0.8116	0.8171	0.7516
70(u) – 70(w)	WM1	0.2080	0.3832	0.5879	0.5691	0.7268
	WM2	0.0911	0.2179	0.3783	0.3244	0.3436
90(u) – 90(w)	WM1	0.4901	0.6882	0.5564	0.8374	0.9250
	WM2	0.3469	0.5627	0.3275	0.7157	0.8185

*Load group comparisons were performed within each rest duration group.
u = unweighted; w = weighted.

($p < 0.0001$), with specimens in the 50% loading group exhibiting significantly higher cumulative load tolerance than those in the 70 and 90% loading groups (figure 1). Implementation of the weighting factor using a point by point basis (WM1) did not alter the main effect conclusions, with rest not significantly altering the cumulative tolerance ($p = 0.3924$) and load magnitude having a significant impact ($p < 0.0001$). As in the unweighted analysis, specimens loaded to a peak of 50% showed significantly higher cumulative load tolerance than those in either the 70 or 90% loading groups (table 3). However, unlike the unweighted cumulative load analysis, implementation of the weighting factor in this method led to an increase in the difference between the 70 and 90% load groups, with this difference becoming significant. Implementing the weighting factors as in WM2 led to the same conclusions regarding the effects of rest duration (non-significant, $p = 0.3706$) and load magnitude (significant, $p = 0.0021$). However, implementation of the weighting factors in this way altered the between-group differences, with the 50 90 and 70 90% differences being significant and the 50 70% group difference being non-significant (table 3). Least square means analysis indicated that neither weighting factor method resulted in significantly increased cumulative load magnitudes at any load magnitude level (table 4).

Based on the observed cumulative load tolerances, the three-dimensional offset sigmoid surface fit was performed, resulting in the production of six coefficients

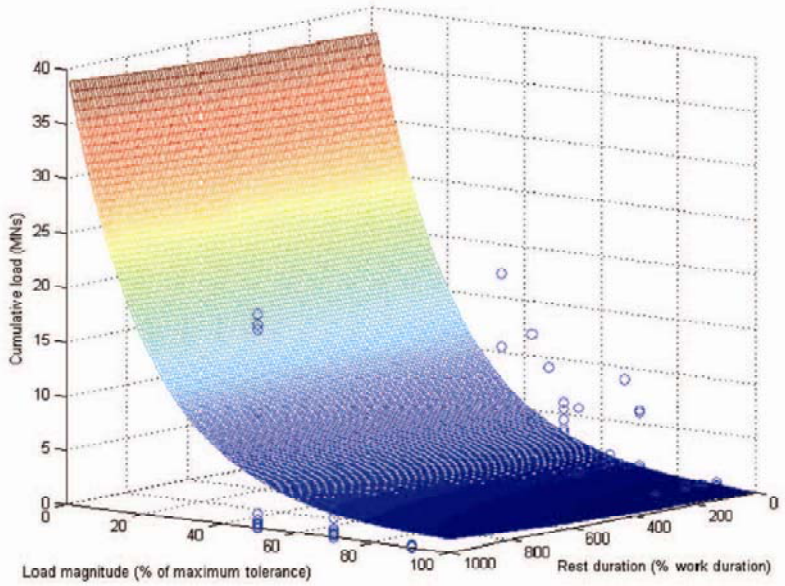

Figure 2. Three-dimensional surface plot (sigmoid function) of predicted cumulative load tolerance (MN) based on load magnitude and rest duration exposure. The original data points are indicated with open circles.

Table 5. Sigmoid coefficients corresponding to variables found in equation 2

Variable	Value
A	$-8.7935186745278279 \times 10^{3}$
B	-9.8201224272378766
C	$-1.2383823459601530 \times 10^{-3}$
D	-5.3884836951142532
E	$4.7976511526969565 \times 10^{-2}$
F	$8.7922770051365042 \times 10^{3}$

corresponding to those in equation 2 (figure 2, table 5). The resulting fit produced a correlation coefficient of 0.44 with a corresponding root mean square difference of 2.9 MNs. In determining the weighting factors as outlined above, it was found that the ratio between the average inverse value for all load magnitude-rest duration combinations and the difference between the average value and one ('ratio' in equation 3) was 13.26309.

4. Discussion

As expected, based on previous research (Parkinson and Callaghan 2007), the relationship between load magnitude and cumulative load tolerance in the

osteoligamentous porcine spine is non-linear. While the insertion of rest did not statistically alter the cumulative load tolerated to failure, it does appear to modify the tolerance. At moderate load magnitudes (50 and 70% of maximum estimated tolerance) it appears that short rest breaks are not beneficial and actually reduce the tolerance of the spinal unit. Rest durations equal in length to the work duration resulted in the lowest cumulative compression tolerance. This result is in opposition to the findings of Sbriccoli *et al.* (2007), who found a ratio of unity to be most beneficial for neuromuscular recovery from cyclic loading. Additionally, it appears that cyclic compression with no rest periods may result in a higher cumulative load tolerance than loading patterns with brief rest periods. This result contrasts with previous work, which found that a high frequency of loading (lifting) resulted in a higher incidence rate of low back pain (Chaffin and Park 1973). However, the same study also found that a low frequency of lifts can increase the low back pain incidence, suggesting that there may be a beneficial exposure level, as moderate amounts of lifting resulted in the lowest incidence rate (Chaffin and Park 1973). For peak loading of 90% of the estimated compressive tolerance, the insertion of rest did not play a role in altering cumulative load sustained at failure.

The implementation of previously determined weighting factors did not result in an adequate adjustment of the cumulative load tolerances, as neither implementation method was able to reduce all significance between load group comparisons and even acted to make some previously non-significant comparisons significant. Further analysis indicated that these weighting factors did not significantly increase the cumulative load tolerance value at any rest level. A re-examination of the methodology employed in generation of the weighting factors determined that, when adjusting the factors to have a minimum weighting factor of 1, the values occurring above the threshold load level (37.5%) were not increased by the same percentage as the values below the threshold as an absolute addition was performed (Parkinson and Callaghan 2007). In generating the weighting factors based on the results of this study, a percentage increase was performed in order to overcome this limitation. By performing this relative increase and multiplying the predicted cumulative load values by the corresponding weighting factor, a constant magnitude prediction is returned.

As with all work, this study is subject to several limitations that should be acknowledged. First, this *in vitro* work was performed using a porcine model. The model allows control over the age, size, genetics, illness history and diet of the animals and has been extensively used for *in vitro* spinal research (Callaghan and McGill 1995, Yingling *et al.* 1997, Tsai *et al.* 1998, Callaghan and McGill 2001, Dickey and Gillespie 2003, Gardner-Morse and Stokes 2003, Goertzen *et al.* 2004). The widespread use of this model is supported by the anatomical and functional similarities between the human and porcine spine, which have been previously documented (Oxland *et al.* 1991, Yingling *et al.* 1999). Given that the fractures created from cyclic compression occur to the endplate and underlying trabecular bone, it is critical that the bone be architecturally similar to the population being modelled (human), which has been previously demonstrated (Lin *et al.* 1997). These similarities do not mean that the findings of this study are directly applicable to the *in vivo* human lumbar spine or that scaling is possible as transference does not yet have empirical support. The use of normalized loads is an attempt to facilitate future work, which may apply these findings to human loading exposures, assuming *in vivo* load exposure can be normalized to an individual worker's estimated

compressive strength. This can be done by predicting individualized *in vivo* compressive strength using factors of age, gender, spinal component and body weight (see Genaidy *et al.* 1993 for a summary of individual predictive equations).

The porcine samples employed in this study were obtained while frozen and thawed prior to use. An examination of the effects of freezing on porcine spinal units found that frozen storage had no effect on the stiffness response, displacement at failure and failure mode of the spinal unit (Callaghan and McGill 1995). However, frozen storage increased the energy absorbed to failure by 33% and increased the ultimate compressive load tolerated by 24% (Callaghan and McGill 1995). As all specimens in this study were obtained frozen and allowed to thaw overnight at room temperature, any effects of freezing are assumed constant and would therefore not alter the relative comparisons contained within this work.

With any *in vitro* fatigue study, the potential effects of repair and recovery should be acknowledged. This study employed cycle numbers much larger than those previously reported (Hansson *et al.* 1987, Brinckmann *et al.* 1988, Holmes and Hukins 1994), with 1000 cycles being stated to replicate an hour's worth of vigorous activity (Hansson *et al.* 1987). Maximum cycle numbers in this study ranged from 21 600 cycles for 0% rest to 1964 cycles for 1000% rest, dictated by the time limit of 12 hours. While this high cycle number allowed fractures to develop at lower load magnitudes than may occur if the maximum cycle number were set lower, there were no physiological repair mechanisms able to act. Clotting can occur at a fracture site 6 to 8 hours after injury (Tortora and Grabowski 1996) and measures of bone repair initiation have been obtained 1 week after injury (Garavello-Freitas *et al.* 2003, Tami *et al.* 2003). On a longer time scale, Lotz *et al.* (1998) concluded that murine intervertebral discs exposed to 1 week of compression failed to fully recover 1 month after removal of compression. Based on these time intervals, it is not expected that tissue healing would have a large effect on the results as 93% of the specimens that failed in this study did so within the first hour of cyclic loading.

The shape of the curve for load magnitudes less than those examined (50% of the estimated compressive tolerance) is extrapolated and should be treated as an estimate of the impact of these load magnitudes on the FSUs' resistance to cumulative compression. Similarly, any extrapolation of the rest effects beyond 1000% should also be treated as an estimate of the influence of rest on cumulative compressive tolerance. Within the dataset there was a large gap in studied rest durations between the 200% and 1000% rest durations. Therefore, predictions of rest effects on cumulative compressive tolerance within this data gap may be made with less certainty than predictions made closer to measured data points.

This work has shown that cumulative load tolerance is greatly influenced by load magnitude, with higher load magnitudes resulting in significantly lower resistance to cumulative compression. Although not significant, rest appears to impact the ability of FSUs to resist cumulative compression at moderate load magnitudes (50 and 70% of estimated compressive tolerance). It appears that very long (1000% rest duration) or no rest periods result in the highest tolerance to cumulative load, with moderate durations of rest (50 and 100%) resulting in lower tolerances. The resulting three-dimensional relationship between load magnitude, rest duration and cumulative load tolerance was used to generate weighting factors to appropriately adjust for the non-linear impact of rest and load magnitude on cumulative injury development. Future work should be conducted to employ these weighting factors *in vivo* to determine

their effectiveness in adjusting *in vivo* load and rest exposures for their impact on cumulative compression injuries.

Acknowledgements

This work was funded by the Natural Sciences and Engineering Research Council Canada and the AUTO21 Network Centers of Excellence, whose funding is provided by the Canadian Federal Government. Jack Callaghan is supported by a Canada Research Chair in Spine Biomechanics and Injury Prevention. The authors would like to thank Erin Harvey for her help with the statistical analysis and Laura Malinowski for assistance with data collection.

References

BRINCKMANN, P., BIGGEMANN, M. and HILWEG, D., 1988, Fatigue fracture of human lumbar vertebrae. *Clinical Biomechanics*, **3**, pp. S1 S23.

CALLAGHAN, J.P., 2006, Cumulative spine loading. In *The Occupational Ergonomics Handbook: Fundamentals and Assessment Tools for Occupational Ergonomics*, W. Marras and W. Karwowski (Eds), pp. 13-1 13-25 (Boca Raton: CRC Press).

CALLAGHAN, J.P. and MCGILL, S.M., 1995, Frozen storage increases the ultimate compressive load of porcine vertebrae. *Journal of Orthopaedic Research*, **13**, pp. 809 812.

CALLAGHAN, J.P. and MCGILL, S.M., 2001, Intervertebral disc herniation: studies on a porcine model exposed to highly repetitive flexion/extension motion with compressive force. *Clinical Biomechanics*, **16**, pp. 28 37.

CHAFFIN, D.B. and PARK, K.S., 1973, A longitudinal study of low-back pain as associated with occupational weight lifting factors. *American Industrial Hygiene Association Journal*, **34**, pp. 513 525.

DICKEY, J.P. and GILLESPIE, K.A., 2003, Representation of passive spinal element contributions to in vitro flexion-extension using a polynomial model: illustration using the porcine lumbar spine. *Journal of Biomechanics*, **36**, pp. 883 888.

FAUCETT, J., MEYERS, J., MILES, J., JANOWITZ, I. and FATHALLAH, F., 2007, Rest break interventions in stoop labor tasks. *Applied Ergonomics*, **38**, pp. 219 226.

GALANTE, J.O., 1967, Tensile properties of the human lumbar annulus fibrosus. *Acta Orthopaedica Scandinavica*, **Suppl. 100**, pp. 1 91.

GALLAGHER, S., MARRAS, W.S., LITSKY, A.S. and BURR, D., 2005, Torso flexion loads and the fatigue failure of human lumbosacral motion segments. *Spine*, **30**, pp. 2265 2273.

GARAVELLO-FREITAS, I., BARANAUSKAS, V., JOAZEIRO, P.P., PADOVANI, C.R., PAI-SILVA, M. and CRUZ-HOFLING, M.A., 2003, Low-power laser irradiation improves histomorphometrical parameters and bone matrix organization during tibia wound healing in rats. *Journal of Photochemistry and Photobiology B, Biology*, **70**, pp. 81 89.

GARDNER-MORSE, M.G. and STOKES, I.A., 2003, Physiological axial compressive preloads increase motion segment stiffness, linearity and hysteresis in all six degrees of freedom for small displacements about the neutral posture. *Journal of Orthopaedic Research*, **21**, pp. 547 552.

GENAIDY, A.M., WALY, S.M., KHALIL, T.M. and HIDALGO, J., 1993, Spinal compression tolerance limits for the design of manual material handling operations in the workplace. *Ergonomics*, **36**, pp. 415 434.

GOERTZEN, D.J., LANE, C. and OXLAND, T.R., 2004, Neutral zone and range of motion in the spine are greater with stepwise loading than with a continuous loading protocol. An in vitro porcine investigation. *Journal of Biomechanics*, **37**, pp. 257 261.

GUNNING, J.L., CALLAGHAN, J.P. and MCGILL, S.M., 2001, Spinal posture and prior loading history modulate compressive strength and type of failure in the spine: a biomechanical study using a porcine cervical spine model. *Clinical Biomechanics*, **16**, pp. 471 480.

HANSSON, T.H., KELLER, T.S. and SPENGLER, D.M., 1987, Mechanical behavior of the human lumbar spine. II. Fatigue strength during dynamic compressive loading. *Journal of Orthopaedic Research*, **5**, pp. 479 487.

HOLMES, A.D. and HUKINS, D.W., 1994, Fatigue-failure at the disc-vertebra interface during cyclic axial compression of cadaveric specimens. *Clinical Biomechanics*, **9**, pp. 133 134.

JAGER, M., JORDAN, C., LUTTMANN, A., LAURIG, W. and DOLLY GROUP, 2000, Evaluation and assessment of lumbar load during total shifts for occupational manual materials handling jobs within the Dortmund Lumbar Load Study DOLLY. *International Journal of Industrial Ergonomics*, **25**, pp. 553 571.

KEYSERLING, W.M., SUDARSAN, S.P., MARTIN, B.J., HAIG, A.J. and ARMSTRONG, T.J., 2005, Effects of low back disability status on lower back discomfort during sustained and cyclical trunk flexion. *Ergonomics*, **48**, pp. 219 233.

KUMAR, S., 1990, Cumulative load as a risk factor for back pain. *Spine*, **15**, pp. 1311 1316.

LIN, R.M., TSAI, K.H. and CHANG, G.L., 1997, Distribution and regional strength of trabecular bone in the porcine lumbar spine. *Clinical Biomechanics*, **12**, pp. 331 336.

LOTZ, J.C., COLLIOU, O.K., CHIN, J.R., DUNCAN, N.A. and LIEBENBERG, E., 1998, Compression-induced degeneration of the intervertebral disc: an in vivo mouse model and finite-element study. *Spine*, **23**, pp. 2493 2506.

NORMAN, R., WELLS, R., NEUMANN, P., FRANK, J., SHANNON, H. and KERR, M., 1998, A comparison of peak vs cumulative physical work exposure risk factors for the reporting of low back pain in the automotive industry. *Clinical Biomechanics*, **13**, pp. 561 573.

OXLAND, T.R., PANJABI, M.M., SOUTHERN, E.P. and DURANCEAU, J.S., 1991, An anatomic basis for spinal instability: a porcine trauma model. *Journal of Orthopaedic Research*, **9**, pp. 452 462.

PARKINSON, R.J. and CALLAGHAN, J.P., 2007, The role of load magnitude as a modifier of the cumulative load tolerance of porcine cervical spinal units: progress towards a force weighting approach. *Theoretical Issues in Ergonomics Science*, **8**, pp. 171 184.

PARKINSON, R.J., DURKIN, J.L. and CALLAGHAN, J.P., 2005, Estimating the compressive strength of the porcine cervical spine: an examination of the utility of DXA. *Spine*, **30**, pp. E492 E498.

SBRICCOLI, P., SOLOMONOW, M., ZHOU, B.H., BARATTA, R.V., LU, Y., ZHU, M.P. and BURGER, E.L., 2004, Static load magnitude is a risk factor in the development of cumulative low back disorder. *Muscle and Nerve*, **29**, pp. 300 308.

SBRICCOLI, P., SOLOMONOW, M., ZHOU, B.H. and LU, Y., 2007, Work to rest durations ratios exceeding unity are a risk factor for low back disorder; a feline model. *Journal of Electromyography and Kinesiology*, **17**, pp. 142 152.

SEIDLER, A., BOLM-AUDORFF, U., HEISKEL, H., HENKEL, N., ROTH-KUVER, B., KAISER, U., BICKEBOLLER, R., WILLINGSTORFER, W.J., BECK, W. and ELSNER, G., 2001, The role of cumulative physical work load in lumbar spine disease: risk factors for lumbar osteochondrosis and spondylosis associated with chronic complaints. *Occupational and Environmental Medicine*, **58**, pp. 735 746.

SEIDLER, A., BOLM-AUDORFF, U., SIOL, T., HENKEL, N., FUCHS, C., SCHUG, H., LEHETA, F., MARQUARDT, G., SCHMITT, E., ULRICH, P.T., BECK, W., MISSALLA, A. and ELSNER, G., 2003, Occupational risk factors for symptomatic lumbar disc herniation; a case-control study. *Occupational and Environmental Medicine*, **60**, pp. 821 830.

SOLOMONOW, M., HE, Z.B., BARATTA, R.V., LU, Y., ZHU, M. and HARRIS, M., 2000, Biexponential recovery model of lumbar viscoelastic laxity and reflexive muscular activity after prolonged cyclic loading. *Clinical Biomechanics*, **15**, pp. 167 175.

TAMI, A.E., NASSER, P., SCHAFFLER, M.B. and KNOTHE TATE, M.L., 2003, Noninvasive fatigue fracture model of the rat ulna. *Journal of Orthopaedic Research*, **21**, pp. 1018 1024.

TORTORA, G.J. and GRABOWSKI, S.R., 1996, *Principles of Anatomy and Physiology* (New York, NY: HarperCollins).

TSAI, K.H., LIN, R.M. and CHANG, G.L., 1998, Rate-related fatigue injury of vertebral disc under axial cyclic loading in a porcine body-disc-body unit. *Clinical Biomechanics*, **13**, pp. S32 S39.

YINGLING, V.R., CALLAGHAN, J.P. and MCGILL, S.M., 1997, Dynamic loading affects the mechanical properties and failure site of porcine spines. *Clinical Biomechanics*, **12**, pp. 301 305.

YINGLING, V.R., CALLAGHAN, J.P. and MCGILL, S.M., 1999, The porcine cervical spine as a model of the human lumbar spine: an anatomical, geometric, and functional comparison. *Journal of Spinal Disorders*, **12**, pp. 415 423.

Rob Parkinson is a PhD Student in the department of Kinesiology at the University of Waterloo, Ontario, Canada. Rob received his undergraduate degree in Kinesiology from the University of Guelph in 2002 and his MSc in Kinesiology from the University of Waterloo in 2004. His research interests involve tissue response to cumulative trauma in the spine.

Jack P. Callaghan received his PhD in Kinesiology from the Faculty of Applied Health Sciences at the University of Waterloo in 1999. From 1998 to 2003 he was a faculty member in the Department of Human Biology at the University of Guelph. In 2003, he was awarded a Canada Research Chair in Spine Biomechanics and Injury Prevention and returned to the Kinesiology Department at the University of Waterloo, where he is cross appointed to the Department of Mechanical and Mechatronics Engineering. He is a project leader in the AUTO21 Network of Centres of Excellence and an NSERC funded researcher. His main research interest is injury mechanisms from exposure to cumulative loading exposure. He is an author on over 50 peer reviewed journal articles and over 100 conference papers.

Bibliography

Adams,M.A., Freeman,B.J., Morrison,H.P., Nelson,I.W., and Dolan,P. (2000) Mechanical initiation of intervertebral disc degeneration. *Spine* **25,** 1625-1636.

Adams,M.A. and Hutton,W.C. (1980) The effect of posture on the role of the apophysial joints in resisting intervertebral compressive forces. *Journal of Bone and Joint Surgery (Br.)* **62,** 358-362.

Adams,M.A. and Hutton,W.C. (1982) Prolapsed intervertebral disc. A hyperflexion injury 1981 Volvo Award in Basic Science. *Spine* **7,** 184-191.

Adams,M.A. and Hutton,W.C. (1983a) The effect of fatigue on the lumbar intervertebral disc. *Journal of Bone and Joint Surgery (Br.)* **65,** 199-203.

Adams,M.A. and Hutton,W.C. (1983b) The effect of posture on the fluid content of lumbar intervertebral discs. *Spine* **8,** 665-671.

Adams,M.A. and Hutton,W.C. (1985) Gradual disc prolapse. *Spine* **10,** 524-531.

Adams,M.A., McMillan,D.W., Green,T.P., and Dolan,P. (1996) Sustained loading generates stress concentrations in lumbar intervertebral discs. *Spine* **21,** 434-438.

Adams,M.A., McNally,D.S., Chinn,H., and Dolan,P. (1994) Posture and the compressive strength of the lumbar spine. *Clin Biomech* **9,** 5-14.

Allan,D.G., Russell,G.G., Moreau,M.J., Raso,V.J., and Budney,D. (1990) Vertebral end-plate failure in porcine and bovine models of spinal fracture instrumentation. *J Orthop Res* **8,** 154-156.

Andersson,G.B. and Schultz,A.B. (1979) Effects of fluid injection on mechanical properties of intervertebral discs. *J Biomechanics* **12,** 453-458.

Asano,S., Kaneda,K., Umehara,S., and Tadano,S. (1992) The mechanical properties of the human L4-5 functional spinal unit during cyclic loading. The structural effects of the posterior elements. *Spine* **17,** 1343-1352.

Bass,E.C., Duncan,N.A., Hariharan,J.S., Dusick,J., Bueff,H.U., and Lotz,J.C. (1997) Frozen storage affects the compressive creep behavior of the porcine intervertebral disc. *Spine* **22,** 2867-2876.

Beach,T.A.C., Coke,S.K., and Callaghan,J.P. (2006) Upper body kinematic and low-back kinetic responses to precision placement challenges and cognitive distractions during repetitive lifting. *Int J Ind Ergonomics* **36,** 637-650.

Bejjani,F.J., Gross,C.M., and Pugh,J.W. (1984) Model for static lifting: relationship of loads on the spine and the knee. *J Biomechanics* **17,** 281-286.

Biggemann,M., Hilweg,D., and Brinckmann,P. (1988) Prediction of the compressive strength of vertebral bodies of the lumbar spine by quantitative computed tomography. *Skeletal Radiol.* **17,** 264-269.

Bishop,J.B., Szpalski,M., Ananthraman,S.K., McIntyre,D.R., and Pope,M.H. (1997) Classification of low back pain from dynamic motion characteristics using an artificial neural network. *Spine* **22,** 2991-2998.

Bowman,S.M., Guo,X.E., Cheng,D.W., Keaveny,T.M., Gibson,L.J., Hayes,W.C., and McMahon,T.A. (1998) Creep contributes to the fatigue behavior of bovine trabecular bone. *J Biomech Eng* **120,** 647-654.

Brereton,L.C. and McGill,S.M. (1998) Frequency response of spine extensors during rapid isometric contractions: effects of muscle length and tension. *J Electromyogr Kinesiol* **8,** 227-232.

Brinckmann,P., Biggemann,M., and Hilweg,D. (1988) Fatigue fracture of human lumbar vertebrae. *Clin Biomech* **3,** S1-S23.

Brinckmann,P., Hoefert,H., and Jongen,H.T. (1981) Sex differences in the skeletal geometry of the human pelvis and hip joint. *J Biomechanics* **14,** 427-430.

Burklein,D., Lochmuller,E., Kuhn,V., Grimm,J., Barkmann,R., Muller,R., and Eckstein,F. (2001) Correlation of thoracic and lumbar vertebral failure loads with in situ vs. ex situ dual energy X-ray absorptiometry. *J Biomechanics* **34,** 579-587.

Burr,D.B., Turner,C.H., Naick,P., Forwood,M.R., Ambrosius,W., Hasan,M.S., and Pidaparti,R. (1998) Does microdamage accumulation affect the mechanical properties of bone? *J.Biomech.* **31,** 337-345.

Buseck,M., Schipplein,O.D., Andersson,G.B., and Andriacchi,T.P. (1988) Influence of dynamic factors and external loads on the moment at the lumbar spine in lifting. *Spine* **13,** 918-921.

Bush,H.D., Horton,W.G., Smare,D.L., and Naylor,A. (1956) Fluid content of the nucleus pulposus as a factor in the disk syndrome. *British Medical Journal* 81-83.

Bush-Joseph,C., Schipplein,O., Andersson,G.B., and Andriacchi,T.P. (1988) Influence of dynamic factors on the lumbar spine moment in lifting. *Ergonomics* **31,** 211-216.

Caler,W.E. and Carter,D.R. (1989) Bone creep-fatigue damage accumulation. *J Biomechanics* **22,** 625-635.

Callaghan,J.P. (1994) Compressive Strength of a Porcine Fracture Model Exposed to Physiologic Pressures. MSc.

Callaghan,J.P. and Dunk,N.M. (2002) Examination of the flexion relaxation phenomenon in erector spinae muscles during short duration slumped sitting. *Clin Biomech* **17,** 353-360.

Callaghan,J.P., Jackson,J.A., Albert,W.J., Andrews,D.M., and Potvin,J.R. (2003) The design and preliminary validation of '3D-Match' - A posture matching tool for estimating three dimensional cumulative loading on the low back., London, Ontario, Canada.

Callaghan,J.P. and McGill,S.M. (1995) Frozen storage increases the ultimate compressive load of porcine vertebrae. *J Orthop Res* **13,** 809-812.

Callaghan,J.P. and McGill,S.M. (2001) Intervertebral disc herniation: studies on a porcine model exposed to highly repetitive flexion/extension motion with compressive force. *Clin Biomech* **16,** 28-37.

Callaghan,J.P., Salewytsch,A.J., and Andrews,D.M. (2001) An evaluation of predictive methods for estimating cumulative spinal loading. *Ergonomics* **44,** 825-837.

Carmichael,B., Dutta,T., and Fernie,G. (2006) Forceshoes: Portable ground reaction sensors for biomechanical analysis in the workplace. University of Waterloo, Waterloo, Ontario, Canada.

Carter,D.R. and Caler,W.E. (1983) Cycle-dependent and time-dependent bone fracture with repeated loading. *J Biomech Eng* **105,** 166-170.

Carter,D.R. and Caler,W.E. (1985) A cumulative damage model for bone fracture. *J Orthop Res* **3,** 84-90.

Carter,D.R. and Hayes,W.C. (1976) Fatigue life of compact bone--I. Effects of stress amplitude, temperature and density. *J Biomechanics* **9,** 27-34.

Chaffin,D.B. (1969) A computerized biomechanical model - Development of and use in studying gross body actions. *J Biomechanics* **2,** 429-441.

Chaffin,D.B., Redfern,M.S., Erig,M., and Goldstein,S.A. (1990) Lumbar muscle size and locations from CT scans of 96 women of age 40 to 63 years. *Clin Biomech* **5,** 9-16.

Ching,C.T., Chow,D.H., Yao,F.Y., and Holmes,A.D. (2003) The effect of cyclic compression on the mechanical properties of the inter-vertebral disc: an in vivo study in a rat tail model. *Clin Biomech* **18,** 182-189.

Choi,B.C., Tennassee,L.M., and Eijkemans,G.J. (2001) Developing regional workplace health and hazard surveillance in the Americas. *Pan American Journal of Public Health* **10,** 376-381.

Choi,K. and Goldstein,S.A. (1992) A comparison of the fatigue behavior of human trabecular and cortical bone tissue. *J.Biomech.* **25,** 1371-1381.

Cooper,R.G., Hollis,S., and Jayson,M.I.V. (1992) Gender Variation of Human Spinal and Paraspinal Structures. *Clin Biomech* **7,** 120-124.

Costi,J.J., Hearn,T.C., and Fazzalari,N.L. (2002) The effect of hydration on the stiffness of intervertebral discs in an ovine model. *Clin Biomech* **17,** 446-455.

Cotton,J.R., Zioupos,P., Winwood,K., and Taylor,M. (2003) Analysis of creep strain during tensile fatigue of cortical bone. *J.Biomech.* **36,** 943-949.

Davis,K.G., Marras,W.S., Heaney,C.A., Waters,T.R., and Gupta,P. (2002) The impact of mental processing and pacing on spine loading: 2002 Volvo Award in biomechanics. *Spine* **27,** 2645-2653.

Davis,K.G., Marras,W.S., and Waters,T.R. (1998) Evaluation of spinal loading during lowering and lifting. *Clin Biomech* **13,** 141-152.

Daynard,D., Yassi,A., Cooper,J.E., Tate,R., Norman,R., and Wells,R. (2001) Biomechanical analysis of peak and cumulative spinal loads during simulated patient-handling activities: a substudy of a randomized controlled trial to prevent lift and transfer injury of health care workers. *Applied Ergonomics* **32,** 199-214.

de Looze,M., Kingma,I., Bussmann,J.B., and Toussaint,H.M. (1992a) Validation of a dynamic linked segment model to calculate joint moments in lifting. *Clin Biomech* **7,** 161-169.

de Looze,M.P., Bussmann,J.B., Kingma,I., and Toussaint,H.M. (1992b) Different methods to estimate total power and its components during lifting. *J Biomechanics* **25,** 1089-1095.

de Looze,M.P., Kingma,I., Thunnissen,W., van Wijk,M.J., and Toussaint,H.M. (1994) The evaluation of a practical biomechanical model estimating lumbar moments in occupational activities. *Ergonomics* **37,** 1495-1502.

Demuth,H., Beale,M., and Hagan,M. (2006) *Neural Network Toolbox User's Guide*. The Mathworks Inc.

Dhillon,N., Bass,E.C., and Lotz,J.C. (2001) Effect of frozen storage on the creep behavior of human intervertebral discs. *Spine* **26,** 883-888.

Dickey,J.P., McNorton,S., and Potvin,J.R. (2003) Repeated spinal flexion modulates the flexion-relaxation phenomenon. *Clin Biomech* **18,** 783-789.

Dipietro,L., Sabatini,A.M., and Dario,P. (2003) Artificial neural network model of the mapping between electromyographic activation and trajectory patterns in free-arm movements. *Medical & Biological Engineering & Computing* **41,** 124-132.

Dolan,P., Mannion,A.F., and Adams,M.A. (1994) Passive tissues help the back muscles to generate extensor moments during lifting. *J.Biomech.* **27,** 1077-1085.

Dolan,P., Mannion,A.F., and Adams,M.A. (1995) Fatigue of the erector spinae muscles: A quantitative assessment using "frequency banding" of the surface electromyography signal. *Spine* **20,** 149-159.

Drake,J.D. and Callaghan,J.P. (2006) Elimination of electrocardiogram contamination from electromyogram signals: An evaluation of currently used removal techniques. *J.Electromyogr.Kinesiol.* **16,** 175-187.

Edmondston,S.J., Singer,K.P., Day,R.E., Price,R.I., and Breidahl,P.D. (1997) Ex vivo estimation of thoracolumbar vertebral body compressive strength: the relative contributions of bone densitometry and vertebral morphometry. *Osteoporosis International* **7,** 142-148.

Ekholm,J., Arborelius,U.P., and Nemeth,G. (1982) The load on the lumbo-sacral joint and trunk muscle activity during lifting. *Ergonomics* **25,** 145-161.

Ekstrom,L., Kaigle,A., Hult,E., Holm,S., Rostedt,M., and Hansson,T. (1996) Intervertebral disc response to cyclic loading--an animal model. *Proc.Inst.Mech.Eng [H.]* **210,** 249-258.

Fathallah,F.A., Marras,W.S., and Parnianpour,M. (1999) Regression models for predicting peak and continuous three-dimensional spinal loads during symmetric and asymmetric lifting tasks. *Hum.Factors* **41,** 373-388.

Fernand,R. and Fox,D.E. (1985) Evaluation of lumbar lordosis. A prospective and retrospective study. *Spine* **10,** 799-803.

Fitzgerald,E.R. (1975) Dynamic mechanical measurements during the life to death transition in animal tissues. *Biorheology* **12,** 397-408.

Freivalds,A., Chaffin,D.B., Garg,A., and Lee,K.S. (1984) A dynamic biomechanical evaluation of lifting maximum acceptable loads. *J Biomechanics* **17,** 251-262.

Fyhrie,D.P. and Schaffler,M.B. (1994) Failure mechanisms in human vertebral cancellous bone. *Bone* **15,** 105-109.

Gagnon,D. and Gagnon,M. (1992) The influence of dynamic factors on triaxial net muscular moments at the L5/S1 joint during asymmetrical lifting and lowering. *J Biomechanics* **25,** 891-901.

Gallagher,S., Marras,W.S., Litsky,A.S., and Burr,D. (2005) Torso flexion loads and the fatigue failure of human lumbosacral motion segments. *Spine* **30,** 2265-2273.

Gallagher,S., Marras,W.S., Litsky,A.S., and Burr,D. (2006) An exploratory study of loading and morphometric factors associated with specific failure modes in fatigue testing of lumbar motion segments. *Clin Biomech* **21,** 228-234.

Ganguly,P., Moore,T.L., and Gibson,L.J. (2004) A phenomenological model for predicting fatigue life in bovine trabecular bone. *J Biomech Eng* **126,** 330-339.

Garavello-Freitas,I., Baranauskas,V., Joazeiro,P.P., Padovani,C.R., Pai-Silva,M., and Cruz-Hofling,M.A. (2003) Low-power laser irradiation improves histomorphometrical parameters and bone matrix organization during tibia wound healing in rats. *Journal of Photochemistry and Photobiology.B, Biology.* **70,** 81-89.

Gardner-Morse,M.G. and Stokes,I.A. (2003) Physiological axial compressive preloads increase motion segment stiffness, linearity and hysteresis in all six degrees of freedom for small displacements about the neutral posture. *J Orthop Res* **21,** 547-552.

Genaidy,A.M., Waly,S.M., Khalil,T.M., and Hidalgo,J. (1993) Spinal compression tolerance limits for the design of manual material handling operations in the workplace. *Ergonomics* **36,** 415-434.

Gleizes,V., Viguier,E., Feron,J.M., Canivet,S., and Lavaste,F. (1998) Effects of freezing on the biomechanics of the intervertebral disc. *Surg.Radiol.Anat.* **20,** 403-407.

Goertzen,D.J., Lane,C., and Oxland,T.R. (2004) Neutral zone and range of motion in the spine are greater with stepwise loading than with a continuous loading protocol. An in vitro porcine investigation. *J Biomechanics* **37,** 257-261.

Gordon,S.J., Yang,K.H., Mayer,P.J., Mace,A.H., Jr., Kish,V.L., and Radin,E.L. (1991) Mechanism of disc rupture. A preliminary report. *Spine* **16,** 450-456.

Gower,W.E. and Pedrini,V. (1969) Age-related variations in proteinpolysaccharides from human nucleus pulposus, annulus fibrosus, and costal cartilage. *J Bone and Jt Surg* **51,** 1154-1162.

Granata,K.P. and Marras,W.S. (1993) An EMG-assisted model of loads on the lumbar spine during asymmetric trunk extensions. *J Biomechanics* **26,** 1429-1438.

Granata,K.P. and Marras,W.S. (1995a) An EMG-assisted model of trunk loading during free-dynamic lifting. *J Biomechanics* **28,** 1309-1317.

Granata,K.P. and Marras,W.S. (1995b) The influence of trunk muscle coactivity on dynamic spinal loads. *Spine* **20,** 913-919.

Grant,J.P., Oxland,T.R., and Dvorak,M.F. (2001) Mapping the structural properties of the lumbosacral vertebral endplates. *Spine* **26,** 889-896.

Grant,J.P., Oxland,T.R., Dvorak,M.F., and Fisher,C.G. (2002) The effects of bone density and disc degeneration on the structural property distributions in the lower lumbar vertebral endplates. *J Orthop Res* **20,** 1115-1120.

Gunning,J.L., Callaghan,J.P., and McGill,S.M. (2001) Spinal posture and prior loading history modulate compressive strength and type of failure in the spine: a biomechanical study using a porcine cervical spine model. *Clin Biomech* **16,** 471-480.

Guo,H.R., Tanaka,S., Cameron,L.L., Seligman,P.J., Behrens,V.J., Ger,J., Wild,D.K., and Putz-Anderson,V. (1995) Back pain among workers in the United States: national estimates and workers at high risk. *American Journal of Industrial Medicine* **28,** 591-602.

Haddock,S.M., Yeh,O.C., Mummaneni,P.V., Rosenberg,W.S., and Keaveny,T.M. (2004) Similarity in the fatigue behavior of trabecular bone across site and species. *J Biomechanics* **37,** 181-187.

Hansson,T. and Roos,B. (1983) The amount of bone mineral and Schmorl's nodes in lumbar vertebrae. *Spine* **8,** 266-271.

Hansson,T., Roos,B., and Nachemson,A. (1980) The bone mineral content and ultimate compressive strength of lumbar vertebrae. *Spine* **5,** 46-55.

Hansson,T.H., Keller,T.S., and Spengler,D.M. (1987) Mechanical behavior of the human lumbar spine. II. Fatigue strength during dynamic compressive loading. *J Orthop Res* **5,** 479-487.

Hasegawa,K., Turner,C.H., Chen,J., and Burr,D.B. (1995) Effect of disc lesion on microdamage accumulation in lumbar vertebrae under cyclic compression loading. *Clinical Orthopaedics* **311,** 190-198.

Herrin,G.D., Jaraiedi,M., and Anderson,C.K. (1986) Prediction of overexertion injuries using biomechanical and psychophysical models. *American Industrial Hygiene Association Journal* **47,** 322-330.

Hickey,D.S. and Hukins,D.W. (1979) Effect of methods of preservation on the arrangement of collagen fibrils in connective tissue matrices: an x-ray diffraction study of annulus fibrosus. *Connect.Tissue Res.* **6,** 223-228.

Hirsch,C. and Galante,J.O. (1967) Laboratory conditions for tensile tests in annulus fibrosus from human intervertebral discs. *Acta Orthop Scand* **38,** 148-162.

Hogan,K.L. (2005) An investigation of industrially transferable data collection techniques to quantify cumulative loading in repetitive tasks. MSc University of Waterloo.

Holmes,A.D. and Hukins,D.W. (1994) Fatigue-failure at the Disc-Vertebra Interface During Cyclic Axial Compression of Cadaveric Specimens. *Clin Biomech* **9,** 133-134.

Holmes,A.D., Hukins,D.W., and Freemont,A.J. (1993) End-plate displacement during compression of lumbar vertebra-disc- vertebra segments and the mechanism of failure. *Spine* **18,** 128-135.

Horst,M. and Brinckmann,P. (1981) 1980 Volvo award in biomechanics. Measurement of the distribution of axial stress on the end-plate of the vertebral body. *Spine* **6,** 217-232.

Hou,Y., Zurada,J., and Karwowski,W. (2004a) Prediction of dynamic forces on lumbar joint using a recurrent neural network model.

Hou,Y., Zurada,J., and Karwowski,W. (2004b) Prediction of EMG signals of trunk muscles in manual lifting using a neural network model.

Hou,Y., Zurada,J., Karwowski,W., and Marras,W. (2005) A hybrid neuro-fuzzy approach for spinal force evaluation in manual materials handling tasks. *Lecture notes in computer science* **3612,** 1216-1225.

Hou,Y., Zurada,J.M., Karwowski,W., Marras,W.S., and Davis,K. (2007) Estimation of the dynamic spinal forces using a recurrent fuzzy neural network. *IEEE Trans.Syst.Man.Cybern.B Cybern.* **37,** 100-109.

Hutton,W.C., Cyron,B.M., and Stott,J.R. (1979) The compressive strength of lumbar vertebrae. *J Anat* **129,** 753-758.

Jager,M., Jordan,C., Luttmann,A., Laurig,W., and DOLLY group (2000) Evaluation and assessment of lumbar load during total shifts for occupational manual materials handling jobs within the Dortmund Lumbar Load Study - DOLLY. *Int J Ind Ergonomics* **25,** 553-571.

Johannessen,W., Vresilovic,E.J., Wright,A.C., and Elliott,D.M. (2004) Intervertebral disc mechanics are restored following cyclic loading and unloaded recovery. *Ann.Biomed.Eng* **32,** 70-76.

Jorgensen,M.J., Marras,W.S., Granata,K.P., and Wiand,J.W. (2001) MRI-derived moment-arms of the female and male spine loading muscles. *Clin Biomech* **16,** 182-193.

Jorgensen,M.J., Marras,W.S., Gupta,P., and Waters,T.R. (2003) Effect of torso flexion on the lumbar torso extensor muscle sagittal plane moment arms. *The Spine Journal* **3,** 363-369.

Jorgensen,M.J., Marras,W.S., Smith,F.W., and Pope,M.H. (2005) Sagittal plane moment arms of the female lumbar region rectus abdominis in an upright neutral torso posture. *Clin Biomech* **20,** 242-246.

Kaigle,A., Ekstrom,L., Holm,S., Rostedt,M., and Hansson,T. (1998) In vivo dynamic stiffness of the porcine lumbar spine exposed to cyclic loading: influence of load and degeneration. *J.Spinal Disord.* **11,** 65-70.

Karwowski,W., Gaweda,A., Marras,W.S., Davis,K.G., Zurada,J., and Rodrick,D. (2006) A fuzzy relational rule network modeling of electromyographical activity of trunk muscles in manual lifting based on trunk angles, moments, pelvic tilt and rotation angles. *Int J Ind Ergonomics* **36,** 847-859.

Keller,T.S., Hansson,T.H., Abram,A.C., Spengler,D.M., and Panjabi,M.M. (1989) Regional variations in the compressive properties of lumbar vertebral trabeculae. Effects of disc degeneration. *Spine* **14,** 1012-1019.

Keller,T.S., Spengler,D.M., and Hansson,T.H. (1987) Mechanical behavior of the human lumbar spine. I. Creep analysis during static compressive loading. *J Orthop Res* **5,** 467-478.

Kelly,M.F., Parker,P.A., and Scott,R.N. (1991) Neural Network Classification of Myoelectric Signal for Prosthesis Control. *J Electromyogr Kinesiol* **1,** 229-236.

Kelsey,J.L. (1975) An epidemiological study of the relationship between occupations and acute herniated lumbar intervertebral discs. *Int.J Epidemiol.* **4,** 197-205.

Kelsey,J.L., Githens,P.B., White,A.A., III, Holford,T.R., Walter,S.D., O'Connor,T., Ostfeld,A.M., Weil,U., Southwick,W.O., and Calogero,J.A. (1984) An epidemiologic study of lifting and twisting on the job and risk for acute prolapsed lumbar intervertebral disc. *J Orthop Res.* **2,** 61-66.

Kettler,A., Wilke,H.J., Haid,C., and Claes,L. (2000) Effects of specimen length on the monosegmental motion behavior of the lumbar spine. *Spine* **25,** 543-550.

Kingma,I., Baten,C.T., Dolan,P., Toussaint,H.M., van Dieen,J.H., de Looze,M.P., and Adams,M.A. (2001) Lumbar loading during lifting: a comparative study of three measurement techniques. *J Electromyogr Kinesiol* **11,** 337-345.

Kingma,I., de Looze,M.P., van Dieen,J.H., Toussaint,H.M., Adams,M.A., and Baten,C.T. (1998a) When is a lifting movement too asymmetric to identify low-back loading by 2-D analysis? *Ergonomics* **41,** 1453-1461.

Kingma,I., deLooze,M.P., Toussaint,H.M., Klijnsma,H.G., and Bruijnen,T.B.M. (1996a) Validation of a full body 3-D dynamic linked segment model. *Human Movement Science* **15,** 833-860.

Kingma,I., Toussaint,H.M., de Looze,M.P., and van Dieen,J.H. (1996b) Segment inertial parameter evaluation in two anthropometric models by application of a dynamic linked segment model. *J Biomechanics* **29,** 693-704.

Kingma,I., van Dieen,J.H., de Looze,M., Toussaint,H.M., Dolan,P., and Baten,C.T. (1998b) Asymmetric low back loading in asymmetric lifting movements is not prevented by pelvic twist. *J Biomechanics* **31,** 527-534.

Knox,J.M., Schwartz,G.S., and Diller,K.R. (1980) Volumetric changes in cells during freezing and thawing. *J.Biomech.Eng* **102,** 91-97.

Koeller,W., Muehlhaus,S., Meier,W., and Hartmann,F. (1986) Biomechanical properties of human intervertebral discs subjected to axial dynamic compression--influence of age and degeneration. *J Biomechanics* **19,** 807-816.

Koike,Y. and Kawato,M. (1995) Estimation of Dynamic Joint Torques and Trajectory Formation from Surface Electromyography Signals Using A Neural-Network Model. *Biological Cybernetics* **73,** 291-300.

Kromodihardjo,S. and Mital,A. (1986) Kinetic analysis of manual lifting activities: Part 1 - Development of a three-dimensional computer model. *Int J Ind Ergonomics* **1,** 77-90.

Kumar,S. (1988a) Moment Arms of Spinal Musculature Determined from CT Scans. *Clin Biomech* **3,** 137-144.

Kumar,S. (1988b) Moment Arms of Spinal Musculature Determined from Ct Scans. *Clinical Biomechanics* **3,** 137-144.

Kumar,S. (1990) Cumulative load as a risk factor for back pain. *Spine* **15,** 1311-1316.

Lariviere,C. and Gagnon,D. (1998) Comparison between two dynamic methods to estimate triaxial net reaction moments at the L5/S1 joint during lifting. *Clin Biomech* **13,** 36-47.

Lavender,S.A., Li,Y.C., Andersson,G.B., and Natarajan,R.N. (1999) The effects of lifting speed on the peak external forward bending, lateral bending, and twisting spine moments. *Ergonomics* **42,** 111-125.

Lee,W., Karwowski,W., Marras,W.S., and Rodrick,D. (2003) A neuro-fuzzy model for estimating electromyographical activity of trunk muscles due to manual lifting. *Ergonomics* **46,** 285-309.

Leskinen,T.P. (1985) Comparison of static and dynamic biomechanical models. *Ergonomics* **28,** 285-291.

Leskinen,T.P., Stalhammar,H.R., Kuorinka,I.A., and Troup,J.D. (1983a) A dynamic analysis of spinal compression with different lifting techniques. *Ergonomics* **26,** 595-604.

Leskinen,T.P., Stalhammar,H.R., Kuorinka,I.A., and Troup,J.D. (1983b) The effect of inertial factors on spinal stress when lifting. *Engineering in Medicine* **12,** 87-89.

Lin,R.M., Tsai,K.H., and Chang,G.L. (1997) Distribution and regional strength of trabecular bone in the porcine lumbar spine. *Clin Biomech* **12,** 331-336.

Lindbeck,L. and Arborelius,U.P. (1991) Inertial effects from single body segments in dynamic analysis of lifting. *Ergonomics* **34,** 421-433.

Linde,F. and Sorensen,H.C. (1993) The effect of different storage methods on the mechanical properties of trabecular bone. *J.Biomech.* **26,** 1249-1252.

Liu,M.M., Herzog,W., and Savelberg,H.H. (1999) Dynamic muscle force predictions from EMG: an artificial neural network approach. *J Electromyogr Kinesiol* **9,** 391-400.

Liu,Y.K., Njus,G., Buckwalter,J., and Wakano,K. (1983) Fatigue response of lumbar intervertebral joints under axial cyclic loading. *Spine* **8,** 857-865.

Lotz,J.C., Colliou,O.K., Chin,J.R., Duncan,N.A., and Liebenberg,E. (1998) Compression-induced degeneration of the intervertebral disc: an in vivo mouse model and finite-element study. *Spine* **23,** 2493-2506.

Lu,W.W., Luk,K.D., Cheung,K.C., Gui-Xing,Q., Shen,J.X., Yuen,L., Ouyang,J., and Leong,J.C. (2004) Microfracture and changes in energy absorption to fracture of young vertebral cancellous bone following physiological fatigue loading. *Spine* **29,** 1196-1201.

Luh,J.J., Chang,G.C., Cheng,C.K., Lai,J.S., and Kuo,T.S. (1999) Isokinetic elbow joint torques estimation from surface EMG and joint kinematic data: using an artificial neural network model. *J Electromyogr Kinesiol* **9,** 173-183.

Marras,W.S. (2005) The future of research in understanding and controlling work-related low back disorders. *Ergonomics* **48,** 464-477.

Marras,W.S., Davis,K.G., and Jorgensen,M. (2002) Spine loading as a function of gender. *Spine* **27,** 2514-2520.

Marras,W.S. and Granata,K.P. (1995) A biomechanical assessment and model of axial twisting in the thoracolumbar spine. *Spine* **20,** 1440-1451.

Marras,W.S. and Granata,K.P. (1997a) Spine loading during trunk lateral bending motions. *J Biomechanics* **30,** 697-703.

Marras,W.S. and Granata,K.P. (1997b) The development of an EMG-assisted model to assess spine loading during whole-body free-dynamic lifting. *J Electromyogr Kinesiol* **7,** 259-268.

Marras,W.S., Granata,K.P., and Davis,K.G. (1999) Variability in spine loading model performance. *Clin Biomech* **14,** 505-514.

Marras,W.S., Jorgensen,M.J., Granata,K.P., and Wiand,B. (2001) Female and male trunk geometry: size and prediction of the spine loading trunk muscles derived from MRI. *Clin Biomech* **16,** 38-46.

Marras,W.S., Lavender,S.A., Leurgans,S.E., Fathallah,F.A., Ferguson,S.A., Allread,W.G., and Rajulu,S.L. (1995) Biomechanical Risk-Factors for Occupationally Related Low-Back Disorders. *Ergonomics* **38,** 377-410.

Marras,W.S., Parakkat,J., Chany,A.M., Yang,G., Burr,D., and Lavender,S.A. (2006) Spine loading as a function of lift frequency, exposure duration, and work experience. *Clin Biomech* **21,** 345-352.

Marras,W.S. and Sommerich,C.M. (1991a) A three-dimensional motion model of loads on the lumbar spine: I. Model structure. *Human Factors* **33,** 123-137.

Marras,W.S. and Sommerich,C.M. (1991b) A three-dimensional motion model of loads on the lumbar spine: II. Model validation. *Human Factors* **33,** 139-149.

McBroom,R.J., Hayes,W.C., Edwards,W.T., Goldberg,R.P., and White,A.A., III (1985) Prediction of vertebral body compressive fracture using quantitative computed tomography. *J Bone and Jt Surg* **67,** 1206-1214.

McCaw,S.T. and DeVita,P. (1995) Errors in alignment of center of pressure and foot coordinates affect predicted lower extremity torques. *J Biomechanics* **28,** 985-988.

McGill,S.M. (1992a) A myoelectrically based dynamic three-dimensional model to predict loads on lumbar spine tissues during lateral bending. *J Biomechanics* **25,** 395-414.

McGill,S.M. (1992b) A myoelectrically based dynamic three-dimensional model to predict loads on lumbar spine tissues during lateral bending. *J Biomechanics* **25,** 395-414.

McGill,S.M. (1997) The biomechanics of low back injury: implications on current practice in industry and the clinic. *J Biomechanics* **30,** 465-475.

McGill,S.M., Juker,D., and Axler,C. (1996a) Correcting trunk muscle geometry obtained from MRI and CT scans of supine postures for use in standing postures. *J Biomechanics* **29,** 643-646.

McGill,S.M. and Norman,R.W. (1985) Dynamically and statically determined low back moments during lifting. *J Biomechanics* **18,** 877-885.

McGill,S.M. and Norman,R.W. (1986) Partitioning of the L4/L5 dynamic moment into disc, ligamentous, and muscular components during lifting. *Spine* **11,** 666-677.

McGill,S.M. and Norman,R.W. (1987) Effects of an anatomically detailed erector spinae model on L4/L5 disc compression and shear. *J Biomechanics* **20,** 591-600.

McGill,S.M., Norman,R.W., and Cholewicki,J. (1996b) A simple polynomial that predicts low-back compression during complex 3-D tasks. *Ergonomics* **39,** 1107-1118.

McGill,S.M., Seguin,J., and Bennett,G. (1994) Passive stiffness of the lumbar torso in flexion, extension, lateral bending, and axial rotation. Effect of belt wearing and breath holding. *Spine* **19,** 696-704.

McLain,R.F., Yerby,S.A., and Moseley,T.A. (2002) Comparative morphometry of L4 vertebrae: comparison of large animal models for the human lumbar spine. *Spine* **27,** E200-E206.

McNally,D.S. and Adams,M.A. (1992) Internal intervertebral disc mechanics as revealed by stress profilometry. *Spine* **17,** 66-73.

Mello,R.G., Oliveira,L.F., and Nadal,J. (2007a) Digital Butterworth filter for subtracting noise from low magnitude surface electromyogram. *Comput.Methods Programs Biomed.* **87,** 28-35.

Mello,R.G., Oliveira,L.F., and Nadal,J. (2007b) Digital Butterworth filter for subtracting noise from low magnitude surface electromyogram. *Comput.Methods Programs Biomed.* **87,** 28-35.

Michel,M.C., Guo,X.D., Gibson,L.J., McMahon,T.A., and Hayes,W.C. (1993) Compressive fatigue behavior of bovine trabecular bone. *J Biomechanics* **26,** 453-463.

Mientjes,M.I., Norman,R.W., Wells,R.P., and McGill,S.M. (1999) Assessment of an EMG-based method for continuous estimates of low back compression during asymmetrical occupational tasks. *Ergonomics* **42,** 868-879.

Mirka,G.A. and Marras,W.S. (1993) A stochastic model of trunk muscle coactivation during trunk bending. *Spine* **18,** 1396-1409.

Mital,A. and Kromodihardjo,S. (1986) Kinetic analysis of manual lifting activities: Part 2 - Biomechanical analysis of task variables. *Int J Ind Ergonomics* **1,** 91-101.

Mitton,D., Rumelhart,C., Hans,D., and Meunier,P.J. (1997) The effects of density and test conditions on measured compression and shear strength of cancellous bone from the lumbar vertebrae of ewes. *Medical Engineering and Physics* **19,** 464-474.

Moga,P.J., Erig,M., Chaffin,D.B., and Nussbaum,M.A. (1993) Torso muscle moment arms at intervertebral levels T10 through L5 from CT scans on eleven male and eight female subjects. *Spine* **18,** 2305-2309.

Moore,T.L. and Gibson,L.J. (2003a) Fatigue microdamage in bovine trabecular bone. *J.Biomech.Eng* **125,** 769-776.

Moore,T.L. and Gibson,L.J. (2003b) Fatigue of bovine trabecular bone. *J Biomech Eng* **125,** 761-768.

Moore,T.L., O'Brien,F.J., and Gibson,L.J. (2004) Creep does not contribute to fatigue in bovine trabecular bone. *J Biomech Eng* **126,** 321-329.

Morris,J.M., Lucas,D.B., and Bresler,B. (1961) Role of the trunk in stability of the spine. *The Journal of Bone and Joint Surgery* **43-A,** 327-351.

Neumann,W.P., Wells,R.P., Norman,R.W., Frank,J., Shannon,H., Kerr,M.S., and the OUBPS Working Group (2001) A posture and load sampling approach to determining low-back pain risk in occupational settings. *Int J Ind Ergonomics* **27,** 65-77.

Nissan,M. (1980) Review of some basic assumptions in knee biomechanics. *J Biomechanics* **13,** 375-381.

Norman,R., Wells,R., Neumann,P., Frank,J., Shannon,H., and Kerr,M. (1998) A comparison of peak vs cumulative physical work exposure risk factors for the reporting of low back pain in the automotive industry. *Clin Biomech* **13,** 561-573.

Nussbaum,M.A., Chaffin,D.B., and Martin,B.J. (1995) A back-propagation neural network model of lumbar muscle recruitment during moderate static exertions. *J Biomechanics* **28,** 1015-1024.

Nussbaum,M.A. and Chaffin,N.B. (1996) Evaluation of artificial neural network modelling to predict torso muscle activity. *Ergonomics* **39,** 1430-1444.

Nussbaum,M.A., Martin,B.J., and Chaffin,D.B. (1997) A neural network model for simulation of torso muscle coordination. *J Biomechanics* **30,** 251-258.

O'Brien,F.J., Taylor,D., and Lee,T.C. (2003) Microcrack accumulation at different intervals during fatigue testing of compact bone. *J.Biomech.* **36,** 973-980.

Oden,Z.M., Selvitelli,D.M., Hayes,W.C., and Myers,E.R. (1998) The effect of trabecular structure on DXA-based predictions of bovine bone failure. *Calcified Tissue International* **63,** 67-73.

Oxland,T.R., Panjabi,M.M., Southern,E.P., and Duranceau,J.S. (1991) An anatomic basis for spinal instability: a porcine trauma model. *J Orthop Res* **9,** 452-462.

Panjabi,M.M., Krag,M.H., Summers,D., and Videman,T. (1985) Biomechanical time-tolerance of fresh cadaveric human spine specimens. *J Orthop Res* **3,** 292-300.

Parkinson,R.J., Beach,T.A., and Callaghan,J.P. (2004) The time-varying response of the in vivo lumbar spine to dynamic repetitive flexion. *Clin.Biomech.(Bristol., Avon.)* **19,** 330-336.

Parkinson,R.J. and Callaghan,J.P. (2006) The role of load magnitude as a modifier of the cumulative load tolerance of porcine cervical spinal units: Progress towards a force weighting approach. *Theoretical Issues in Ergonomics Science*.

Parkinson,R.J. and Callaghan,J.P. (2007a) Can periods of static loading be used to enhance the resistance of the spine to cumulative compression? *J Biomechanics* **40,** 2944-2952.

Parkinson,R.J. and Callaghan,J.P. (2007b) The role of load magnitude as a modifier of the cumulative load tolerance of porcine cervical spinal units: Progress towards a force weighting approach. *Theoretical Issues in Ergonomics Science* **8,** 171-184.

Parkinson,R.J., Durkin,J.L., and Callaghan,J.P. (2005) Estimating the compressive strength of the porcine cervical spine: an examination of the utility of DXA. *Spine* **30,** E492-E498.

Parnianpour,M., Wang,J.L., Shirazi-Adl,A., Sparto,P., and Wilke,H.J. (1997) The effect of variations in trunk models in predicting muscle strength and spinal loading. *Journal of Musculoskeletal Research* **1,** 55-69.

Pattin,C.A., Caler,W.E., and Carter,D.R. (1996) Cyclic mechanical property degradation during fatigue loading of cortical bone. *J Biomechanics* **29,** 69-79.

Pearsall,D.J., Reid,J.G., and Ross,R. (1994) Inertial properties of the human trunk of males determined from magnetic resonance imaging. *Annals of Biomedical Engineering* **22,** 692-706.

Pflaster,D.S., Krag,M.H., Johnson,C.C., Haugh,L.D., and Pope,M.H. (1997) Effect of test environment on intervertebral disc hydration. *Spine* **22,** 133-139.

Plagenhoef,S., Evans,F.G., and Abdelnour,T. (1983) Anatomical Data for Analyzing Human Motion. *Research Quarterly for Exercise and Sport* **54,** 169-178.

Plamondon,A., Gagnon,M., and Desjardins,P. (1996) Validation of two 3-D segment models to calculate the net reaction forces and moments at the L(5)/S(1) joint in lifting. *Clin Biomech* **11,** 101-110.

Porter,R.W., Adams,M.A., and Hutton,W.C. (1989) Physical activity and the strength of the lumbar spine. *Spine* **14,** 201-203.

Postacchini,F., Ripani,M., and Carpano,S. (1983) Morphometry of the lumbar vertebrae. An anatomic study in two caucasoid ethnic groups. *Clinical Orthopaedics* 296-303.

Potvin,J.R. (1997) Use of NIOSH equation inputs to calculate lumbosacral compression forces. *Ergonomics* **40,** 691-707.

Potvin,J.R., Norman,R., and Wells,R. (1990) A field method for continuous estimation of dynamic compressive forces on the L4/L5 disc during the performance of repetitive industrial tasks., Ottawa, Ontario.

Potvin,J.R. and Norman,R.W. (1993) Quantification of erector spinae muscle fatigue during prolonged, dynamic lifting tasks. *Eur.J.Appl.Physiol Occup.Physiol* **67,** 554-562.

Potvin,J.R., Norman,R.W., Eckenrath,M.E., McGill,S.M., and Bennett,G.W. (1992) Regression models for the prediction of dynamic L4/L5 compression forces during lifting. *Ergonomics* **35,** 187-201.

Prentice,S.D. and Patla,A.E. (2006) Modelling of some aspects of skilled locomotor behaviour using artificial neural networks. In *Computational intelligence for movement sciences: Neural networks and other emerging techniques* (Edited by Begg,R. and Palaniswami,M.) Pp. 172-196. Idea Group Publishing, Hershey.

Prentice,S.D., Patla,A.E., and Stacey,D.A. (1998) Simple artificial neural network models can generate basic muscle activity patterns for human locomotion at different speeds. *Experimental Brain Research* **123,** 474-480.

Prentice,S.D., Patla,A.E., and Stacey,D.A. (2001) Artificial neural network model for the generation of muscle activation patterns for human locomotion. *J Electromyogr Kinesiol* **11,** 19-30.

Race,A., Broom,N.D., and Robertson,P. (2000b) Effect of loading rate and hydration on the mechanical properties of the disc. *Spine* **25,** 662-669.

Race,A., Broom,N.D., and Robertson,P. (2000a) Effect of loading rate and hydration on the mechanical properties of the disc. *Spine* **25,** 662-669.

Rapillard,L., Charlebois,M., and Zysset,P.K. (2006) Compressive fatigue behavior of human vertebral trabecular bone. *J Biomechanics* **39,** 2133-2139.

Reid,J.G. and Costigan,P.A. (1985) Geometry of adult rectus abdominus and erector spinae muscles. *The Journal of Orthopaedic and Sports Physical Therapy* **6,** 278-280.

Reilly,C.H. and Marras,W.S. (1989) Simulift: a simulation model of human trunk motion. *Spine* **14,** 5-11.

Roaf,R. (1960) A Study of the Mechanics of Spinal Injuries. *The Journal of Bone and Joint Surgery* **42,** 810-823.

Rockoff,S.D., Sweet,E., and Bleustein,J. (1969) The relative contribution of trabecular and cortical bone to the strength of human lumbar vertebrae. *Calcified Tissue Research* **3,** 163-175.

Rosen,J., Fuchs,M.B., and Arcan,M. (1999) Performances of hill-type and neural network muscle models-toward a myosignal-based exoskeleton. *Computers and biomedical research, an international journal* **32,** 415-439.

Rubinsky,B., Lee,C.Y., Bastacky,J., and Onik,G. (1990) The process of freezing and the mechanism of damage during hepatic cryosurgery. *Cryobiology* **27,** 85-97.

Schultz,A.B., Andersson,G.B., Haderspeck,K., Ortengren,R., Nordin,M., and Bjork,R. (1982) Analysis and measurement of lumbar trunk loads in tasks involving bends and twists. *J Biomechanics* **15,** 669-675.

Schultz,A.B. and Andersson,G.B.J. (1981) Analysis of Loads on the Lumbar Spine. *Spine* **6,** 76-82.

Seidler,A., Bolm-Audorff,U., Heiskel,H., Henkel,N., Roth-Kuver,B., Kaiser,U., Bickeboller,R., Willingstorfer,W.J., Beck,W., and Elsner,G. (2001) The role of cumulative physical work load in lumbar spine disease: risk factors for lumbar osteochondrosis and spondylosis associated with chronic complaints. *Occupational and Environmental Medicine* **58,** 735-746.

Seidler,A., Bolm-Audorff,U., Siol,T., Henkel,N., Fuchs,C., Schug,H., Leheta,F., Marquardt,G., Schmitt,E., Ulrich,P.T., Beck,W., Missalla,A., and Elsner,G. (2003) Occupational risk factors for symptomatic lumbar disc herniation; a case-control study. *Occupational and Environmental Medicine* **60,** 821-830.

Sepulveda,F., Wells,D.M., and Vaughan,C.L. (1993) A neural network representation of electromyography and joint dynamics in human gait. *J Biomechanics* **26,** 101-109.

Sietsma,J. and Dow,R.J.F. (1991) Creating Artificial Neural Networks That Generalize. *Neural Networks* **4,** 67-79.

Smeathers,J.E. and Joanes,D.N. (1988) Dynamic compressive properties of human lumbar intervertebral joints: a comparison between fresh and thawed specimens. *J Biomechanics* **21,** 425-433.

Smit,T.H. (2002) The use of a quadruped as an in vivo model for the study of the spine - biomechanical considerations. *European Spine Journal* **11,** 137-144.

Smith,J.L., Smith,L.A., and McLaughlin,T.M. (1982) A Biomechanical Analysis of Industrial Manual Materials Handlers. *Ergonomics* **25,** 299-308.

Sobelman,O.S., Gibeling,J.C., Stover,S.M., Hazelwood,S.J., Yeh,O.C., Shelton,D.R., and Martin,R.B. (2004) Do microcracks decrease or increase fatigue resistance in cortical bone? *J Biomechanics* **37,** 1295-1303.

Song,R. and Tong,K.Y. (2005) Using recurrent artificial neural network model to estimate voluntary elbow torque in dynamic situations. *Medical & Biological Engineering & Computing* **43,** 473-480.

Sutherland,C.A., Albert,W.J., Wrigley,A.T., and Callaghan,J.P. (2008) A validation of a posture matching approach for the determination of 3D cumulative back loads. *Appl.Ergon.* **39,** 199-208.

Taha,Z., Brown,R., and Wright,D. (1997) Modelling and simulation of the hand grasping using neural networks. *Medical Engineering and Physics* **19,** 536-538.

Tami,A.E., Nasser,P., Schaffler,M.B., and Knothe Tate,M.L. (2003) Noninvasive fatigue fracture model of the rat ulna. *J Orthop Res* **21,** 1018-1024.

Tampier,C. (2006) Progressive disc herniation: An investigation of the mechanism using hitochemical and microscopic techniques. MSc University of Waterloo.

Thomsen,J.S., Ebbesen,E.N., and Mosekilde,L. (2002) Predicting human vertebral bone strength by vertebral static histomorphometry. *Bone* **30,** 502-508.

Tortora,G.J. and Grabowski,S.R. (1996) *Principles of anatomy and physiology*. HarperCollins, New York, NY.

Tsai,K.H., Lin,R.M., and Chang,G.L. (1998) Rate-related fatigue injury of vertebral disc under axial cyclic loading in a porcine body-disc-body unit. *Clin Biomech* **13,** S32-S39.

Uchiyama,T., Bessho,T., and Akazawa,K. (1998) Static torque-angle relation of human elbow joint estimated with artificial neural network technique. *J Biomechanics* **31,** 545-554.

van Dieen,J.H. (1997) Are recruitment patterns of the trunk musculature compatible with a synergy based on the maximization of endurance? *J.Biomech* **30,** 1095-1100.

van Dieen,J.H. and Kingma,I. (2005) Effects of antagonistic co-contraction on differences between electromyography based and optimization based estimates of spinal forces. *Ergonomics* **48,** 411-426.

van Dieen,J.H., Kingma,I., Meijer,R., Hansel,L., and Huiskes,R. (2001) Stress distribution changes in bovine vertebrae just below the endplate after sustained loading. *Clin Biomech* **16 Suppl 1,** S135-S142.

Van Herp,G., Rowe,P., Salter,P., and Paul,J.P. (2000) Three-dimensional lumbar spinal kinematics: a study of range of movement in 100 healthy subjects aged 20 to 60+ years. *Rheumatology.(Oxford)* **39,** 1337-1340.

Veiersted,K.B., Westgaard,R.H., and Andersen,P. (1993) Electromyographic evaluation of muscular work pattern as a predictor of trapezius myalgia. *Scand J Work Environ.Health* **19,** 284-290.

Wang,L. and Buchanan,T.S. (2002) Prediction of joint moments using a neural network model of muscle activations from EMG signals. *IEEE Transactions on Neural Systems and Rehabilitation Engineering* **10,** 30-37.

Waters,T., Yeung,S., Genaidy,A.M., Callaghan,J.P., Barriera-Viruet,H., Abdallah,S., and Kumar,S. (2006) Cumulative spinal loading exposure methods for manual material handling tasks. Part 2: methodological issues and applicability for use in epidemiological studies. *Theoretical Issues in Ergonomics Science* **7,** 131-148.

Waters,T.R., Putz-Anderson,V., Garg,A., and Fine,L.J. (1993) Revised NIOSH equation for the design and evaluation of manual lifting tasks. *Ergonomics* **36,** 749-776.

Wilke,H.J., Jungkunz,B., Wenger,K., and Claes,L.E. (1998) Spinal segment range of motion as a function of in vitro test conditions: effects of exposure period, accumulated cycles, angular-deformation rate, and moisture condition. *The Anatomical Record* **251,** 15-19.

Woo,S.L., Orlando,C.A., Camp,J.F., and Akeson,W.H. (1986) Effects of postmortem storage by freezing on ligament tensile behavior. *J.Biomech.* **19,** 399-404.

Wood,G.A. and Hayes,K.C. (1974) A kinetic model of intervertebral stress during lifting. *British Journal of Sports Medicine* **8,** 74-79.

Yingling,V.R., Callaghan,J.P., and McGill,S.M. (1997) Dynamic loading affects the mechanical properties and failure site of porcine spines. *Clin Biomech* **12,** 301-305.

Yingling,V.R., Callaghan,J.P., and McGill,S.M. (1999) The porcine cervical spine as a model of the human lumbar spine: an anatomical, geometric, and functional comparison. *Journal of Spinal Disorders* **12,** 415-423.

Yoganandan,N., Kumaresan,S., Voo,L., and Pintar,F.A. (1996) Finite element applications in human cervical spine modeling. *Spine* **21,** 1824-1834.

Yu,C.Y., Tsai,K.H., Hu,W.P., Lin,R.M., Song,H.W., and Chang,G.L. (2003) Geometric and morphological changes of the intervertebral disc under fatigue testing. *Clin.Biomech.(Bristol., Avon.)* **18,** S3-S9.

Zatsiorsky,V.M., Gregory,R.W., and Latash,M.L. (2002) Force and torque production in static multifinger prehension: biomechanics and control. I. Biomechanics. *Biological Cybernetics* **87,** 50-57.

Zioupos,P. and Casinos,A. (1998) Cumulative damage and the response of human bone in two-step loading fatigue. *J Biomechanics* **31,** 825-833.

Zioupos,P., Currey,J.D., and Casinos,A. (2001) Tensile fatigue in bone: are cycles-, or time to failure, or both, important? *Journal of Theoretical Biology* **210,** 389-399.

Zurada,J., Karwowski,W., and Marras,W.S. (1997) A neural network-based system for classification of industrial jobs with respect to risk of low back disorders due to workplace design. *Applied Ergonomics* **28,** 49-58.